UNIVERSIDAD CARLOS III DE MADRID

TESIS DOCTORAL

INFLUENCIA DE LA COMPOSICIÓN Y EL CONFORMADO EN EL COMPORTAMIENTO FRENTE A LA CORROSIÓN DE LOS CORRUGADOS DE ACERO INOXIDABLE

Autora

Sandra Milena Álvarez Arboleda

Directores

Dra. María Asunción Bautista Arija

Dr. Francisco Javier Velasco López

Departamento de Ciencia e Ingeniería de Materiales e Ingeniería Química

Leganés, Marzo de 2014

TESIS DOCTORAL

INFLUENCIA DE LA COMPOSICIÓN Y EL CONFORMADO EN EL COMPORTAMIENTO FRENTE A LA CORROSIÓN DE LOS CORRUGADOS DE ACERO INOXIDABLE

Autora: Sandra Milena Álvarez Arboleda

Directores: Dra. María Asunción Bautista Arija

Dr. Francisco Javier Velasco López

Firma del Tribunal Calificador:

Firma

Presidente:

Vocal:

Vocal:

Vocal:

Secretario:

Calificación:

Leganés, Marzo de 2014

A mi familia

Por toda su paciencia, apoyo y confianza durante este tiempo desde la distancia, sus palabras de aliento y la energía que me trasmiten con cada conversación. Especialmente a mi madre y hermana, dos grandes mujeres humildes, trabajadoras, amigas y emprendedoras, gracias por darme siempre un buen consejo. A mi hermano (que con un, *te amo*, me cambia la vida) y mis sobrinos (mis dos pequeños soles). A Iván y a Jaime, que siempre están y nunca me fallan. A José por su apoyo, por darme su cariño y sobrellevar todo este proceso.

AGRADECIMIENTOS

En primer lugar, quiero agradecer a mis directores por la realización de esta tesis, Asunción Bautista y Francisco Velasco, sin ustedes no habría sido posible cumplir este reto en mi vida profesional y personal, gracias por la dedicación, optimismo y el apoyo incondicional que me han brindado en estos años de trabajo. Gracias por confiar en mí y por haber hecho buenos, todos los que yo creía malos momentos ya que siempre he podido contar con ustedes.

Quiero agradecer a todo el Departamento de Ciencia e Ingeniería de Materiales e Ingeniería Química de la Universidad Carlos III de Madrid, a mis compañeros del grupo de Comportamiento en Servicio, a los que están y a los que han estado, con los que compartí el día a día y que siempre encontraron palabras de ánimo, sumado al tiempo para ayudarme con sus experiencias, sugerencias y aportaciones.

A todos mis amigos que han vivido de cerca estos últimos años: Mariu, Susana, Cristina Moral, Marta, Ana, Tamara, Teresa, Blanca, Carlos, Mariola, Belén B., Miguel Ángel y Juani. Mención especial merecen dos amigas, Noe y Cris (por los momentos de risas, tristezas y eternas conversaciones, ha sido un autentico placer encontrarlas en mi camino). A mis *Latín Brother´s:* Carol, María Crespo, Amaia (eres una de los nuestros), Freddy, Edwin y Kesman (descubrí en ustedes unas personas maravillosas, estos cuatro años no habrían sido igual sin ustedes a mi lado). A mis amigas Dayana y Shirley que me han aguantado desde la distancia y que tantas veces han tenido que contagiarme de su energía y de su alegría. Y a todos aquellos cuyo nombre no figure, púes han sido cuatro años de duro trabajo y esfuerzo personal, pero no hubiera sido posible sin la ayuda incondicional y el cariño de un gran número de personas que han estado siempre a mi lado y que he tenido la gran suerte de conocer durante estos últimos años, todos ellos están incluidos en este párrafo. Gracias por darme buenos momentos y por haber estado en esta etapa de mi vida.

Agradecer también al Ministerio de Ciencia e Innovación de España por haberme facilitado los medios necesarios para llevar a cabo este doctorado a través de una beca FPI.

ÍNDICE

RESUMEN

En la presente Tesis Doctoral se evalúa el comportamiento frente a la corrosión de barras corrugadas de aceros inoxidables (que pueden ser utilizadas como refuerzo en las partes más expuestas de las estructuras de hormigón) y se analizan en profundidad diversos factores que pueden influir en su durabilidad.

El estudio de la influencia de la composición química de las barras ha demostrado el gran interés de los nuevos grados 2001 y el 2304 (dúplex de baja aleación), que ofrecen excelentes resultados en disoluciones que simulan las contenidas en los poros del hormigón, especialmente teniendo en cuenta su precio.

Las barras corrugadas están altamente deformadas, especialmente en determinados puntos de su superficie, y poseen características microestructurales muy específicas que determinan su comportamiento frente a la corrosión. La influencia del procesado (en frío o en caliente) y la tendencia a la corrosión selectiva de las diferentes fases presentes se ha evaluado en disoluciones que simulan las contenidas en los poros del hormigón y también en medios ácidos (para simular posibles acidificaciones locales).

El interés del empleo de armaduras de acero inoxidable en general (resaltando las limitaciones que puede tener un grado austenítico de baja aleación como el 204Cu en ambiente de agresividad extrema) quedan demostrados mediante resultados de 9 años de duración obtenidos en mortero.

ABSTRACT

This Thesis evaluates the corrosion performance of stainless steel corrugated bars that can be used as reinforcement in the most exposed areas of concrete structures. Moreover, factors that can affect their durability are deeply analysed.

The study about the influence of the chemical composition of the bars has demonstrated the interest of new grades, 2001 and 2304 low-alloy duplex stainless steels, that offer excellent results in solutions simulating those contained in concrete pores, in particular taking their price into account.

The corrugated bars are strongly strained, mainly in particular areas of their surface, and they show specific microstructural features that determine their corrosion performance. The influence of processing (cold or hot working) and the trend to selective corrosion of different microstructural phases have been evaluated both in solutions simulating those contained in the pores of concrete and in acid media (to simulate possible local acidifications).

The interest of general use of stainless steel bars (standing out the limitations of a low alloyed austenitic grade like 204Cu y strongly aggressive environments) is demonstrated through long term results obtained embedding bars in mortar for 9 years.

Capítulo I

Introducción

1.1 ORIGEN Y CARACTERÍSTICAS DE LOS ACEROS INOXIDABLES

El acero inoxidable es un producto típico del siglo XX, cuyo nacimiento se sitúa entre los años 1913 y 1935. La mayoría de las aleaciones que se utilizan actualmente fueron inventadas en Inglaterra, Alemania, Estados Unidos y Francia. Una vez consolidadas las aleaciones, las investigaciones se centraron en encontrar nuevos sistemas de producción más económicos y en popularizar el uso del material [1].

En España, a finales de los años 50 e inicio de los 60, se inicia la fabricación de productos largos de acero inoxidable (barras y pletinas), destacando las empresas Olarra, S.A. y Roldán, S.A. En 1970, inicia su actividad la Compañía Española para la Fabricación de Aceros Inoxidables (Acerinox, S.A.), dedicada a la fabricación de productos planos (chapas y flejes) [1].

A partir de 1970 se empezaron a desarrollar los aceros inoxidables dúplex, más económicos y de mayor resistencia mecánica y a la corrosión, los cuales suponen el futuro del material para su empleo estructural. El acero inoxidable ha pasado de ser un producto de alto coste con usos muy restringidos, a una situación en la que se ha estandarizado la tecnología de fabricación, mejorando su eficiencia, disminuyendo sus costes y ampliando sus aplicaciones.

Los datos mundiales de producción y consumo del acero inoxidable, tomados del *International Stainless Steel Forum* (ISSF) [2], muestran una evolución en aumento del uso del mismo (Figura 1.1).

Los aceros inoxidables son aleaciones Fe-Cr, con un contenido mínimo de Cr en peso superior al 10,5% según la norma europea EN 10088-1 [3] y otros autores [1,4], aunque tradicionalmente se indica que debe ser superior al 12% [5,6]. El Cr es un elemento de aleación que tiene una alta afinidad por el oxígeno molecular, formando una capa protectora de Cr_2O_3 [7]. Esta capa, al ser impermeable al aire e insoluble, impide la corrosión del acero [1,6].

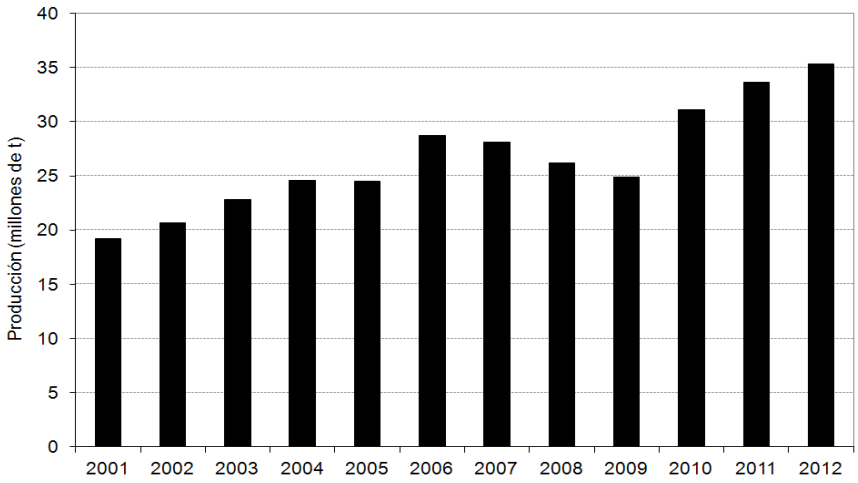

Figura 1.1. Producción mundial de los aceros inoxidables en la última década.

Los aceros inoxidables presentan un conjunto de propiedades dadas por los porcentajes de los elementos aleantes que pueden estar presentes; en el esquema de la Figura 1.2 se resumen algunas características importantes.

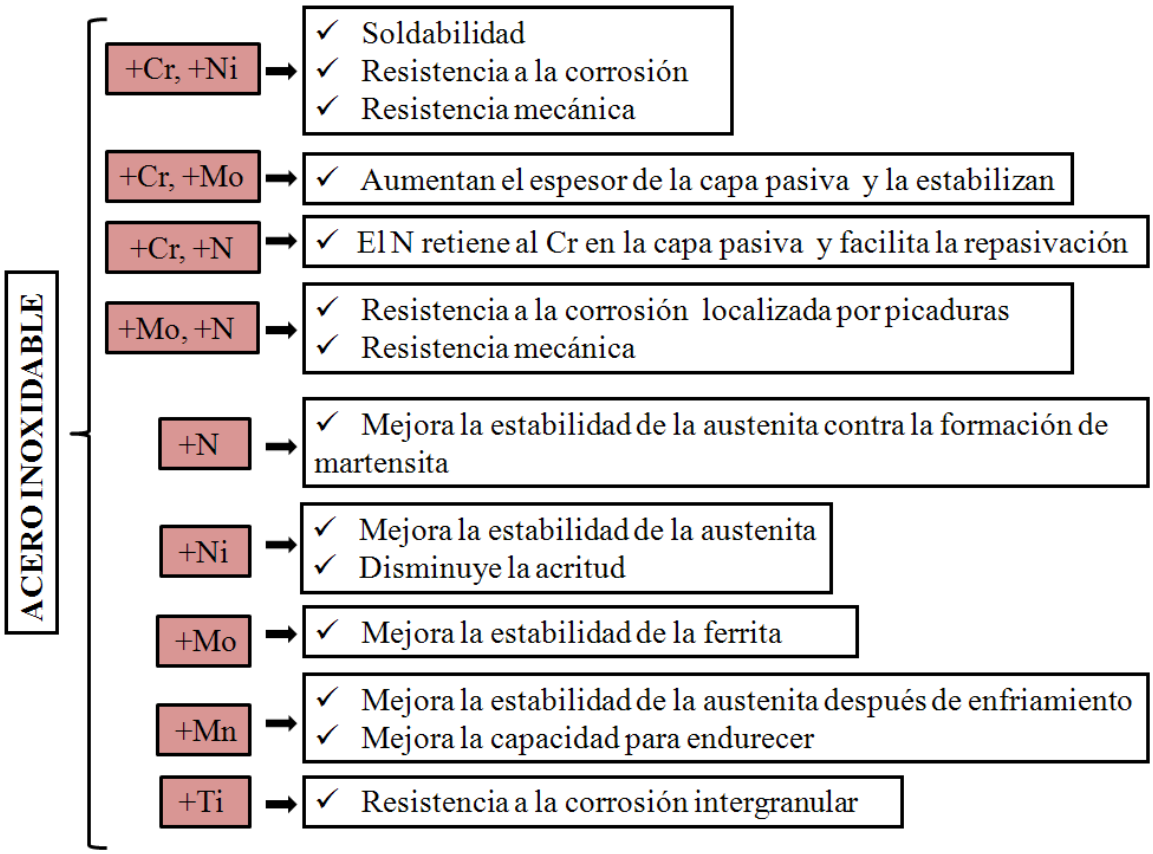

Figura 1.2. Influencia de los aleantes en algunas propiedades de aceros inoxidables.

En general, hay cinco tipos básicos o familias de aceros inoxidables que se encuentran divididos según su microestructura:

- Los aceros inoxidables endurecibles por precipitación: presentan la posibilidad de elevar sus características de resistencia mecánica mediante tratamientos térmicos adecuados, con altos valores de límite elástico y resistencia, manteniendo al mismo tiempo una notable tenacidad y plasticidad, así como elevadas características de resistencia a la corrosión y maquinabilidad [1,4].

- Los aceros inoxidables martensíticos: presentan propiedades magnéticas, con una estructura tetragonal centrada en el cuerpo (BCT). La principal característica de estos aceros es su gran dureza y resistencia al desgaste debidas al tratamiento térmico. Para prevenir la corrosión y aumentar la resistencia, se pueden adicionar elementos tales como molibdeno y níquel [4].

- Los aceros inoxidables ferríticos: presentan una microestructura de ferrita, cuya estructura es cúbica centrada en el cuerpo (BCC). Son aceros magnéticos, no se les puede endurecer mediante tratamiento térmico y su forma habitual de empleo es en estado recocido [4]. Poseen bajas propiedades de tenacidad, ductilidad y soldabilidad, son relativamente frágiles y su resistencia final no es muy alta [4].

- Los aceros inoxidables austeníticos: presentan una estructura cúbica centrada en las caras (FCC). Se caracterizan por su elevada plasticidad y tenacidad, resistencia a la corrosión, comportamiento no magnético y facilidad para ser soldados. En cambio, tienen una baja resistencia a tracción, son susceptibles a la fisuración por corrosión bajo tensiones y su estructura monofásica no permite el endurecimiento mediante tratamiento térmico (temple) [4].

- Los aceros inoxidables dúplex: son aceros con una microestructura combinada de austenita y ferrita en proporciones generalmente cercanas al 50-50%. Combinan propiedades atractivas de aceros inoxidables austeníticos y ferríticos. Llegan a tener elevadas características mecánicas (límite elástico casi el doble que los aceros austeníticos) y mejor comportamiento frente a la corrosión bajo tensiones y por picaduras [1].

Es oportuno, antes de comenzar a tratar específicamente estos materiales, suministrar alguna información sobre su designación e identificación, dado que la literatura científica usa diferentes nomenclaturas según las normas aplicables. Entre las clasificaciones más conocidas en el sector de los aceros inoxidables se encuentran la AISI (*American Iron and Steel Institute*), la EN (Norma Europea) y la UNS (*Unified Numbering System*). En la Tabla 1.1 se encuentran algunas de las designaciones y en la Tabla 1.2 se recogen los límites de la composición química de los aceros inoxidables utilizados en esta Tesis Doctoral.

Tabla 1.1. Designación de aleaciones para algunos aceros inoxidables utilizados.

EN - DIN	AISI	UNS
1.4597	204Cu	S20430
1.4301	304	S30400
1.4307	304L	S30403
1.4401	316	S31600
1.4404	316L	S31603
1.4571	316Ti	S31635
1.4482	2001	S32001
1.4362	2304	S32304
1.4462	2205	S32205

Tabla 1.2. Límites de la composición química de los aceros inoxidables austeníticos corrugados empleados.

Elemento (%)	S20430	S30400	S30403	S31600	S31603	S31635
C	< 0,15	< 0,07	< 0,03	< 0,07	< 0,03	< 0,08
S	< 0,03	< 0,03	< 0,03	< 0,03	< 0,03	< 0,03
Si	< 2,00	< 1,00	< 1,00	< 1,00	< 1,00	< 1,00
Mn	6,50-8,50	< 2,00	< 2,00	< 2,00	< 2,00	< 2,00
Cr	15,50-17,50	17,00-19,50	18,00-19,50	16,50-18,50	16,50-18,50	16,50-18,00
Ni	< 3,50	8,00-10,50	8,00-10,50	10,00-13,00	10,00-13,00	10,50-13,50
Mo				2,00-2,50	2,00-2,50	2,00-2,50
Ti						5*C/0,70
N	< 0,30	< 0,11	< 0,11	< 0,10	< 0,10	
Cu	2,00-3,50					

Tabla 1.2. (Continuación). Límites de la composición química de los aceros inoxidables dúplex corrugados empleados.

Elemento (%)	S32001	S32304	S32205
C	< 0,03	< 0,03	< 0,03
S	< 0,02	< 0,02	< 0,02
Si	< 1,00	< 1,00	< 1,00
Mn	4,00-6,00	< 2,00	< 2,00
Cr	19,50-21,50	22,00-24,00	21,00-23,00
Ni	1,50-3,00	3,50-5,50	4,50-6,50
Mo	≤ 0,60	0,10-0,60	2,50-3,50
Ti			
N	0,05-0,17	0,05-0,20	0,10-0,22
Cu		0,10-0,60	

Existen dos parámetros que relacionan los aleantes con la resistencia a la corrosión: el número de resistencia equivalente uniforme (*Uniform Resistance Equivalent*, URE) y el número de resistencia equivalente a picaduras (*Pitting Resistance Equivalent Number*, PREN). El URE se propone para predecir el comportamiento frente a la corrosión uniforme de los aceros inoxidables ferríticos [8]. El PREN se emplea para caracterizar la resistencia frente a la corrosión por picaduras, especialmente en los aceros inoxidables austeníticos [9], aunque su uso se ha extendido también a veces a los inoxidables dúplex [10-14].

La dificultad que presentan el PREN y el URE cuando se pretende emplearlos para aceros inoxidables dúplex, se basa en que en estos materiales existen dos fases con diferentes composiciones [15]. El PREN en aceros dúplex se calcula a partir de la composición química de las dos fases. Esto puede suponer una simplificación demasiado peligrosa, y no se debe utilizar para elegir el grado adecuado de acero inoxidable ni para hacer cálculos teóricos del comportamiento a la corrosión de los aceros dúplex, tal y como ha sido sugerido anteriormente por otros autores [15].

Varios estudios intentan explicar la mayor o menor resistencia a la corrosión en las fases de los grados dúplex utilizando el cálculo del índice PREN para la austenita y la ferrita de forma independiente [12,15,16]. Sin embargo, su éxito está limitado por la dificultad para determinar la composición exacta de cada fase, y en particular el contenido de N, que tiene un peso muy alto en la expresión del PREN. Éste se calcula teniendo en

cuenta el contenido de los aleantes que favorecen dicha resistencia, mediante la fórmula 1.1:

$$PREN_{\mathbf{X}} = [\%\ Cr\ (p/p)] + 3{,}3\ [\%\ Mo\ (p/p)] + \mathbf{X}\ [\%\ N\ (p/p)] \quad (1.1)$$

Donde **X** es el factor de multiplicidad que define el tipo de acero inoxidable. Los valores de este factor encontrados varían en su mayoría entre 16 y 30, tanto para austeníticos como dúplex [8,10,17,18]. Incluso ciertos autores consideran el efecto perjudicial del Mn restando dicho contenido de la ecuación [12], aunque, tal y como definen Lo et al., los elementos que más contribuyen a la resistencia a corrosión por picadura en aceros inoxidables son el molibdeno y nitrógeno [19].

El URE está relacionado con el PREN, y tiene en cuenta además el efecto del níquel [8], mediante la fórmula 1.2:

$$URE = \%\ Ni + PREN \quad (1.2)$$

Al igual que ocurría con la fórmula 1.1, la expresión del URE tendría inconvenientes para ser utilizada al momento de elegir un acero inoxidable dúplex. Existen muchos factores, además de la composición química, que influyen en el comportamiento frente a la corrosión y que no están incluidos en el cálculo del índice PREN. Por ejemplo, para un determinado dúplex S32205 en medio ácido, la tendencia de la corrosión selectiva de la austenita o la ferrita depende de las condiciones del entorno agresivo [20,21].

Existen estudios relevantes sobre la influencia de la formación de martensita por deformación en aceros austeníticos y el efecto perjudicial de ésta sobre las picaduras [22-24], las propiedades mecánicas, el desgaste y la resistencia a la corrosión [25]. De igual modo, se ha evaluado la importancia de la disminución del tamaño de grano, ya que ralentiza la corrosión intergranular y mejora la resistencia a la corrosión en general [25,26].

1.2 ACEROS INOXIDABLES DE BAJA ALEACIÓN

El interés por encontrar aceros inoxidables más económicos, pero capaces de garantizar la durabilidad de los componentes en ambientes agresivos, ha llevado a las empresas a desarrollar nuevos aceros de bajo grado de aleación. Uno de los elementos que más encarece el precio de los aceros inoxidables austeníticos y dúplex es el níquel, muy por encima de otros aleantes mayoritarios como el cromo. Por ello, la mayoría de los desarrollos se han centrado en reducir el contenido del mismo de los aceros.

1.2.1 Austeníticos de baja aleación

Los aceros inoxidables austeníticos de la serie AISI 300 son un grupo muy importante, dado que a él pertenecen la mayor parte de los comúnmente empleados. Su contenido en Ni y la volatilidad del precio de este elemento, llevó a la fabricación y estudio de aceros inoxidables austeníticos de baja aleación, desarrollándose los aceros inoxidables austeníticos de la serie AISI 200. Algunos tipos destacados de esta serie son el S20100, S20200, S20400 ó S20500, que se caracterizan por contenidos en Ni inferiores al 6% y la adición de Mn (entre un 5,5 y un 15,5%) como elemento que favorece la solubilidad del N y tiene un comportamiento gammágeno o estabilizador de la austenita. Existen trabajos sobre esta familia de aceros austeníticos, en los cuales se destacan sus propiedades mecánicas (más elevadas que las de un S30400) o su buen equilibrio entre dureza y propiedades de tracción [27,28]. También se ha evaluado el nivel de ductilidad [27,29], o el efecto de la laminación en frío sobre el tamaño de grano, que a su vez influye sobre las propiedades mecánicas del acero [22]. Además, se ha estudiado la transformación de la austenita en martensita inducida por deformación [30,31], ya que ésta afecta a las propiedades mecánicas [32], ocasionando el endurecimiento del material [31,33].

La resistencia a la corrosión de los aceros austeníticos de bajo Ni se encuentra aproximadamente entre la de los austeníticos y los ferríticos estándar [28]. Se ha estudiado la importancia de las capas de óxidos formadas sobre estos aceros a altas temperaturas, observando la formación de óxidos bien adheridos al sustrato [34], la

influencia de la temperatura de oxidación en el espesor y desprendimiento de los óxidos formados [35], o la oxidación a alta temperatura al variar el porcentaje de Ni [36].

Hay que tener en cuenta la influencia de algunos elementos en las propiedades mecánicas y frente a la corrosión de estos aceros. Por ejemplo, la adición de Cu aumenta la susceptibilidad al agrietamiento, aunque aumenta la resistencia a la corrosión por picaduras [29,32,37]. El N, por otro lado, aumenta la estabilidad de la austenita frente a la formación de martensita inducida mediante la deformación, e incrementa de forma muy pronunciada la resistencia a la corrosión por picaduras [27].

1.2.2 Dúplex de baja aleación

En general, debido a su microestructura, los aceros dúplex siempre han demostrado una excepcional combinación de propiedades mecánicas y estabilidad química [38-41]. Por ello, desde hace años, los aceros inoxidables dúplex son de interés para aplicaciones tales como la industria del petróleo, las refinerías de gas y ambientes marinos en particular [42-45].

La imposibilidad de producir aceros inoxidables austeníticos de baja aleación con buena durabilidad en ambientes agresivos ha propiciado el desarrollo de aceros dúplex de baja aleación. Así, han aparecido en el mercado aceros dúplex con alto contenido en Mn y menor Ni (más económicos), así como otros con menor porcentaje en Mo [12,16,46,47].

Los aceros inoxidables dúplex de baja aleación parecen ser una excelente alternativa, desde el punto de vista económico y tecnológico, para remplazar a aquellos grados más tradicionales como el S30400 o el S31600 en múltiples aplicaciones. Se han estudiado aspectos como su caracterización microestructural [48], mecánica [49], su tendencia a la fragilización a alta temperatura [50], su buena resistencia a la erosión y a la erosión-corrosión [51] o su comportamiento frente a la soldadura [50] y la formación de los óxidos durante la misma [52]. Se ha demostrado que con estos materiales se pueden logar propiedades mecánicas comparables a los austeníticos tradicionales [53], siendo más baratos que el dúplex S32205 y que el austenítico S30400. Algunos dúplex de baja aleación han demostrado, en determinados medios, una resistencia a la corrosión por

picaduras superior a la de los austeníticos, a un precio, además, mucho más competitivo [54-56].

Ya han surgido ejemplos de la utilización de acero inoxidable dúplex de baja aleación en la construcción [57], incluidos puentes peatonales en Førde (Noruega) y en Siena (Italia) [58].

Para aplicaciones en ingeniería civil, suele interesar llevar a cabo una evaluación adecuada de las propiedades y la resistencia al fuego de las estructuras de acero, que depende en gran medida de la capacidad de predecir con claridad la respuesta del material a temperatura elevada. El acero inoxidable austenítico, en particular, ya ha sido empleado con éxito durante muchos años en aplicaciones de alta temperatura. Estudios recientes han demostrado un mejor comportamiento al fuego de los aceros inoxidables dúplex de baja aleación respecto al acero al carbono, ya que mantienen su resistencia por más tiempo a temperaturas elevadas [59-61]. Por ello, los dúplex presentan en ese campo grandes posibilidades de aplicación práctica, debido a la creciente importancia del diseño de la seguridad contra incendios y a la reducción de consecuencias sociales y económicas derivadas de la pérdida [62].

Teniendo en cuenta las propiedades térmicas de los aceros inoxidables, se podrían considerar dos aspectos importantes al momento de valorar su comportamiento a temperaturas elevadas: el tipo de conformado del acero, ya que las propiedades mecánicas, tales como resistencia a la fluencia y el módulo elástico se reducen rápidamente con el conformado en frío [63], y a la composición química de cada una de las aleaciones. Esto último se debe a que las propiedades de los aceros inoxidables pueden variar considerablemente a altas temperaturas entre diferentes grados [64], viéndose mejoradas, por ejemplo, con mayores contenidos en Cr y Mo.

Un grado novedoso dúplex de baja aleación y de gran interés en el mercado actual es el S32101 [12,16,56,58,64-66]. Se trata de un inoxidable con buenas propiedades mecánicas [58,66]. Por ejemplo, su resistencia mecánica es dos veces superior a la de un austenítico convencional [67], presenta alta resistencia a la fractura [68], una adecuada capacidad de soldadura [58] y buenas propiedades a alta temperatura [64]. Otros estudios sobre el S32101 se han centrado en evaluar la temperatura crítica para el inicio, la propagación y el crecimiento de picaduras [56,69,70]. También se han publicado estudios en medios neutros con cloruros o con sulfatos, para analizar el comportamiento frente a la

corrosión [71,72], la formación de precipitados que afectan la resistencia a la corrosión por picaduras [12] o los cambios en la microestructura del acero inoxidable dúplex causados por la deformación a altas temperaturas [73]. Todas estas investigaciones se han realizado en condiciones muy diferentes a las que supondría su empleo real como armadura en hormigón.

El acero inoxidable dúplex S32304 ha tenido desde el año 2003 un uso creciente en la industria desalinizadora, aplicaciones marinas o procesos de producción, donde está desplazando al austenítico S31600. Es posible encontrar en la bibliografía estudios relativos a su comportamiento mecánico y frente a la soldadura [74-79]. Se han publicado estudios centrados en el comportamiento en medios neutros conteniendo cloruros y sulfatos, propios de la industria papelera [80-82], así como el efecto de los tratamientos térmicos en el comportamiento frente a corrosión por picaduras [83,84]. Sin embargo, es una aleación de la que se dispone de muy limitada información sobre su comportamiento frente a la corrosión desde el punto de vista científico en cuanto a su uso como armaduras en hormigón, aunque algún trabajo pionero ya ha hecho patente el interés del uso de este acero dúplex como refuerzo en estructuras de hormigón [85].

Por todo ello, resulta de gran atractivo la evaluación de la dependencia del conformado, la microestructura y los aleantes con la corrosión de los nuevos dúplex, dada su posible repercusión económica en la construcción de armaduras con aceros inoxidables y su resistencia frente a la corrosión por picaduras [83].

1.3 RESISTENCIA A LA CORROSION EN HORMIGÓN

1.3.1 Tipos de corrosión del acero en hormigón

La primera barrera para impedir el ataque químico externo es el grado de compactación del hormigón. La penetración de agua o aire y otro tipo de agentes químicos agresivos, claves para el desarrollo de un ataque corrosivo de las armaduras, depende de la porosidad del hormigón, estructura de poros y su grado de conectividad [86] (Figura 1.3). La penetración de agentes agresivos a través de los poros puede verse favorecida mediante los mecanismos de absorción capilar, permeabilidad y difusión.

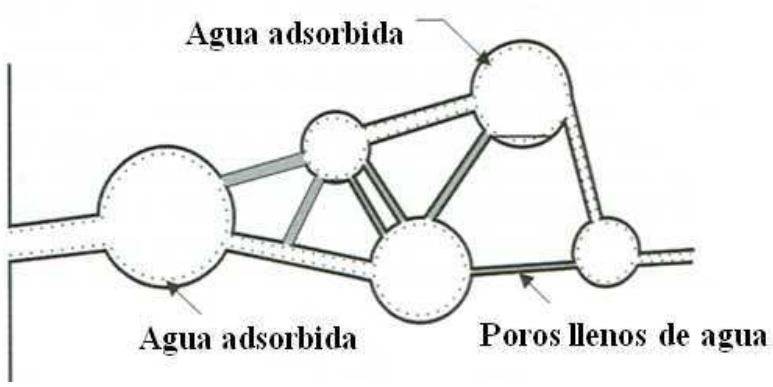

Figura 1.3. Representación de la estructura porosa del hormigón [87].

Según los agentes agresivos presentes en el ambiente, los refuerzos metálicos de las estructuras de hormigón, en general, podrían ser susceptibles a diferentes tipos de corrosión. Los más comunes son los que se muestran en la Figura 1.4: localizada (por cloruros) o generalizada (por carbonatación).

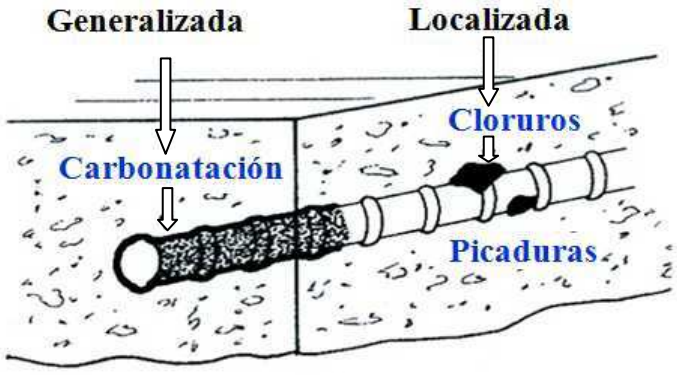

Figura 1.4. Esquema de los modos de corrosión de armadura mostrando los factores que originan la misma [88].

Por otro lado, en estructuras que utilizan armaduras pretensadas, existe un importante riesgo de desarrollar corrosión bajo tensión en ambientes con cloruros [89], que es una forma de ataque que conduce fácilmente al fallo de las estructuras de hormigón armado (EHA).

- ✓ **Corrosión por cloruros**

Los iones cloruro pueden estar presentes dentro del mismo hormigón, ligados con el cemento, y/o como cloruros libres en la disolución de los poros que penetra en las estructuras desde el exterior, difundiéndose hasta alcanzar la armadura. La corrosión por picaduras causada por cloruros es una de las formas más normales de fallo de un acero embebido en hormigón, y sólo llega a producirse en algunos casos en medios altamente contaminados con estos iones. El mecanismo por el que se desarrolla este tipo de ataque aparece esquematizado en la Figura 1.5.

Los cloruros causan la destrucción localizada de la capa pasiva del acero en determinados puntos. Por tanto, la corrosión por cloruros es localizada (corrosión por picaduras), con ataques penetrantes de área limitada rodeadas de áreas no corroídas. González *et al*. prueban que los cloruros por sí solos no son capaces de iniciar la corrosión de las armaduras, necesitando de la presencia de resquicios u otro tipo de heterogeneidades geométricas, oxígeno y humedad [90]. Los resquicios característicos de la interfase acero/hormigón juegan un papel clave en el inicio de las picaduras.

Excepcionalmente, cuando están presentes niveles muy altos de cloruros, la capa pasiva puede ser destruida en grandes extensiones de la armadura, y la corrosión será de naturaleza generalizada.

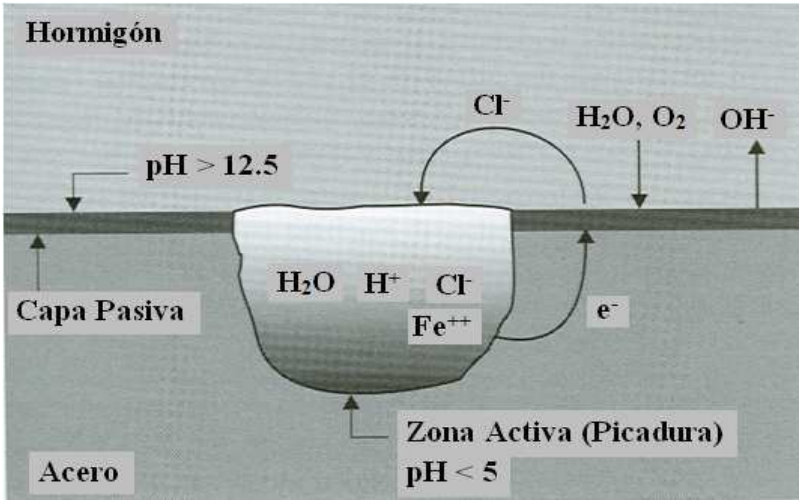

Figura 1.5. Esquema del proceso de corrosión por picadura en una armadura embebida en hormigón contaminado con cloruros [87].

El tiempo que tardan los cloruros en llegar hasta la armadura y alcanzar una concentración suficiente para desencadenar la corrosión (llamado periodo de iniciación en el modelo propuesto por Tuutti [91], Figura 1.6) dependerá principalmente de los siguientes factores:

- La concentración de cloruros en el medio exterior.
- La naturaleza del catión que acompaña al cloruro.
- La calidad del hormigón: tipo de cemento, proporción de aluminato tricálcico, relación agua/cemento, etc.
- La temperatura.
- El tamaño y cantidad de las fisuras.

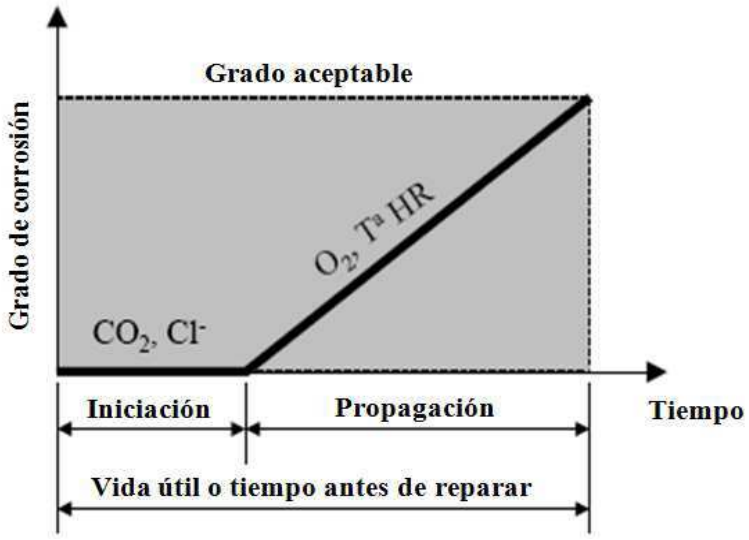

Figura 1.6. Modelo de Tuutti sobre la vida útil respecto de la corrosión [91].

Se asume que el inicio de la etapa de propagación tiene lugar cuando la relación molar de los iones cloruro e hidroxilo en la disolución de los poros supera un cierto valor [92,93]. Se han propuesto valores para esta relación molar $[Cl^-]/[OH^-]$ alrededor de 0,6 para el inicio de la corrosión [94,95], pero la realidad es que existe una gran variabilidad para el valor experimental de este parámetro umbral [96]. Esto es debido a la importante influencia que tienen en la relación $[Cl^-]/[OH^-]$ las condiciones físicas de la interfase acero-hormigón [97].

Una vez se inicia la corrosión, se forman óxidos de naturaleza expansiva que agrietan el hormigón, lo que facilita la entrada de más agentes agresivos, pudiendo llegar a situaciones de riesgo y hasta de colapso de la estructura.

- ✓ **Corrosión por carbonatación**

La carbonatación del hormigón, es una causa importante en la disminución del pH superficial. Se produce por la acción del CO_2 atmosférico que se combina con el $Ca(OH)_2$ producido como subproducto de hidratación del cemento Portland [98], formando carbonato de calcio, según la siguiente reacción 1.1:

$$Ca(OH)_2 + CO_2 \rightarrow CaCO_3 + H_2O \qquad (1.1)$$

El proceso de carbonatación es un fenómeno lento pero progresivo. La reacción se produce necesariamente en presencia de un cierto grado de humedad, favoreciendo la reacción con CO_2 hasta formar un tampón carbonato/bicarbonato (Figura 1.7).

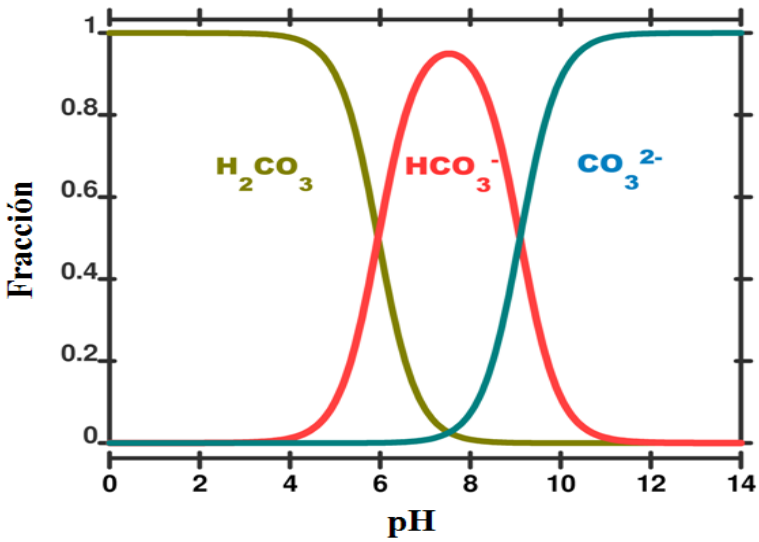

Figura 1.7. Esquema de la relación entre pH y sistema ácido carbónico-bicarbonato-carbonato.

Este proceso genera una importante disminución del pH por debajo de 9 que, al generalizarse en el espesor del recubrimiento, lleva a una completa disolución de la capa

protectora y a la despasivación de las armaduras (pasando de la zona de pasividad a la zona de corrosión del diagrama de Pourbaix, tal y como puede verse en la Figura 1.8.).

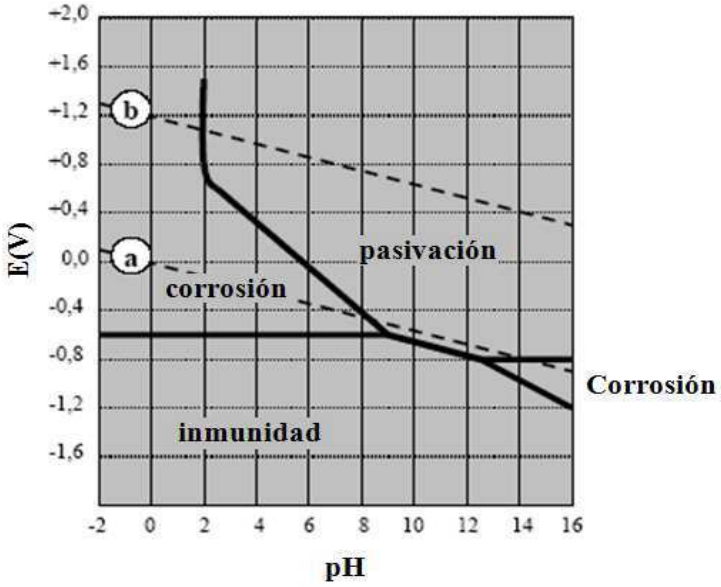

Figura 1.8. Diagrama de Pourbaix para el Fe a 25ºC.

La humedad relativa (HR) del ambiente donde se encuentre la estructura puede relacionarse con la velocidad de penetración del frente de carbonatación en el hormigón [99,100], como se muestra en la Figura 1.9. El intervalo de HR crítico para fomentar la carbonatación varía desde 60% hasta 80% [99,100]. Puede observarse cómo hormigones sometidos a ambientes secos, con HR menor del 20%, presentan un grado de carbonatación relativamente bajo. Por otro lado, a HR muy altas, los poros están saturados de agua y la difusión del CO_2 en H_2O está más dificultada que en aire, por lo que la reacción de carbonatación no se produce.

La iniciación y propagación de la corrosión de las armaduras por carbonatación del hormigón también puede modelizarse según el modelo propuesto por Tuutti (Figura 1.6).

La determinación del espesor carbonatado en el hormigón resulta especialmente sencilla a través del uso de indicadores tales como la fenoftaleína, con un viraje de color que dependerá del pH, o bien colocando electrodos de titanio activado junto a las

armaduras, ya que por medio de éstos se puede controlar el avance del perfil de carbonatación, observándose un cambio en el potencial con la disminución del pH [101].

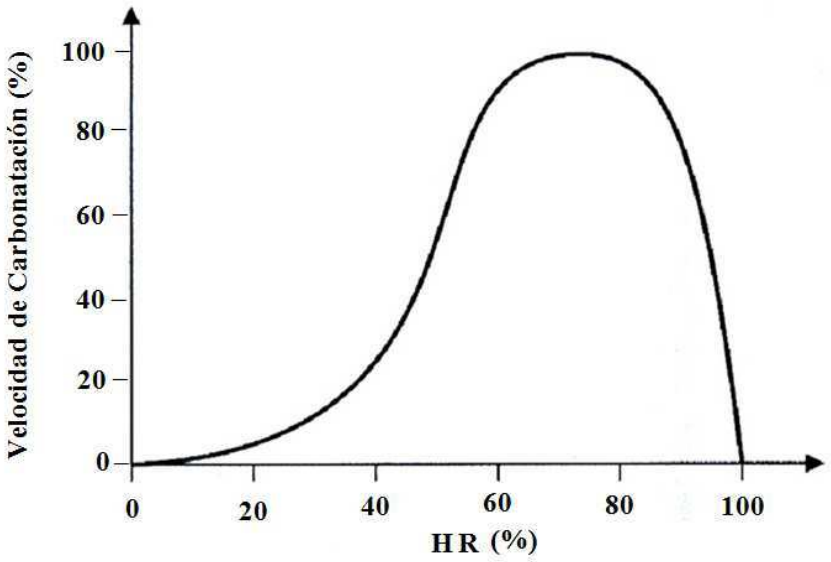

Figura 1.9. Grado de carbonatación del hormigón en función de la HR atmosférica de exposición [87].

1.3.2 Factores acelerantes de la corrosión

El ataque puede avanzar tan lentamente que no afecte a la vida útil de la estructura. Los factores que determinan en mayor medida la velocidad de corrosión son [102,103]:

- Contenido de humedad
- Concentración de cloruros
- Temperatura
- Formación de macropares galvánicos

✓ **Contenido de humedad**

Una de las características del hormigón es su capacidad de absorción de humedad ambiental, proceso que se desarrolla con gran facilidad, al contrario que su secado. Si la

humedad exterior es constante, se puede llegar a establecer un equilibrio entre la existente en el interior del hormigón y la ambiental. Si la humedad externa no es constante, el interior del hormigón no puede mantener el equilibrio, permaneciendo únicamente la capa superior del hormigón en equilibrio con la humedad ambiental. El contenido en humedad es el factor que más influye en la velocidad de corrosión, pudiéndose considerar las tres situaciones mostradas en la Figura 1.10:

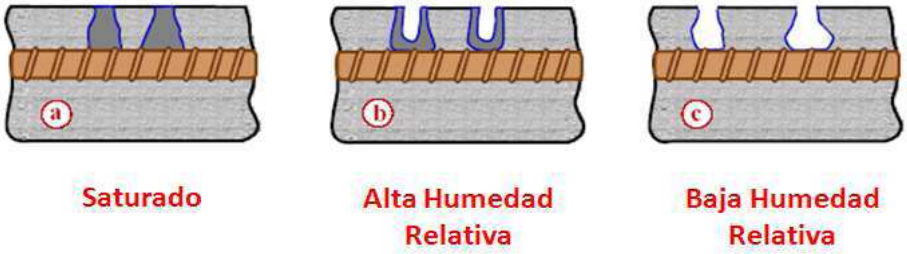

Figura 1.10. Contenido en humedad de los poros de hormigón en función de la humedad ambiental.

- **Saturado:** Los poros están saturados de humedad (Figura 1.10a). En esta situación, a pesar de que la resistividad es la menor posible y que la formación de una pila de corrosión estará favorecida, el oxígeno tendrá primero que disolverse en el agua para poder alcanzar la armadura. En estas condiciones, el proceso está controlado por la velocidad de acceso del oxígeno, y las velocidades de corrosión serán moderadas o bajas.

- **Alta humedad relativa:** Los poros contienen un grado de humedad alto, pero sin llegar a la saturación (Figura 1.10b). El acceso del oxígeno hasta la armadura es fácil, pues la distancia de difusión es corta. Además, la baja resistividad del medio permite elevadas velocidades de reacción. En este caso las velocidades de corrosión son las máximas.

- **Baja humedad relativa:** Los poros contienen muy poca humedad (Figura 1.10c). La resistividad es muy elevada y el proceso de corrosión se encuentra dificultado debido al control resistivo. En esta situación, la velocidad de corrosión también será baja, a pesar de que el hormigón se encuentre carbonatado o contaminado con iones despasivantes.

- ✓ **La concentración de cloruros**

Los iones cloruro, una vez alcanzan las armaduras, destruyen localmente la capa de óxido que protege las armaduras de la corrosión. Una vez despasivada, el proceso de corrosión de la armadura se podrá desencadenar cuando se alcanzan concentraciones suficientes de O_2 y agua, tal y como se ha explicado antes. Además, los iones cloruros son higroscópicos, es decir, si su concentración es elevada en el hormigón, éste retiene una mayor cantidad de agua, con el consiguiente aumento de la velocidad de corrosión del acero al disminuir la resistividad iónica del hormigón.

En la Figura 1.11 se muestra cuantitativamente cómo la concentración de estos iones no sólo favorece el inicio de la corrosión, sino que además aumenta la velocidad con que se desarrolla el ataque.

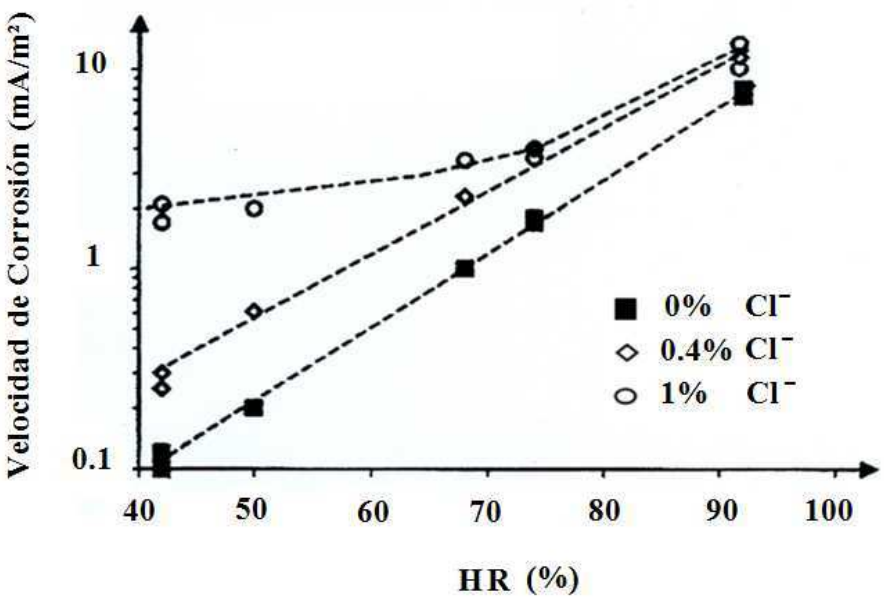

Figura 1.11. Relación entre la HR y la velocidad de corrosión en hormigón carbonatado con y sin presencia de cloruros [104].

- ✓ **Temperatura**

La temperatura suele acelerar el proceso de corrosión de dos maneras: por un lado, genera un incremento en la velocidad de corrosión, tal y como predice la teoría de

Arrhenius; por otro, favorece la movilidad de los iones a través de la película de óxido homogéneo que se forma "in situ" sobre la superficie metálica [105] y a través del hormigón.

Sin embargo un aumento próximo a la temperatura de ebullición del agua puede provocar un descenso del contenido en agua retenido en los poros del hormigón, lo que inhibiría la corrosión (Figura 1.10).

- ✓ **Formación de macropares galvánicos**

Se trata de macropilas de corrosión generadas entre dos áreas de la estructura situadas a cierta distancia. Se forman cuando un área de las armaduras está corroída y actúa como ánodo, y la otra actúa como cátodo permaneciendo pasiva. Estas macropilas son un caso común, por ejemplo, en tableros de puente, donde los cloruros acceden por la parte superior y la inferior permanece sin contaminar. En este caso, la macropila se forma a través de los estribos. La corrosión comienza en las armaduras superiores, mientras que las inferiores permanecerán pasivas más tiempo.

Cuando una situación como esta se produce sobre la EHA, la corrosión propia de las micropilas (debidas al ataque por cloruros) se suma a la acción de la macropila, aumentando la velocidad de corrosión. El incremento producido dependerá de los potenciales de corrosión del ánodo y del cátodo cuando empiece la acción de la macropila, así como de la resistencia óhmica entre ambos. Sin embargo, se ha comprobado que, en general, la resistividad del hormigón hace que la actividad de los macropares galvánicos sea casi despreciable frente a la actividad de las micropilas de corrosión [106-108].

1.4 MÉTODOS DE PROTECCIÓN FRENTE A LA CORROSIÓN DE LAS ARMADURAS

Las EHA se fabrican tradicionalmente con acero al carbono, dado su bajo precio, buenas propiedades mecánicas, conformabilidad y capacidad para conseguir la adhesión

con el hormigón y permitir la transferencia de carga. Además, en ausencia de agentes agresivos en el ambiente, permanece en estado pasivo al estar embebido en el hormigón. Sin embargo, la corrosión de las barras corrugadas es la principal causa de fallo en servicio de las EHA.

Para impedir la pérdida de pasividad de las armaduras y los problemas que esto supone para las EHA, se ha venido actuando en los últimos años desde dos posiciones diferentes:

- Con *medidas que actúan sobre el hormigón*, modificando su química o creando barreras que lo hacen más resistente al ataque o penetración de los agentes agresivos para el acero.
- Con *medidas que actúan sobre las armaduras*, mejorando la resistencia a la corrosión del material empleado para reforzar las EHA.

1.4.1 Medidas que actúan sobre el hormigón

Las principales características y limitaciones de los métodos utilizados para tratar de controlar la corrosión de las armaduras de acero actuando sobre el hormigón se exponen a continuación.

- **Adición de inhibidores de corrosión**

Los inhibidores son sustancias que se añaden al hormigón para disminuir la velocidad de corrosión [109,110]. Esta medida suele resultar atractiva debido al bajo coste de los inhibidores y a su fácil aplicación en comparación con otros métodos [111]. Existen muchos tipos de inhibidores, pero los más tradicionales son los nitritos, cuya efectividad está probada en determinadas condiciones [112-116]. Los nitritos se han añadido normalmente en forma de $NaNO_2$ al agua de amasado. Su presencia da lugar a un descenso de la resistencia a compresión del hormigón [117], pero esta pérdida de propiedades mecánicas es despreciable en las concentraciones necesarias para inhibir la corrosión [118].

Es necesario un contenido mínimo de NO_2^- para garantizar la pasividad de las armaduras, que depende del grado de contaminación del hormigón por cloruros. El valor umbral para la relación $[NO_2^-]/[Cl^-]$ capaz de evitar la corrosión oscila entre el 0,5 señalado por Berke [119], y las recomendaciones más estrictas de otros autores [120,121], que proponen que este valor se mantenga siempre por encima de 0,7-1,0. Królikowski y Kuziak han evaluado la capacidad de penetración de un inhibidor en la estructura capilar del hormigón para reducir la corrosión ya iniciadas del acero, utilizando diferentes tasas de aumento para la relación molar [122]. También se ha demostrado el efecto sinérgico del uso de revestimientos galvanizados e inhibidores, que actúan de manera complementaria para retrasar la corrosión [123].

Durante años se han buscado inhibidores de corrosión de las armaduras alternativos a los nitritos, entre otras razones porque se ha sugerido que estos últimos son potencialmente cancerígenos. Se han propuesto los monofluoruro-fosfatos sódicos [124-126], o compuestos orgánicos basados en mezclas de alcanoaminas, aminas o aminoácidos o basados en una emulsión de estos [127-132]. Pero su eficacia suele ser inferior a la de los nitritos, por lo que estos últimos son los únicos que se han usado en la práctica de forma significativa [133].

Estudios más recientes se han enfocado en comparar más de 80 sustancias orgánicas como candidatos a ser utilizados como inhibidores de la corrosión [134]. Hu *et al.* proponen la incorporación de vesículas poliméricas, vacías o con contenidos de Ca, en la mezcla del hormigón, determinando que las vesículas con Ca aumentan la resistencia a corrosión del acero y conducen a la recuperación de la capa de superficie del acero [135].

Sin embargo, el principal riesgo que entraña el uso de inhibidores químicos en la corrosión, es la durabilidad de su eficacia, aunque en gran parte el rendimiento de estos se puede considerar parcialmente satisfactorio. Hay que señalar, por ejemplo, su tendencia a la lixiviación en estructuras sumergidas [136]. Además, se han demostrado incapaces de pasivar armaduras con un fuerte grado de precorrosión [137].

- **Aditivos para reducir la porosidad del hormigón**

Este tipo de aditivos son sustancias que también se añaden al hormigón para evitar la formación de redes de poros en su interior a través de las cuales se favorece la entrada

de los agentes que provocan la corrosión electroquímica de las armaduras de acero [138-140].

Los aditivos reductores de la porosidad alargan la etapa de iniciación de la corrosión definida en el modelo de Tuutti (Figura 1.6). Por esta última razón, su eficacia puede ser cuestionable en ambientes de agresividad extrema o estructuras de vida en servicio prevista muy larga. Además, otro de los inconvenientes de los aditivos reductores de la porosidad es que provocan la fijación de un menor número de cloruros en el cemento.

Hay un gran interés en estudiar la microestructura y las propiedades mecánicas del hormigón al utilizar polímeros, cenizas volantes u otras puzolanas con el fin de reducir la porosidad de este [141,142]. Huang *et al.* han investigado la combinación de látex y fibras adicionados en la mezcla del hormigón, obteniendo un hormigón con buenas propiedades de resistencia y buena permeabilidad [143].

La utilización de cenizas volantes y otras adiciones puzolánicas presenta beneficios ambientales y económicos [144]. Además de refinar la estructura de los poros, los productos de hidratación producidos por la reacción de cenizas volantes con el hidróxido de calcio llenan los poros, lo que no sólo reduciría el volumen, sino también el tamaño de los poros [142]. Sin embargo, la disminución de la reserva alcalina causada por las cenizas volantes u otros aditivos reductores de la porosidad de naturaleza puzolánica puede favorecer la corrosión por carbonatación de las armaduras [145,146]. Además, este tipo de aditivos afecta a la velocidad de curado, disminuyéndola [147].

Las trasformaciones causadas por aditivos reductores de la porosidad además pueden mejorar el comportamiento mecánico en otros aspectos muy relacionados con el comportamiento en servicio de la estructura. El tamaño, la conectividad, la rugosidad de la superficie y la fracción de volumen de los poros están directamente relacionados con la resistencia mecánica del hormigón [148]. Además, la porosidad favorece la absorción de agua y las reacciones internas de ésta con el CaO, formando cristales de $Ca(OH)_2$, y determinando el deterioro de un hormigón expuesto a elevadas temperaturas [149].

- **Recubrimientos poliméricos del hormigón**

Debido a la problemática existente con la absorción de agua, la permeabilidad y la difusión del cloruro y del dióxido de carbono en la matriz del hormigón, se pueden usar una extensa variedad de pinturas y recubrimientos con el fin de proteger el deterioro del hormigón.

La selección correcta entre los diversos recubrimientos orgánicos utilizados para proteger la superficie del hormigón es difícil, ya que pueden proporcionar diferentes niveles de protección. De todos ellos, los que parecen resultar más impermeables son los base epoxi, si bien presentan el inconveniente del elevado coste relativo y su propia estabilidad a los agentes atmosféricos [150-152]. Los resultados obtenidos con un epoxi y un poliuretano acrílico-alifático han demostrado su eficiencia en la reducción de la penetración de cloruros y mejora de la vida en servicio de las EHA [153].

Mediante la impregnación del hormigón con silanos de tamaño nanométrico (60-70 nm) se inhibe eficazmente la corrosión de las armaduras por cloruros, así como la absorción de agua [154].

Otros estudios han optado por investigar la posibilidad de utilizar un geopolímero como un innovador revestimiento inorgánico de protección de hormigón en ambientes marinos. Los geopolímeros investigados poseen baja permeabilidad y excelente propiedad anticorrosiva [155].

Aunque los recubrimientos pueden extender la vida útil de las EHA, no todos son capaces de resistir la exposición en terrenos ácidos. Además, se ha demostrado que ninguno es capaz de detener la corrosión una vez iniciada [137].

- **Prevención y protección catódica**

La polarización catódica del acero al carbono es uno de los métodos más efectivos para inhibir la corrosión de EHA expuestas en ambientes agresivos. Esta técnica se ha utilizado bajo la denominación de “prevención catódica” durante las últimas décadas para evitar el inicio de la corrosión en EHA construidas en ambientes marinos [156-158].

Por otro lado, la polarización catódica de las armaduras es el único método que se ha demostrado capaz de detener la corrosión una vez se ha iniciado el ataque. En este

caso, la técnica se denomina "protección catódica" [157,159-161], y las corrientes impuestas para polarizar catódicamente son mayores que en el caso anterior. A nivel mundial se utiliza cada vez más para detener la corrosión del acero de refuerzo, normalmente se debe reparar también el hormigón para minimizar las posibles grietas y mantener una estructura integra y estética [162,163].

En ambos casos, tal y como se observa en la Figura 1.12, se fija un ánodo externo en la estructura (frecuentemente mallas de titanio activado) y se fuerza a las armaduras a actuar como cátodo. La aplicación de una corriente catódica (cuyo valor está comprendido dentro del intervalo de las normalmente usadas en estas aplicaciones) implica una desaceleración del proceso anódico de oxidación del hierro y una aceleración del proceso de reducción de oxígeno. Este último tiene lugar mediante la reacción 1.2:

$$O_2 + 2H_2O + 4e^- \rightarrow 4OH^- \qquad (1.2)$$

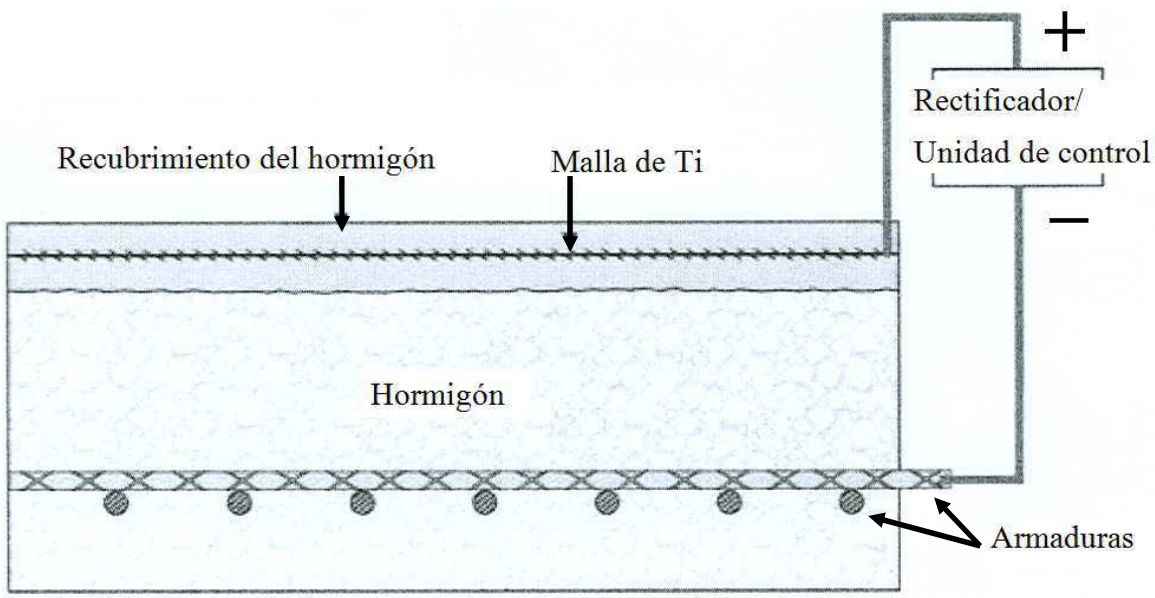

Figura 1.12. Sistema de protección catódica en EHA.

El potencial de una EHA debe ser inferior a -710 mV frente al electrodo de calomelanos saturado (SCE) para que se considere catódicamente protegida [164]. Además, existe un límite inferior para el potencial a fin de evitar problemas causados por

la evolución de hidrógeno. El valor de ese límite inferior es de -1090 mV vs. SCE para EHA normales y de -890 mV si las armaduras están pretensadas [164].

En otros sistemas diferentes a EHA, la durabilidad de los metales protegidos catódicamente se asegura por la aplicación de una corriente lo suficientemente alta para polarizar instantáneamente en dirección catódica hasta los valores adecuados, lo que reduce la velocidad del proceso anódico hasta valores despreciables. Sin embargo, en EHA las corrientes impuestas en protección catódica no pueden ser mayores que 20 mA/m^2, según limita la normativa vigente [164]. Además, los valores de corriente límite son todavía menores para EHA con recubrimientos orgánicos o si lo que se quiere aplicar es prevención catódica.

Para EHA sumergidas, en las que la velocidad de difusión de oxígeno es muy baja debido a la saturación de los poros con agua, los valores de corriente permitidos por la norma son capaces de polarizar las armaduras hasta valores de potencial suficientemente negativos para garantizar la durabilidad de la EHA [165]. Sin embargo, este caso no es el más interesante, pues es difícil que las armaduras en estas condiciones alcancen elevadas velocidades de corrosión, debido al control por difusión de la cinética que ejerce el proceso catódico.

En EHA expuestas a la atmósfera, la cinética de corrosión presenta un control por activación. En este caso se necesitarían corrientes mucho mayores que las normalizadas para inducir inmediatamente la pasividad de las armaduras activas [166]. La efectividad de la protección catódica en EHA no sumergidas y usando corrientes normalizadas se basa esencialmente en dos fenómenos diferentes:

- ✓ La corriente impuesta favorece la generación de iones OH^-, tal y como se ve en la reacción 1.2. Estos iones mantienen (en la prevención catódica) o regeneran (en la protección catódica) el pH de las EHA, equilibrando la acidificación que el CO_2 o los cloruros pueden causar [90]. Además, esta reacción favorece la eliminación del O_2 que se encuentra alrededor del acero polarizado catódicamente.
- ✓ La carga eléctrica de signo positivo que adquieren las armaduras repele a los iones cloruro y fuerza su migración hacia el ánodo externo.

Además, también se ha detectado que la polarización catódica promueve transformaciones electroquímicas y morfológicas de los óxidos de la superficie de las

armaduras incrementando sus propiedades protectoras [167,168]. Todos estos procesos son lentos y la protección catódica de las EHA aéreas puede tardar en producirse meses o años, hasta que se alcanzan los valores de potencial característicos de estructuras bien protegidas [159].

La razón de que exista un límite máximo para el valor de la corriente catódica que se puede utilizar para polarizar las armaduras es que la aplicación de una corriente eléctrica induce transformaciones físico-químicas alrededor de las armaduras. Estas transformaciones han sido monitorizadas mediante espectroscopia de impedancia electroquímica (EIS) [169]. La corriente catódica produce una acumulación de iones Na^+ y K^+ [170] en el hormigón alrededor del acero que dan lugar a una ablandamiento del gel de silicato cálcico hidratado (C-S-H). Además, puede favorecer reacciones árido-álcali en esa zona [171]. Ambos factores implican una disminución de la adherencia acero-hormigón y, consecuentemente, [172] una pérdida de propiedades mecánicas de la EHA.

García *et al.* [173] han comparado el comportamiento de la protección catódica en dos tipos de probetas de hormigón: 100% cemento Portland y otras probetas con un 85% cemento Portland y un 15% de cenizas volantes, sumergidas en una solución de NaCl al 3,5%. Los estudios han demostrado una acumulación de los iones Na^+, K^+ y H^+ en la interfase acero-hormigón, que ocasiona la pérdida de unión entre estos bajo la protección catódica. Como consecuencia de ello se observó que las propiedades mecánicas de las muestras eran más pobres a nivel de sobreprotección que de protección.

Como consecuencia de estas limitaciones, la protección catódica es una técnica relativamente compleja que requiere un mantenimiento constante y especializado no siempre disponible, por lo que puede resultar cara a largo plazo [174,175].

- **Métodos electroquímicos de realcalinización y extracción de cloruros**

Son técnicas no destructivas que se han venido desarrollando desde finales del siglo pasado [176-181] para evitar la corrosión de las barras de acero utilizadas como refuerzo. Aunque se aplican en la práctica, su eficacia y otros aspectos se pueden considerar todavía en fase de investigación.

La realcalinización se aplica a EHA carbonatadas. Externamente, y al igual que en protección catódica se sitúa un ánodo (Figura 1.12) y las armaduras se conectan a un

cátodo. A diferencia de la protección catódica, este dispositivo se sitúa sólo de forma temporal sobre la EHA. Pérez *et al.* han optado por utilizar un cemento conductivo para ser utilizado como ánodo para la extracción electroquímica de cloruro en muestras de hormigón armado, con una eficacia similar a la que se obtiene con un clásico ánodo de malla Ti-RuO_2 [182].

En la reacalinización se busca la formación de iones hidroxilo, según la reacción 1.2, para elevar el pH junto a la armadura a sus valores originales. Para ello se aplica una corriente que nunca puede superar 1 A/m^2 (unos 2 órdenes de magnitud mayores que las empleadas en protección catódica) durante un corto periodo de tiempo (4-7 días). El medio conductor externo se encuentra con disolución alcalina, como Na_2CO_3 o K_2CO_3.

La extracción de cloruros es otra técnica bastante similar que se emplea en estructuras de hormigón armado contaminadas con cloruros. También se aplican corrientes que nunca pueden superar 1 A/m^2, pero en este caso los tiempos de aplicación son mayores (4-8 semanas). Para la extracción de cloruros, el medio conductor externo con el que se fija el ánodo atrapa los iones cloro.

Estas técnicas electroquímicas no garantizan la eliminación total del contenido de Cl^- presentes en hormigones contaminados. Guimarães *et al.* indican la fuerte dependencia que existe entre el grado de saturación del hormigón y el coeficiente de difusión, debido principalmente a la porosidad total y a la distribución del tamaño del poro [183].

Para mejorar la eficiencia de estos métodos, estudios actuales tratan de introducir cambios para acelerar la extracción de cloruros [184,185]. Un aumento de la temperatura de la solución del electrolito aumenta notablemente el porcentaje de eliminación de los iones Cl^- [186].

En cualquier caso, la eficacia de los métodos depende fuertemente del grado de precorrosión de las armaduras, de manera que pueden considerarse como métodos adecuados de prevención, pero no estrictamente como métodos de rehabilitación de estructuras de hormigón dañadas [187].

1.4.2 Medidas que actúan sobre las armaduras

Entre las medidas que actúan sobre el material de las armaduras destaca, por su eficacia y creciente implantación en la práctica, el empleo de corrugados de acero inoxidable. Las principales características y limitaciones de otros métodos utilizados para tratar de controlar la corrosión de las EHA actuando sobre el hormigón se exponen a continuación.

- **Galvanización de las armaduras**

El galvanizado de las armaduras ha sido uno de los medios más empleados para tratar de evitar la corrosión de las mismas [188]. Sin embargo, se ha demostrado científicamente que en hormigones expuestos en ambientes con cloruros, el galvanizado no ofrece suficientes garantías, pues sólo es capaz de evitar la corrosión del acero durante un espacio limitado de tiempo [189-191]. La galvanización resulta un método muy eficaz de protección cuando la corrosión es debida a la carbonatación del hormigón [192], debido a su buen comportamiento a esos pHs, pero no asegura la durabilidad de las EHA frente a otros tipos de ataque.

La combinación del acero galvanizado y la adición de inhibidores en la mezcla del hormigón pueden mejorar la resistencia sobre la corrosión del acero de refuerzo [123,193]. Resultaría interesante un análisis de costes y eficacia a largo plazo, para determinar si esta combinación podría ser una alternativa eficaz (e interesante desde el punto de vista económico) para asegurar la durabilidad de las EHA.

- **Recubrimientos epoxídicos aplicados sobre las armaduras**

Sus inicios a mediados de la década de los setenta fueron muy prometedores y fueron utilizados masivamente en Estados Unidos por la "Federal Highway Administration", aunque posteriormente se ha comprobado que presentan graves deficiencias. Estas radican en la durabilidad de la propia resina en el medio alcalino y la presencia de posibles defectos en el recubrimiento desencadenan procesos de corrosión localizada [194].

Estudios microestructurales realizados a diferentes métodos de recubrimientos, han mostrado la importancia de los poros en la capa de esmalte frente a la resistencia a la

corrosión [195]. Dong *et al.* han estudiado la posibilidad de galvanizar y recubrimiento epoxi; sin embargo, una vez dañado el recubrimiento mecánicamente, pueden ocurrir graves problemas de corrosión [196]. La posibilidad de utilizar inhibidores químicos en las barras con daños en su superficie podría ser beneficioso y disminuir la velocidad de corrosión [110].

Además, es conocida la disminución de la adherencia metal/hormigón que su uso implica [197], y, en ambientes con una alta concentración de cloruros se ha demostrado que no son capaces de proteger al acero [198,199]. El "Florida Department of Transportation" ha dejado de recomendar la utilización de estos recubrimientos debido a los severos daños por corrosión detectados en puentes de su ámbito de competencias después de 10 años de servicio [200].

Todos estos motivos, junto con el relativamente elevado coste del recubrimiento epoxi de las armaduras, han hecho que está técnica no se haya arraigado demasiado en Europa y que, en la actualidad, también se esté abandonando su empleo en países de Oriente Medio y del Golfo Pérsico.

1.5 ARMADURAS DE ACERO INOXIDABLE

Los aceros inoxidables son excelentes candidatos para mejorar la durabilidad de las EHA. Se ha establecido que la característica que singulariza el acero corrugado inoxidable frente al acero al carbono es su excelente resistencia a la corrosión por cloruros. El nivel crítico de cloruros para iniciar la corrosión se establece de cinco a diez veces superior en austeníticos y dúplex respecto al acero al carbono [41,201].

Se ha demostrado que el coste global y las repercusiones ambientales de los problemas de corrosión se han convertido en un gran desafío para los ingenieros, ya que el deterioro de las EHA conduce a la adopción de medidas preventivas, de costosas reparaciones, o incluso a la demolición en pocos años. Las reparaciones convencionales de las EHA implican la eliminación del hormigón carbonatado o contaminado por cloruros, la limpieza de las armaduras en todo su perímetro, el reemplazamiento del hormigón afectado y, frecuentemente, la aplicación de algún método de protección que

evite nuevas reparaciones. El proceso es muy caro y nocivo para los trabajadores y el entorno ambiental, llegando a generar millones de dólares en pérdidas anuales.

Incluso en el más grave de los entornos, la sustitución del acero al carbono como refuerzo por aceros inoxidables austeníticos (grados S30400 y S31600) y/o dúplex (grados S32205, S32101 y S32304) [202-204] disminuye los costes de mantenimiento más de un 50% proyectándolo a 100-120 años en servicio [9,202-204].

1.5.1 Uso actual de las armaduras de inoxidable en hormigón

En la actualidad, las armaduras de acero inoxidable tienen diferentes aplicaciones. Parece ser que las únicas limitaciones para el empleo de armaduras de acero inoxidable son de tipo económico. Su precio hace que el empleo de corrugado inoxidable se recomiende exclusivamente en las zonas más críticas de las EHA, que son las que podrían estar afectadas por la corrosión, siendo el resto de acero al carbono. Para garantizar la durabilidad, en las zonas más críticas de nuevas EHA expuestas en ambientes agresivos, una cantidad de acero inoxidable comprendida entre el 5-10% del volumen total de la armadura en la estructura es suficiente [174]. Estudios previos descartan riesgos de pares galvánicos entre el acero inoxidable y carbono en el hormigón [205] y evalúan las implicaciones estructurales de la soldadura del acero inoxidable [206,207].

El uso de refuerzo de acero inoxidable eleva el precio inicial de las obras entre 5% y 15%, dependiendo en gran medida del grado de acero inoxidable seleccionado y de la estructura [208]. Medina, en su Tesis Doctoral, obtuvo resultados interesantes en el estudio comparativo de las propiedades mecánicas, económicas y comportamiento frente a corrosión por cloruros durante 20 meses de vida del acero dúplex S32001 frente al S32304 y al austenítico S30400 [209].

Además, se cuenta con la valiosa experiencia del muelle del Progreso (Figura 1.13) en Yucatán (México), construido entre 1937 y 1941. En este muelle, de hormigón masivo, hay embebidas barras de acero inoxidable S30400 para evitar problemas de agrietamientos por contracción del hormigón. Dicho hormigón es extremadamente poroso (22-25%) [210], y su comportamiento frente a la corrosión ha sido excelente durante más de 60 años [211]. Sólo recientemente ha mostrado indicios de corrosión, cuando en la

estructura han empezado a aparecer grietas de origen mecánico, debido a los sobredimensionados esfuerzos de fatiga a los que estaba sometida [212] y que han dejado al inoxidable expuesto directamente a la atmósfera.

Figura 1.13. Muelle del Progreso en México. Muelle con barras de inoxidable al fondo y restos del muelle con barras de acero al carbono (construido tres décadas después) en primer plano.

Se pueden considerar que las principales aplicaciones actuales de las armaduras de acero inoxidable son:

- ✓ Las armaduras situadas en la zona de mareas o de salpicaduras en EHA parcialmente sumergidas en ambiente marino, donde el riesgo de corrosión es elevado.
- ✓ En las zonas más externas de los puentes (debido a los cloruros de las sales vertidas en el caso de heladas o del agua de mar en el caso de las construcciones costeras). Esta estrategia permite una disminución de las inspecciones y de las operaciones de mantenimiento, y se elimina la necesidad de cortar el tráfico para las reparaciones [53,204].
- ✓ Para la fabricación de EHA que han de tener un espesor de recubrimiento de hormigón pequeño.

- ✓ En la reparación de EHA dañadas por corrosión [213] en las que no se permite aumentar el espesor inicial del recubrimiento.

- ✓ En elementos situados a gran altura, como por ejemplo, cúpulas de edificios singulares, donde evitar gastos de inspección y mantenimiento supone un gran ahorro. Un ejemplo son las cúpulas de la Sagrada Familia de Barcelona.

- ✓ En elementos especialmente sensibles para la seguridad [214] y expuestos, como los voladizos y balcones de edificios situados en ambientes marinos frente a la costa y en estructuras para piscinas cubiertas. Por ejemplo, en Alemania, Dinamarca o Finlandia, el empleo de armaduras de acero inoxidable es obligatorio en balcones y piscinas, a fin de evitar los problemas de seguridad que acarrearía la corrosión de los refuerzos [214].

En los últimos 20-30 años, en Europa, Norte América, Australia y Oriente Medio, un gran número de EHA se han construido o reparado utilizando armaduras de acero inoxidable [215]. Algunos ejemplos de EHA donde se han utilizado estos materiales más recientemente son:

- Acero inoxidable dúplex S32205:
  - ✓ Puente de Sitra (Bahrain)
  - ✓ Puente sobre el río Colorado (Montana, EE.UU.)
  - ✓ Puente Eiffel (Portugal)
- Acero inoxidable austenítico S31653 y dúplex S32205:
  - ✓ Puente Driscoll, sobre el río Raritan (New Jersey, EE.UU.)
  - ✓ Puente Woodrow Wilson, sobre el río Potomac (EE.UU.)
- Acero inoxidable austenítico S30400 y dúplex S32205:
  - ✓ Museo de Arte Moderno (Vitoria, España)
- Acero inoxidable dúplex S32304:
  - ✓ Puente Hastings en la TH 61 (Minnesota, EE.UU.)
  - ✓ Puente Hong Kong-Macao (China, en construcción)
- Acero inoxidable dúplex S32001:
  - ✓ AVE Palencia-León (España)
  - ✓ Puente Gateway (Brisbane, Australia)

1.5.2 Influencia de la composición de los inoxidables en su comportamiento frente a la corrosión en hormigón

Se ha investigado la influencia de la composición del acero inoxidable base en el comportamiento frente a la corrosión de EHA, especialmente sobre aceros austeníticos tradicionales tipo S30400 y S31600. En general, los estudios concluyeron que no hay diferencias significativas entre la resistencia a la corrosión por picaduras de ambos materiales en este medio [9,208,216-219]. Hay autores, sin embargo, que detectan un comportamiento ligeramente mejor en el S31603 debido a las adiciones de Mo [208,220,221]. Estas diferencias pueden explicarse considerándose el tipo de ensayos realizados para evaluar la resistencia a la corrosión y su diferente agresividad, pero también la falta de uniformidad en el estado del material evaluado.

La bibliografía encontrada sobre el comportamiento de inoxidables ferríticos se encuentra limitada, en gran medida, por los agresivos métodos definidos en los años 70, que llevaban a resultados negativos de resistencia en hormigón [208,222]. Sin embargo, existen datos posteriores sobre el comportamiento de estos aceros con bajo contenido en Cr (tipo S40900), que demuestran que su comportamiento es significativamente mejor que el del acero al carbono, y lo proponen como la mejor opción para ambientes de agresividad moderada [223]. Producto, quizás, de estos resultados fue la fabricación de armaduras con este material en Alemania y Sudáfrica a lo largo de la década de los 90.

Además, durante la primera década del presente siglo, hubo un gran interés en la caracterización y comercialización de aceros inoxidables austeníticos de bajo contenido en Ni y alto contenido en Mn. Se han publicado estudios de austeníticos de baja aleación en medios alcalinos que simulan la disolución contenida dentro de los poros del hormigón y se han estudiado los cambios ocurridos en las capas de pasivas con el pH [224] y la resistencia a la corrosión en presencia de cloruros [225,226]. Su comportamiento frente a la corrosión en hormigón ha demostrado ser solo ligeramente inferior al del tradicional AISI 304 [10,227-229].

También a principios del siglo XXI se empezaron a fabricar corrugados dúplex tipo S32205. Estos aceros ofrecían la gran ventaja de tener un menor contenido en Ni que los austeníticos tradicionales, a un precio que podía ser algo inferior. Dependiendo de las condiciones y las técnicas empleadas en el estudio, se han obtenido resultados que

sugieren que los aceros inoxidables dúplex ofrecen una excelente resistencia frente a la corrosión comparable o incluso superior a la de los aceros austeníticos S30400 y S31600 [10,53,84,202,203,208,215,230-233]. Esto ha hecho que, en la práctica, el uso a gran escala de las armaduras de acero inoxidable dúplex S32205 se haya introducido en el mercado en los últimos años.

Actualmente existe un gran interés en el desarrollo y caracterización de aceros inoxidables dúplex de baja aleación (bajo contenido en Ni o en Mo, generalmente). Aceros como el S32304 (dúplex de bajo contenido en Mo) se conocen desde hace años, pero su uso en aplicaciones de hormigón armado es muy novedoso. Además otro producto de muy reciente comercialización es el S32001, acero inoxidable dúplex de menor grado de aleación que el S32304, por lo que, el menor contenido en Ni y Cr reduce su coste.

1.5.3 Propiedades mecánicas

Un problema que planteó en un principio el empleo de armaduras de acero inoxidable fue que las barras corrugadas debían cumplir con los requisitos mecánicos que ofrece el acero al carbono en términos de límite elástico, módulo de elasticidad y ductilidad, para poder sustituirlo como material estructural [213]. Las armaduras de acero inoxidable presentan importantes diferencias respecto a las elaboradas con acero al carbono: su microestructura, su composición química, y al tratamiento de laminado aplicado a cada uno de ellos. Los aceros inoxidables poseen una menor dureza, lo que hace indispensable un tratamiento que, aunque encarece el material, le otorga las propiedades mecánicas adecuadas.

Actualmente es posible encontrar en el mercado europeo barras de acero corrugadas que se utilizan como refuerzo en hormigón endurecidos por conformado en frío (CW), así como endurecidos por conformado en caliente (HW). En general, la dureza media de las barras de inoxidable corrugado depende de cómo se haya llevado a cabo su conformado. Algunos autores han publicado que las barras CW tienen una dureza media algo mayor que las HW [221,234]. Además, el proceso de corrugado supone un endurecimiento de la superficie de las barras. La profundidad de la región endurecida es

de 1-2 mm [221,235], mucho más marcado en las barras CW donde la dureza aumenta linealmente con la deformación en frío [234].

En el estudio sobre la influencia del procesado en el comportamiento mecánico de las barras corrugadas de acero inoxidable es importante conocer diversos factores. El procesado implica cambios microestructurales, variaciones del tamaño de grano y/o formación de martensita en su microestructura, que modifican el comportamiento mecánico de los aceros inoxidables [16,22,24,25,31-33,234].

Las armaduras de acero inoxidable CW presentan valores de límite elástico hasta un 50% superior a los valores de las armaduras equivalentes de acero al carbono, y valores de resistencia máxima un 14% superior. Sin embargo, la deformación máxima alcanzada por las barras de acero inoxidable, 6,31% de media, es inferior a la obtenida por las barras de acero al carbono.

Las barras corrugadas de acero inoxidable, HW y CW, tienen un módulo de elasticidad inferior que las de acero al carbono. El menor valor del módulo de elasticidad contrarresta la ventaja que supone para las armaduras de acero inoxidable el poder relajar las medidas de durabilidad del hormigón, como son la disminución (entre 10 y 15 mm) de los espesores del recubrimiento necesario y el aumento (en 0,1 mm) de la abertura característica de fisura máxima permitida, de forma que no se produce ahorro en la cuantía de armado de los elementos estructurales cuando se tiene en cuenta en los cálculos [209].

Los corrugados de acero inoxidable austenítico con una resistencia a tracción similar al acero al carbono muestran, a la vez, mejor ductilidad y tenacidad que éste [221, 236]. El acero inoxidable dúplex, por su parte, presenta mejores resistencias a tracción que los austeníticos y aceros al carbono, conservando al mismo tiempo una tenacidad similar a la del acero al carbono [236,237]. El CW aumenta la resistencia a tracción y el límite elástico y disminuye la tenacidad con respecto al HW de un mismo tipo de inoxidable [221].

E. Medina ha estudiado las características mecánicas y el comportamiento estructural de las barras corrugadas de los aceros inoxidables austenítico S30400, dúplex S32304 y dúplex de bajo contenido en níquel S32001, y su comparación con las del acero al carbono B-500-SD [209]. Sus estudios han demostrado que las armaduras de acero

inoxidable HW tienen el límite elástico y la resistencia a rotura similares a las armaduras de acero al carbono. Sin embargo, alcanzan valores de deformación máxima que llegan a duplicar los valores de las armaduras de acero al carbono, lo que se traduce en que presentan una ductilidad muy superior.

Otra variable que influye en el comportamiento a fatiga de los corrugados inoxidables es la presencia de precipitados de TiN en aquellos grados que llevan Ti en su composición (S31635, S32304 o S32205, por ejemplo). Los TiN presentes en zonas superficiales actúan como concentradores de tensiones [236]. En cualquier caso, el comportamiento a fatiga de los corrugados inoxidables HW, en ausencia de defectos o precipitados de TiN en su superficie, es similar al del acero al carbono [236]. Además, la presencia de marcas superficiales o defectos del conformado producidos por las herramientas que imprimen las corrugas tiene una mala influencia en la resistencia a fatiga [236].

1.5.4 Influencia de las soldaduras en el comportamiento de las armaduras

El empleo de soldaduras no es una práctica habitual en la construcción de nuevas EHA. Sin embargo, sí se emplea en rehabilitación o sustitución, reemplazando trozos de armaduras dañadas por la corrosión por otros nuevos, siendo esta la única opción en este tipo de reparaciones. La unión entre un acero inoxidable dúplex y un acero al carbono debe llevarse a cabo utilizando un corto período de tiempo de soldadura, evitando que se produzca una descarburación del acero al carbono y así disminuir los riesgos de fractura por fatiga cíclica [238].

La presencia de soldaduras ha demostrado ser capaz de disminuir de forma muy pronunciada la resistencia a la corrosión de los aceros inoxidables. En medios con alta concentración de cloruros tienden a aparecer pequeñas picaduras aisladas [208], lo cual se ve favorecido, además de por una alta concentración de iones, por la carbonatación del hormigón. La influencia del procedimiento de soldadura en el aumento de la susceptibilidad a la corrosión se ha demostrado ser mucho más débil que la del estado superficial de acero inoxidable [239].

Se ha demostrado que esa disminución de la resistencia a la corrosión se debe a la formación de películas de óxidos (llamadas "*heat tints*"), debido a las altas temperaturas que implica el proceso de soldadura. Se ha culpado del efecto adverso de las "*heat tints*" a la formación de una capa empobrecida en Cr justo bajo los óxidos de soldadura [240,241]. Otras posibles causas sugeridas para explicar el efecto de la soldadura en el comportamiento frente a la corrosión son la composición química de los óxidos de soldadura [242-245], su estructura [246] o las tensiones y defectos reticulares en la película de óxido y substrato metálico que supone su formación [247].

Se ha sugerido que la probabilidad de fallo por corrosión en las soldaduras de las armaduras de acero inoxidable podría reducirse mediante un tratamiento superficial de granallado o una limpieza química [174,208].

Las características microestructurales específicas en la zona de soldadura y la variación en las propiedades mecánicas que ésta ocasiona, dan lugar a una disminución de la resistencia a la tracción y la fatiga en la zona de la unión [248]. Sin embargo, se ha estimado que esta variación de las propiedades mecánicas no es significativa ni es capaz de comprometer los requisitos mecánicos exigidos a las EHA [207]. Kumar *et al*. analizaron el efecto generado al disminuir la temperatura durante el proceso, y obtuvieron buena resistencia a la tracción y ductilidad [249]. Obviamente esto último es cierto, siempre que el proceso de soldadura se lleve a cabo de forma adecuada y se evite la aparición de una o varias discontinuidades producidas durante el proceso, grietas, cambios en el tamaño de grano y posibles inclusiones que actúan como concentradores de esfuerzos, disminuyendo la resistencia de la unión [250].

1.6 INFLUENCIA DE UN MEDIO ÁCIDO EN EL ACERO INOXIDABLE

La selección de un acero inoxidable para el servicio en medios corrosivos, requiere la consideración del tipo de corrosión que puede presentar. En medio ácido, la corrosión de los aceros inoxidables se desarrolla a través de un mecanismo muy diferente que a otros pHs. A bajos pHs puede ocurrir un ataque más generalizado en lugar de una corrosión localizada típica de los inoxidables en otros medios.

La resistencia de los diferentes aceros inoxidables a la corrosión generalizada en medio ácido varía según las composiciones de los grados y según el ambiente agresivo. Sin embargo, también es necesario conocer a profundidad cómo el procesado y los cambios microestructurales pueden afectar su durabilidad. Por ejemplo, la presencia de níquel y cobre en algunos grados austeníticos mejora en gran medida la resistencia frente al H_2SO_4 en comparación con la resistencia de los ferríticos.

La resistencia del acero inoxidable a los ácidos depende de la concentración del ion H^+ y la capacidad de oxidación del ácido, junto con el contenido de cromo, níquel y carbono y el tratamiento térmico del acero.

Un acero inoxidable recocido resiste muy bien el HNO_3 a pesar del bajo pH del ácido, ya que el HNO_3 es altamente oxidante y forma una película pasiva debido al contenido de cromo de la aleación. Los inoxidables tienden a corroerse fácilmente en HCl, ya que no se forma fácilmente una película pasiva estable en presencia de iones fuertemente depasivantes como los cloruros [251].

El comportamiento del acero inoxidable en un ácido diluido es complejo y es bien sabido que la transición activa a pasiva puede ser muy sensible a pequeños cambios en la composición de la aleación [252].

A pHs bajos, la microestructura también puede condicionar el desarrollo del ataque. La disminución en la resistencia a la corrosión de los aceros inoxidables austeníticos en medio ácido con cloruros tras laminación en frío se ha relacionado con los cambios en la microestructura. Estos pueden ser no sólo la formación de martensita, sino también la morfología de grano o la textura cristalográfica, ya que no es posible evaluar la contribución de cada factor microestructural para el comportamiento de la corrosión [253]. Otros autores han encontrado una relación entre el aumento en la velocidad de corrosión en soluciones ácidas de NaCl y la fracción de martensita en la microestructura de acero inoxidable austenítico [254].

Las curvas de polarización anódicas en medios ácidos son un método útil para el estudio de la resistencia a la corrosión de los aceros inoxidables y su transición activa a pasiva. Tradicionalmente, las curvas anódicas en diferentes soluciones de H_2SO_4 se han utilizado para evaluar el grado de sensibilización de acero inoxidable austenítico después de un tratamiento térmico [255,256] o de otros procedimientos de fabricación [257]. La

solución de prueba típica consiste en una mezcla de 0,5 M H_2SO_4 y 0,01 M KSCN [258], extendiéndose hoy en día su aplicación a otros tipos de aceros inoxidables o aleaciones base níquel [256,258]. Además, se han sugerido algunas optimizaciones del método estándar para el acero austenítico [259], y se ha propuesto un método modificado de la polarización en solución 1 M HCl [260] para estudiar el efecto de los tratamientos térmicos en aceros inoxidables dúplex.

Una disolución de H_2SO_4 y HCl se ha aplicado anteriormente como medio de prueba para estudiar el comportamiento de la corrosión de nuevos aceros inoxidables super-dúplex altamente aleados [261]. En estos casos, en las curvas de polarización, sólo aparece un pico de activación en la zona de corrosión activa, antes de la pasivación anódica de los materiales.

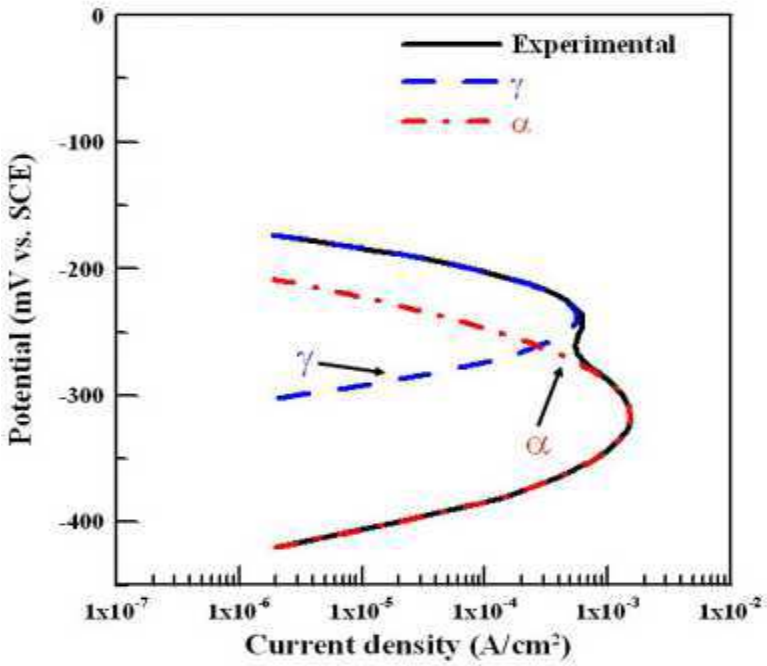

Figura 1.14. Picos de activación en una curva de polarización [21].

Sin embargo, para el grado dúplex tradicional tipo S32205 en la disolución mixta de H_2SO_4 + HCl, se han encontrado dos picos de activación [20,262], como se ve en la Figura 1.14. Cada fase en un acero inoxidable dúplex (austenita o ferrita) alcanza su máxima velocidad de corrosión a un potencial electroquímico diferente de la otra, lo que puede facilitar la aparición de la corrosión galvánica entre las fases del S32205 [21].

1.7 BIBLIOGRAFÍA

[1] G. Di Caprio, "*Los aceros inoxidables",* 2ª edición GRUPINOX, Barcelona, España (1999).

[2] www.worldstainless.org. Mayo 2013.

[3] UNE-EN 10088-1, "*Aceros inoxidables. Parte I: Relacion de aceros inoxidables*", AENOR (2006).

[4] N.M. Piris, "*Ciencia de materiales para ingenieros",* 1ª edición, Pearson Educación S.A., Madrid, España (2012).

[5] J.F. Shackelford, "*Introducción a la ciencia de materiales para ingenieros",* 7ª edición, Pearson Educación S.A., Madrid, España (2010).

[6] W.F. Smith, "*Fundamentos de la ciencia e ingeniería de materiales",* 3ª edición, Mc Graw Hill S.A., Madrid, España (1998).

[7] G. Krauss, "*Steels, heat treatment and processing principles",* ASM International, (1995).

[8] M. Romero, V. Matres, *"Comparative evaluation on uniform corrosion resistance behavior of ferritic stainless steels: Experimental studies of electrochemical test"*, in: 7th European Stainless Steel Conference: Science and Market, Paper Nº 5, Como, Italia (2011).

[9] M. Kouřil, P. Novák, M. Bojko, *"Threshold chloride concentration for stainless steels activation in concrete pore solutions"*, Cement and Concrete Research, 40, pp. 431-436 (2010).

[10] M. Serdar, L.V. Žulj, D. Bjegović, *"Long-term corrosion behaviour of stainless reinforcing steel in mortar exposed to chloride environment"*, Corrosion Science, 69, pp. 149-157 (2013).

[11] M. Martins, L.C. Casteletti, *"Microstructural characteristics and corrosion behavior of a super duplex stainless steel casting"*, Materials Characterization, 60, pp. 150-155 (2009).

[12] L. Zhang, W. Zhang, Y. Jiang, B. Deng, D. Sun, J. Li, "*Influence of annealing treatment on the corrosion resistance of lean duplex stainless steel 2101"*, Electrochimica Acta, 54, pp. 5387-5392 (2009).

[13] J. Li, Z. Ma, X. Xiao, J. Zhao, L. Jiang, *"On the behavior of nitrogen in a low-Ni high-Mn super duplex stainless steel"*, Materials and Design, 32, pp. 2199-2205 (2011).

[14] N. Ebrahimi, M.H. Moayed, A. Davoodi, *"Critical pitting temperature dependence of 2205 duplex stainless steel on dichromate ion concentration in chloride medium"*, Corrosion Science, 53, pp. 1278-1287 (2011).

[15] L.F. Garfias-Mesias, J.M. Sykes, C.D.S. Tuck, *"The effect of phase compositions on the pitting corrosion of 25 Cr duplex stainless steel in chloride solutions",* Corrosion Science, 38, pp. 1319-1330 (1996).

[16] L. Zhang, Y. Jiang, B. Deng, W. Zhang, J. Xu, J. Li, *"Effect of aging on the corrosion resistance of 2101 lean duplex stainless steel",* Materials Characterization, 60, pp. 1522-1528 (2009).

[17] V.M. Linton, N.J. Laycock, S.J. Thomsen, A. Klumpers, *"Failure of a super duplex stainless steel reaction vessel"*, Engineering Failure Analysis, 11, pp. 243-256 (2004).

[18] T.J. Mesquita, E. Chauveau, M. Mantel, *"Study of molybdenum effect on pitting corrosion of stainless steel concrete reinforcements"*, in: 7th European Stainless Steel Conference: Science and Market, Paper No. 47, Como, Italia (2011).

[19] K.H. Lo, C.H. Shek, J.K.L. Lai, *"Recent developments in stainless steels",* Materials Science and Engineering R: Reports, 65, pp. 39-104 (2009).

[20] I.H. Lo, Y. Fu, C.-J. Lin, W.-T. Tsai, *"Effect of electrolyte composition on the active-to-passive transition behavior of 2205 duplex stainless steel in H_2SO_4/HCl solutions",* Corrosion Science, 48, pp. 696-708 (2006).

[21] W.-T. Tsai, J.-R. Chen, *"Galvanic corrosion between the constituent phases in duplex stainless steel",* Corrosion Science, 49, pp. 3659-3668 (2007).

[22] A. Di Schino, J.M. Kenny, I. Salvatori, G. Abbruzzese, *"Modelling primary recrystallization and grain growth in a low nickel austenitic stainless steel",* Journal of Materials Science, 36, pp. 593-601 (2001).

[23] L. Peguet, B. Malki, B. Baroux, *"Effect of austenite stability on the pitting corrosion resistance of cold worked stainless steels",* Corrosion Science, 51, pp. 493-498 (2009).

[24] L. Peguet, B. Malki, B. Baroux, *"Influence of cold working on the pitting corrosion resistance of stainless steels",* Corrosion Science, 49, pp. 1933-1948 (2007).

[25] A. Di Schino, M. Barteri, J.M. Kenny, "*Effects of grain size on the properties of a low nickel austenitic stainless steel",* Journal of Materials Science, 38, pp. 4725-4733 (2003).

[26] A. Di Schino, J.M. Kenny, *"Effect of grain size on the corrosion resistance of a high nitrogen-low nickel austenitic stainless steel",* Journal of Materials Science Letters, 21, pp. 1969-1971 (2002).

[27] A. Di Schino, J.M. Kenny, M. Barteri, *"High temperature resistance of a high nitrogen and low nickel austenitic stainless steel"*, Journal of Materials Science Letters, 22, pp. 619-693 (2003).

[28] A. Di Schino, J.M. Kenny, M.G. Mecozzi, M. Barteri, *"Development of high nitrogen, low nickel, 18% Cr austenitic stainless steels"*, Journal of Materials Science, 35, pp. 4803-4808 (2000).

[29] M. Sibanda, S.L. Vismer, R.D. Knutsen, *"Consideration of reduced nickel containing austenitic stainless steels for forming applications"*, Materials Letters, 21, pp. 203-207 (1994).

[30] S.S.M. Tavares, J.M. Pardal, M.J. Gomes da Silva, H.F.G. Abreu, M.R. da Silva, "*Deformation induced martensitic transformation in a 201 modified austenitic stainless steel"*, Materials Characterization, 60, pp. 907-911 (2009).

[31] A. Kanni Raj, K.A. Padmanabhan, "*Tensile properties and formability of low Ni (1.2 mass% Ni) metastable austenitic stainless steel sheets"*, Materials Transactions, 39, pp. 613-616 (1998).

[32] A. Kanni Raj, K.A. Padmanabhan, "*Room-temperature plastic flow and strain-induced martensitic transformation in 1.2 wt.% Ni metastable austenitic stainless steel sheets"*, Journal of Materials Science Letters, 16, pp. 1920-1924 (1997).

[33] M. Mililitsky, N. De Wispelaere, R. Petrov, J.E. Ramos, A. Reguly, H. Hänninen, "*Characterization of the mechanical properties of low-nickel austenitic stainless steels"*, Materials Science and Engineering. A, 498, pp. 289-295 (2008).

[34] F.J. Pérez, M.J. Cristóbal, G. Arnau, M.P. Hierro, J.J. Saura, *"High-temperature oxidation studies of low-nickel austenitic stainless steel. Part I: Isothermal oxidation"*, Oxidation of Metals, 55, pp. 105-118 (2001).

[35] F.J. Pérez, M.J. Cristóbal, M.P. Hierro, *"High-temperature oxidation studies of low-nickel austenitic stainless steel. Part II: Cyclic oxidation",* Oxidation of Metals, 55, pp. 165-175 (2001).

[36] J. Botella, C. Merino, E. Otero, *"A comparison of the high-temperature oxidation of 17Cr-2Ni and 18Cr-8Ni austenitic stainless steels at 973 K"*, Oxidation of Metals, 49, pp. 297-324 (1998).

[37] T. Sourisseau, E. Chauveau, B. Baroux, *"Mechanism of copper action on pitting phenomena observed on stainless steels in chloride media"*, Corrosion Science, 47, pp. 1097-1117 (2005).

[38] C.-J. Park, H.-S. Kwon, *"Effects of aging at 475 °C on corrosion properties of tungsten-containing duplex stainless steels"*, Corrosion Science, 44, pp. 2817-2830 (2002).

[39] B. Deng, Y. Jiang, J. Gong, C. Zhong, J. Gao, J. Li, *"Critical pitting and repassivation temperatures for duplex stainless steel in chloride solutions"*, Electrochimica Acta, 53, pp. 5220-5225 (2008).

[40] A. Igual Muñoz, J. García Antón, J.L. Guiñón, V. Pérez Herranz, *"Inhibition effect of chromate on the passivation and pitting corrosion of a duplex stainless steel in LiBr solutions using electrochemical techniques"*, Corrosion Science, 49, pp. 3200-3225 (2007).

[41] A. Igual Muñoz, J. García Antón, J.L. Guiñón, V. Pérez Herranz, *"The effect of chromate in the corrosion behavior of duplex stainless steel in LiBr solutions"*, Corrosion Science, 48, pp. 4127-4151 (2006).

[42] A.M. do Nascimento, M.C.F. Ierardi, A.Y. Kina, S.S.M. Tavares, *"Pitting corrosion resistance of cast duplex stainless steels in 3.5% NaCl solution"*, Materials Characterization, 59, pp. 1736-1740 (2008).

[43] V.S. Moura, L.D. Lima, J.M. Pardal, A.Y. Kina, R.R.A. Corte, S.S.M. Tavares, *"Influence of microstructure on the corrosion resistance of the duplex stainless steel UNS S31803"*, Materials Characterization, 59, pp. 1127-1132 (2008).

[44] V. Muthupandi, P. Bala Srinivasan, S.K. Seshadri, S. Sundaresan, *"Effect of weld metal chemistry and heat input on the structure and properties of duplex stainless steel welds"*, Materials Science and Engineering: A, 358, pp. 9-16 (2003).

[45] S.A. Távara, M.D. Chapetti, J.L. Otegui, C. Manfredi, *"Influence of nickel on the susceptibility to corrosion fatigue of duplex stainless steel welds"*, International Journal of Fatigue, 23, pp. 619-626 (2001).

[46] I.-U.-H. Toor, P.J. Hyun, H.S. Kwon, *"Development of high Mn–N duplex stainless steel for automobile structural components"*, Corrosion Science, 50, pp. 404-410 (2008).

[47] T. Laitinen, L. Wegrelius, A. Bergquist, *"Mill exposure test of duplex stainless steel LDX 2101 in recycled fiber applications"*, in: 6th Stainless Steel Conference, Helsinki, Finlandia (2008).

[48] H. Liu, P. Johansson, M. Lijias, *"Structural evolution of LDX 2101 1.41162 during isothermal ageing at 600-850 ºC"*, in: 6th Stainless Steel Conference Helsinki, Finlandia (2008).

[49] I. Calliari, J. Dobransky, E. Ramous, G. Straffelini, G. Rebuffi, *"Investigation on low Ni duplex stainless steel grades"*, in: 6th Stainless Steel Conference, Helsinki, Finlandia (2008).

[50] C. Fosca, J. Sakima, *"Detection of the 475 ºC embrittlement in a lean duplex stainless steel using a electrochemical potentiodynamic reactivation (EPR) test"*, in: 6th Stainless Steel Conference, Helsinki, Finlandia (2008).

[51] S. Aribo, R. Barker, X. Hu, A. Neville, *"Erosion-corrosion behavior of lean duplex stainless steels in 3.5% NaCl solution"*, Wear, 302, pp. 1602-1608 (2013).

[52] E.M. Westin, C.-O.A. Olsson, S. Hertzman, *"Weld oxide formation on lean duplex stainless steel"*, Corrosion Science, 50, pp. 2620-2634 (2008).

[53] E. Medina, A. Cobo, D.M. Bastidas, *"Evaluación del comportamiento estructural y de resistencia a la corrosión de armaduras de acero inoxidable austenítico AISI 304 y dúplex AISI 2304 embebidas en morteros de cemento Portland"*, Revista de Metalurgia, 48, pp. 445-458 (2012).

[54] R. Sánchez, J. Botella, V. Matres, I. Fernandez de Castillo, J. Fullea, J.L. Enríquez, L. Coco, *"Avances en ciencia y tecnología del acero inoxidable"*, J.A. Odiozola, J. Botella, C. Merino, Vol., II CICIC, Sevilla, España (2003).

[55] J. Peutier, E. Chaveau, S. Jacques, M. Mantel, *"A new lean duplex stainless steel with high mechanical and corrosion properties: 1.4062"*, in: 6th Stainless Steel Conference, Helsinki, Finlandia (2008).

[56] A. Burkert, J. Lehemann, A. Burkert, J. Mietz, P. Gümple, *"Technical and economical stainless steel alternatives for civil engineering applications"*, Materials and Corrosion, 64 (DOI:10.1002/201307057) (2013).

[57] G. Gedge, *"Structural uses of stainless steel-buildings and civil engineering"*, Journal of Constructional Steel Research, 64, pp.1194-1198 (2008).

[58] M. Theofanous, L. Gardner, *"Testing and numerical modeling of lean duplex stainless steel hollow section columns"*, Engineering Structures, 31, pp. 3047-3058 (2009).

[59] L. Gardner, N.R. Baddoo, *"Fire testing and design of stainless steel structures"*, Journal of Constructional Steel Research, 62, pp. 532-543 (2006).

[60] L. Gardner, A. Talja, N.R. Baddoo, *"Structural design of high-strength austenitic stainless steel"*, Thin-Walled Structures, 44, pp. 517-528 (2006).

[61] E.C.-Y. To, B. Young, *"Performance of cold-formed stainless steel tubular columns at elevated temperatures"*, Engineering Structures, 30, pp. 2012-2021 (2008).

[62] I. Payá-Zaforteza, M.E.M. Garlock, *"A numerical investigation on the fire response of a steel girder bridge"*, Journal of Constructional Steel Research, 75, pp. 93-103 (2012).

[63] N.D. Kankanamge, M. Mahendran, *"Mechanical properties of cold-formed steels at elevated temperatures"*, Thin-Walled Structures, 49, pp. 26-44 (2011).

[64] L. Gardner, A. Insausti, K.T. Ng, M. Ashraf, *"Elevated temperature material properties of stainless steel alloys"*, Journal of Constructional Steel Research, 66, pp. 634-647 (2010).

[65] N. Saliba, L. Gardner, *"Cross-section stability of lean duplex stainless steel welded I-sections"*, Journal of Constructional Steel Research, 80, pp. 1-14 (2013).

[66] M.F. Hassanein, *" Numerical modeling of concrete-filled lean duplex slender stainless steel tubular stub columns*", Journal of Constructional Steel Research, 66, pp. 1057-1068 (2010).

[67] M. Longshithung Patton, K. D. Singh, *"Numerical modeling of lean duplex stainless steel hollow columns of square, L-, T-, and + -shaped cross sections under pure axial compression"*, Thin-Walled Structures, 53, pp.1-8 (2012).

[68] H. Sieurin, R. Sandstrom, E. M. Westin, *"Fracture toughness of lean duplex stainless steel LDX 2101"*, Metallurgical and Materials Transactions A, 37, pp. 2975-2981 (2006).

[69] J. Xu, T. Sun, L. Zhang, J. Li, Y. Jiang, *"Potentiostatic electrochemical noise analysis of 2101 lean duplex stainless steel in 1 mol/L NaCl"*, Journal of Materials Science and Technology, 28, pp. 474-480 (2012).

[70] Z. Wei, J. Laizhu, H. Jincheng, S. Hongmei, *"Study of mechanical and corrosion properties of a Fe-21.4Cr-6Mn-1.5Ni-0.24N-0.6Mo duplex stainless steel"*, Materials Science and Engineering A, 497, pp. 501-504 (2008).

[71] J. Gao, Y. Jiang, B. Deng, W. Zhang, C. Zhong, J. Li, *"Investigation of selective corrosion resistance of aged lean duplex stainless steel 2101 by non-destructive electrochemical techniques"*, Electrochimica Acta, 54, pp. 5830-5835 (2009).

[72] Y.Z. Yang, Y.M. Jiang, J. Li, *"In situ investigation of crevice corrosion on UNS S32101 duplex stainless steel in sodium chloride solution"*, Corrosion Science, 76, pp. 163-169 (2013).

[73] Y. Liu, H. Yan, X. Wang, M. Yan, *"Effect of hot deformation mode on the microstructure evolution of lean duplex stainless steel 2101"*, Materials Science and Engineering A, 575, pp. 41-47 (2013).

[74] J. Linder, A. Melander, *"Fatigue strength of spot welded stainless sheet steels exposed to 3% NaCl solution"*, International Journal of Fatigue, 20, pp. 383-388 (1998).

[75] J. Johansson, M. Odén, *"Load sharing between austenite and ferrite in a duplex stainless steel during cyclic loading"*, Metallurgical and Materials Transactions A, 31, pp. 1557-1570 (2000).

[76] J.L. Song, P.L. Blackwell, *"Superplastic behavior of commercial duplex stainless steel SAF 2304"*, Materials Science and Technology, 15, pp. 1285-1292 (1999).

[77] J. Johansson, M. Odén, X.H. Zeng, *"Evolution of the residual stress state in a duplex stainless steel during loading"*, Acta Materialia, 47, pp. 2669-2684 (1999).

[78] J.L. Song, P.S. Bate, *"Plastic anisotropy in superplastic duplex stainless steel"*, Acta Materialia, 45, pp. 2747-2757 (1997).

[79] S. Beretta, M. Boniardi, *"Microstucture and fatigue properties of a welded duplex stainless steel"*, Fatigue and Fracture of Engineering Materials and Structures, 19, pp. 647-654 (1996).

[80] J. Mietz, J. Rueckert, B. Isecke, *"Electrochemical investigations on austenitic and duplex stainless steels for use as ground anchor materials"*, Materials Science Forum, 247, pp. 25-36 (1997).

[81] D. Han, Y. Jiang, C. Shi, Z. Li, J. Li, *"Influence of the microstructure and alloying element on the polarization behavior within the crevice of UNS S32304 duplex stainless steel"*, Corrosion Science, 53, pp. 3796-3804 (2011).

[82] P.E. Hazlewood, P.M. Singh, J.S. Hsieh, *"Effect of black liquor oxidation on the stress corrosion cracking"*, Corrosion, 62, pp. 765-772 (2006).

[83] Z. Zhang, D. Han, Y. Jiang, C. Shi, J. Li, *"Microstructural evolution and pitting resistance of annealed lean duplex stainless steel UNS S32304"*, Nuclear Engineering and Design, 243, pp. 56-62 (2012).

[84] R. Merello, F.J. Botana, J. Botella, M.V. Matres, M. Marcos, *"Influence of chemical composition on the pitting corrosion resistance of non-standard low-Ni high-Mn–N duplex stainless steels"*, Corrosion Science, 45, pp. 909-921 (2003).

[85] E. Chaveau, B. Demelin, T. Sourisseau, *"New lean duplex stainless steel rebar: Pitting corrosion resistance and galvanic coupling behavior"*, in: 6th Stainless Steel Conference, Helsinki, Finlandia (2008).

[86] E.F. Irassar, *"Ataque químico al hormigón"*, AATH - Durabilidad del hormigón estructural, (2001).

[87] L. Bertolini, B. Elsener, P. Pedeferri, R. Polder, "*Corrosion of steel in concrete: prevention, diagnosis, repair*", Wiley-VCH, Weinheim (2004).

[88] P. Garcés, M.A. Climent, E.Z. Gómez, "*Corrosión de armaduras en estructuras de hormigón armado*", Club Universitario, Alicante (2008).

[89] J. Sánchez, J. Fullea, C. Andrade, J.J. Gaitero, A. Porro, *"AFM study of the early corrosion of a high strength steel in a diluted sodium chloride solution"*, Corrosion Science, 50, pp. 1820-1824 (2008).

[90] J.A. González, E. Otero, S. Feliú, A. Bautista, E. Ramírez, E. Rodríguez, W. López, *"Some considerations on the effect of chloride ion on the corrosion of steel reinforcements embedded in concrete structures"*, Magazine of Concrete Research, 50, pp. 189-199 (1998).

[91] K. Tuutti, *"Corrosion of steel in concrete",* Swedish Foundation for Concrete Research Institute, ed. 82-84, Estocolmo, Suecia (1982).

[92] C.L. Page, P. Lambert, P.R.W. Vassie, *"Investigation of reinforcement corrosion: 1. The pore electrolyte phase in chloride-contaminated concrete"*, Materials and Structures, 24, pp. 243-252 (1991).

[93] P. Lambert, C.L. Page, P.R.W. Vassie, *"Investigation of reinforcement corrosion: 2. Electrochemical monitoring of steel in chloride-contaminate concrete"*, Materials and Structures, 24, pp. 351-358 (1991).

[94] C. Andrade, J. González, "*Vida útil de las estructuras de hormigón armado: obras nuevas y deterioradas",* Curso de Estudios Mayores de la Construcción, CEMCO-95, Seminario reparación de estructuras de hormigón dañadas por corrosión, Instituto Eduardo Torroja, (1995).

[95] D.A. Haussmann, *"Steel corrosión in concrete: How does it occur?"*, Material Protection, 6, pp. 19-23 (1967).

[96] G.K. Glass, N.R. Buenfeld, *"Chloride threshold level for corrosion of steel in concrete"*, Corrosion Science, 39, pp. 1001-1013 (1997).

[97] K.Y. Ann, H.-W. Song, *"Chloride threshold level for corrosion of steel in concrete"*, Corrosion Science, 49, pp. 4113-4133 (2007).

[98] E. Becker, *"Cemento Portland – Características y Recomendaciones de Uso"*, en: Seminario sobre Cemento Portland y Patología del Hormigón, (2001).

[99] H.J. Wierig, *"Long-time studies in the carbonation of concrete under normal outdoor exposure"*, in: Rilem Seminar on Durability of Concrete Structures under Normal Outdoor Exposure, Hannover, Alemania, pp. 26-27, (1984).

[100] L.J. Parrott, *"Carbonation, moisture and empty pores"*, Advances in Cement Research, 4, pp. 111-118 (1991/92).

[101] K. Kinoshita, M.J. Madou, *"Electrochemical measurements on Pt, Ir, and Ti oxides as pH probes"*, Journal of the Electrochemical Society, 131, pp. 1089-1094 (1984).

[102] *"Encuesta sobre patologías de estructuras de hormigón"*, Grupo Español de Hormigón (GEHO), Boletín Nº 10, pp. (1992).

[103] J. González, W. López, P. Rodríguez, *"Mecanismos de corrosión en el hormigón armado y factores que controlan su cinética"*, Revista de Metalurgia (Madrid), 28, pp. 297-305 (1992).

[104] G.K. Glass, C.L. Page, N.R. Short, *"Factors affecting the corrosion rate of steel in carbonated mortars"*, Corrosion Science, 32, pp. 1283-1294 (1991).

[105] E. Otero, *"Corrosión y degradación de materiales"*, Síntesis S.A., Madrid, España (1997).

[106] M.F. Cánovas, *"Patología y terapéutica del hormigón armado"*, 3ª edición, Colegio de ICCP, Madrid, España (1994).

[107] P. Rodríguez, E. Ramírez, S. Feliú, J.A. González, W. López, *"Significance of coplanar macrocells to corrosion in concrete-embedded steel"*, Corrosion, 55, pp. 319-325 (1999).

[108] J.A. González, E. Ramírez, A. Bautista, *"Behaviour of steel reinforcement under the effect of strong cathodic or anodic polarizations"*, Magazine of Concrete Research, 50, pp. 201-208 (1998).

[109] M. Ormellese, M. Berra, F. Bolzoni, T. Pastore, *"Corrosion inhibitors for chlorides induced corrosion in reinforced concrete structures"*, Cement and Concrete Research, 36, pp. 536-547 (2006).

[110] S.U. Al-Dulaijan, M. Maslehuddin, M. Shameem, M. Ibrahim, M. Al-Mehthel, *"Corrosion protection provided by chemical inhibitors to damage FBEC bars"*, Construction and Building Materials, 29, pp.487-495 (2012).

[111] B. Elsener, *"Corrosiono inhibitors for steel in concrete — State of the art report (EFC 35)"*, Maney Publishing, Londres, Reino Unido (2001).

[112] N.S. Berke, *"Review of corrosion inhibitors in concrete"*, Materials Performance, 28, pp. 41-45 (1989).

[113] N.S. Berke, T.G. Weil, *"World-wide review of corrosion inhibitors in concrete; Advances in concrete technology"*, CANMET, Atenas, Grecia, pp. 899–924 (1992).

[114] R. Cigna, G. Familiari, F. Gianetti, E. Proverbio, *"Influence of calcium nitrite on the reinforcement corrosion in concrete mixtures containing different cements"*, International Conference on Corrosion and Corrosion Protection of Steel in Concrete, Sheffield, Reino Unido, pp. 878-892 (1994).

[115] I.A. Callander, F. Gianetti, *"A review on the use of C.N. corrosion inhibitor to improve the durability of reinforced concrete"*, 2nd Annual Middle East Protection and Rehabilitation of Reinforced Concrete Conference, Dubai, Emiratos Árabes Unidos, pp. 1-12 (1996).

[116] N.S. Berke, M.C. Hicks, *"Predicting long-term durability of steel reinforced concrete with calcium nitrite corrosion inhibitor"*, Cement and Concrete Composites, 26, pp. 191-198 (2004).

[117] R.J. Craig, L.E. Wood, *"Effectiveness of corrosion inhibitors and their influence on the physical properties of Portland cement mortars"*, Highway Research Record, 328, pp. 77-78 (1970).

[118] C. Andrade, Tesis Doctoral, "*Nuevas técnicas electroquímicas para la medida de la velocidad de corrosión*", Universidad Complutense de Madrid (1973).

[119] B. El-Jazairi, N.S. Berke, *"The use of calcium nitrite as corrosion inhibiting admixture to steel reinforcement in concrete"*, en Corrosion of Reinforcement in Concrete, C.L. Page, K. W. Treadaway, P.B. Bandford (Eds.). SCI, Londres, Reino Unido, pp. 571-585 (1990).

[120] C. Andrade, C. Alonso, J.A. González, *"Some laboratory experiments on the inhibitor effect of sodium nitrite on reinforcement corrosion"*, Cement, Concrete and Aggregates, 8, pp. 110-116 (1986).

[121] A.M. Rosemberg, J.M. Gaidis, *"The inhibition of chloride-induced corrosion in reinforced concrete by calcium nitrite"*, Cement, Concrete and Aggregates, 9, pp. 30-33 (1987).

[122] A. Królokowski. J. Kuziak, *"Impedance study on calcium nitrite as a penetrating corrosion inhibitor for steel in concrete"*, Electrochimica Acta, 56, pp. 7845-7853 (2011).

[123] I. Fayala, L. Dhouibi, X.R. Nóvoa, M. Ben Ouezdou, *"Effect of inhibitors on the corrosion of galvanized steel and on mortar properties"*, Cement and Concrete Composites, 35, pp. 181-189 (2013).

[124] C. Andrade, C. Alonso, M. Acha, B. Malric, *"Na_2PO_4F as inhibitor of corroding reinforcement in carbonated concrete"*, Cement and Concrete Research, 26, pp. 405-415 (1996).

[125] V.T. Ngala, C.L. Page, M.M. Page, *"Corrosion inhibitor system for remedial treatment of reinforced concrete: Part 2. Sodium monofluorophosphate"*, Corrosion Science, 45, pp. 1523-1537 (2003).

[126] A. Raharinaivo, B. Malric, *"Performance of MFP for inhibiting corrosion of steel in reinforced concrete structures"*, International Conference on Corrosion and Rehabilitation of Reinforced Concrete Structures, FHWA, Orlando, EE.UU. (1998).

[127] U. Mäder, *"A new class of corrosion inhibitors for reinforced concrete"*, Concrete, 9, pp. 215-223 (1999).

[128] J.M. Gaidis, *"Chemistry of corrosion inhibitors"*, Cement and Concrete Composites, 26, pp. 181-189 (2004).

[129] F. Wombacher, U. Maeder, B. Marazzani, *"Aminoalcohol based mixed corrosion inhibitors"*, Cement and Concrete Composites, 26, pp. 209-216 (2004).

[130] C.K. Nmai, *"Multi-functional organic corrosion inhibitor"*, Cement and Concrete Composites, 26, pp. 199-207 (2004).

[131] B. Elsener, M. Büchler, F. Stalder, H. Böhni, *"Migrating corrosion inhibitor blend for reinforced concrete: Part 1. Prevention of corrosion"*, Corrosion, 55, pp. 1155-1163 (1999).

[132] B. Elsener, M. Büchler, F. Stalder, H. Böhni, *"Migrating corrosion inhibitor blend for reinforced concrete: Part 2. Inhibitor as repair strategy"*, Corrosion, 56, pp. 727-732 (2000).

[133] J.A. González Fernández, J. Miranda Vidales, *"Corrosión de estructuras de hormigón armado: fundamentos, medida, diagnosis y prevención"*, CSIC, Madrid, España, (2007).

[134] M. Ormellese, L. Lazzari, S. Goidanich, G. Fumagalli, A. Brenna, *"A study of organic substances as inhibitors for chloride-induced corrosion in concrete"*, Corrosion Science, 51, pp. 2959-2968 (2009).

[135] J. Hu, D. A. Koleva, P. Petrov, K. van Breugel, *"Polymeric vesicles for corrosion control in reinforced mortar: Electrochemical behavior, steel surface analysis and bulk matrix properties"*, Corrosion Science, 65, pp. 414-430 (2012).

[136] J.A. González, E. Ramírez, A. Bautista, *"Protection of steel embedded in chloride-containing concrete by means of inhibitors"*, Cement and Concrete Research, 28, pp. 577-589 (1998).

[137] J.A. González, E. Ramírez, A. Bautista, S. Feliú, *"The behaviour of pre-rusted steel in concrete"*, Cement and Concrete Research, 26, pp. 501-511 (1996).

[138] K. Videm, *"Electrochemical studies of steel in cement mortar containing chloride and micro-silica"*, Corrosion Science, 49, pp. 1702-1717 (2007).

[139] P. Garcés, P. Saura, A. Méndez, E. Zornoza, C. Andrade, *"Effect of nitrite in corrosion of reinforcing steel in neutral and acid solutions simulating the electrolytic environments of micropores of concrete in the propagation period"*, Corrosion Science, 50, pp. 498-509 (2008).

[140] E. Zornoza, J. Payá, P. Garcés, *"Chloride-induced corrosion of steel embedded in mortars containing fly ash and spent cracking"*, Corrosion Science, 50, pp. 1567-1575 (2008).

[141] H. Ma, Z. Li, *"Microstructure and mechanical properties of polymer modified mortars under distinct mechanisms"*, Construction and Building Materials, 47, pp. 579-587 (2013).

[142] Z. Yu, G. Ye, *"The pore structure of cement paste blended with fly ash"*, Construction and Building Materials, 45, pp. 30-35 (2013).

[143] B. Huang, H. Wu, X. Shu, E. G. Burdette, *"Laboratory evaluation of permeability and strength of polymer-modified pervious concrete"*, Construction and Building Materials, 24, pp. 818-823 (2010).

[144] C. Meyer, *"The greening of the concrete industry"*, Cement and Concrete Composites, 31, pp. 601-605 (2009).

[145] E. Zornoza, J. Payá, J. Monzó, M.V. Borrachero, P. Garcés, *"The carbonation of OPC mortars partially substituted with spent fluid catalytic catalyst (FC3R) and its influence on their mechanical properties"*, Construction and Building Materials, 23,pp. 1323-1328 (2009).

[146] E. Zornoza, P. Garcés, J. Monzó, M.V. Borrachero, J. Payá, *"Accelerated carbonation of cement pastes partially substituted with fluid catalytic cracking catalyst residue (FC3R) "*, Cement and Concrete Composites, 31, pp. 134-138 (2009).

[147] I. De la Varga, J. Castro, D. Bentz, J. Weiss, *"Application of internal curing for mixtures containing high volumes of fly ash"*, Cement and Concrete Composites, 34, pp. 1001-1008 (2012).

[148] C. Lian, Y. Zhuge, S. Beecham, *"The relationship between porosity and strength for porous concrete"*, Construction and Building Materials, 25, pp. 4294-4298 (2011).

[149] A. Mendes, J. G. Sanjayan, W. P. Gates, F. Collins, "*"The influence of water absorption and porosity on the deterioration of cement paste and concrete exposed to elevated temperatures, as in a fire event"*, Cement and Composites, 34, pp. 1067-1074 (2012).

[150] A.B. Darwin, J.D. Scantlebury, *"Retarding of corrosion processes on reinforcement bar in concrete with an FBE coating"*, Cement and Concrete Composites, 24, pp. 73-78 (2002).

[151] M.M. Al-Zahrani, S.U. Al-Dulaijan, M. Ibrahim, H. Saricimen, F.M. Sharif, *"Effect of waterproofing coatings on steel reinforcement corrosion and physical properties of concrete"*, Cement and Concrete Composites, 24, pp. 127-137 (2002).

[152] L.K. Spainhour, I.A. Wootton, *"Corrosion process and abatement in reinforced concrete wrapped by fibre reinforced polymer"*, Cement and Concrete Composites, 30, pp. 535-543 (2008).

[153] M.K. Moradllo, M. S.hekarchi, M. Hoseini, *"Time-dependent performance of concrete surface coatings in tidal zone of marine environment"*, Construction and Building Materials, 30, pp. 198-205 (2012).

[154] F.F. Bamoharram, M.M. Heravi, S. Saneinezhad, A. Ayati, *"Synthesis of a nano organo-silicon compound for building materials waterproofing, using heteropolyacids as a green and eco-friendly catalyst"*, Progress in Organic Coatings, 76, pp. 384-387 (2013).

[155] Z. Zhang, X. Yao, H. Zhu, *"Potential application of geopolymers as protection coatings for marine concrete I. Basic properties"*, Applied Clay Science, 49, pp.1-6 (2010).

[156] L. Bertolini, M. Gastaldi, M.P. Pedeferri, E. Redaelli, *"Prevention of steel corrosion in concrete exposed to seawater with submerged sacrificial anodes"*, Corrosion Science, 44, pp. 1497-1513 (2002).

[157] L. Bertolini, F. Bolsón, A. Cigada, T. Pastore, P. Pedeferri, *"Cathodic protection of new and old reinforced concrete structures"*, Corrosion Science, 35, pp. 1633-1639 (2003).

[158] F.J. Presuel-Moreno, A.A. Sagües, S.C. Krac, *"Steel activation in concrete following interruption of long-term cathodic polarization"*, Corrosion, 61, pp. 428-436 (2005).

[159] Z. Chaudhary, A.K. Bairamov, R. Fernández, F. Al-Mutlaq, *"Cathodic protection of reinforced concrete seawater structures in petrochemical plants"*, Materials Performance, 46, pp. 26-29 (2004).

[160] I. Martínez, C. Andrade, O. Vennesland, U. Evensen, R.B. Polder, J. Leggedor, *"Efficiency control of cathodic protection measured using passivation verification technique in different concrete structures"*, Corrosion, 63, pp. 880-892 (2007).

[161] I. Martínez, C. Andrade, I. Lasa, O. Tronconis de Rincón, A.A. Torres-Acosta, *"Control of cathodic protection in bridges without disconnecting protection current: passivity verification technique (PVT) "*, Corrosion Engineering, Science and Technology, 42, pp. 215-223 (2007).

[162] K. Wilson, M. Jawed, V. Ngala, *"The selection and used of cathodic protection systems for the repair of reinforced concrete structures"*, Construction and Building Materials, 39, pp. 19-25 (2013).

[163] E. Radaelli, F. Lollini, L. Bertolini, *"Throwing power of localized anodes for the cathodic protection of slender carbonated concrete elements in atmospheric conditions"*, Construction and Building Materials, 39, pp. 95-104 (2013).

[164] UNE-EN 12696, "*Protección catódica del acero en el hormigón*", 2001.

[165] G.K. Glass, A.M. Hassanein, N.R. Buenfeld, *"CP criteria for reinforced concrete in marine exposure zones"*, Journal of Materials in Civil Engineering, 12, pp. 164-171 (2000).

[166] P. Pedeferri, *"Cathodic protection and cathodic prevention"*, Construction and Building Materials, 10, pp. 391-402 (1996).

[167] D.A. Koleva, J. Hu, A.L.A. Fraaij, P. Stroeven, N. Boshkov, K. van Breugel, *"Cathodic protection revisited: Impact on structural morphology sheds new light on its efficiency"*, Cement and Concrete Composites, 28, pp. 696-706 (2006).

[168] D.A. Koleva, K. van Breugel, J.H.W. De Wit, E. van Westing, O. Copuroglu, L Veleva, A.L.A. Fraaij, *"Correlation of microstructure, electrical properties and electrochemical phenomena in reinforced mortar. Breakdown to multi-phase interface structures. Part I: Microstructural observations and electrical properties"*, Materials Characterization, 154, pp. 290-300 (2008).

[169] D.A. Koleva, K. van Breugel, J.H.W. De Wit, L.P. Veleva, E. van Westing, O. Copuroglu, A.L.A. Fraaij, *"Correlation of microstructure, electrical properties and electrochemical phenomena in reinforced mortar. Breakdown to multi-phase interface structures. Part II: Pore network, electrical properties and electrochemical response"*, Materials Characterization, 154, pp. 801-815 (2008).

[170] Rasheeduzzafar, M.G. Ali, G.J. Al-Sulaimini, *"Degradation bond between reinforcing steel and concrete due to cathodic protection current"*, ACI Materials Journal, 90, pp. 8-15 (1993).

[171] M.G. Ali, Rasheeduzzafar, *"Polarization Period, current density, and the cathodic protection criteria"*, ACI Materials Journal, 89**,** pp. 247-252 (1993).

[172] J.J. Chang, *"A study of the bond degradation of rebar due to cathodic protection current"*, Cement and Concrete Research, 32, pp. 657-663 (2002).

[173] J. García, F. Almeraya, C. Barrios, C. Gaona, R. Núñez, I. López, M. Rodríguez, A. Martínez-Villafañe, J.M. Bastidas, *"Effect of cathodic protection on steel-concrete bond strength using ion migration measurements"*, Cement and Concrete Composites, 34, pp. 242-247 (2012).

[174] O. Klinghoffer, T. Frolung, B. Kofoed, A. Knudsen, F. M. Jensen, T. Skovsgaard, *"Practical an economical aspects of application of austenitic stainless steel, AISI 316, as reinforcement in concrete"*, in Corrosion of Reinforcement in Concrete, pp. 121- 133. Ed. J. Mietz, R. Polder, B. Elserner, European Federation of Corrosion, Londres, Reino Unido (2000).

[175] A. Knudsen, F.M. Jensen, O. Klinghoffer, T. Skovsgaard, *"Cost-effective enhancement of durability of concrete structures by intelligent use of stainless steel reinforcement"*, Conference on Corrosion and Rehabilitation of Reinforced Concrete Structures, Florida, EE. UU. (1998).

[176] A.M. Hassanein, G.K. Glass, N.R. Buenfeld, *"A mathematical model for electrochemical removal of chloride from concrete structures"*, Corrosion, 54, pp. 323-332 (1998).

[177] P. Castro, *"Corrosión en estructuras de concreto armado - Teoría, inspección, diagnóstico, vida útil y reparaciones"*, IMCYT, México D.F., México, pp. 93–116 (1998).

[178] M. Castellote, C. Andrade, C. Alonso, *"Electrochemical removal of chlorides. Modelling of the extraction, resulting profiles and determination of the efficient time of treatment"*, Cement and Concrete Research, 30, pp. 615-621 (2000).

[179] J.C. Orellan, G. Escadeillas, G. Arliguie, *"Electrochemical chloride extraction: Efficiency and side effects"*, Cement and Concrete Research, 34, pp. 227-234 (2004).

[180] A. Cobo, E. Otero, M.N. González, J.A. González, *"Electrochemical chloride removal from reinforced concrete structures and its ability to repassivate prerusted steel surfaces"*, Materials and Corrosion, 52, pp. 581-589 (2001).

[181] P. Garcés, M.J. Sánchez de Rojas, M.A. Climent, *"Effect of the reinforcement bar arrangement on the efficiency of electrochemical chloride removal technique applied to reinforced concrete structures"*, Corrosion Science, 48, pp. 531-545 (2006).

[182] A. Pérez, M.A. Climent, P. Garcés, *"Electrochemical extraction of chlorides from reinforced concrete using a conductive cement paste as the anode"*, Corrosion Science, 52, pp. 1576-1581 (2010).

[183] A.T.C. Guimarães, M.A. Climent, G. de Vera, F. J. Vicente, F.T. Rodrigues, C. Andrade, *"Determination of chloride diffusivity through partially saturated Portland cement concrete by a simplified procedure"*, Construction and Building Materials, 25, pp. 785-790 (2011).

[184] M. Sánchez, M. C. Alonso, *"Electrochemical chloride removal in reinforced concrete structures: Improvement of effectiveness by simultaneous migration of calcium nitrite"*, Construction and Building Materials, 25, pp. 873-878 (2011).

[185] Y. Liu, X. Shi, *"Ionic transport in cementitious materials under an externally applied electric field: Finite element modeling"*, Construction and Building Materials, 27, pp. 450-460 (2012).

[186] T. Ueda, K. Wakitani, A. Nanasawa, *"Influence of electrolyte temperature on efficiency of electrochemical chloride removal from concrete"*, Electrochimica Acta, 86, pp. 23-27 (2012).

[187] J.M. Miranda, A. Cobo, E. Otero, J.A. González, *"Limitations and advantages of electrochemical chloride removal in corroded reinforced concrete structures"*, Cement and Concrete Research, 37, pp. 596-603 (2007).

[188] Z.Q. Tan, C.M. Hansson, *"Effect of surface condition on the initial corrosion of galvanized reinforcing steel embedded in concrete",* Corrosion Science, 50, pp. 2512-2522 (2008).

[189] E. Ramírez, J.A. González, A. Bautista, *"The protective efficiency of galvanized against corrosion of steel in mortar and in $Ca(OH)_2$ solutions containing chlorides"*, Cement and Concrete Research, 26, pp. 1525-1536 (1996).

[190] A. Bautista, J.A. González, *"Analysis of the protective efficiency of galvanizing against corrosion of reinforcements embedded in chloride contaminated concrete"*, Cement and Concrete Research, 26, pp. 215-224 (1996).

[191] B.S. Hamad, G.K. Jumaa, *"Bond strength of hot-dip galvanized hooked bars in high strength concrete structures"*, Construction and Building Materials, 22, pp. 2042-2052 (2008).

[192] A. Macías, C. Andrade, *"The behaviour of galvanized steel in chloride-containing alkaline solutions - I. The influence of the cation"*, Corrosion Science, 30, pp. 393-407 (1990).

[193] F. Tittarelli, G. Moriconi, *"The effect of silane-based hydrophobic admixture on corrosion of galvanized reinforcing steel in concrete"*, Corrosion Science, 52, pp. 2958-2963 (2010).

[194] S. Rostam, *"Vida útil de las estructuras de hormigón",* Cuadernos INTEMAC, nº 61, Madrid, España (2006).

[195] F. Tang, G. Chen, J. S. Volz, R.K. Brow, M. Koenigstein, *"Microstructure and corrosion resistance of enamel coatings applied to smooth reinforcing steel"*, Construction and Building Materials, 35, pp. 376-384 (2012).

[196] S. Dong, B. Zhao, C. Lin, R. Du, R. Hu, G.X. Zhang, *"Corrosion behavior of epoxy/zinc duplex coated rebar embedded in concrete in ocean environment"*, Construction and Building Materials, 28, pp. 72-78 (2012).

[197] J.J. Assaad, C.A. Issa, *"Bond strength of epoxy-coated bars in underwater concrete"*, Construction and Building Materials, 30, pp. 667-674 (2012).

[198] F. Rasheedduzzafar, F.H. Dakhil, M.A. Bader, M.M. Khan, *"Performance of corrosion resistant steel in chloride bearing concrete"*, ACI Materials Journal, 89, pp. 439-448 (1992).

[199] R.J. Kesser, R.G. Powers, "*Corrosion Report 88-8A*", Florida Department of Transportation, August (1988).

[200] A. Zayed, A. Sagües, R.G. Powers, *"Corrosion of epoxy-coated reinforcing steel"*, NACE - CORROSION/89, Houston, Texas, EE. UU., paper Nº 379, (1989).

[201] A. Knudsen, A. Skoysgaard, *"Stainless steel reinforcement"*, Concrete Engineering International, 5, pp. 59-62 (2001).

[202] R.D. Moser, P.M. Singh, L.F. Kahn, K.E. Kurtis, *"Chloride-induced corrosion resistance of high-strength stainless steels in simulated alkaline and carbonated concrete pore solutions"*, Corrosion Science, 57, pp. 241-253 (2012).

[203] M.F. Hurley, J.R. Scully, *"Threshold chloride concentrations of selected corrosion-resistant rebar materials compared to carbon steel"*, Corrosion, 62, pp. 892-904 (2006).

[204] R. El Sarraf, W. Mandeno, J. Xia, *"Stainless steel in bridges: A discussion"*, in: Steel Innovations Conference, Christchurch, Nueva Zelanda (2013).

[205] J.T. Pérez-Quiroz, J. Terán, M.J. Herrera, M. Martínez, J. Genescá, *"Assessment of stainless steel reinforcement for concrete structures rehabilitation"*, Journal of Constructional Steel Research, 64, pp. 1317-1324 (2008).

[206] A. Bautista, G. Blanco, F. Velasco, M.A. Martínez, *"Corrosion performance of welded stainless steels reinforcements in simulated pore solutions"*, Construction and Building Materials, 21, pp. 1267-1276 (2007).

[207] F. Velasco, G. Blanco, A. Bautista, M.A. Martínez, *"Effect of welding on local mechanical properties of stainless steels for concrete structures using universal hardness tests"*, Construction and Building Materials, 23, pp. 1883-1891 (2009).

[208] U. Nürberger, *"Stainless steel in concrete. State of the art report"*, in: Publication Nº 18, Institute of Materials, London (1996).

[209] E. Medina, Tesis Doctoral, "*Evaluación del comportamiento mecánico, estructural y frente a la corrosión, de una nueva armadura de acero inoxidable dúplex bajo en níquel*", Universidad Politécnica de Madrid, Septiembre (2012).

[210] E.I. Moreno, P. Castro-Borges, A.A. Torres-Acosta, A. Cárdenas, O. Tronconis de Rincón, *"Chloride analysis in a 62-years-old concrete pier reinforcement with type 304 SS bars"*, in: NACE International Corrosion Conference, Tennessee, EE.UU. (2007).

[211] P. Castro-Borges, O. Tronconis de Rincón, E.I. Moreno, A.A. Torres-Acosta, M. Martinez-Madrid, A. Knudsen, *"Performance of a 60-years-old concrete pier with stainless steel reinforcement"*, Materials Perfomance, 41, Paper Nº 07240, pp. 50-55 (2002).

[212] A.A. Torres-Acosta, M.J. Fabela-Gallegos, D. Vazquez-Vega, M. Martínez-Madrid, P. Castro-Borges, E.I. Moreno, H.D. Cuadros-Abad, *"Structural evaluation and rehabilitation of conference arches in the Progreso pier"*, in: International Congress in Concrete Repair, Rehabilitation and Retrofitting. Ciudad del Cabo, Sudáfrica, 2005, H. Benhaussen, Taylor and Francis, Londres, Reino Unido, pp. 603-608 (2005).

[213] "*Guidance on the use of stainless steel reinforcement"*, British Concrete Society, Camberley, Reino Unido, Technical Report Nº 51, (1998).

[214] *"Stainless steel for outdor swimming pools"*, in: A refurbishment and upgrading initiative Bruselas, Munich (2003).

[215] F.N. Smith, *"Stainless steel reinforcement for concrete construction"*, in: 12th Middle East Conference and Exhibition, Paper Nº 08032, Manama, Bahrain (2008).

[216] J.M. Deus, L. Freire, M.F. Montemor, X.R. Nóvoa, *"The corrosion potential of stainless steel rebars in concrete: Temperature effect"*, Corrosion Science, 65, pp. 556-560 (2012).

[217] L. Bertolini, F. Bolzoni, T. Pastore, P. Pedeferri, *"Stainless steel behavior in simulated concrete pore solution"*, British Corrosion Journal, 31, pp. 218-222 (1996).

[218] D.B. McDonald, M.R. Sherman, D.W. Pfeifer, Y.P. Virmany, *"Stainless steel reinforcing as corrosion protection"*, Concrete International, 17, pp. 65-70 (1995).

[219] L. Freire, M.A. Catarino, M.I. Godinho, M.J. Ferreira, M.G.S. Ferreira, A.M.P. Simões, M.F. Montemor, *"Electrochemical and analytical investigation of passive films formed on stainless steels in alkaline media"*, Cement and Concrete Composites, 34, pp. 1075-1081 (2012).

[220] B. Soerensen, P. Jensen, E. Maahn, *"The corrosion properties of stainless steel reinforcement"*, in 3rd International Symposium on Corrosion of Reinforcement in Concrete Construction, Wishaw, Reino Unido, pp. 601-610 (1990).

[221] H. Castro, C. Rodríguez, F.J. Belzunce, A.F. Cantelli, *"Mechanical properties and corrosion behaviour of stainless steel reinforcing bars"*, Journal of Materials Processing Technology, 143–144, pp. 134-137 (2003).

[222] M.W.K. Treadaway, *"Corrosion of steel reinforcement in concrete construction",* in: Materials Preservation Group, Symposium Society of Chemical Industry, Londres, Reino Unido (1978).

[223] B.G. Callaghan, *"The use of 3CR12 as reinforcing in concrete"*, Construction and Building Materials, 7, pp. 131-136 (1993).

[224] S. Fajardo, D.M. Bastidas, M.P. Ryan, M. Criado, D.S. McPhail, J.M. Bastidas, *"Low-nickel stainless steel passive film in simulated concrete pore solution: A SIMS study"*, Applied Surface Science, 256, pp. 6139-6143 (2010).

[225] M. Criado, S. Fajardo, J.M. Bastidas, *"Corrosion Behaviour of a New Low-Nickel Stainless Steel Reinforcement: A Study in Simulated Pore Solutions and in Fly Ash Mortars"*, International Journal of Corrosion, 13, ID 847323, pp. 8 pages, (2012).

[226] M. Criado, D.M. Bastidas, S. Fajardo, A. Fernández-Jimenez, J.M. Bastidas, *"Corrosion behaviour of a new low-nickel stainless steel embedded in activated fly ash mortars"*, Cement and Concrete Composites, 33, pp. 644-652 (2011).

[227] M.C. García-Alonso, M.L. Escudero, J.M. Miranda, M.I. Vega, F. Capilla, M.J. Correia, M. Salta, A. Bennani, J.A. González, *"Corrosion behaviour of new stainless steels reinforcing bars embedded in concrete"*, Cement and Concrete Research, 37, pp. 1463-1471 (2007).

[228] M.C. García-Alonso, J.A. González, J. Miranda, M.L. Escudero, M.J. Correia, M. Salta, A. Bennani, *"Corrosion behaviour of innovative stainless steels in mortar"*, Cement and Concrete Research, 37, pp. 1562-1569 (2007).

[229] A. Bautista, G. Blanco, F. Velasco, *"Corrosion behaviour of low-nickel austenitic stainless steels reinforcements: A comparative study in simulated pore solutions"*, Cement and Concrete Research, 36, pp. 1922-1930 (2006).

[230] T. Pastore, P. Pedeferri, *"Corrosion behavior of a duplex stainless steel in chloride contaminated concrete"*, in: International Conference of Stainless Steel, Chiba, Japan (1991).

[231] T. Pastore, P. Pedeferri, L. Bertolini, F. Bolzoni, A. Cigada, *"Electrochemical study on the use of duplex stainless steel in concrete"*, in: International Conference of Duplex Stainless Steels, Beaune, France (1991).

[232] L. Bertolini, M. Gastaldi, P. Pedeferri, E. Redealli, *"Factors influencing the corrosion resistance of austenitic and duplex stainless steel bars in chloride bearing concrete"*, in: 15th International Corrosion Congress, Granada, España (2002).

[233] A. Bautista, G. Blanco, F. Velasco, A. Gutiérrez, S. Palacín, H. Soriano, H. Takenouti, *"Passivation of duplex stainless steels in solutions simulating chloride-contaminated concrete"*, Materiales de Cosntrucción, 57, pp. 17-32 (2007).

[234] S. Baldo, I. Mészáros, *"Effect of cold rolling on microstructure and magnetic properties in a metastable lean duplex stainless steel"*, Journal of Materials Science, 45, pp. 5339-5346 (2010).

[235] E. Berjón, F.J. Belzunce, C. Rodriguez, H. Castro, *"Análisis de la resistencia a la corrosión de barras corrugadas de aceros inoxidables en medios acuosos que simulan el hormigón"*, en: VII Congreso Nacional de Materiales, Madrid, España (2002).

[236] H. Castro, C. Rodriguez, F.J. Belzunce, M.L. Aenlle, A.F. Cantelli, *"Propiedades mecánicas de armaduras de refuerzo fabricadas con distintos tipos de acero"*, en: VIII Congreso Nacional de Propiedades Mecánicas de los Sólidos, Gandía, España (2002).

[237] H. Castro, C. Rodriguez, F.J. Belzunce, *"Mechanical behaviour and corrosion resistance of stainless steel cold rolled bars"*, Materials Science Forum, 426-432, pp. 1541-1546 (2003).

[238] M. Matsushita, H. Ogiyama, T. Suko, S. Matsuda, *"Study on solid-phase welding of dúplex stainless steel with carbon steel based on superplasticity and consideration of the cyclic fatigue fracture behavior"*, Materials Chemistry and Physics, 114, pp. 599-603 (2009).

[239] I. Juraga, I. Esih, F. Simunovic, *"Effect of the welding procedure on the pitting susceptibility of stainless steel"*, in: 15th International Corrosion Congress, Granada, España (2002).

[240] M.E. Somervouri, L.S. Johanson, M.H. Heinonen, D.H.D. van Hoecke, N. Akdut, H.E. Hánninnen, *"Characterization and corrosion of spot welds of austenitic stainless steels"*, Materials and Corrosion, 55, pp. 421-436 (2004).

[241] T. Trickl, G. Mori, *"Corrosion of welds in automotive fuel tanks"*, in: 15th International Corrosion Congress, Granada, España (2002).

[242] R.F.A. Petterson, J. Fly, *"Influence of weld oxides on the corrosion of 316L stainless steel"*, in: EUROCORR, Lisboa, Portugal (2005).

[243] P.K. Rastogi, B.K. Shah, A.K. Sinha, P.G. Kulkarni, *"Technical note: Effect of oxide film on pitting susceptibility of 304 austenitic stainless steel"*, British Corrosion Journal, 29, pp. 78-80 (1994).

[244] H. Liu, X. Jin, *"Electrochemical corrosion behavior of the laser continuous heat treatment welded joints of 2205 duplex stainless steel"*, Journal of Wuhan University of Technology-Materials Science, 26, pp. 1140-1147 (2011).

[245] B. Kurt, A. Çalik, *"Interface structure of diffusion bonded duplex stainless steel and medium carbon steel couple"*, Materials Characterization, 60, pp. 1035-1040 (2009).

[246] J.R. Kearns, G.E. Moller, *"Reducing heat tint effects on the corrosions-resistance of austenitic stainless alloys"*, Materials Perfomance, 33, pp. 57-61 (1994).

[247] I. Esih, V. Alar, I. Juraga, *"Influence of thermal oxides on pitting corrosion of stainless steel in chloride solutions"*, Corrosion Engineering Science and Technology, 40, pp. 110-120 (2005).

[248] M. Sharifitabar, A. Halvaee, S. Khorshahian, *"Microstrucure and mechanical properties of resistance upset butt welded 304 austenitic stainless steel joints"*, Materials and Design, 32, pp. 3854-3864 (2011).

[249] S. Kumar, A.S. Shahi, *"Effect of heat input on the microstructure and mechanical properties of gas tungsten arc welded AISI 304 stainless steel joints"*, Materials and Design, 32, pp. 3617-3623 (2011).

[250] A.R. Galvis, W. Hormaza, *"Characterization of failure modes for different welding processes of AISI/SAE 304 stainless steels"*, Engineering Failure Analysis, 18, pp. 1791-1799 (2011).

[251] ASM Handbook, "*Corrosion*", Vol. 13, 4th ed., ASM International, Materials Park, EE.UU. (1992).

[252] A. Pardo, M.C. Merino, M. Carboneras, F. Viejo, R. Arrabal, J. Muñoz, *"Influence of Cu and Sn content in the corrosion of AISI 304 and 316 stainless steels in H_2SO_4"*, Corrosion Science, 48, pp. 1075-1092 (2006).

[253] A. Barbucci, M. Delucchi, M. Panizza, M. Sacco, G. Cerisola, *"Electrochemical and corrosion behaviour of cold rolled AISI 301 in 1 M H_2SO_4"*, Journal of Alloys and Compounds, 317–318, pp. 607-611 (2001).

[254] A.S. Hamada, L.P. Karjalainen, M.C. Somani, *"Electrochemical corrosion behaviour of a novel submicron-grained austenitic stainless steel in an acidic NaCl solution"*, Materials Science and Engineering: A, 431, pp. 211-217 (2006).

[255] P. De Tiedra, Ó. Martín, M. López, M. San-Juan, *"Use of EPR test to study the degree of sensitization in resistance spot welding joints of AISI 304 austenitic stainless steel"*, Corrosion Science, 53, pp. 1563-1570 (2011).

[256] V. Číhal, R. Štefec, *"On the development of the electrochemical potentiokinetic method"*, Electrochimica Acta, 46, pp. 3867-3877 (2001).

[257] A. Bautista, F. Velasco, S. Guzmán, D. de la Fuente, F. Cayuela, M. Morcillo, *"Corrosion behaviour of powder metallurgical stainless steels after two years of exposure in atmosphere"*, Corrosion Engineering, Science and Technology, 41, pp. 284-290 (2006).

[258] ASTM G 108-94, *"Standard test method for electrochemical reactivation (EPR) for detecting sensitization of AISI type 304 and 304L stainless steels*", ASTM International (2012).

[259] V. Číhal, S. Lasek, M. Blahetova, E. Kalabisova, Z. Krhutova, *"Trends in electrochemical polarization pontentiodynamic reactivation methods - EPR"*, Chemical and Biochemical Engineering Quarterly, 21, pp. 47-54 (2007).

[260] Ó. Martín, P. De Tiedra, C. García, F. Martín, M. López, *"Comparative study between large-scale and small-scale electrochemical potentiokinetic reactivation performed on AISI 316L austenitic stainless steel"*, Corrosion Science, 54, pp. 119-126 (2012).

[261] I.N. Bastos, S.S.M. Tavares, F. Dalard, R.P. Nogueira, *"Effect of microstructure on corrosion behavior of superduplex stainless steel at critical environment conditions",* Scripta Materialia, 57, pp. 913-916 (2007).

[262] S. Zor, M. Soncu, L. Çapan, *"Corrosion behavior of G-X CrNiMoNb 18-10 austenitic stainless steel in acidic solutions",* Journal of Alloys and Compounds, 480, pp. 885-888 (2009).

Capítulo II

Objetivos

Como se ha visto en el Capítulo I, el empleo de barras corrugadas de acero inoxidable tiene un gran potencial en estructuras con riesgo de sufrir corrosión, bien sea por el ingreso de iones cloruros o bien por carbonatación del hormigón. El principal inconveniente de los corrugados de acero inoxidable es su precio (cuando el coste de la estructura se valora solo a corto plazo, sin incluir el mantenimiento), pero la posibilidad de emplear aleaciones más económicas ha relanzado el interés por esta forma de optimizar la durabilidad de estructuras de hormigón armado.

Los resultados obtenidos a lo largo de la investigación planteada en esta tesis doctoral pretenden aportar datos sobre tres aspectos fundamentales para garantizar la viabilidad y revelar posibles limitaciones de esta estrategia:

- Conocer el comportamiento frente a la corrosión y las características de las capas pasivas formadas en nuevos aceros inoxidables dúplex de baja aleación (grados S32001 y S32304) en un medio de elevada alcalinidad. Por ello, se ha estudiado los aceros inoxidables dúplex de baja aleación en medios que simulan los contenidos en los poros del hormigón, tanto sin carbonatar como carbonatados, y con diferentes contenidos de cloruro, utilizando otros aceros inoxidables corrugados cuyo comportamiento es algo más conocido como referencia.

- Evaluar la influencia del proceso de conformado de los corrugados de acero inoxidable en su resistencia a la corrosión, puesto que la gran mayoría de los estudios publicados hasta la fecha recurren a muestras de inoxidable que no han sido conformadas como las barras corrugadas. Las barras corrugadas están altamente deformadas y presentan características microestructurales específicas que pueden determinar su durabilidad. Se ha recurrido tanto a estudios en disoluciones alcalinas como a estudios en disoluciones ácidas (que reproducen el pH en el interior de resquicios y picaduras cuando hay corrosión).

- Estudiar el comportamiento de los corrugados de acero inoxidable en mortero tras largas exposiciones a condiciones agresivas. Dado que la bibliografía publicada en el tema se basa esencialmente en resultados de ensayos en disolución, la obtención de datos sobre en comportamiento en mortero es indispensable para validarlos, pues hay características del desarrollo de la corrosión en hormigón que no se pueden reproducir en ensayos en disolución.

Capítulo III

Materiales y

Procedimiento Experimental

3.1 BARRAS CORRUGADAS DE ACERO ESTUDIADAS

En la presente Tesis se han estudiado a fondo las barras de aceros inoxidables dúplex corrugados UNS S32001, de bajo contenido en molibdeno y en níquel, y el UNS S32304, de bajo contenido en molibdeno, que son materiales novedosos en su utilización como refuerzo en estructuras de hormigón armado.

Con fines comparativos, sus resultados serán analizados con otros aceros inoxidables dúplex y austeníticos, convencionales en el mercado de la construcción, con notables diferencias entre ellos en su contenido de Ni, Mo, Mn, Cr y N. Dichos elementos son muy importantes y decisivos en el momento de evaluar la corrosión. También se comparará la influencia del procesado en las barras de aceros inoxidables corrugados, estudiandose algunos de ellos en dos estados de conformado: en frío (*Cold Worked*, CW) y en caliente (*Hot Worked*, HW).

La Tabla 3.1 recoge los aceros estudiados tanto en disolución como en mortero, habiendo sido, algunos de ellos, evaluados en ambos casos.

Tabla 3.1. Aceros inoxidables estudiados en las distintas partes de esta Tesis Doctoral.

Materiales		**Ensayos**	
		Disolución	**Mortero**
Dúplex	HW S32001	X	X
	HW S32304	X	X
	HW S32205 a	X	X
	HW S32205 b		X
	CW S32205 a	X	X
	CW S32205 b		X
Austeníticos	CW S20430 a		X
	CW S20430 b		X
	CW S30400		X
	HW S30403	X	
	CW S30403	X	X
	CW S31600		X
	HW S31603	X	
	CW S31603 a	X	X
	CW S31603 b		X
	CW S31603 c		X
	CW S31635		X

Para los ensayos en disolución se han utilizado 8 tipos de aceros inoxidables y para el estudio en morteros, se han utilizado 15 tipos de aceros inoxidables. Se utilizaron un total de 17 aceros diferentes. Además, para algunas composiciones y condiciones de conformado, se han empleado varias coladas, indicadas con una letra tras el acero.

El objetivo de utilizar coladas distintas es observar como una diferencia en alguno de sus elementos, microestructura y características propias del conformado, podrían afectar a su comportamiento frente a la corrosión. Todos los aceros fueron proporcionados por la empresa ROLDÁN S.A. (Grupo Acerinox).

La composición química, el diámetro y algunas propiedades mecánicas de cada una de ellas se recogen en las Tablas 3.2 y 3.3. Estos datos han sido proporcionados por la empresa proveedora ROLDÁN S.A.

Tabla 3.2. Composición química, diámetro y algunas propiedades mecánicas de los aceros inoxidables dúplex corrugados empleados.

Elemento (%)	HW S32001	HW S32304	HW S32205 *a*	HW S32205 b	CW S32205 *a*	CW S32205 b
C	0,025	0,017	0,020	0,019	0,018	0,029
S	0,002	0,002	0,003	0,002	0,001	0,001
Si	0,75	0,57	0,37	0,32	0,39	0,39
Mn	4,39	1,68	1,67	1,50	1,82	1,72
Cr	20,58	23,66	22,17	22,41	22,32	22,49
Ni	1,74	4,32	4,71	4,88	4,92	4,72
Mo	0,221	0,243	3,500	2,749	3,408	3,221
Ti	0,012	0,046	0,048	0,006	0,044	0,027
N	0,124	0,153	0,178	0,144	0,184	0,174
Cu	0,073	0,186	0,093	0,084	0,074	0,237
Fe	Bal.	Bal.	Bal.	Bal.	Bal.	Bal.
Diámetro (mm)	16	16	20	12,7	14	12
Resistencia a la tracción (MPa)	824	769	855	846	1132	1156
Límite elástico (MPa)	554	568	583	539	950	968
Alargamiento (%)	44	38	33	37	14	12

Tabla 3.3. Composición química, diámetro y algunas propiedades mecánicas de los aceros inoxidables austeníticos corrugados empleados.

Elemento (%)	CW S20430 a	CW S20430 b	CW S30400	CW S30403	HW S30403
C	0,049	0,052	0,063	0,023	0,026
S	0,002	0,004	0,002	0,001	0,002
Si	0,23	0,30	0,31	0,36	1,00
Mn	8,26	8,01	1,42	1,45	1,48
Cr	16,12	16,55	18,33	18,30	18,66
Ni	1,89	1,97	8,12	8,68	8,56
Mo	0,015	0,316	0,297	0,275	0,249
Ti	0,003	0,004	0,004	0,004	0,039
N	0,130	0,138	0,050	0,051	0,055
Cu	2,65	2,72	0,32	0,49	0,51
Fe	Bal.	Bal.	Bal.	Bal.	Bal.
Diámetro (mm)	5	8	8	10	16
Resistencia a la tracción (MPa)	918	808	1035	747	780
Límite elástico (MPa)	756	620	923	580	580
Alargamiento (%)	32	20	21	38	15

Tabla 3.3. (Continuación). Composición química, diámetro y algunas propiedades mecánicas de los aceros inoxidables austeníticos corrugados empleados.

Elemento (%)	CW S31600	CW S31603 *a*	CW S31603 b	CW S31603 c	HW S31603	CW S31635
C	0,052	0,025	0,021	0,014	0,013	0,029
S	0,001	0,003	0,006	0,004	0,002	0,001
Si	0,29	0,35	0,21	0,37	0,40	0,45
Mn	1,48	1,40	1,67	1,62	2,02	1,21
Cr	17,03	17,05	17,05	17,10	18,41	16,68
Ni	10,38	10,12	10,25	11,38	10,79	11,25
Mo	2,206	2,11	2,171	2,039	2,488	2,232
Ti	0,004	0,005	0,003	0,004	0,005	0,251
N	0,040	0,043	0,047	0,045	0,044	0,020
Cu	0,37	0,49	0,32	0,50	0,26	0,41
Fe	Bal.	Bal.	Bal.	Bal.	Bal.	Bal.
Diámetro (mm)	6	14	10	10	16	12
Resistencia a la tracción (MPa)	874	734	805	822	800	860
Límite elástico (MPa)	693	623	651	656	603	726
Alargamiento (%)	27	30	26	26	12	22

Al finalizar el proceso industrial del conformado, cada barra corrugada es sometida a un pasivado. Dicho proceso consiste en un tratamiento químico (inmersión en disolución de ácido nítrico con una pureza de un 60% en peso y durante un tiempo de 2 min). Este proceso genera sobre la superficie de los aceros inoxidables una capa pasiva formada por óxidos más protectores, con el fin de optimizar su comportamiento frente a la corrosión. Todos los aceros evaluados se han estudiado en este estado de recepción, y se ha seguido ese mismo proceso cuando ha sido necesario pasivar cortes transversales de las barras en el laboratorio.

Además, en alguna fase de esta tesis, se han empleado barras corrugadas de acero al carbono con un diámetro de 10mm, dado su común utilización en estructuras de hormigón armado. La composición química de las barras de acero al carbono empleado se recoge en la Tabla 3.4. Cumpliéndose con lo establecido en la Norma UNE 36065:2000 EX.

Tabla 3.4. Composición química del acero al carbono corrugado ensayado en mortero.

Elemento (%)	C	S	P	Si	Mn	Cr	Ni	Mo	Cu
	0,245	0,002	0,030	0,552	0,760	0,236	0,093	0,023	0,605

3.2 PROCEDIMIENTO EXPERIMENTAL

En este trabajo se han utilizado barras de aceros inoxidables corrugados que abarcan una amplia gama de composiciones. Debido al gran número de muestras bajo estudio, se presenta un esquema dividido en dos partes, en función de los medios evaluados: estudios en disoluciones o estudios en morteros.

3.2.1 Ensayos electroquímicos en disolución

a) Ensayos en medio alcalino

Se pretende analizar la susceptibilidad a la corrosión por picaduras en las barras de los diferentes materiales que se estudian, caracterizándose en medios que simulan las disoluciones contenidas en los poros del hormigón.

Las medidas se han realizado en disoluciones saturadas de $Ca(OH)_2$, principal compuesto responsable de la alcalinidad en la disolución de los poros del hormigón en estructuras envejecidas. Se estudió el comportamiento en medios sin carbonatar (pH≅13) y carbonatados (pH≅9), con 4 concentraciones de cloruro sódico diferentes (0, 0,5, 1 y 5% de NaCl en peso).

El pH≅9 (utilizado con el fin de investigar el efecto de la carbonatación sobre la pasividad de los aceros inoxidables corrugados) se consigue carbonatando mediante burbujeo en la disolución de aire enriquecido con un 10% de CO_2 a una velocidad muy lenta. Esto hace que se forme una disolución reguladora CO_3^{2-}/HCO_3^- de menor alcalinidad que la disolución original.

- **Curvas de polarización anódicas cíclicas**

Los ensayos se han realizado siguiendo un procedimiento basado en la norma ASTM G61 [1]. La velocidad de barrido del potencial ha sido de 0,17 mV/s. El sentido del barrido del potencial ha sido invertido cuando se ha alcanzado una densidad de corriente de 10^{-4} A/cm^2. El barrido en sentido catódico termina al llegar al potencial de corrosión (E_{corr}).

La polarización comenzó a potenciales catódicos (100 mV vs SCE) por debajo del potencial de corrosión (E_{corr}), obteniendo la relación entre el potencial (E) y la intensidad (i). A partir de las curvas de polarización se obtienen los valores del E_{corr}, así como las intensidades de corrosión (i_{corr}). Para la determinación de este último parámetro se ha utilizado el procedimiento de las pendientes de Tafel.

El potencial de picadura (E_{pit}) ha sido identificado para pH≅13 como el potencial anódico donde se observa un incremento brusco de corriente. Para pH≅9, dado que la

zona pasiva está definida en la curva y resulta subjetivo identificar el potencial al cual hay un incremento brusco de corriente, se han usado como criterio para evaluar el comportamiento a corrosión los sobrepotenciales requeridos para alcanzar una determinada corriente entre 0,5 y 1 x 10^{-5} A/cm^2.

En todos los ensayos electroquímicos en disolución, la celda electroquímica empleada ha estado compuesta por tres electrodos:

- Electrodo de trabajo: probeta de acero objeto de estudio.
- Electrodo de referencia: electrodo de calomelanos saturado (SCE).
- Contraelectrodo: espiral de acero inoxidable rodeando el electrodo de trabajo.

Para los estudios del comportamiento de la superficie real de las armaduras, el electrodo de trabajo empleado ha sido un trozo de material corrugado, sumergido 2 cm en la disolución y con su sección transversal desbastada hasta grado 320. Para todos los casos, los ensayos se han realizado tras 48 h de exposición del material corrugado a la disolución para asegurar una estabilización del E_{corr} lo más correcta posible.

En lo que se refiere al estudio del comportamiento del centro de las barras, los ensayos se realizaron en la celda Avesta. Las pruebas realizadas en la celda Avesta buscan evitar cualquier riesgo de corrosión en resquicio que interfiera en las medidas de susceptibilidad a corrosión por picaduras. Las probetas fueron trozos de barra cortados transversalmente, embutidos y desbastados hasta grado 320. Estos ensayos se han realizado para comparar el comportamiento del núcleo con la superficie corrugada en los aceros.

Debido a la dispersión intrínseca del proceso de corrosión y a la heterogeneidad de las superficies del corrugado, se han ensayado 6 probetas por condición, con el fin de obtener resultados fiables y significativos.

b) Ensayos en medio ácido

En medios ácidos, la corrosión de los aceros inoxidables se desarrolla a través de un mecanismo muy diferente que en medio alcalino, ya que puede ocurrir un ataque más generalizado en lugar de la corrosión localizada. Aunque las barras corrugadas son un

material fabricado para estar expuesto en hormigón, y este es un medio alcalino, cuando se ha iniciado un proceso de corrosión, la hidrólisis ácida de los productos de corrosión da lugar, en el interior de las picaduras y en los resquicios como los que hay en la interfase acero-hormigón, a una disminución del pH. Se han medido pHs tan ácidos como 1-2 a través de grietas o macroporos de probetas armadas que se corroían activamente [2].

Se trabajó con una disolución H_2SO_4 2 M y HCl 0,5 M [3], que es una disolución empleada anteriormente para estudiar las transiciones actividad/pasividad de los aceros dúplex [3-6].

- **Curvas de polarización anódicas**

Las polarizaciones se realizaron a partir de -550 mV hasta 400 mV vs SCE, con una velocidad de barrido de 1 mV/s [3,4,6]. Las curvas de polarización anódicas para cada material se repiten entre 5-7 veces para asegurar la fiabilidad de los resultados.

Se emplea la misma configuración de la celda electroquímica utilizada en las curvas de polarización en medio alcalino, con tres electrodos. Para estudiar el comportamiento de la superficie corrugada, el electrodo de trabajo empleado ha sido un trozo de material corrugado, sumergido 2 cm en la disolución y con su sección transversal pulida a 0,3 μm. En el caso del centro de las barras, las probetas fueron trozos cortados transversalmente, embutidos, desbastados y pulidos a 0,3 μm, para su ensayo en celda Avesta.

La deconvolución matemática de los picos en las curvas de polarización anódica se llevó a cabo por un software específicamente programado. El software fue desarrollado utilizando la interfaz gráfica de usuario (GUI), herramienta de creación en lenguaje Matlab (Matlab versión R2010b). El software utiliza una función GEV (*Generalized Extreme Value*), para obtener curvas que se ajustan a los datos experimentales. La distribución GEV se define por la ecuación 3.1:

$$F(x;\mu;\sigma;\xi) = \exp\left\{-\left[1+\xi\left(\frac{x-\mu}{\sigma}\right)\right]^{-1/\xi}\right\} \qquad (3.1)$$

Donde x son los valores de potencial, F son los valores de densidad de corriente, μ es el parámetro de ubicación (en función de los potenciales en las que aparece el máximo del pico de corriente), σ es el parámetro de escala (relacionada con el área del pico) y ξ es el parámetro de forma (que permite simular la característica de asimetría de los picos de activación).

Esta herramienta permite realizar un ajuste gráfico de curvas con formas complejas, orientado específicamente a la adaptación de gráficas, intensidades frente potencial de corriente, relativas a ensayos de polarización anódica. Los antecedentes teóricos y aplicaciones físicas de las funciones de GEV, se pueden encontrar fácilmente en la literatura [7,8]. La aplicación de ingeniería y los límites de la GEV se han discutido previamente [9].

El ajuste permite obtener los valores de la densidad de carga que participan en los diferentes fenómenos que ocurren durante la polarización anódica, además de otros parámetros pertinentes, tales como la densidad de corriente máxima (i_{max}) de cada fenómeno y el potencial máximo (E_{max}) en que el correspondiente i_{max} aparece.

- **Polarización potenciostática anódica**

Las pruebas potenciostáticas se llevaron a cabo para los aceros en diferentes potenciales anódicos que se consideraron significativos, para comprobar la influencia de la polarización en la morfología del ataque. Los valores de los potenciales fueron seleccionados dentro de la región de activación de las curvas de polarización. Para determinar el tiempo de exposición del ensayo, se tuvo en cuenta la resistencia de cada material y se realizaron múltiples ensayos por condición, hasta llegar a obtener resultados fiables y significativos. En la Tabla 3.5 se resumen los potenciales y los tiempos de exposición que se consideraron óptimos para cada ensayo.

Se expusieron también trozos de cada acero en la disolución ácida, cada uno por separado, durante varios días a su respectivo E_{corr}, observándose visualmente cambios de color y/o deterioro en la superficie en cada muestra. En la Tabla 3.6 se coloca el tiempo que estuvo cada acero en la disolución.

Tabla 3.5. Condiciones utilizadas para los ensayos potenciostáticos.

MATERIALES	CENTRO		SUPERFICIE CORRUGADA	
	E (mV vs SCE)	TIEMPO (h)	E (mV vs SCE)	TIEMPO (h)
CW S31603	-185	4	-185	4
	-230		-235	
CW S30403	-184	4	-184	4
	-272		-275	
HW S30403	-172	4		
	-350			
HW S32001	-200	7	-200	4
	-255	4	-255	
	-325		-325	
	-400		-400	
HW S32304	-244	4	-244	4
	-344		-344	
HW S32205	-295	7	-230	7
	-355		-330	
CW S32205	-250	7	-250	7
	-355		-330	

Tabla 3.6. Condiciones utilizadas para los ensayos E_{corr}.

MATERIALES	CW S30403	HW S32001	HW S32304	HW S32205 a	CW S32205 a
Tiempo	4 días	2 días	4 días	12 días	8 meses

En la Figura 3.1 se muestra en un esquema general un resumen del procedimiento experimental seguido para llevar a cabo los ensayos electroquímicos en disolución en cada uno de los aceros inoxidables.

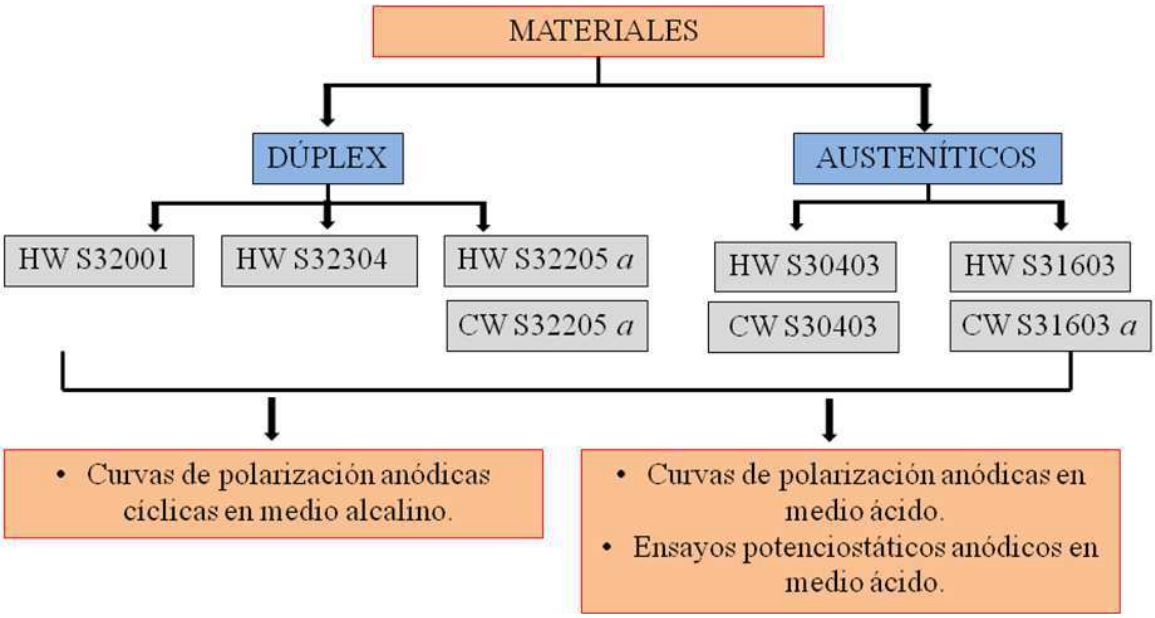

Figura 3.1. Esquema general utilizado en los ensayos electroquímicos en disolución.

3.2.2 Ensayos electroquímicos en mortero

Un objetivo importante en la presente Tesis Doctoral es el estudio y la evaluación frente a la corrosión de los aceros inoxidables embebidos en mortero mediante estudios a largo plazo, pues los existentes hasta el momento consideran composiciones de poco interés en el mercado actual [10,11].

La construcción de estructuras de hormigón genera la unión de dos fases (armadura-hormigón). Aunque la química de las disoluciones contenidas en sus poros pueda ser similar a la de los ensayos en disolución, existen otros factores (irreproducibles en ensayos en disolución) que pueden afectar al desarrollo de los procesos de corrosión/pasividad de las armaduras. Esencialmente estos factores son:

- Resquicios en la intercara armadura/recubrimiento que favorecen la formación de pilas de corrosión mucho más potentes que las que pueden aparecer en medios acuosos.
- Velocidad de difusión de oxigeno mucho más limitada.

Por estos motivos, y por la posibilidad que ofrece de realizar ensayos de durabilidad con resultados a largo plazo, se consideró necesario corroborar la estabilidad de la pasividad del acero inoxidable en probetas de mortero.

a) Fabricación de probetas

En los morteros se han embebido armaduras de aceros inoxidables, acero al carbono y distintos aceros soldados.

Para las probetas, las barras de acero corrugadas fueron cortadas en trozos. La sección transversal de la armadura que quedó dentro del mortero fue desbastada hasta grado 320 y pasivada en laboratorio (apdo. 3.1). Para facilitar la posterior monitorización de las probetas con espectroscopía de impedancia electroquímica (EIS), las armaduras se han embebido en probetas de mortero cilíndricas [12]. La configuración y las medidas de las armaduras se muestran en la Figura 3.2. Se colocó cinta aislante en la intercara mortero-aire-acero para evitar influencias indeseadas de agentes contaminantes, principalmente de la carbonatación. De este modo, se pretende que no aparezcan durante la exposición las zonas anódicas y garantizar que los fenómenos de corrosión ocurran en las condiciones de trabajo inicialmente diseñadas. Se han utilizado diferentes moldes, teniendo en cuenta el diámetro de la barra, tratando de mantener siempre una distancia entre la barra y el exterior del hormigón de 1.5 cm.

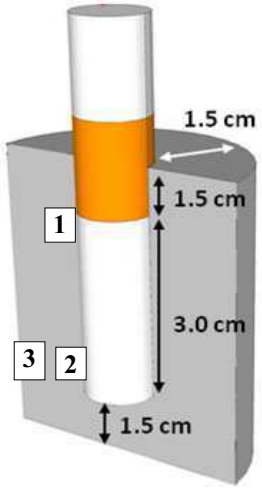

Figura 3.2. Esquema de las probetas embebidas en mortero.

Para la fabricación del mortero se utilizó una relación de 1 parte de cemento, 3 de arena y 0,6 de agua en todas las probetas. En algunos casos, para forzar la corrosión, también se añadió durante el amasado un 3% de $CaCl_2$ con respecto al peso de cemento, a fin de lograr condiciones de agresividad que pudieran favorecer la corrosión en un tiempo relativamente corto. Se escogió esta sal para no añadir artificialmente cationes diferentes a los que dominan normalmente en el mortero.

Los materiales empleados para la fabricación de los morteros en estudio fueron: Cemento CEM IV/B (P-V) 32,5 V (de Cementos Portland LAFARGE), arena CEN_NORMSAND S7142/143 MPA GmbH (arena normalizada de acuerdo a DIN EN 196 Parte 1, de Normensand GmbH) y agua potable. Para la elaboración de los morteros se utilizó una amasadora de la marca IIC, modelo C-2.

El proceso de curado que se ha utilizado en todas las probetas tras su amasado ha sido en condiciones de alta humedad relativa (HR) controlada durante 30 días.

Para este estudio se colocaron electrodos de titanio activado en la mitad de las probetas embebidas en el mortero, junto a la armadura. Una vez finalizado su curado, se sometieron a una carbonatación acelerada, con los electrodos de Ti se pretende controlar el avance del perfil de carbonatación, pues el potencial de estos electrodos cambia con el pH [13].

El proceso de carbonatación se realizó en una cámara donde se inyectó aire enriquecido con un 10% de CO_2 hasta llenar totalmente su volumen. Se monitorizaron periódicamente los potenciales de los electrodos de Ti activado, repitiendo una nueva inyección de aire enriquecido en CO_2 a los 7 días. Transcurridos 15 días, el frente de carbonatación había llegado hasta la armadura, según informaron los electrodos de Ti activado mediante un cambio en su potencial (medido frente a un SCE externo).

Las probetas se han expuesto en 6 condiciones diferentes y a temperatura ambiente, como se resumen a continuación:

- **PI**: Parcialmente sumergidos en agua con 3,5% de NaCl.
- **PI9**: Carbonatados y parcialmente sumergidos en agua con 3,5% de NaCl.
- **HRHCl**: 90-95% de HR y con adición de $CaCl_2$ durante la fabricación del mortero.

- **HRH9**: Carbonatados y con un 90-95% de HR.
- **HRH9Cl**: Carbonatados, con un 90-95% de HR y con adición de $CaCl_2$ durante la fabricación del mortero.
- **PICl**: Parcialmente sumergidos en agua con 3,5% de NaCl y con adición de $CaCl_2$ durante la fabricación del mortero.

En la Figura 3.3 se resume el esquema del procedimiento experimental llevado a cabo en las barras embebidas en mortero para realizar los ensayos electroquímicos.

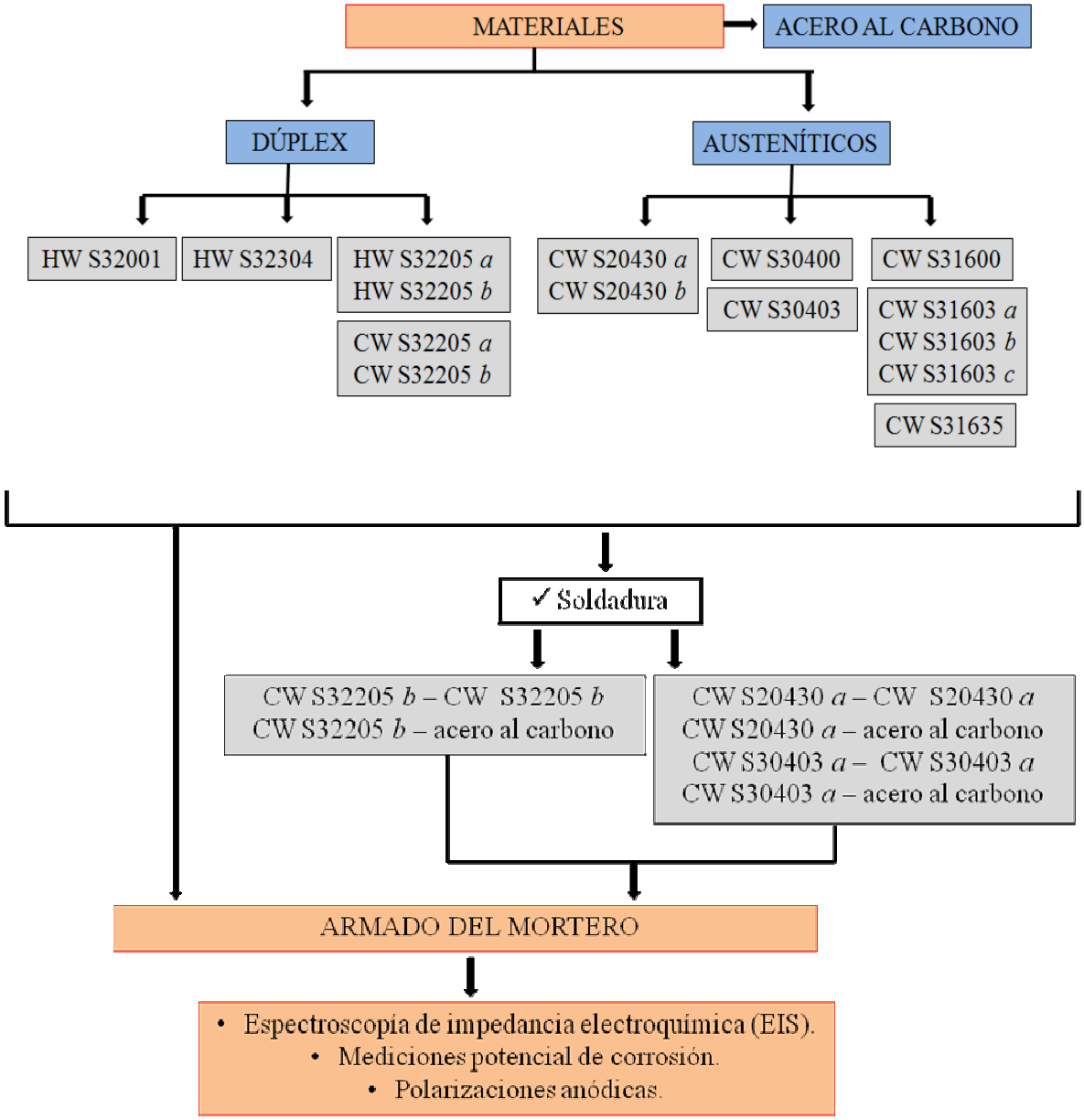

Figura 3.3. Esquema general utilizado en los aceros embebidos en mortero.

b) Soldadura

Una de las aplicaciones de las armaduras de acero inoxidable es la sustitución de trozos de armaduras de acero al carbono en determinadas zonas de la estructura durante las reparaciones. La soldadura no es una técnica habitual para unir armaduras en obra, pero a veces en la única opción en este tipo de reparaciones.

Se trabajó con barras de aceros inoxidables corrugados soldadas para estudiar el efecto de la soldadura en probetas embebidas en hormigón. Las propiedades mecánicas [14] y la corrosión de las barras soldadas en disolución habían sido estudiadas previamente [15]. Algunos de los materiales se han soldado frente a sí mismos y también frente a barras de acero al carbono de similar diámetro. En la Figura 3.4 puede observarse el aspecto de las barras corrugadas soldadas.

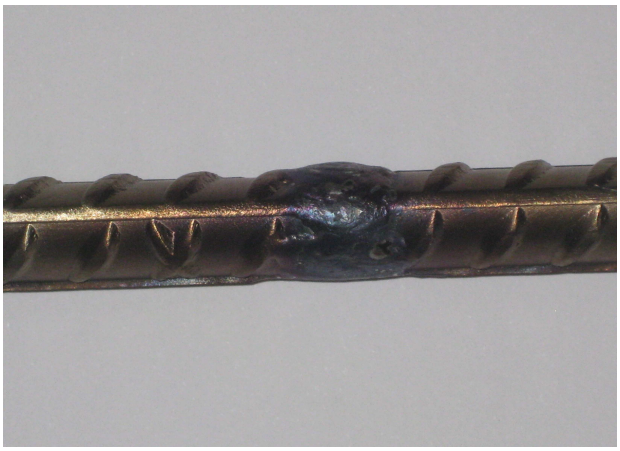

Figura 3.4. Barra de acero inoxidable corrugado.

En este estudio se optó por un método fácilmente implementable en obra, que es la soldadura manual con electrodo revestido (*Shielded Metal Arc Welding*, SMAW), Los parámetros del proceso fueron:

- Longitud de las barras: 10 cm.
- Tensión aplicada: 50-60 V.
- Corriente aplicada: 45-90 A.

Se utilizó un electrodo revestido como material de aporte distinto en función del tipo de acero inoxidable a soldar. Para los aceros inoxidables austeníticos se ha utilizado el electrodo OK 61.30 de 2 mm de diámetro y para los dúplex el OK 67.50 de 2,5 mm de diámetro (Tabla 3.7).

Tabla 3.7. Características de los electrodos de aporte empleados en la soldadura.

	Tipo	**Revestimiento**	**%Cr**	**%Ni**	**%Mn**
OK 61.30	AISI 308L	LMA*	19,5	10,0	0,9
OK 67.50	SAF E 2209	Rutilo	22,5	9,5	0,9

* de baja absorción de humedad

Después del proceso de soldadura es necesario llevar a cabo una limpieza del metal. Existían estudios previos sobre la efectividad de diversos métodos de limpieza de los óxidos de soldadura en disolución [15], pero era necesario corroborarlos en mortero. En el presente estudio se utilizaron 2 métodos diferentes para evaluar la efectividad en la eliminación de los óxidos, los cuales se citan a continuación:

- Chorreado en arena. La arena utilizada estaba principalmente formada por SiO_2, FeO y Al_2O_3, y el tamaño empleado ha sido de 120 mallas (0,122 mm).
- Limpieza con decapante de Grupinox (GX). El decapante empleado es un producto químico compuesto básicamente por ácido nítrico y ácido sulfúrico.

En la Figura 3.5 se muestra el aspecto de las barras soldadas antes y después de los procedimientos de limpieza. Como se puede ver, el decapante químico no es capaz de eliminar totalmente los óxidos formados durante la soldadura, y el chorreado en arena deja partículas embebidas en la superficie del material [15].

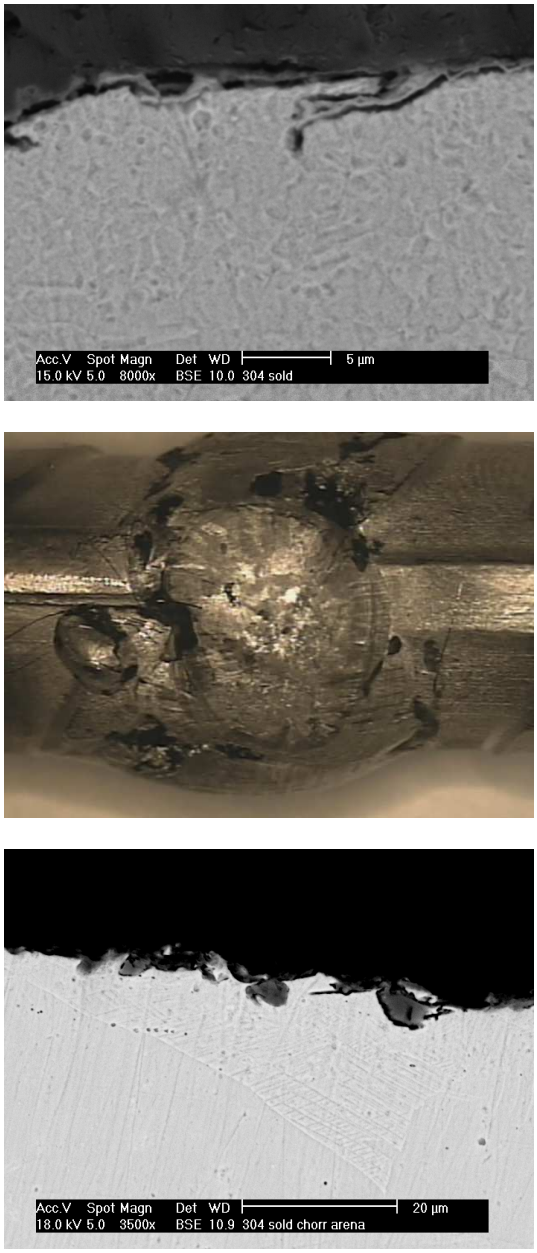

Figura 3.5. Acero corrugado S30403 soldado. Arriba, tras el soldeo. Centro: limpieza con decapante. Abajo: Tras chorreado en arena.

El procedimiento para las probetas amasadas con refuerzos soldados es el mismo explicado anteriormente en este mismo apartado. Las armaduras se han embebido en probetas de mortero cilíndricas [12], mostrándose la configuración y las medidas de las armaduras en la Figura 3.6.

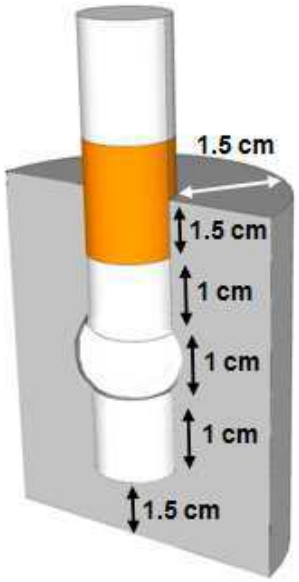

Figura 3.6. Esquema de las probetas de mortero soldadas.

c) Ensayos electroquímicos

Las transformaciones electroquímicas de la capa pasiva y el posible inicio de la corrosión de los aceros inoxidables corrugados han sido evaluadas mediante tres técnicas. Estas técnicas se has empleado para estudiar los aceros en mortero (soldados y sin soldar).

La configuración de la celda electroquímica sigue siendo con tres electrodos, pero modificando el contraelectrodo y el medio, el cual ha sido el propio mortero donde se encontraban embebidas las barras de acero:

- El electrodo de referencia empleado ha sido nuevamente un SCE, pero en este caso se encontraba en contacto con el mortero a través de una bayeta húmeda.
- El contraelectrodo utilizado ha sido un tubo de cobre dispuesto concéntricamente alrededor de las probetas de mortero, manteniendo el contacto con el mortero mediante otra bayeta húmeda.
- Los electrodos de trabajo empleados son las barras de los aceros inoxidables que se encuentran embebidas en el mortero, las barras sobresalen del mortero aproximadamente 2 cm de longitud (Figuras 3.2 y 3.6).

A algunos de los materiales embebidos en mortero se les ha hecho un seguimiento durante cinco años en el grupo de investigación previo al inicio de este Trabajo Doctoral. Durante el actual doctorado se han embebido otros aceros de interés y se ha iniciado y continuado con el seguimiento a todas las probetas y se han realizados ensayos destructivos.

- **Espectroscopía de impedancia electroquímica (EIS)**

La amplitud de la señal sinusoidal aplicada a los materiales ha sido de 10 mV en torno al E_{corr}. Los aceros inoxidables han sido estudiados en el intervalo de frecuencias de 10^3 a 10^{-3} Hz. Los tiempos a los cuales se han realizado las medidas de EIS han sido, desde los 3 meses hasta los 8 años de curado de las probetas en cada uno de los medios preparados. El objetivo era/ha sido observar transformaciones electroquímicas de la capa pasiva y el posible inicio de la corrosión de los aceros inoxidables corrugados.

Tras los ensayos EIS realizados en mortero sobre las barras de los aceros inoxidables, los espectros han sido ajustados mediante un programa basado en el método Simplex.

- **Mediciones potencial de corrosión**

El comportamiento frente a la corrosión de las armaduras embebidas en hormigón, se ha estudiado desde los 3 meses hasta los 8 años de curado de las probetas en cada uno de los medios preparados, monitorizando periódicamente su E_{corr}.

Este método es adecuado para la evaluación del comportamiento en servicio de los aceros, ya que puede ser utilizado en cualquier momento de las probetas acero-hormigón o de una estructura en servicio, sin flujo de corriente externa.

La utilización de este método se consideró como apoyo para la estimación de las propiedades estructurales del acero dentro del hormigón, siguiendo las indicaciones de la norma ASTM C876–09 [16].

➢ **Polarizaciones anódicas**

Se ha evaluado la probabilidad de picadura de morteros armados que permanecían pasivos tras largas exposiciones en diferentes medios, mediante ensayos de polarización anódica. La prueba de polarización se ha empleado en los morteros que llevaban ocho años embebidos. Se aplicaron al sistema pequeños escalones de potencial ΔE con el tiempo, y se registró la corriente. El test potenciostático registra la corriente anódica a escalones de potencial sucesivos y crecientes, iniciando en el E_{corr} y aumentando 20 mV cada 10 min hasta completar 1 h. Luego se aumentó 20 mV cada 1 h hasta alcanzar 900 mV. Los escalones son pequeños para obtener más sensibilidad en la prueba.

3.2.3 Técnicas de caracterización complementarias

Para explicar el comportamiento frente a la corrosión de los aceros inoxidables corrugados, se han empleado diversas técnicas que se detallan a continuación. Para complementar y explicar los resultados de los ensayos de corrosión se resumen en la Figura 3.7, los aceros y las técnicas utilizadas en cada uno de ellos.

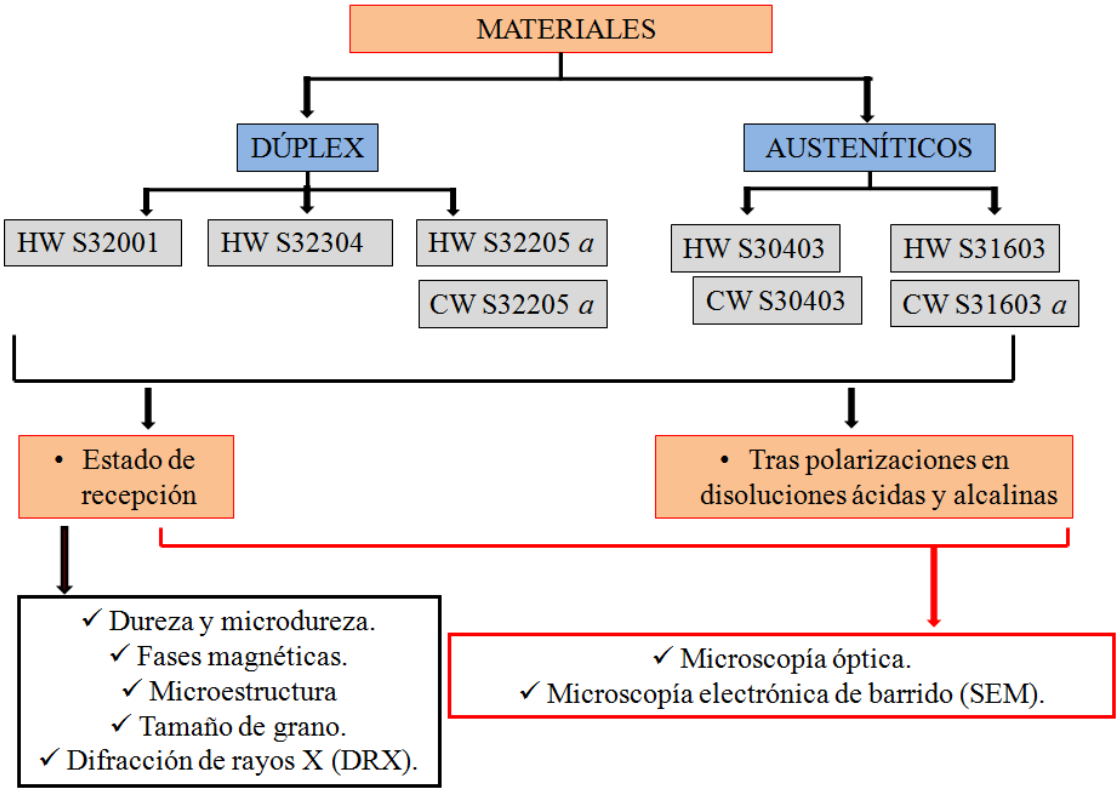

Figura 3.7. Esquema general utilizado en la caracterización de los aceros.

a) Análisis microestructural

Se estudió la microestructura de todos los materiales utilizados en esta investigación. La caracterización se ha utilizado a fin de evaluar el tamaño de grano y la variación microestructural de los aceros inoxidables dúplex y austeníticos debido a su conformado en frío o en caliente (CW y HW).

El análisis microestructural se ha llevado a cabo mediante microscopía óptica y microscopía electrónica de barrido (SEM). El SEM, de la marca *Philips* XL-30, es un instrumento que proyecta un haz de electrones a un punto exactamente focalizado de la superficie de una muestra y recoge la señal electrónica emitida en un detector. Consta de un detector de electrones donde se pueden obtener micrografías correspondientes a interacciones de tipo electrones secundarios (SE) y retrodispersados (BSE), además se encuentra equipado con un analizador *EDAX* de espectroscopía de energía de rayos X (EDS) que nos permite realizar análisis semicuantitativos. Es una poderosa herramienta de caracterización morfológica [17].

Para ello, tanto las secciones transversales como las longitudinales han sido preparadas metalográficamente, mediante desbastado hasta grado 1000, pulido con polvo de alúmina de tamaño 0,3 μm y atacado químicamente por inmersión con los reactivos siguientes:

- Agua Regia: Cuya composición química es ¼ en vol. de HNO_3 con una concentración del 37% en peso y ¾ en vol. de HCl con una concentración del 65% en peso. Este reactivo se utilizó para mostrar la microestructura del acero inoxidable austenítico, atacando los bordes de grano preferentemente.

- Bloech and Weld: Cuya composición química es 100 ml de H_2O destilada, 10-20 ml de HCl con una concentración del 37% en peso y 0,6 g de $K_2S_2O_5$. Este reactivo se utilizó para revelar la microestructura de los aceros inoxidables dúplex, coloreando de forma diferencial la capa pasiva de las dos fases presentes en el material (austenita y ferrita).

Para realizar el estudio del tamaño de grano, se han tomado fotos sobre las superficies de las muestras pulidas y atacadas, manteniendo constantes los aumentos en las muestras. En los aceros inoxidables dúplex y en los aceros inoxidables austeníticos HW las fotos se han tomado a 1500 aumentos, mientras que en los aceros inoxidables

austeníticos CW se han tomado a 100 aumentos. Esto vino condicionado por la gran diferencia en el tamaño de grano que presentan los materiales.

Se determinó el tamaño de grano de los aceros inoxidables mediante microscopía óptica, utilizando el programa (Image Pro-plus 5.0) y teniendo en cuenta las normas UNE-EN ISO-643 [18] y ASTM E1-12 [19]. El método se basa en contar el número de granos interceptados o el número de intersecciones de bordes de grano, mediante una circunferencia cuyo diámetro es conocido. La precisión en la determinación del tamaño de grano es mayor cuantas más probetas se examinen, por lo tanto se llevó a cabo el análisis en 20 fotos y se dio el valor promedio del tamaño de grano en cada material.

Tras los ensayos potenciostáticos y potenciodinámicos de polarización anódica, los materiales corroídos se han sometido a cortes transversales y longitudinales para estudiar la morfología del ataque en las secciones obtenidas.

b) Dureza

El ensayo simultaneo de microdureza Vickers (HV20) y dureza universal (HU) [20], de las barras de aceros inoxidables dúplex y austeníticos comparados en este estudio, se llevó a cabo en un durómetro universal de la marca Zwick/Roell. La dureza se midió sobre la sección transversal de las barras, tanto en el centro como en la zona corrugada.

Se cortaron trozos de aproximadamente 5 mm de longitud, se pulieron las zonas donde se realizarían las medidas y se embutieron de la forma convencional para tener un soporte. El ensayo se realizó en diferentes puntos de la sección transversal, realizando 10 medidas en cada zona, y determinando el valor medio y la desviación estándar. Ambas durezas se han analizado en el mismo instante del ensayo, al momento de aplicar la carga. La microdureza HV20 usa la diagonal de la huella después de la medida y la dureza HU la profundidad máxima de la huella (valores geométricamente relacionados) [21,22]. Todas las medidas fueron realizadas a una velocidad de 1 mm/min, empleando una carga máxima de 20 N durante 20 s.

c) Cuantificación de fases magnéticas

Se determinó el porcentaje de la fase magnética presente en las muestras de acero inoxidables dúplex y austeníticos, mediante un ferritómetro manual de marca FERITSCOPE® FMP30. El equipo se calibra previamente basado en estándares de calibración que contienen distintos porcentajes de fase magnética.

Las medidas se realizaron en el corte transversal de las barras, tanto en el centro de la barra como en la zona corrugada. Se realizaron 10 medidas para cada tipo de material y se determinó el valor medio y la desviación estándar.

d) Difracción de rayos X (DRX)

La técnica de difracción de rayos X se ha utilizado para identificar las distintas fases presentes en los aceros estudiados. Se obtuvieron los difractogramas correspondientes al núcleo y la corruga de las barras de aceros inoxidables dúplex y a los núcleos de las barras corrugadas de los aceros austeníticos.

La radiación empleada fue la correspondiente a la línea Kα del Cu (λ = 1,5418 Å). Los ensayos se realizaron para un ángulo 2θ comprendido entre 40 y 95º para los aceros inoxidables austeníticos y de 40 a 120º para los aceros inoxidables dúplex. Con un tamaño de paso de 0,02º, tiempo por paso de 5 s y una velocidad de 0,04 º/s. La tensión se fijó a 40 kV y la intensidad a 40 mA. De esta forma, se observó la evolución de los máximos de difracción correspondientes a las distintas fases presentes en función de las variables que afectan a los diferentes aceros.

e) Valoración de cloruros

El contenido de cloruro total del mortero se valora después de la exposición durante 9 años al medio agresivo. La localización de las regiones estudiadas se marca en la Figura 3.2. En todos los casos, se ha obtenido el valor promedio de al menos 5 mediciones en cada región de las muestras, que fueron molidas a 800 μm.

Para determinar la concentración de cloruro, se comprobó en el laboratorio la eficiencia de la técnica Fluorescencia de Rayos X (XRF), como ya habían hecho otros

autores [23], y se decidió emplearla para medir el porcentaje de cloruros. Se utilizó un equipo SPECTRO XEPOS, con una exactitud de 0.2% y un límite de detección > 100 ppm.

3.3 BIBLIOGRAFÍA

[1] ASTM, "*Standard test method for conducting cyclic potentiodynamic polarization measurements for localized corrosion susceptibility of Iron-, Nickel-, or Cobalt-based alloys*", ASTM International (2009).

[2] J.A. González, E. Otero, S. Feliu, A. Bautista, E. Ramírez, E. Rodríguez, W. López, "*Some considerations on the effect of chloride ion on the corrosion of steel reinforcements embedded in concrete structures",* Magazine of Concrete Research 50, pp. 189-199 (1998).

[3] W.-T. Tsai, J.-R. Chen, "*Galvanic corrosion between the constituent phases in duplex stainless steel",* Corrosion Science 49, (9), pp. 3659-3668 (2007).

[4] S. Zor, M. Soncu, L. Çapan, "*Corrosion behavior of G-X CrNiMoNb 18-10 austenitic stainless steel in acidic solutions",* Journal of Alloys and Compounds 480, (2), pp. 885-888 (2009).

[5] S.-J. Pan, Y.-J. Shih, J.-R. Chen, J.-K. Chang, W.-T. Tsai, "*Selective micro-etching of duplex stainless steel for preparing manganese oxide supercapacitor electrode",* Journal of Power Sources 187, (1), pp. 261-267 (2009).

[6] I.H. Lo, Y. Fu, C.-J. Lin, W.-T. Tsai, "*Effect of electrolyte composition on the active-to-passive transition behavior of 2205 duplex stainless steel in H_2SO_4/HCl solutions",* Corrosion Science 48, (3), pp. 696-708 (2006).

[7] J. Swait, "*Choice set generation within the generalized extreme value family of discrete choice models",* Transportation Research Part B: Methodological 35, (7), pp. 643-666 (2001).

[8] M. Clusel, E. Bertin, "*Global fluctuations in physical systems: A subtle interplay between sum and extreme value stastics",* International Journal of Modern Physics B 22, (20), pp. 3311-3368 (2008).

[9] J.D. Holmes, W.W. Moriarty, "*Application of the generalized Pareto distribution to extreme value analysis in wind engineering",* Journal of Wind Engineering and Industrial Aerodynamics 83, (1–3), pp. 1-10 (1999).

[10] B.G. Callaghan, "*The performance of a 12% chromium steel in concrete in severe marine environments",* Corrosion Science 35, (5–8), pp. 1535-1541 (1993).

[11] G.N. Flint, R.N. Cox, "*The resistance of stainless steel partly embedded in concrete to corrosion by seawater",* Magazine of Concrete Research 40, pp. 13-17 (1988).

[12] C. Andrade, L. Soler, C. Alonso, X.R. Nóvoa, M. Keddam, "*The importance of geometrical considerations in the measurement of steel corrosion in concrete by means of AC impedance",* Corrosion Science 37, (12), pp. 2013-2023 (1995).

[13] K. Kinoshita, M.J. Madou, "*Electrochemical measurements on Pt, Ir, and Ti oxides as pH probes",* Journal of the Electrochemical Society 131, pp. 1089-1094 (1984).

[14] F. Velasco, G. Blanco, A. Bautista, M.A. Martínez, "*Effect of welding on local mechanical properties of stainless steels for concrete structures using universal hardness tests",* Construction and Building Materials 23, (5), pp. 1883-1891 (2009).

[15] A. Bautista, G. Blanco, F. Velasco, M.A. Martı´nez, "*Corrosion performance of welded stainless steels reinforcements in simulated pore solutions",* Construction and Building Materials 21, (6), pp. 1267-1276 (2007).

[16] ASTM C876–09, "*Standard test method for corrosion potentials of uncoated reinforcing steel in concrete*", ASTM International (2009).

[17] K.C.A. Smith, C.W. Oatley, "*The scanning electron microscope and its fields of application",* British Journal of Applied Physics 6, (11), pp. 391-399 (1955).

[18] UNE-EN ISO-643, "*Acero: Determinación micrográfica del tamaño de grano aparente*", AENOR (2004).

[19] ASTM E1-12, "*Standard test methods for determining average grain size*", ASTM International (2007).

[20] DIN 50359-1, "*Testing of metallic materials – Universal hardness test – Part 1: test method*", DIN Publisher (1997).

[21] S.A. Shahdad, J.F. McCabe, S. Bull, S. Rusby, R.W. Wassell, "*Hardness measured with traditional Vickers and Martens hardness methods",* Dental Materials 23, (9), pp. 1079-1085 (2007).

[22] W.C. Oliver, G.M. Pharr, "*An improved technique for determining hardness and elastic modulus using load and displacement sensing indentation experiments",* Journal of Materials Research 7, (06), pp. 1564-1583 (1992).

[23] R.K. Dhir, M.R. Jones, H.E.H. Ahmed. "*Determination of total and soluble chlorides in concrete*", Cement and Concrete Research, 20, pp. 579-590 (1990).

Capítulo IV

Resumen de las publicaciones

Los resultados más relevantes obtenidos durante esta Tesis Doctoral han sido recogidos y publicados en diferentes artículos y congresos. En concreto, se incluyen 8 artículos publicados en revistas incluidas en el JCR. Los resúmenes de estos trabajos se presentarán en tres bloques: ensayos en medio alcalino, ensayos en medio ácido y ensayos en mortero.

En los artículos que han resultado de esta investigación se han utilizado diferentes nomenclaturas, dado que hay varias designaciones, como se mostró en la Tabla 2.1. En el resumen del presente capítulo se utilizará siempre la nomenclatura UNS.

4.1 ENSAYOS EN MEDIO ALCALINO

Los diferentes estudios realizados para analizar el comportamiento frente a la corrosión de los aceros inoxidables dúplex de baja aleación S32001 HW y S32304 HW se comparan con los aceros más convencionales tipo austeníticos S31603 y S30403 y el dúplex S32205. Estos tres últimos grados, se han estudiado en CW y HW. Los resultados obtenidos en las curvas de polarización en medio alcalino, se han resumido en tres publicaciones:

Publicación 1: P1

S.M. Alvarez, A. Bautista, F. Velasco, "*Corrosion behaviour of corrugated lean duplex stainless steels in simulated concrete pore solutions*", Corrosion Science, vol. 53, p. 1748-1755, 2011. Índice de impacto: 3,734 (2 de 75 – 1er cuartil). Área: Metallurgy and Metallurgical Engineering.

Publicación 2: P2

E.C. Paredes, A. Bautista, S.M. Alvarez, F. Velasco, "*Influence of the forming process of corrugated stainless steels on their corrosion behaviour in simulated pore solutions*", Corrosion Science, vol. 58, p. 52-61, 2012. Índice de impacto: 3,615 (2 de 75 – 1er cuartil). Área: Metallurgy and Metallurgical Engineering.

Nota: Hay que señalar que este es un trabajo de varios miembros del grupo de investigación. La caracterización mediante Mott-Schottky realizada de la superficie corrugada y del centro no se discutirán en esta Tesis Doctoral, ya que no han sido realizados dentro del trabajo de esta Tesis.

Publicación 3: P3

S.M. Alvarez, A. Bautista, F. Velasco, "*Influence of process parameters on the corrosion resistance of corrugated austenitic and duplex stainless steels*", Materials and technology (Materiali in tehnologije), vol. 47, p. 317–321, 2013. Índice de impacto: 0,571 (189 de 241 – 4º cuartil, datos de 2012). Área: Materials Science, Multidisciplinary.

El primer aspecto evaluado fue el comportamiento frente a la corrosión utilizando los grados dúplex de baja aleación S32304 HW y S32001 HW, comparándolos con aceros convencionales (S32205 HW y S30403 HW). Como se indicó en el capítulo 3, el estudio se realizó mediante curvas de polarización en soluciones alcalinas saturadas con $Ca(OH)_2$, carbonatadas y no carbonatadas, con cantidades diferentes de NaCl.

En las Figs. 1 y 2 de la **P1,** se muestran las curvas de polarización correspondientes a los dos nuevos aceros inoxidables dúplex, evaluados en la superficie real de las barras corrugadas. En soluciones sin carbonatar, los materiales presentan una amplia región pasiva en ausencia de cloruros, sin presentar picaduras ni ningún otro tipo de ataque significativo. En estas disoluciones, se ha apreciado la presencia de dos reacciones:

$$Cr_2O_3 + 10OH^- \longrightarrow 5H_2O + 2CrO^{2-}_4 + 6e^- \quad \text{(Reacción 1)}$$

$$4OH^- \longrightarrow 2H_2O + O_2 + 4e^- \quad \text{(Reacción 2)}$$

La reacción (1), a 300 mV vs SCE aproximadamente, se debe a la disolución del óxido de Cr cuando el material sufre polarizaciones anódicas altas. Esta reacción aparece en todos los inoxidables en soluciones saturadas con $Ca(OH)_2$ sin cloruros. La reacción (1) no se puede entender como un proceso de corrosión, ya que no hay rotura de la capa pasiva y no implica la disolución de los metales básicos. Sin embargo, la reacción sugiere una posible disminución de la capacidad de protección de la capa pasiva cuando se expone en este rango de potencial.

La reacción (2), a 700 mV vs SCE, corresponde a la reacción de desprendimiento de oxígeno, pudiendo apreciarse que la curva no tiene ciclo de histéresis (típico de la

corrosión por picaduras) se produce con $Ca(OH)_2$, sin cloruros. Esta reacción también se aprecia en la Fig. 7 de la **P2**.

En disoluciones sin carbonatar y con cloruros, el dúplex S32304 HW sufre picaduras a sobrepotenciales anódicos muy altos, cercanos a la evolución del oxígeno (**P1**, Fig. 1a), como se ve por el ciclo de histéresis que aparece durante el barrido de vuelta. Las picaduras se producen después de que la reacción (1) haya tenido lugar, las propiedades protectoras de la capa pasiva han disminuido y la pasividad se deba garantizar (al menos parcialmente) por el Fe_3O_4. Por lo tanto, el material se vuelve más vulnerable al ataque por los cloruros. El incremento en el contenido de cloruros en la solución obstaculiza la repasivación, como se puede observar por el aumento del bucle de la histéresis durante el barrido de vuelta. De todos modos, las picaduras en el grado S32304 HW bajo estas condiciones de pH siempre se repasivan fácilmente.

El acero dúplex S32001 HW de baja aleación en soluciones no carbonatadas con cloruros presenta una mayor susceptibilidad a la corrosión por picadura que el dúplex S32304 HW (**P1**, Fig. 1b). Para el grado S32001 HW, disminuye la longitud de las regiones pasivas con el aumento en el contenido de cloruro de la solución y las picaduras formadas no son capaces de repasivarse durante el barrido de vuelta de las curvas de polarización. Además, para las soluciones con altas concentraciones de NaCl, la corriente continúa aumentando al comienzo del barrido inverso, a pesar de que los valores del potencial empiezan a disminuir. Este comportamiento puede demostrar el proceso de corrosión notablemente desarrollado en estas condiciones.

En las soluciones a pH ≈ 9 sin cloruros (**P1**, Fig. 2), ambos aceros dúplex muestran un comportamiento excelente. La forma de la curva es muy similar a la detectada en soluciones sin cloruros no carbonatadas (**P1**, Fig. 1), y las diferencias observadas a muy altos sobrepotenciales anódicos son debidos al pH y su influencia en la reacción (2).

En soluciones carbonatadas con cloruros, el dúplex S32304 HW desarrolla la corrosión por picadura a un alto sobrepotencial anódico (**P1**, Fig. 2a). La repasivación tras el ataque en el dúplex S32304 HW parece más difícil que en las soluciones no carbonatadas. Además, aparecen a menudo picaduras metaestables a sobrepotenciales anódicos moderados, especialmente en soluciones con alto contenido de cloruro.

En las curvas correspondientes al dúplex S32001 HW en soluciones carbonatadas con cloruros, las picaduras aparecen sin la necesidad de alcanzar altas sobretensiones anódicas (**P1**, Fig. 2b). La forma de las curvas sugiere un ataque distribuido en muchas y pequeñas picaduras. Esto podría estar relacionado con el hecho de que las capas pasivas del acero inoxidable S32001 HW son menos ricas en Cr_2O_3 a pH 9 que a pH 12,6. Por consiguiente, si las capas pasivas son más débiles a este pH, probablemente se rompería casi al mismo tiempo en muchos puntos cuando se polariza.

Además de la discusión de la forma de las curvas, se ha realizado un análisis numérico, con diferentes parámetros obtenidos del ensayo, para comparar estos aceros inoxidables con otros más convencionales (e incluso con el acero al carbono, típico en EHA). Así, los valores de la i_{corr} y el E_{corr} de todos los aceros inoxidables, incluidos los dúplex de baja aleación, son característicos del estado pasivo (**P1**, Fig. 3), sin observarse diferencias significativas entre ellos. La presencia del Cr_2O_3 junto con el Fe_3O_4 en su capa pasiva hace que la i_{corr} de los aceros inoxidables sea casi un orden de magnitud más bajas que la i_{corr} del acero al carbono cuando se pasiva (en soluciones no carbonatadas sin cloruros, la durabilidad del acero al carbono sólo se concede por la presencia de Fe_3O_4 en la superficie). Las diferencias entre la i_{corr} de los aceros inoxidables y el acero al carbono aumentan a medida que la agresividad del medio lo hace, al igual que ocurre con el E_{corr}.

Debido a las heterogeneidades inevitables de la intercara entre hormigón/refuerzo, es interesante analizar la respuesta de estos diferentes aceros inoxidables bajo polarizaciones, para conocer si la resistencia a la corrosión de estos nuevos grados es adecuada y si podrían ser utilizados en lugar de los más convencionales (un poco más caros). En soluciones con cloruros a pH ≈ 12,6, el parámetro utilizado para evaluar la estabilidad del estado pasivo bajo polarizaciones es el E_{pit}. Los valores obtenidos del E_{pit} a partir de las curvas de polarización se representan en la Fig. 4, **P1**. Para el acero inoxidable dúplex S32205 HW, la evolución del oxígeno, reacción (1), siempre aparece antes de que el E_{pit} pueda ser alcanzado, a pesar de la baja velocidad de barrido del potencial y el contenido de cloruro de las soluciones (Fig. 4 de **P1**), esté el acero deformado en frío o en caliente (Fig. 7 de **P2**). Para los otros tres aceros inoxidables corrugados (S32001 HW, S32304 HW y el S30403 HW), el E_{pit} disminuye cuando el contenido de cloruro de la solución aumenta, como se esperaba.

El acero inoxidable dúplex S32001 HW presenta valores del E_{pit} muy similares a los obtenidos para el austenítico S30403 HW. Por lo tanto, se puede suponer que este nuevo dúplex, más barato que el austenítico S30403 HW, puede tener una excelente resistencia a las picaduras en medios no carbonatados u hormigón contaminado con cloruros, similar a la del austenítico S30403 HW. El acero inoxidable dúplex S32304 HW muestra mayores valores del E_{pit} que los obtenidos en el S30403 HW (es decir, este grado dúplex es más resistente a la corrosión localizada y más barato que el austenítico S30403 HW). El comportamiento del dúplex S32304 HW se encuentra entre el grado dúplex S32205 HW y el grado austenítico S30403 HW, lo que sugiere que puede ser un material muy interesante para entornos altamente contaminados con cloruros.

Es interesante evaluar el riesgo que implica la presencia de carbonatación y cloruros en el mismo momento en la estructura, por su agresividad. Aunque, en la práctica, un alto contenido de cloruro por lo general aparece en estructuras expuestas a ambientes marinos, donde la humedad relativa es alta y la carbonatación no se ve favorecida, el uso de sales de deshielo en el entorno urbano puede dar lugar a esta situación mixta (carbonatación más cloruros).

La determinación del E_{pit} en estas condiciones puede ser complicada. Por ello, se eligió como parámetro de comparación en soluciones carbonatadas el sobrepotencial requerido para alcanzar una cierta densidad de corriente. Los valores fueron elegidos teniendo en cuenta que el E_{pit} generalmente en las soluciones no carbonatadas se define entre 5×10^{-6} y 10^{-5} A/cm^2 (**P1**, Fig. 2), y el hecho de que, por debajo del 5×10^{-6} A/cm^2, los datos pueden estar muy influenciados por la reacción (1). Los aceros inoxidables dúplex S32205 HW y S32304 HW requieren sobrepotenciales anódicos muy altos para llegar a esas intensidades. Sin embargo, debe señalarse que el dúplex S32304 HW muestra un comportamiento algo peor que el dúplex más aleado S32205 HW. La resistencia a la corrosión para llegar a 5×10^{-6} A/cm^2 es muy similar para el dúplex S32001 HW y el austenítico S30403 HW.

Además de los excelentes resultados que muestran en los ensayos de polarización los aceros dúplex de baja aleación, el hecho de tener una microestructura dúplex hace que la morfología del ataque no sea tan peligrosa como en un acero austenítico convencional. El acero S32001 HW, que tiene una i_{corr} similar al S30403 HW, presenta picaduras más pequeñas y numerosas que el S30403 HW (**P1**, Fig. 6) tras las curvas de polarización,

tanto en medios carbonatados como sin carbonatar. Además, las picaduras en el acero inoxidable dúplex de baja aleación siempre muestran bocas con formas irregulares, en contraste con las picaduras en el acero austenítico ensayado que a menudo son picaduras con bocas circulares. El grado S32001 HW tiende a desarrollar una morfología menos peligrosa y muestra una alta capacidad en la reducción de la intensidad de la corrosión durante el barrido inverso del potencial (**P1**, Fig. 2).

Como es bien sabido, los aceros inoxidables dúplex están formados por dos fases (austenita y ferrita) con diferentes resistencias a la corrosión. Esto significa que se inicia la corrosión en la fase más débil del acero inoxidable dúplex y probablemente podría tener lugar la corrosión preferencial de una de las fases.

En el dúplex S32304 HW, la extensión del ataque después de realizar las curvas de polarización es limitada. Además, se ha detectado una diferencia en la velocidad de corrosión de las fases que determinan claramente el desarrollo del proceso de corrosión (**P1**, Fig. 7). En las muestras ensayadas en soluciones con cloruros, la ferrita (la fase continua de color oscuro) actúa como la fase menos resistente a la corrosión. El progreso del ataque está limitado por la austenita (la fase discontinua de color claro). Este hecho se verificó en soluciones con diferentes contenidos de cloruro, y se observa también que es independiente de la carbonatación o no de las soluciones. Teniendo en cuenta el excelente comportamiento del grado S32205 HW durante las pruebas de polarización, el comportamiento ligeramente peor del grado S32304 HW puede entenderse considerando la composición química diferente de la ferrita en ambos grados dúplex. El menor contenido de Mo, elemento alfágeno, del grado S32304 HW (**P1**, Tabla 1) explica por qué la ferrita en este material se corroe durante las pruebas (**P1**, Fig. 7), mientras que el grado S32205 HW es totalmente inmune durante las pruebas.

Por otro lado, para el grado dúplex S32001 HW, se observa la corrosión preferencial de la austenita (**P1**, Fig. 8), en las soluciones con cloruros no carbonatadas y carbonatadas. En el acero S32001 HW, no sólo el contenido de Mo se reduce, sino también el contenido de Cr y Ni son menores que en el acero S32304 HW (**P1,** Tabla 1). El Cr es un elemento alfágeno y el Ni es gammágeno, por lo que se puede suponer que en ambas fases del grado S32001 HW se reduce su resistencia a la corrosión en comparación con el grado S32304 HW. Sin embargo, los resultados demuestran que la reducción en el contenido de Ni, es mucho más significativo que la reducción del contenido de Cr, por lo

cual se ha detectado la corrosión selectiva de la austenita en el acero S32001 HW. Además, el Mn, que es un elemento de aleación con efecto perjudicial sobre la resistencia a la corrosión, se añade al grado S32001 HW. El papel del Mn en la estabilidad de la fase es complejo, pero se supone que actúa como un elemento gammágeno a estas concentraciones. La presencia de Mn en la austenita contribuye a justificar la corrosión selectiva observada en los dúplex S32001 HW y S32304 HW.

La corrosión selectiva de las fases y la microestructura deformada en la zona de las corrugas explican la forma irregular de las picaduras en los aceros inoxidables dúplex de baja aleación (**P1**, Fig. 9a). Cuando los picaduras aparecen en las corrugas que son las regiones fuertemente deformadas, a menudo crecen en forma semi-paralelas a la superficie, siguiendo las características de la microestructura local (**P1**, Fig. 9b). Su fácil repasivación puede estar relacionado con la forma abierta de estas picaduras (**P1**, Fig. 1a).

El segundo aspecto evaluado en medio alcalino fue la influencia del proceso en el conformado de los aceros. Este aspecto se ha evaluado desde dos puntos de vista: la deformación superficial que sufren las corrugas durante el conformado, y el efecto de conformar el acero en frío o en caliente. Las publicaciones 2 y 3 recogen los resultados de este estudio, en medios alcalinos carbonatados y sin carbonatar con cloruros.

La diferencia entre la corruga y el centro en las propiedades mecánicas se pueden ver en la (Fig.1 de **P2**). Las corrugas son siempre mucho más duras que el centro de las barras. Las mayores diferencias se observaron entre el centro y la corrugas en los diferentes grados HW. Las diferencias locales con respecto al comportamiento mecánico en las diferentes áreas de las barras corrugadas se pueden explicar por las diferencias observadas entre las microestructuras de las corrugas y los centros. Las corrugas siempre tienen menor tamaño de grano que el centro (**P2**, Tabla 3). Esto conduce a una menor dureza en el centro que en la superficie de las barras. Los grados austeníticos HW tienen menor tamaño de grano que los CW. Este tamaño de grano más pequeño que explica el mayor limite elástico de las barras HW, a pesar de ser procesado a alta temperatura (**P2**, Tabla 2). Por otra parte, se observó una notable diferencia entre los tamaños de grano de las barras de austeníticos y dúplex. Estas diferencias se trasladan, como es obvio a la resistencia a la corrosión.

En la Fig. 6 de **P2**, se pueden observar que las diferencias en las curvas de polarización anódica del acero inoxidable austenítico S30403 CW y HW. En disoluciones

no carbonatadas, en el caso S30403 CW se observa un área pasiva bien definida. Una vez superado el E_{pit}, la intensidad de corriente aumenta muy rápidamente. Sin embargo, en los grados austeníticos HW, la corrosión parece comenzar a un menor sobrepotencial anódico y los aumentos en la intensidad de la corrosión después del inicio del ataque son más leves que en los grados austeníticos CW. La Fig. 7 de la **P2** muestra que para llegar a intensidades de corriente en torno a 5 $\mu A/cm^2$, que caracterizan a la corrosión activa, el sobrepotencial anódico que presentan los grados CW es mayor que en los grados HW para un mismo tipo austenítico. Esto quiere decir, es más probable que comience el ataque corrosivo en los grados HW que en los grados CW en medios agresivos.

La morfología del ataque es diferente entre CW y HW. La polarización de los austeníticos CW en medios con cloruros, en soluciones tanto carbonatadas y no carbonatadas, da lugar a la aparición de picaduras globulares en la superficie de barras (**P2**, Fig. 11a). Las picaduras tienden a aparecer en la zona de las corrugas, que se caracterizan por tener una mayor concentración de tensiones (**P2**, Fig. 1). La morfología de ataque que prevalece en el austenítico HW son picaduras muy pequeñas (**P2**, Fig. 11b), numerosas y bien distribuidas en aquellas zonas con mayor deformación mecánica (**P2**, Fig. 2d). Este tipo de morfología explica la forma de la curva observada para los grados HW (**P2**, Fig. 6), donde la rotura capa pasiva no conduce a un fuerte crecimiento de la intensidad, a diferencia de lo que ocurre con los grados de CW. El estudio morfológico de los ataques confirma que para los grados HW, donde la corrosión se desarrolla a un menor sobrepotencial anódico, el ataque tiende a adoptar un mecanismo menos agresivo. El mayor peligro de la corrosión localizada vs generalizada se vuelve particularmente relevante cuando se trata de refuerzos de hormigón. Los esfuerzos de tracción creados en el hormigón por la corrosión localizada de los refuerzos son mucho más peligrosos que las tensiones creadas por la corrosión uniforme. Las presiones para provocar el agrietamiento de la capa de hormigón, en ausencia de condiciones uniformes de corrosión han demostrado ser mucho menor que en la corrosión uniforme.

Por otro lado, las diferencias de comportamiento entre centro y corruga quedan patentes. La diferente microestructura entre el centro y la corruga es clara, así como sus propiedades mecánicas (**P2**, Tabla 3, Figs. 1 y 2). La resistencia a la corrosión en el centro de los aceros austeníticos es mayor (**P2**, Fig. 9), las zonas pasivas son mayores y los valores de potencial de picadura también. Esto mismo aparece en los aceros dúplex de baja aleación (**P3**, Fig. 1). La formación de las corrugas conlleva que estas tengan un E_{pit}

menores que los del centro de las barras, tanto en medios carbonatados como sin carbonatar (**P3**, Figs. 2 y 3); incluso en algunas condiciones, los núcleos no se corroen mientras que las corrugas sí. La menor resistencia a la corrosión de la superficie corrugada del acero inoxidable se explica por tener una microestructura más deformada y una mayor concentración de tensiones en las corrugas que el encontrado en el centro de las barras (**P1**, Tabla 2, y **P2**, Tabla 2).

La marcada diferencia entre los valores del E_{pit}, correspondiente a la superficie corrugada y al centro de la barra, hace hincapié en el efecto de los parámetros del proceso del conformado. Sería arriesgado extrapolar los resultados del comportamiento en hormigón de los aceros inoxidables procesados de forma diferente al de las barras corrugadas, a pesar de que a menudo se ha hecho en la literatura.

Es destacable mencionar que el centro de la barra del dúplex S32304 HW ha demostrado ser inmune a la corrosión durante las pruebas de polarización llevadas a cabo con diferentes contenidos de NaCl en la solución carbonatada. Sin embargo, durante la polarización de las superficies corrugadas el grado S32304 HW en presencia de cloruros, se detecta un aumento en la corriente, lo que corresponde a un ataque corrosivo, incluso con 0,5 % de NaCl.

El dúplex de baja aleación S32001 HW y en el austenítico S30403 CW y HW presentan siempre corrosión localizada en las soluciones carbonatadas con cloruros. Se puede observar también en la Fig. 2 de **P3**, que en todos los materiales el E_{pit} de la superficie corrugada es mucho más bajo que el E_{pit} del centro de una barra y como era de esperar, en todos los casos se observa que un aumento en el contenido de cloruro en la solución, provoca una disminución en la resistencia a la corrosión localizada, es decir, una disminución en el E_{pit}.

En la Fig. 3 de **P3**, se resumieron gráficamente los valores del E_{pit} en las soluciones no carbonatadas. Se puede observar que, con un pH más alto, es más difícil que ocurra la corrosión durante los ensayos. En las soluciones sin cloruros, no se produce corrosión en ninguno de los casos y el centro del dúplex S32304 HW mostró ser inmune a la corrosión en las pruebas realizadas con diferentes contenidos de cloruros, como se informó para pH ~ 9. Tampoco ocurre corrosión durante la polarización en los centros de las barras de los demás aceros estudiados en las soluciones con un 0,5% NaCl.

Este comportamiento también se puede obtener a partir de la i_{max} alcanzada durante las curvas de polarización (Fig. 4, **P3**). Todas las curvas están programadas para invertir el barrido de potencial cuando se alcanza una intensidad de corriente de 10^{-4} A/cm^2. Cuando no se produce corrosión, la corriente disminuye rápidamente cuando empieza a disminuir el potencial.

Cuando se forman picaduras durante la polarización anódica, la corriente todavía aumenta a medida que el potencial comienza a disminuir debido al importante efecto autocatalítico de la corrosión localizada. Cuanta más alta es la i_{max}, más peligrosa es la morfología de las picaduras. Como un ejemplo, se representan en la Fig. 4 de **P3**, los valores de este parámetro obtenidos en el dúplex S32001 HW. Se puede observar que las muestras en el centro de la barra, aunque son menos susceptibles a la corrosión que las superficies corrugadas, sufren un ataque más agresivo que cuando se produce en la superficie. Se llega a la misma conclusión para los resultados obtenidos en los otros tres materiales estudiados.

Una observación en la morfología de las picaduras después de las curvas de polarización confirma la idea deducida a partir de los valores de la i_{max}. Como se puede observar en la Fig. 5 de **P3**, la polarización provoca picaduras pequeñas y poco profundas, ampliamente distribuidas en las regiones más deformadas de la superficie de la corruga. En el centro de la barra, las polarizaciones causan picaduras mucho más grandes y que pueden ser mucho más peligrosas.

4.2 ENSAYOS EN MEDIO ÁCIDO

El objetivo de este apartado era evaluar el comportamiento de los aceros inoxidables corrugados frente a acidificaciones puntuales que pudieran ocurrir en el hormigón, haciendo hincapié en el efecto de la microestructura. El resultado de esta investigación en medio ácido se ha discutido en tres publicaciones:

Publicación 4: P4

S.M. Alvarez, A. Bautista, F. Velasco, "*Influence of strain-induced martensite in the anodic dissolution of austenitic stainless steels in acid medium*", Corrosion Science, vol.

69, p. 130-138, 2013. Índice de impacto: 3,615 (2 de 75 – 1er cuartil, datos de 2012). Área: Metallurgy and Metallurgical Engineering.

Publicación 5: P5

A. Bautista, S.M. Alvarez, F. Velasco, "*Selective corrosion of duplex stainless steel bars in acid. Part 1: effect of the composition, microstructure and anodic polarizations*", Materials and Corrosion, aceptado. DOI: 10.1002/maco.201307419. Índice de impacto: 1,208 (17 de 76 – 1er cuartil, datos de 2012). Área: Metallurgy and Metallurgical Engineering.

Publicación 6: P6

A. Bautista, S.M. Alvarez, F. Velasco, "*Selective corrosion of duplex stainless steel bars in acid. Part 2: effect of the surface strain and numerical analysis*", Materials and Corrosion, aceptado. DOI: 10.1002/maco.201307420. Índice de impacto: 1,208 (17 de 76 – 1er cuartil, datos de 2012). Área: Metallurgy and Metallurgical Engineering.

Teniendo en cuenta la composición química de los aceros inoxidables, se podría esperar una microestructura completamente austenítica en los aceros austeníticos (**P4**, Tabla 1) o austenita–ferrita en los aceros dúplex (**P5**, Tabla 1). Sin embargo, el proceso de conformado puede provocar la formación de martensita en ambos tipos de aceros. Esto se ha comprobado mediante difracción de rayos X (**P4**, Fig. 2) y mediciones magnéticas (**P4**, Fig. 3) para los aceros austeníticos, y microestructuralmente para los aceros dúplex (**P5**, Fig. 1).

La influencia del conformado en la cantidad de martensita formada puede ser difícil de predecir. La tendencia a la formación de la martensita se ha ligado, para los aceros inoxidables austeníticos, con la energía de defecto de apilamiento, inferior para el acero S30403 que para el S31603, por lo que el S30403 es más propenso a la precipitación de martensita inducida. Además, se esperaba que la cantidad de martensita fuera más baja cuando el proceso de conformado se lleva a cabo a una temperatura superior y, obviamente, el HW se produce a una temperatura más alta que el CW. Teniendo estos criterios en cuenta, las barras del CW de una composición dada deben tener más martensita inducida por deformación que las barras del HW. Esto ocurre para el S30403 CW, pero no para el S31603 CW (**P4**, Figs. 2 y 3). Además de la temperatura,

otro parámetro importante para determinar la precipitación de martensita es la cantidad de deformación. La alta resistencia a la tracción del S31603 HW (**P4**, Tabla 2) sugiere que esta barra puede haber sido sometida a un proceso de conformado más fuerte.

Para los aceros dúplex, la formación de martensita en la austenita también es función de la deformación plástica. Para todos los materiales, la presencia de martensita es mayor en las regiones cercanas a la superficie que en el centro de las barras. Esto es fácil de entender teniendo en cuenta que las superficies siempre han sufrido una mayor deformación plástica. En la literatura se han propuesto diferentes parámetros para estimar la susceptibilidad a la formación de martensita inducida por deformación en función de la composición, siendo el más importante la temperatura M_D (30/50). El M_D (30/50) mide la temperatura a la que se produce el 50% de martensita después de deformación verdadera del 30% en condiciones de tracción.

Los valores más altos de este parámetro implican una formación más fácil de martensita. Hay diferentes expresiones propuestas para calcular M_D (30/50). Todas las expresiones se han propuesto para aceros inoxidables austeníticos puros y cuando se aplican a los DSS pueden aparecer algunas imprecisiones. Sin embargo, pueden ser útiles de una forma cualitativa. En este trabajo se han calculado utilizando dos enfoques. Por una parte, se ha utilizado el procedimiento habitual de considerar los datos de la composición de los DSS (**P5**, Tabla 1). Por otro lado, se ha utilizado la composición de la austenita (**P5**, Tabla 2). En la Fig. 2 de **P5**, se muestran los datos obtenidos de M_D (30/50) para los cuatro aceros dúplex estudiados. Todos los datos sugieren que la tendencia en la formación de la martensita disminuye como sigue: S32001>S32304>S32205. Por lo tanto, la composición química de los DSS puede ser capaz de explicar, al menos en parte, las diferencias en la cantidad de martensita que se han encontrado en las barras estudiadas. Los DSS de baja aleación, a causa de su composición, son más propensos a formar martensita cuando son conformados. Otro punto relevante de los resultados de la Fig. 2 de **P5**, es que se aprecia más claramente esta tendencia al emplear la composición química de la austenita. Es esencialmente debido al marcado carácter gammágeno del N. Los resultados son consistentes con las microestructuras en la Fig. 1 de la **P5**.

La resistencia a corrosión en medio ácido se midió en todos los materiales mediante curvas de polarización anódica. Todas ellas muestran la típica forma de pico de activación y posterior generación de una capa pasiva. En el caso de los aceros austeníticos

(**P4**, Fig. 1), la curva del acero S31603 CW muestra un solo pico de activación, mientras que para los otros tres materiales estudiados aparecen dos picos. En los aceros dúplex se encuentran curvas anódicas con uno o dos picos. Así, los núcleos de las barras presentan claramente dos picos de activación excepto el acero S32001 HW (**P5**, Fig. 7), mientras que, al analizar las corrugas, solo el acero S32205 HW y CW mantienen los dos picos de activación (**P6**, Fig. 2).

Con el objetivo de identificar los fenómenos que causan los diferentes picos en las curvas, se llevan a cabo pruebas potenciostáticas a potenciales anódicos significativos dentro de la región de activación y en E_{corr}. El estudio del grado S30403 CW (**P4**, Fig. 4) muestra que, a bajos sobrepotenciales anódicos cerca del E_{corr}, tiene lugar una disolución anódica selectiva (**P4**, Fig. 4a). La disolución electroquímica afecta bandas alternadas que se producen dentro de los granos austeníticos con diferentes orientaciones (**P4**, Fig. 4b), y parece lógico suponer que la martensita inducida por deformación es la fase que se disuelve en esta condición.

Cuando se aplica un aumento en el sobrepotencial anódico, se observan cambios en la morfología del ataque (**P4**, Fig. 4c). Las condiciones también se vuelven agresivas para la austenita y todo el material metálico se disuelve, llevándose a cabo un ataque generalizado con una morfología bastante ondulada, que no tiene ninguna relación aparente con la microestructura de la barra. Estos resultados son consistentes con los dos picos de activación que aparecen en las curvas de polarización anódica (Fig. 1, **P4**).

El otro acero austenítico deformado en frío (S31603 CW) presenta un solo pico en la región de activación (**P4**, Fig. 1). La morfología del ataque a polarizaciones bajas y altas (**P4**, Figs. 5a y 5b), coincide con la esperada para un acero inoxidable austenítico puro en medio ácido. Sin embargo, un estudio muy detallado mediante SEM pone de manifiesto (**P4**, Fig. 5c) un ataque selectivo en algunos puntos de la superficie polarizada a pequeños sobrepotenciales anódicos. Sin tener en cuenta la intensidad del ataque, su morfología podría parecerse a la observada en el S30403 CW (**P4**, Figs. 4a y b). Este hecho parece indicar que la martensita podría estar presente en la microestructura del S31603 CW, aunque en una cantidad que está por debajo de los límites de detecciones mediante difracción de rayos X, de las mediciones magnéticas y que no es capaz de revelarse claramente con un doble pico de activación.

En los aceros austeníticos deformados en caliente, el ataque selectivo es similar, aunque su observación es más compleja debido a su reducido tamaño de grano (**P4**, Tabla 2). A bajos sobrepotenciales anódicos, las superficies ensayadas exhiben pequeñas ondulaciones irregulares (**P4**, Fig. 6a), con ataques puntuales en la superficie (**P4**, Fig. 7a). Este fenómeno parece ser dependiente de la microestructura. A altas sobrepolarizaciones (**P4**, Fig. 6b y 7b), la morfología de la superficie se asemeja a la observada cuando los grados CW sufren un ataque general (**P4**, Figs. 4c y 5b), es decir, en esta región de potencial los materiales se someten a un proceso de disolución anódica sin ninguna influencia evidente de la microestructura. Parece lógico suponer que esta disolución anódica selectiva está relacionada con la presencia de martensita inducida por deformación. Además el acero S31603 HW muestra la presencia adicional de numerosas picaduras, cuyo progreso parece estar claramente relacionado con la forma del grano, ocurriendo disolución selectiva del grano. Cuanto mayor sea la localización de la martensita inducida por deformación en las barras del S31603 HW podría explicar el progreso del ataque localizado, incluso en los potenciales donde también se está disolviendo la austenita.

La microestructura de los DSS también determina el desarrollo del ataque de corrosión. Cuando las muestras son expuestas a la disolución de ensayo HCl + H_2SO_4 por diferentes periodos de tiempo, se puede observar que, para todos los DSS, el principal mecanismo de ataque es la disolución de la ferrita. Este fenómeno ha sido claramente observado para los grados S32304 HW y S32205 HW (**P5**, Figs. 4b y 4c). Para el grado de baja aleación S32001 HW (**P5**, Fig. 4a), el comportamiento de la corrosión entre la ferrita y la austenita es muy similar, aunque se puede intuir que la austenita presenta una resistencia a la corrosión un poco más alta.

Por otra parte, también se ha obtenido información sobre el comportamiento de corrosión de la martensita inducida por deformación. En la Fig. 4c de **P5**, se muestra que la martensita en el S32205 HW es más resistente a la corrosión que la ferrita. A pesar de la duración de la exposición, se observa martensita sin corroer. Además cuando los grados S32001 HW y S32304 HW están expuestos en el medio ácido durante un tiempo corto, se puede observar que la martensita no se ha corroído (marcado con elipses blancas, **P5**, Fig. 5), mientras que la ferrita sí se ha disuelto. Estos resultados demuestran que la martensita presente en los DSS estudiados es más resistente a la corrosión que la ferrita en el E_{corr}. Por lo tanto, el ataque a este pH estaría controlado principalmente por la

velocidad de disolución de la ferrita, a pesar de la formación de martensita durante el proceso de conformado. Desde un punto de vista práctico, estos resultados sugieren que no hay ningún efecto perjudicial relevante que se pueda esperar a partir de la precipitación de martensita durante el conformado, a diferencia de lo que ocurre en los aceros inoxidables austeníticos puros.

Por otro lado, cuando la exposición en la solución se extiende, y la ferrita ha desaparecido por completo, la martensita puede empezar a disolverse preferentemente, como se ve en el S32304 HW (**P5**, Fig. 6a). Este resultado demuestra que la resistencia a la corrosión de la martensita es inferior a la resistencia a la corrosión de la austenita, como se esperaba.

En los aceros dúplex también se han llevado a cabo pruebas potenciostáticas en diferentes potenciales en la región de activación. A sobrepotenciales anódicos bajos, coincidentes con el primer pico de activación, se puede observar un fenómeno similar al observado en E_{corr} (**P5**, Fig. 8), pero tiene lugar una mayor velocidad de disolución. En el S32001 HW se puede ver que la ferrita se corroe selectivamente en estas condiciones, pero la austenita en este material presenta una tendencia también a disolverse. La disolución de la austenita es insignificante en estas condiciones para los grados más aleados. La martensita (marcada con elipses blancas en la **P5**, Figs. 8a y 8c) demuestra otra vez tener una mayor resistencia a la corrosión que la ferrita. También está claro que la estabilidad de la martensita en estas polarizaciones es ligeramente menor que la de austenita pura, se puede ver como en algunas zonas hay disolución de la martensita.

A altas polarizaciones anódicas se observa una corrosión selectiva de la austenita para todos los DSS (**P5**, Fig. 9), mientras que la ferrita se mantiene casi sin ataque, especialmente para los grados del S32205 HW. Las pruebas potenciostáticas demuestran que la corrosión selectiva de la austenita también se produce en el S32001 HW (**P5**, Fig. 9a), a pesar de que no pueda verse la doble estructura del pico de activación en la curva de polarización (**P5**, Fig. 7). Estos resultados confirman que, para todos los grados estudiados, el pico a sobrepotenciales más bajos se asocia con la disolución preferencial de la ferrita, mientras que la austenita se corroe preferentemente a sobrepotenciales más altos. La martensita se disuelve completamente en las mismas condiciones que la austenita (**P5**, Fig. 9).

A altas polarizaciones, se puede detectar a veces durante un efecto galvánico entre las fases. Para el S32304 HW y el S32205 HW (**P5**, Figs. 9b y c), las flechas negras marcan la regiones en las que se corroe la austenita en los límites de grano a una velocidad más alta. Esto es debido a la micro-pila galvánica formada entre los granos continuos de la austenita y la ferrita, que tienen un comportamiento más noble en estas condiciones. Para el S32205 CW (**P5**, Fig. 9d), el fenómeno es menos visible debido al menor tamaño de grano, pero también tiende a ocurrir. Sin embargo, no se observa acoplamiento galvánico para el S32001 HW (**P5**, Fig. 9a), lo que concuerda con el alto solapamiento de los picos entre la austenita y la ferrita en la curva de polarización anódica.

Los aceros inoxidables dúplex presentan nitruros de titanio (identificados como TiN por EDS) en su microestructura (**P5**, Fig. 1e). El número y tamaño de los precipitados de los TiN son más pequeños en las barras del dúplex S32001 HW que en los otros grados DSS, probablemente debido al menor contenido de Ti y/o el contenido de N del grado S32001 HW (**P5**, Tabla 1). Después de varios días de exposición a E_{corr}, los TiN también tienden a disolverse (**P5**, Fig. 6b). Son claramente más estables que la ferrita, pero menos que la austenita, en los grados S32304 HW y S32205 HW. Para el S32001 HW, el número de precipitados de TiN es muy bajo, pero presentan una velocidad de disolución más baja que la ferrita y la austenita. Las polarizaciones anódicas (**P5**, Fig. 10) no muestran disolución de estos precipitados. Desde un punto de vista práctico, se puede concluir que los precipitados de TiN en los DSS no serían la fase más propensa a la corrosión donde el ataque en medio ácido se iniciaría, aunque a largo plazo, los TiN pueden tener una mayor tendencia a la disolución que la austenita en los grados S32304 HW y S32205 HW y CW.

En el caso de los aceros dúplex, también se estudió la superficie de las barras, que tiene mayor dureza (**P6**, Fig. 9) al sufrir una mayor deformación durante el conformado. Si bien no todas las curvas de polarización anódicas de la superficie tienen dos picos de activación (**P6**, Fig. 2), los ensayos potenciostáticos muestran, inicialmente, resultados similares al centro. A bajos sobrepotenciales, se corroe selectivamente la ferrita en todos los aceros (**P6**, Figs. 4a, 4b y 5). A altos sobrepotenciales sí que se aprecian diferencias. Para los aceros S32205 HW y CW, se corroe la austenita (**P6**, Figs. 4c y 4d). Sin embargo, a potenciales anódicos más altos, es fácil ver que hay regiones en las superficies del S32001 HW y del S32304 HW donde existe una clara corrosión preferencial de la

ferrita (**P6**, Fig. 6 y 7). Al mismo tiempo, las regiones de la superficie de estos dos DSS de baja aleación donde se corroe preferentemente la austenita también existen. Se comprobó que la austenita se disuelve en las regiones menos deformadas de la superficie y que la ferrita se disuelve en las regiones más deformadas.

Los fenómenos mixtos que ocurren en la superficie del S32001 HW y del S32304 HW a altas polarizaciones anódicas dentro de las regiones activas, explica por qué el pico de la ferrita se superpone marcadamente sobre el pico de la austenita (**P6**, Fig. 3b). Es bien conocido que los cambios microestructurales causados durante el conformado tienden a reducir la resistencia a la corrosión de los metales. Estos resultados sugieren que la ferrita es más sensible a la deformación que la austenita y por lo tanto la resistencia a la corrosión de la fase ferrítica en los DSS disminuye en mayor grado. Estas pruebas experimentales se pueden entender teniendo en cuenta las características cristalográficas de ambas fases. La estructura cúbica centrada en el cuerpo de la ferrita es menos dúctil que la estructura cúbica centrada en la cara de la austenita. La microestructura austenítica tiene más planos de deslizamiento, que probablemente conduce a menos defectos microestructurales que puedan aparecer durante el proceso de conformado. Como una primera aproximación, se puede suponer que cuanto mayor es el número de defectos microestructurales, menor sería la resistencia a la corrosión.

Además, en la superficie de las barras, se demuestra de nuevo que la martensita es más resistente a la corrosión que la ferrita en polarizaciones anódicas bajas y que presenta un comportamiento frente a la corrosión cercano a la austenita. La martensita se disuelve a potenciales próximos al E_{corr} a un ritmo muy lento donde la velocidad de corrosión de la austenita no es significativa (**P6**, Fig. 8).

A la vista de las curvas de polarización y el análisis microestructural, se utilizó un software especialmente diseñado para ver la contribución de la disolución de la martensita en los inoxidables austeníticos y de la ferrita y la austenita en los dúplex. En estos últimos, la inclusión de un tercer pico y tratar de distinguir entre el comportamiento de la austenita y la martensita implicaría un gran riesgo, por lo que la disolución relativa de la martensita está incluido en la curva de la austenita. Por otra parte, está claro que los picos de austenita se hacen claramente asimétricos y desarrollan una cola hacia bajos potenciales en las curvas de las muestras en las que se ha detectado más martensita en la microestructura. Así, esta cola (**P6**, Fig. 3b) debe estar relacionada con la martensita y

contribuir al pico de la austenita. La deconvolución matemática de las curvas permite separar los fenómenos tanto en los aceros austeníticos (**P4**, Fig. 9) como en los dúplex (**P6**, Fig. 3), tanto cuando hay dos picos de activación (S32205 CW, **P6**, Fig. 3a) como cuando no los hay (S32001 HW, **P6**, Fig. 3b). En este caso, la estructura de doble pico de la región no es visible, pero la forma de la curva no puede ser simulada por un solo pico. Este proceso permite calcular densidades de carga, intensidades máximas de cada pico, y potenciales a los que aparecen los picos. Los valores de densidad de carga se obtienen a partir del área bajo las curvas correspondientes. Este parámetro puede ser considerado como la forma más precisa de la evaluación de la intensidad relativa de los dos tipos de ataque en los diferentes materiales. La región total de la activación implica densidades de carga más altas, causadas por la disolución general del material de las barras.

En los aceros austeníticos, la disolución selectiva de la martensita implica densidades de carga más bajas que el ataque general de la superficie (**P4**, Fig. 10). Esto es debido a la menor cantidad de material que reacciona durante este tipo de ataque durante la corrosión en los potenciales más altos. Se observa que los rangos de pico se encuentran entre 0,18 y 0,27 en relación de las áreas del pico de la corrosión de la martensita y la corrosión general de la austenita. Estos valores son mucho más altos que los que se podrían predecir a partir de la simple cantidad de martensita en la microestructura de cada material (**P4**, Fig. 3). La velocidad de corrosión más alta de la martensita en comparación con la austenita es la responsable de la significativa contribución de esta fase para el proceso de corrosión, a pesar de su reducida presencia en la microestructura.

Las densidades de carga son más altas en los grados del S30403 que para los grados del S31603 (**P4**, Fig. 10). Este resultado probablemente está influenciado por el contenido de martensita en la microestructura (**P4**, Fig. 3). Sin embargo, es importante señalar que la distribución de la martensita en la microestructura, no sólo su cantidad, influye en el proceso de corrosión. Los grados HW, con un tamaño de grano más pequeño que los grados CW parecen ser más propensos a desarrollar ataques más agresivos.

El análisis de los valores i_{max} (**P4**, Fig. 11), es menos sensible para detectar diferencias entre los materiales que el área de los picos (**P4**, Fig. 10). Las áreas de los picos exhiben claramente una proporcionalidad directa con la cantidad de especies disueltas a través de los diferentes mecanismos durante las polarizaciones anódicas,

mientras que la relación entre la magnitud de la disolución anódica y la i_{max} se puede enmascarar parcialmente cuando se producen fenómenos complejos, como en este caso.

El E_{corr} de la barra (**P4**, Fig. 12) disminuye a medida que aumenta la cantidad de martensita en las barras. El mismo fenómeno se puede ver para el E_{max} correspondiente al pico de la martensita (**P4**, Fig. 12). Estos datos confirman que el valor del E_{corr} depende de las características electroquímicas y la relativa abundancia de la fase menos resistente a la corrosión en los aceros inoxidables. Como el E_{corr} es un potencial mixto cuyo valor se rige por el equilibrio más rápido, estos resultados sugieren que el ataque de la martensita es el proceso anódico más rápido que tiene lugar en estos medios ácidos en ausencia de polarizaciones. Estos resultados también sugieren que en un medio ácido más concentrado, donde la semireacción catódica se trasladaría a los valores de potenciales más altos, el equilibrio podría establecerse a valores más altos del E_{corr}, donde el ataque general sería el proceso anódico más rápido. Por otra parte para la disolución de la austenita (**P4**, Fig. 12), el E_{max} sigue siendo constante para todos los materiales estudiados, independientemente de la composición y el proceso de conformado.

En los aceros dúplex, como era de esperar, los valores en la densidad de carga en los DSS de baja aleación (**P6**, Fig. 9) es superior en ambas fases, más que los grados del S32205. Al tener un menor grado de aleación, el comportamiento de corrosión de todas las fases es peor. Esto es debido al carácter gammágeno o alfágeno de los elementos de aleación que se distribuyen, de una manera más o menos desequilibrada, entre ferrita y austenita, determinando diferencias entre los grados, por lo que los elementos de aleación afectan la resistencia a la corrosión de las dos fases.

La relación entre las densidades de carga de los picos puede ser utilizada como un indicador de la relación de la resistencia a la corrosión de las fases. En la **P6**, Fig. 9a, se puede ver que, para los grados del S32205 y S32304 HW, la ferrita tiene una mayor contribución en la región de la corrosión activa que la austenita. El menor contenido de Mo (elemento alfágeno) en el grado del S32304 HW puede haber causado una aumento relativo de la velocidad de corrosión de la ferrita. Sin embargo, teniendo en cuenta que la corrosión de la martensita está incluida en la austenita y a la mayor tendencia del grado S32304 HW para formar martensita que los grados del S32205 HW y CW, se puede concluir, que la corrosión de la martensita ha equilibrado el efecto de la ausencia de Mo en la relación de densidad de carga de las fases. Por otro lado, para la barra de S32001

HW, se encuentra una mayor contribución de corrosión de la austenita en la región activa. En este caso, el efecto de la mayor cantidad de martensita inducida por deformación así como el contenido más bajo en la aleación de elementos gammágenos resistentes a la corrosión pueden fácilmente explicar este hecho.

Podría ser un poco extraño, observar que las superficies de los grados del S32205 HW y CW (**P6**, Fig. 9b) presenten valores más bajos en las densidades de carga asociados a la corrosión de la austenita y la ferrita que en el centro (**P6**, Fig. 9a). Este hecho se puede explicar teniendo encuenta la alta anisotropía de los granos (alargados en la dirección paralela a la superficie expuesta) y a la manera en que progresa la corrosión en los DSS. Para un DSS, el ataque se inicia en la fase menos resistente a la corrosión y, si hay diferencia significativa entre la resistencia a la corrosión de ferrita y austenita, la fase más resistente a la corrosión dificulta la progreso del ataque.

Cuando se estudian las secciones transversales de las barras, el ataque penetra en la misma dirección alargada de los granos (**P6**, Figs. 7b, 7c y 8b). Si el ataque corrosivo profundiza fácilmente en el material a través de la fase menos resistente a la corrosión, la fase más resistente a la corrosión sería apenas capaz de ralentizar el ataque corrosivo, ya que esta queda expuesta y su disolución se puede aumentar un poco. Por lo tanto, la interacción entre la microestructura, la composición química, y las tensiones, pueden conducir a resultados muy diferentes en cuanto al comportamiento de la corrosión de los DSS.

Cuando se calculan los resultados de densidad de carga en la superficie de las barras de los DSS con bajo contenido en Mo (**P6**, Fig. 9b), se puede observar que la ferrita aumenta significativamente su contribución a la región activa. El aumento en la carga asociada a la corrosión de la ferrita es coherente con las observaciones acerca de la corrosión selectiva de las fases en la superficie a altas polarizaciones (**P6**, Figs. 6 y 7). El aumento en la densidad de carga correspondiente a la corrosión de la austenita debe analizarse teniendo en cuenta el aumento en la velocidad de corrosión de la austenita debido a la tensión y a la mayor cantidad de martensita inducida por deformación en la superficie, como se comentó en la **P5**.

En la **P6**, Fig. 10, se puede observar que el E_{corr} es sensible a las composiciones de los DSS. Su valor disminuye a medida que disminuye el grado de aleación, llegando a ser más activo. Sin embargo, los valores del E_{corr} parecen ser bastante independiente del nivel

de deformación de las muestras. El E_{max} correspondiente a la corrosión activa tanto de la ferrita y la austenita, presentan valores relativamente similares para todas las pruebas realizadas en el estudio de los DSS (**P6**, Fig. 10a). Al comparar las muestras de las barras del grado S32205 HW y CW de la superficie de las barras (**P6**, Fig. 10b) con las muestras del centro, el pico del E_{max} de la ferrita y la austenita no cambian de manera significativa sus valores, pero en los DSS de baja aleación se desplazan fuertemente hacia valores más anódicos. Esto significa que el aumento en la densidad de carga de los picos debidos a la deformación se asocia con una expansión en la región de corrosión activa hacia mayores potenciales. El aumento del E_{max} de la austenita y la tendencia de la martensita a disolverse lentamente a potenciales ligeramente más cercanos al E_{corr}, explican la asimetría de los picos, tales como los de la contribución austenita + martensita en la (**P6**, Fig. 3b).

Por otra parte, cuando se comparan para cada material los resultados obtenidos en la i_{max} de las fases, en el centro (**P6**, Fig. 11a) o para las superficies con tensión (**P6**, Fig. 11b), se puede observar que las barras del S32205 HW y CW presentan valores inferiores cuando se consideran las muestras de la superficie. Sin embargo, para el S32304 HW y el S32001 HW, la tendencia observada es justo lo contrario. Esta tendencia coincide con la densidad de carga (**P6**, Fig. 9). Sin embargo, debe recordarse que los valores de la i_{max} son un indicador mucho menos sensible que la densidad de carga, sobre el efecto de las deformaciones en el comportamiento a la corrosión.

En cuanto a la intensidad de pasivación (i_{pass}) medida durante las polarizaciones, no se observan diferencias significativas entre materiales (**P6**, Fig. 11a), por lo que la composición química de los DSS no es un parámetro clave para la determinación de los valores de la i_{pass}. Los resultados interesantes se obtienen cuando los valores de la i_{pass} en el centro (**P6**, Fig. 11a) se comparan con los resultados de la superficie (**P6**, Fig. 11b). Para los DSS de baja aleación, la i_{pass} de la superficie es claramente superior que en el centro de los mismos materiales. Este hecho no ha sido previamente observado para materiales similares cuando se han ensayado en medios mucho menos agresivos, con valores de pH más altos. Con los resultados anteriores se puede concluir que la naturaleza de la película pasiva en los aceros inoxidables puede depender del nivel de deformación del material base. Se ha publicado que capas pasivas menos estequiométricas, menos protectoras, se forman en la superficie. En este caso, se puede llegar a la misma conclusión para las barras del S32304 HW y del S32001 HW. En las condiciones

estudiadas, las tensiones en la superficie de las barras de los DSS de baja aleación deben favorecer la generación de óxidos menos estequiométricos con menor capacidad de aislamiento. Eso explicaría los altos valores de la i_{pass} observados en las superficies que aquellos hallados para el centro de las barras. Los resultados presentados en este trabajo muestran que los valores de la deformación que limitan el predominio del efecto de la textura sobre el efecto de la cantidad de defectos son altamente depende de la composición química del material. Por tanto en las barras del S32205, no se detecta ningún aumento en la i_{pass} cuando la superficie se compara con el centro.

4.3 ENSAYOS EN HORMIGÓN

El objetivo de este apartado era estudiar el comportamiento electroquímico de los aceros inoxidables corrugados incrustados en el mortero, que han sido expuestos a ambientes muy agresivos durante 9 años. El resultado de esta investigación en medio ácido se ha discutido en dos publicaciones que han sido enviados a publicación.

Nota: En esta investigación se analizó el comportamiento frente a la corrosión y su influencia en la composición química, la microestructura y las propiedades mecánicas de las barras de acero inoxidables estudiadas mediante varias técnicas electroquímicas. Sin embargo, cabe señalar que es un trabajo de varios miembros del grupo de investigación. Por tanto, la caracterización de los resultados obtenidos mediante EIS realizada al comportamiento electroquímico de la superficie corrugada embebida en el mortero, no se discutirán en esta Tesis Doctoral.

Publicación 7: P7

A. Bautista, S.M. Alvarez, E.C. Paredes, F. Velasco, "*Corrosion performance of stainless steels corrugated bars after 9 years of exposure. Part I: Non-carbonated, chloride-contaminated mortar*", Enviado a Corrosion Science.

Publicación 8: P8

A. Bautista, S.M. Alvarez, E.C. Paredes, F. Velasco, S. Guzmán, "*Corrosion performance of stainless steels corrugated bars after 9 years of exposure. Part II: carbonated mortars with and without chlorides*", Enviado a Corrosion Science.

La norma ASTM C876 sugiere un criterio para determinar la probabilidad de corrosión de las barras corrugadas que se han incluido en las figuras de E_{corr} de **P7** (medios sin carbonatar) y **P8** (medios carbonatados). Se puede ver en la Figs. 3 y 4 de **P7** que los valores del E_{corr} monitorizados en las barras de acero al carbono corrugadas en mortero, después de sólo 3 meses en condiciones de inmersión parcial, son muy bajos. Estos valores (<-426 mV vs SCE) son típicos de un ataque severo de corrosión y en el laboratorio se ha comprobado que estas muestras se agrietaron completamente después de 6-8 meses de pruebas. En el caso de los medios carbonatados (Figs. 1 a 3, **P8**), los aceros al carbono también han presentado condiciones activas durante toda la exposición.

Los aceros inoxidables, por el contrario, han estado mayoritariamente en estado pasivo. En el caso de morteros carbonatados expuestos a alta humedad (Fig. 1, **P8**), los resultados de E_{corr} muestran que los aceros inoxidables permanecen en estado pasivo cuando no hay cloruros. Cuando los cloruros se añaden durante la fabricación del mortero, los aceros inoxidables tampoco muestran signos de corrosión, ni en mortero sin carbonatar (Fig. 4, **P7**) ni carbonatado (Fig. 3, **P8**).

Solo en el caso de los morteros sometidos a inmersión parcial se han detectado algunos casos de corrosión. En medios sin carbonatar, todos los aceros han tendido a permanecer en la región en la que el riesgo de corrosión es inferior al 10% (Fig. 3, **P7**), con algún valor aleatorio en la región con riesgo intermedio de corrosión. Solo para el acero austenítico de baja aleación S20430 se puede observar una evolución significativa del E_{corr} durante el último año de la exposición cuando el mortero sin carbonatar se ha expuesto a inmersión parcial (Fig. 3, **P7**). El E_{corr} de este material exhibe valores correspondientes a un alto riesgo de corrosión. Aunque esta relación entre E_{corr} y las condiciones de corrosión no ha sido validado específicamente para aceros inoxidables, estos resultados sugieren un excelente rendimiento para la mayoría de los aceros inoxidables probados (especialmente teniendo en cuenta que la resistividad del mortero no puede enmascarar el ataque debido a su humedad). Es decir, todos los inoxidables, excepto un material en una condición, son capaces de mantener su pasividad en medios sin carbonatar.

Cuando el mortero carbonatado se sumerge parcialmente en agua salada (Fig. 2, **P8**), el acero S20430 vuelve a mostrar una caída importante del E_{corr} a zonas de actividad, pero en este caso tras solo 3 años de exposición, lo que muestra la mayor agresividad de

esta condición (inmersión parcial más carbonatada). El acero S30400 también ha presentado valores de E_{corr} en la zona intermedia de corrosión, aunque al final recupera valores propios de la pasividad. Estos resultados son coherentes con el hecho de que la inmersión parcial es una condición especialmente agresiva si la concentración de cloruros en los poros han alcanzado un valor crítico en la superficie de la armadura. Además, se pueden formar celdas de aireación diferencial, al tener el oxigeno diferentes accesos entre la zona sumergida y la expuesta al aire, favoreciendo la localización de ánodos, en la zona sumergida de las barras corrugadas.

Además, los datos medidos sobre la concentración de cloruros evaluados al final de la exposición, (Fig. 5, **P7**; Fig. 4, **P8**) contribuyen a comprender los diferentes comportamientos. La concentración de cloruro en las muestras en las que se ha añadido el ion despasivante durante la fabricación del mortero, se mantiene constante en todas las regiones de las muestras. Este nivel de cloruro (en relación con el peso del mortero) puede ser comparable, por ejemplo, con las que se encuentran (en relación con el peso de cemento) a 7-8 cm de la superficie de la región no sumergida de una estructura expuesta de 60 años en un ambiente marino tropical. Los cloruros añadidos se pueden unir física y químicamente al mortero durante su fraguado, por lo que se reduce su riesgo de provocar picaduras, como se ha comprobado en los datos de E_{corr}.

Cuando los cloruros entran desde el exterior, se produce un gradiente, que la larga exposición (9 años) ha anulado. En morteros sin carbonatar, el nivel de cloruros (Fig. 5, **P7**) alcanza valores mayores, y ha promovido la corrosión del acero S20430. En morteros carbonatados, menos poros, la difusión ha sido menor (Fig. 4, **P8**), por lo que el efecto combinado de pH y cloruros (junto a la aireación diferencial), ha sido el desencadenante de la corrosión.

A los 8 años de la exposición de las probetas reforzadas con acero inoxidable fueron sometidos a pruebas de polarización anódica para obtener información acerca de la calidad de la capa pasiva en estas condiciones y cómo la resistencia a la picadura del acero inoxidable se ha modificado. A partir de experimentos tales como los que se muestran en la Fig. 2 de **P7**, se pueden obtener los datos típicos a las curvas de polarización (**P7**, Fig. 12; **P8**, Fig. 10), observándose en algunas de las barras de los aceros inoxidables, que la polarización anódica causa un ataque por picaduras en la superficie corrugada.

Para comparar las curvas de polarización de los materiales, se han utilizado los valores de potencial necesarias para llegar a una densidad de corriente de 2 x 10^{-6} A/cm^2 (**P7**, Fig. 13; **P8**, Fig. 11). Este valor es típico para la velocidad de corrosión de refuerzos de acero al carbono en las condiciones de exposición considerados en el estudio, y está dentro del rango de las densidades de corriente habituales utilizados para definir el potencial de picadura o para comparar el comportamiento frente a la corrosión de los refuerzos de acero inoxidable.

Hay que destacar el excelente comportamiento del acero S32205 en todas las condiciones, sin haber mostrado corrosión en ningún caso. La alta resistencia a la corrosión se puede entender teniendo en cuenta la naturaleza protectora de la capa pasiva formada sobre este grado en medios alcalinos. Para condiciones muy agresivas, el S32205 es una opción mucho más interesante que el S31603, algo más barato y mucho más resistente a la corrosión.

Después de las pruebas de polarización, es claro que las muestras en inmersión parcial son mucho más propensas a desarrollar la corrosión por picadura que las muestras expuestas a alta humedad relativa. En morteros sin carbonatar con cloruros añadidos, o en morteros carbonatados sin cloruros, los aceros S30400 y S31603 no muestran corrosión (los potenciales corresponden a la reacción de desprendimiento de oxigeno), y los otros aceros austeníticos requieren muy altos sobrepotenciales para provocar la corrosión, por lo que todos los aceros pueden asegurar la durabilidad en estructuras bajo esas condiciones. La inmersión parcial, tanto en mortero sin carbonatar como carbonatado, es capaz de provocar corrosión en todos los aceros austeníticos y en particular en el S20430.

Después de las polarizaciones realizadas, las muestras analizadas permanecieron un año más en inmersión parcial y en alta humedad relativa, manteniendo las condiciones previas, con el fin de permitir el desarrollo o repasivasion de las picaduras. Entonces, las muestras de mortero fueron rotas para permitir la observación visual de los refuerzos. No se observaron picaduras en el S32205 estudiado en ninguna condición de exposición, ni en el S30400 y S31603 en las condiciones en los que se alcanzaba el potencial de descomposición del agua, lo que es coherente con esta hipótesis.

Por otra parte, el ataque corrosivo en el S31635 en medio sin carbonatar (donde la polarización había causado la corrosión, como sugeriría el resultado en la **P7**, Fig. 13) no se pueden confirmar picaduras mediante observaciones con el SEM. Estos datos sugieren

un cierto grado de capacidad del S31635 a repasivarse o limitar el ataque cuando se exponen los morteros en un medio sin carbonatar contaminado con cloruros.

En el S30400 expuesto en inmersión parcial se pueden observan numerosas picaduras redondeadas, la mayoría de ellas con una ubicación claramente relacionada con las regiones más deformadas de la superficie de la barra tanto en medios sin carbonatar (**P7**, Fig. 14b) como carbonatados (P8, Fig. 13).

En las barras S31603 y S31635 expuestas en inmersión parcial, la morfología del ataque es diferente. Las picaduras son irregulares y de poca profundidad y su ubicación no parece estar relacionada con las corrugas u otras zonas deformadas en la superficie de las barras tanto en medios sin carbonatar (**P7**, Fig. 14c) como carbonatadas (**P8**, Fig. 13b), aunque en este ultimo parece existir una cierta relación con las zonas más deformadas. Esta morfología de corrosión parece menos peligrosa que la observada para los refuerzos austeníticos con bajo contenido de Mo. Sin embargo, la diferencia no puede ser debida a la composición química de los aceros inoxidables. El nivel de deformación inferior de estas barras en comparación con el S30400 ensayado, puede explicar fácilmente este hecho.

El acero S20430 si que muestra picaduras en todas las condiciones. En medios sin carbonatar, las picaduras irregulares y grandes (**P7**, Fig. 14a), cuando el mortero ha sufrido inmersión parcial y son más aisladas y redondeadas (**P7**, Fig. 14d) en alta humedad relativa. En medios carbonatados (**P8**, Fig. 12), las picaduras tienden a ser redondeadas en la barra y menos geométricas en las corrugas para todas las condiciones.

Capítulo V

Publicaciones

5.1 PUBLICACION 1: P1

S.M. Alvarez, A. Bautista, F. Velasco.

"*Corrosion behaviour of corrugated lean duplex stainless steels in simulated concrete pore solutions*".

Corrosion Science, vol. 53, p. 1748-1755, 2011.

Corrosion Science 53 (2011) 1748–1755

Contents lists available at ScienceDirect

Corrosion Science

journal homepage: www.elsevier.com/locate/corsci

Corrosion behaviour of corrugated lean duplex stainless steels in simulated concrete pore solutions

S.M. Alvarez, A. Bautista *, F. Velasco

Material Science and Engineering Department – I.A.A.B., Universidad Carlos III de Madrid, Leganés, Madrid, Spain

ARTICLE INFO

Article history:
Received 29 October 2010
Accepted 24 January 2011
Available online 4 February 2011

Keywords:
A. Stainless steel
A. Steel reinforced concrete
B. Polarization
C. Pitting corrosion

ABSTRACT

This work studies the corrosion behaviour of two corrugated lean duplex stainless steels (SAF 2001 and 2304 grades) in eight alkaline solutions (carbonated and non-carbonated, saturated $Ca(OH)_2$ solutions with different chloride contents). 2001 stainless steel is a new grade in market because of its composition. 2304 is a grade previously studied under different conditions. However, its use as reinforcement in concrete is new. Studies are carried out by polarization curves following scanning electronic microscopy (SEM) and optical observations. Results are compared to those of carbon steel and austenitic AISI 304 and duplex SAF 2205 under similar conditions. After corrosion tests in alkaline media with chloride, ferrite tends to corrode selectively in 2304 duplex, while austenite corrodes selectively in 2001 under the same conditions. The influence of the duplex microstructure on attack development and morphology is analyzed. The electrochemical parameters obtained from the polarization curves suggest 2001 could replace 304 keeping the structure its corrosion performance (and with clear economical advantages). 2304 shows better corrosion behaviour than the more expensive 304, but somewhat lower than the excellent behaviour shown by 2205.

1. Introduction

Stainless steel is sometimes used as reinforcement in the most critical areas of reinforced concrete structures (such as tidal zones in partially-submerged structures or external areas in bridges) to guarantee their durability. A stainless steel amount of 5–10% total volume of the structure is enough to assure appropriate performance in highly-aggressive environments [1]. Previous studies rule out risks of galvanic pairs between stainless and carbon steels in concrete [2] and evaluate the structural implications of welding stainless steel [3,4].

The use of stainless steel reinforcement rises the initial price of the works between 5% and 15%, depending to a large extent on the selected stainless steel grade [5]. However, they have been proven a profitable alternative to cathodic protection in aggressive environments in the long term [6].

The corrosion resistance of many stainless steels in the atmosphere and many other environments is well-known, but the special features of concrete (pH, Na^+, Ca^{2+}, differential aeration, etc.) introduce factors which affect passive layer structure. These factors must be analyzed prior to recommending their use as reinforcements. For example, research on the surface of austenitic stainless steels in solutions simulating that contained in concrete pores has proven the particular passive layers generated in this environment [7–10].

Although, in practice the large-scale use of stainless steel rebars began only a few years ago, AISI 304 steel in concrete in highly-aggressive environments has offered a good performance for more than 8 decades [11]. There are long-term laboratory studies that show clearly positive results about the corrosion performance of austenitic stainless steels [12–14]. Negative results can also be found in the literature, but they are probably related to a non-adequate processing of the bars [15]. It can be considered that the performance of austenitic stainless steel such as AISI 304 and 316 grades in concrete has been widely studied. [8,10,16,17]. The use of duplex stainless steels SAF 2205 grade (somewhat more expensive than 304 austenitic grades) has been a very interesting option for the market in last years, given its excellent corrosion resistance in concrete, better than austenitic [18].

Volatility of Ni price – together with the lower corrosion resistance of low-Ni, high-Mn stainless steels [19] – has focused interest in the development of low alloy duplex steels (generally low Ni or Mo contents) [20,21], cheaper than 2205 duplex. Those lean, low alloyed duplex steels are aimed at replacing austenitic steels (such as 304 or 316) in multiple applications.

SAF 2304 duplex stainless steel, one of those selected in this study, has low Mo-content and has been known for years. Its use has grown up in desalinization industries, marine applications or production processes since 2003, thus displacing austenitic 316.

* Corresponding author.
E-mail address: mbautist@ing.uc3m.es (A. Bautista).

0010-938X/$ - see front matter © 2011 Elsevier Ltd. All rights reserved.
doi:10.1016/j.corsci.2011.01.050

However, there is scarce scientific information regarding its corrosion performance. Besides, it often focuses on environmental conditions highly different from those usually found in reinforcement of structures [22–24].

SAF 2001 is a duplex stainless grade, lower alloyed than 2304, containing less Ni and Cr (i.e., cheaper). Its corrosion performance should generally be lower than other highly-alloyed duplex grades, but can be enough to assure the durability of concrete structures (duplex steels outstand in this kind of environments). This is a very novel grade, and very scarce references can be found regarding the corrosion performance of a very close grade, 2101 [25], with a slightly higher Cr content. XPS analysis shows that the passive film formed on this lean duplex in H_2SO_4 is Cr^{3+}-richer than that formed on 316 [26]. There are also some studies on other non-standardized duplex grades with high Mn–N content [26,27]. Although there are exclusively-mechanical studies on the possible use of the 2101 or similar grades in civil engineering [28,29], no information on the corrosion performance of those lean duplex grades in alkaline media (such as concrete) was found.

Despite market volatility, the use of lean duplex reinforcements may involve important saving opportunities relative to more traditional stainless steels. The use of 2304 reinforcements, instead of traditional 304, may allow 9% savings on stainless steel costs. Compared to a more traditional duplex grade such as 2205, 2304 steel may be 15% cheaper. Manufacturers of stainless reinforcements have recently estimated that 2001 rebars are 15% cheaper than 304.

2. Experimental procedures

Corrugated bars of three different duplex stainless steels were used in this study: 2304 and 2001 (used as reinforcements for the first time) and traditional 2205. The austenitic 304 type is also included, as the new lean corrugated stainless steels could be proposed as economically-advantageous replacements of traditional 304 corrugated bars. Moreover, corrugated carbon steel bars were also studied for comparison purposes.

The diameter and chemical composition of these four corrugated stainless steels is shown in Table 1. The main difference between 2304 and 2205 duplex grades is the lower Mo content in the first, which makes it more economical, but potentially less corrosion-resistant. 2001 does not only have a very reduced amount of Mo, but also less Ni and more Mn than any other stainless steel grade considered in the study.

The corrosion behaviour of the materials was studied in saturated $Ca(OH)_2$ solutions using cyclic polarization curves. Fresh, non-carbonated solutions (pH ≈12.6) were used to simulate, aged, non-carbonated concrete pore solutions. This solution has been extensively used by numerous authors to study the corrosion behaviour of reinforced metals in non-carbonated media. Higher pHs, typical of fresh concretes – when no lixiviation of cations such as K^+ or Na^+ has taken place – have not been included in this study. Solutions in which the pH had been reduced to about 9 by bubbling 10% CO_2-enriched air were used to simulate carbonated concrete. With this process, a CO_3^{2-}/HCO_3^- buffer solution is obtained, reproducing the chemical reaction that takes place in the concrete during carbonation, and avoiding the need of adding other chemical compounds than can hardly be found in the pore solution of aged concrete exposed to aggressive environments. The bubbling was carried out at very slow rate, just before the immersion of the corrugated bars in the solutions. The pH of the solution was continuously monitorized during the tests to check that an undesirable reaction with the atmospheric CO_2 has not modified the testing conditions. Four different amounts of NaCl were added (without NaCl and with 0.5%, 1% and 5% (w/w)) to both types of solutions (carbonated and non-carbonated) to test the effect of chloride contamination.

Electrochemical measurements were carried out after 48 h of exposure of the reinforcement to the test solution, to reach complete stabilization of the corrosion potential (E_{corr}). Two centimeters long reinforcement regions with the cross section polished to 320 acted as working electrodes. Saturated calomel electrode (SCE) and an AISI 316 stainless steel mesh were used as reference electrode and counter-electrode, respectively. The polarization started at cathodic potentials and the potential value was increased monotonously. The sweeping rate of the potential was 0.17 mV/s, following the advice of the ASTM G61 standard. The current limit for reversing the sign of the potential sweep was 10^{-4} A/cm^2. The reversal sweep ended at the E_{corr}. The multiplicity of the measurements (3–4) assures the reliability of the results. The E_{corr} values considered in the work have been obtained from these curves as well as the corrosion rates (i_{corr}). For the calculation of this last parameter the Tafel procedure has been used. The pitting potential (E_{pit}) has been identified as the anodic potential where a sharp current increase can be observed. It has been always born in mind that E_{pit} must be lower than the potential value corresponding to the oxygen evolution reaction at the pH of the testing solution. Moreover, it has always been identified for current values between 0.5 and 1×10^{-5} A/cm^2, to avoid interferences with other electrochemical processes different form pitting corrosion that can also occurs during anodic polarization.

Metallographical samples of the studied materials were prepared. The etching solutions were Bloech and Wedl reagent for duplex stainless steels and aqua regia for the austenitic grade. The grain size of the stainless steels was measured following the ASTM E112 standard. The morphology of the attack after the corrosion test and the influence of the microstructure on its development were studied by optical microscopy using cross-sectional views. The study of the distribution of the attack on the surface of the corrugated bars was completed with scanning electronic microscopy (SEM) observations to take advantage of the greater depth of focus of this technique.

3. Results and discussion

Some of the polarization curves corresponding to both new corrugated duplex stainless steels in carbonated and non-carbonated, saturated $Ca(OH)_2$ solutions are shown in Figs. 1 and 2. Neither Fig. 1 nor Fig. 2 includes the results corresponding to 1% NaCl solutions. Their behaviour in these solutions is always intermedi-

Table 1
Chemical compositions and nominal diameter of the corrugated steels considered in the study.

Corrugated material	∅ (mm)	Chemical composition (% w/w)							
		C	S	Si	Mn	Cr	Ni	Mo	N
Stainless steel 2205	20	0.020	0.003	0.39	1.77	22.47	4.88	3.500	0.177
Stainless steel 2304	16	0.017	0.002	0.65	1.54	22.70	4.46	0.259	0.153
Stainless steel 2001	16	0.025	0.001	0.68	4.14	19.98	1.78	0.238	0.124
Stainless steel304L	16	0.026	0.001	0.30	1.42	18.37	9.74	0.275	0.055
Black steel B500	10	0.19	0.022	0.10	0.62	0.07	0.02	–	0.005

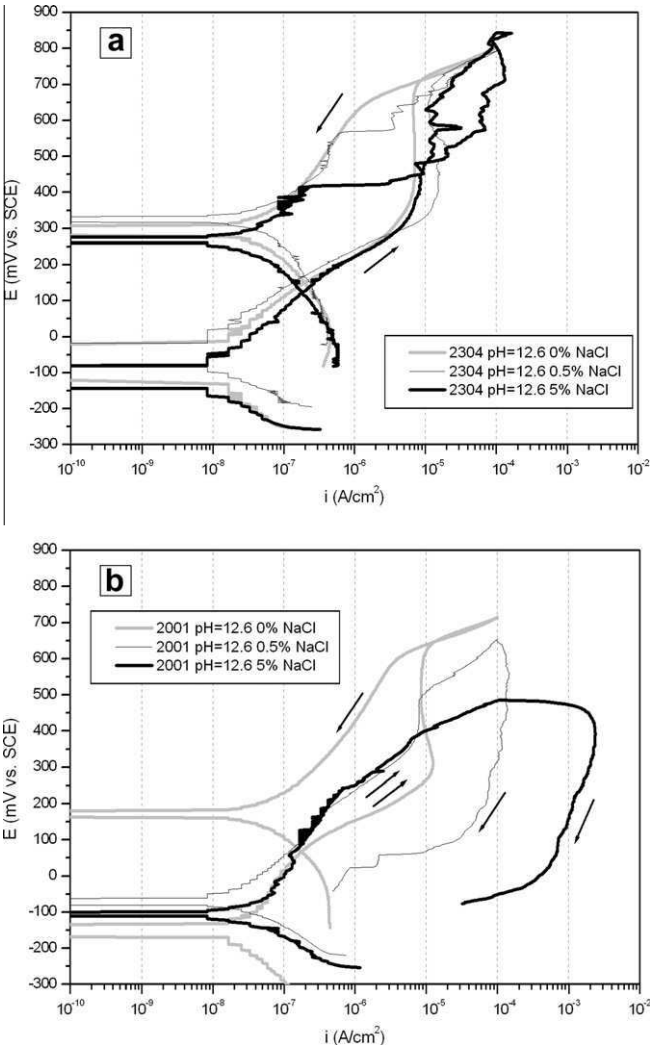

Fig. 1. Examples of the polarization curves of lean duplex in non-carbonated, saturated $Ca(OH)_2$ solutions (a) 2304 and (b) 2001.

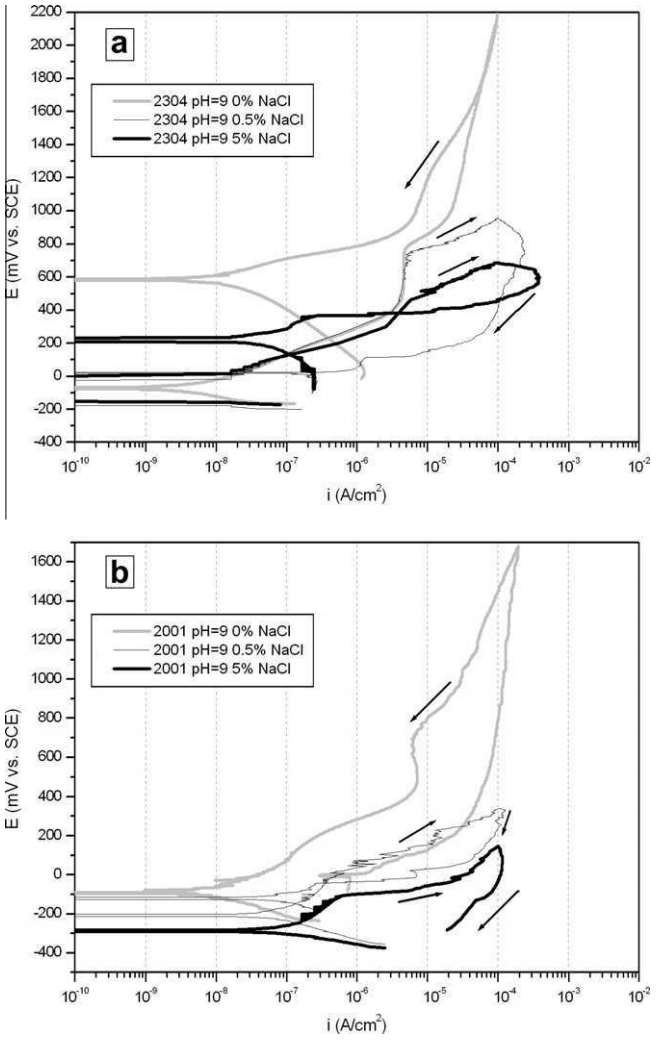

Fig. 2. Examples of the polarization curves of lean duplex in carbonated, saturated $Ca(OH)_2$ solutions (a) 2304 and (b) 2001.

ate between that in 0.5% and 5% NaCl solutions. However, including all concentrations in these graphs may make them confusing.

In non-carbonated solutions all curves correspond to passive materials with a wide passive region (Fig. 1). At pH 12.6 and in absence of chlorides, neither pitting nor any kind of meaningful corrosive attack corresponding to any of the tested materials was observed during the tests. However, the current increase observed at about 300 mV vs. SCE reveals that chromium oxide dissolution is taking place through the Reaction (1) when the material suffers high anodic polarizations:

$$Cr_2O_3 + 10OH^- \rightarrow 5H_2O + 2CrO_4^{2-} + 6e^- \qquad \text{(Reaction 1)}$$

This hypothesis is validated by the fact that similar current increases at this potential are observed in the curves of all stainless steels in saturated $Ca(OH)_2$ solutions without chlorides, but not in carbon steel bars testing. Other authors report this increase with chromium oxides' activity, in particular with transformation from Cr^{3+} to Cr^{6+} in both ferritic and austenitic stainless steels [30,31]. Moreover, thermodynamic analysis predicts the instability of Cr_2O_3 within this range of potentials [32]. The current densities due to the process described in Reaction (1) are around 10^{-5} A/cm^2 or below during the tests. Reaction (1) cannot be understood as a corrosion process, as there is no break of the passive layer and it does not imply base metal dissolution. However, the reaction suggests a possible decrease of protective ability of the passive layer when it is exposed at this potential range (the protective ability of the passive layers on stainless steels has been traditionally related with their Cr_2O_3 content [7]).

The current increases detected from 700 mV vs. SCE correspond to the oxygen evolution reaction:

$$4OH^- \rightarrow 2H_2O + O_2 + 4e^- \qquad \text{(Reaction 2)}$$

The potentials where the current increases take place and the shape of the curve (without the hysteresis loop typical from pitting corrosion) confirm that Reaction (2) occurs during the polarization curves in non-carbonated $Ca(OH)_2$ solutions without chlorides, but no corrosion of the corrugated lean duplex bars.

In non-carbonated solution with chlorides, 2304 suffers pitting at very high anodic overpotentials, close to those where oxygen evolution takes place (Fig. 1a). The attack is mainly noticed due to changes in the shape of the polarization curves (a hysteresis loop appears during the reverse scan). Pitting occurs after Reaction (1) takes place and the protective properties of the passive layer decrease and the passivity must be guaranteed (at least partially) by the Fe_3O_4 [7]. Hence, the material becomes more vulnerable to chloride attack. The increase of the chloride content in the solution hinders repassivation, as it can be observed by the increasing size of the hysteresis loop during the reverse potential scan with

NaCl concentration. Anyway, pits on 2304 under these pH conditions always repassivate easily, as protection potentials (E_{prot}) are always defined close to E_{pit}.

Lower alloyed 2001 duplex type in non-carbonated solutions with chlorides reveals higher susceptibility to pitting corrosion than 2304 (Fig. 1b). For 2001, the length of the passive regions clearly decreases with the increase in the chloride content of the solution. Pits formed on the 2001 type are not able to repassivate during the reverse scan of the polarization curves. Moreover, for solutions with higher NaCl concentrations, the current continues increasing at the beginning of the reverse loop, in spite of the decreasing potential values. This behaviour may prove the markedly-autocatalytic corrosion mechanism developed in these conditions.

At pH 9 (Fig. 2) in solutions without chlorides, both new duplex steels show an excellent behaviour. Cr_2O_3 activity takes place at potentials higher than those found at pH 12.6 in accordance with thermodynamic predictions [34]. Up to potentials of 600–700 mV vs. SCE, the shape of the curve is very similar to that detected in non-carbonated solutions without chlorides (Fig. 1). The differences at very high anodic overpotentials observed between the curves without chlorides are due to the pH and its influence on the Reaction (2).

Fig. 2a shows that, in carbonated solution, 2304 duplex develops pitting corrosion at high anodic overpotentials. E_{pit} decreases as the NaCl concentration of the testing solution increases. Metastable pitting is often observed at moderate anodic overpotentials, especially in solutions with high chloride content. In carbonated solutions, the repassivation of the attack on 2304 seems more difficult than in non-carbonated solutions (Fig. 1a), although the current behaviour for this material during the reverse scan seems to be mainly related with the E_{pit} values. Pitting at high polarizations usually implies higher currents during the reverse scan.

In curves corresponding to 2001 duplex type in carbonated solutions with chlorides, pitting attack appears without the need of reaching high anodic overpotentials (Fig. 2b). The influence of Reaction (1) cannot be observed in the curves. The determination of E_{pit} is often less objective in these conditions and the use of other parameters to evaluate the corrosion performance is advisable. The shape of the curves suggests an attack distributed in many small pits. This could be related with the fact that passive layers on stainless steel are less Cr_2O_3-rich at pH 9 than at pH 12.6. If the passive layers are weaker, they would probably break almost simultaneously in many points when they are polarized.

For a more complete understanding of their practical implications, the results of these new materials were compared to other more known reinforcements tested under the same conditions. Fig. 3 compares the i_{corr} and E_{corr} of the five corrugated materials considered in this study. In all tested conditions, the four studied stainless steels show i_{corr} and E_{corr} values characteristic of the passive state. No meaningful differences were detected among their i_{corr} and E_{corr} values. They reflect the normal dispersion in the experimental measurement of such a low i_{corr}, and the usual oscillations of the E_{corr} of passive metals. The presence of Cr_2O_3 together with the Fe_3O_4 in their passive layer [7,10] makes the i_{corr} of the stainless steels nearly one order of magnitude lower than the i_{corr} of the black steel when passive (i.e., the durability of black steel in non-carbonated solutions without chlorides is only granted by the presence of Fe_3O_4 on the surface). In other conditions considered aggressive for black steel, the measured i_{corr} are always about two orders of magnitude lower for stainless steels, and a difference of about of 500 mV was observed between the E_{corr} of the stainless steels and the carbon steel in all studied solutions. The differences between the i_{corr} of stainless steels and carbon steel increases as the aggressivity of the medium does.

In spite of the good behaviour of the stainless steels in alkaline media in presence of chlorides, the strength of the corrosion cells that appear in reinforced concrete due to the unavoidable heterogeneities of the concrete/reinforcement interface demands analysing the response of these different stainless steels under polarizations. This analysis can indicate if their corrosion resistances make these new grades adequate for being used instead of other better-known,

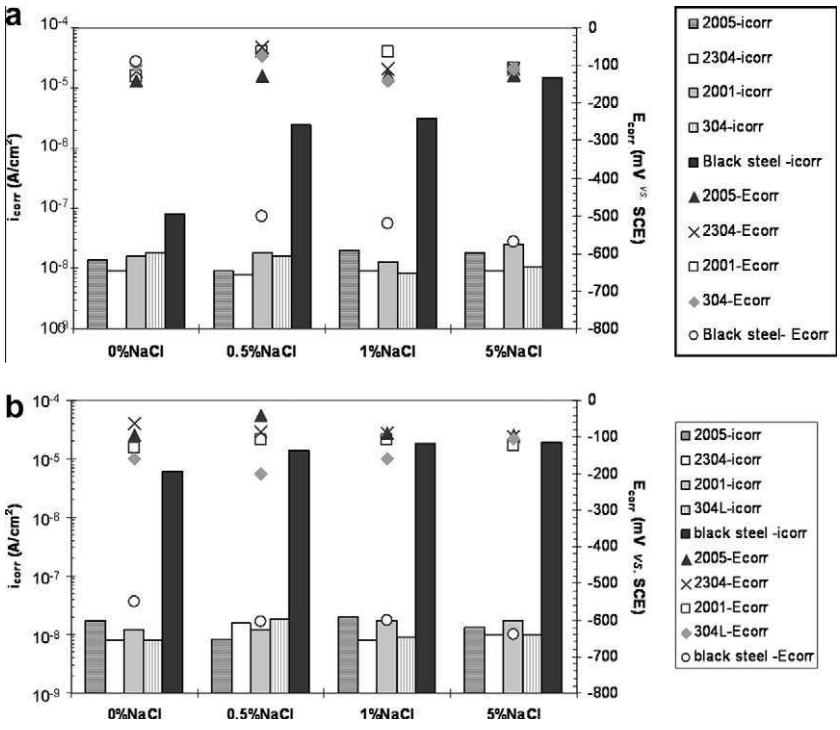

Fig. 3. i_{corr} and E_{corr} of the five corrugated materials in solutions with different chloride contents (a) pH 12.6 and (b) pH 9.

more expensive grades. For solutions with chlorides at pH 12.6, the parameter used to evaluate the stability of the passive state under polarizations is E_{pit}. As no meaningful differences were observed among the E_{corr} of the different stainless steels (Fig. 3a), the value of E_{pit} can be used directly to compare the corrosion resistance of the new lean duplex stainless steels with those of better-known stainless steel reinforcements such as 304 and 2205. The E_{pit} values obtained from the polarization curves are plotted in Fig. 4. For duplex 2205 stainless steel, the oxygen evolution (Reaction (1)) always appear before the E_{pit} could be reached, in spite of the low potential sweeping rate and the high chloride contents considered in this study. That is, for 2205 the curves in solutions with chlorides have similar shape to that of the curves in solutions without chlorides (the only effect of these aggressive ions that could be observed is some metastable pitting at high concentrations) [20]. For the other three corrugated stainless steels, E_{pit} decreases when the chloride content of the solution increases, as expected. 2001 shows very similar E_{pit} values to those of 304. Hence, it can be assumed that this new duplex – cheaper than austenitic 304 – may have an excellent pitting resistance in non-carbonated, chloride contaminated concrete, similar to that of austenitic 304 [11]. 2304 shows higher E_{pit} than that of 304 (i.e., the duplex grade is more resistant to localized corrosion and cheaper than the austenitic). The behaviour of 2304, intermediate between 2205 and 304, suggests that it can be a very interesting material for highly chloride-contaminated environments.

In carbonated concrete without chlorides, no risk of corrosion was observed when stainless steels reinforcements are used, and the curves in Fig. 2 are repeated for all stainless steels, regardless of their grade. The risk involved by the presence of carbonation and chlorides at the same time in the structure should be evaluated. This can be a very aggressive condition [21]. Although, in practice, higher chloride contents usually appears in structures exposed to marine environments, where relative humidity is high and carbonation is not favoured [33], the use of de-icing salts in urban environments may lead to this situation. With the aim of evaluating the risk involved by the strength of the cell formed on the concrete reinforcement interface for bar durability, the potentials necessary for reaching certain anodic current intensity are compared for new and traditional materials [21]. As it has been previously pointed out, the determination of E_{pit} in these conditions can be complicated. Fig. 5 shows an example for 1% NaCl carbonated solutions. The current values were chosen bearing in mind the current values at which E_{pit} are usually defined in non-carbonated solutions (between 5×10^{-6} and 10^{-5} A/cm^2) and the fact that,

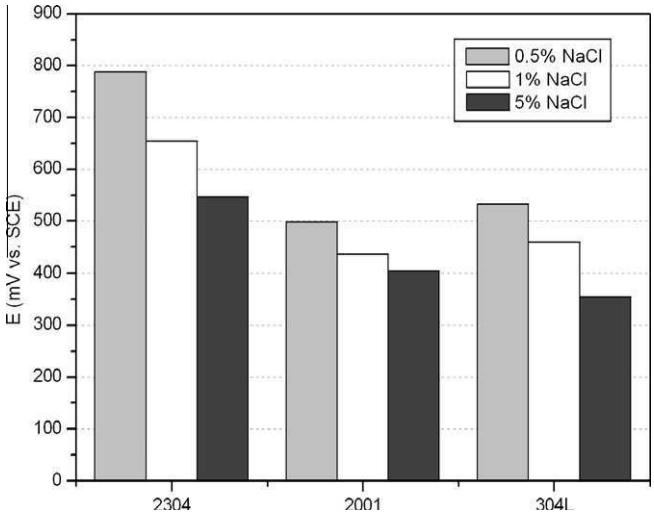

Fig. 4. E_{pit} values for the studied stainless steels that corrode during the tests in non-carbonated, saturated $Ca(OH)_2$ solutions with different Cl^- contents.

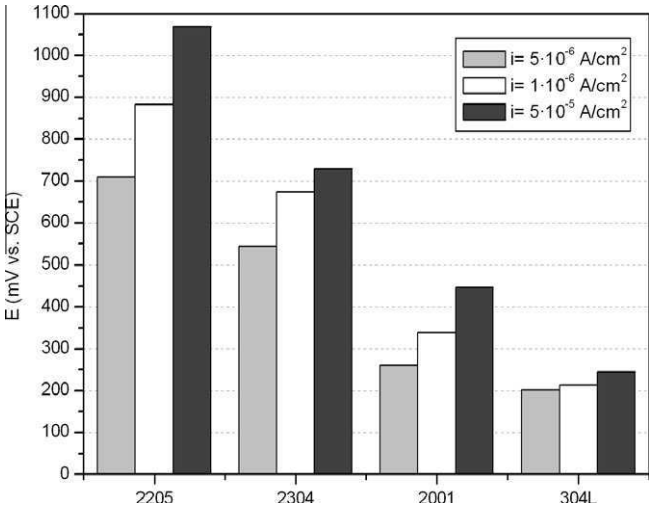

Fig. 5. Anodic potentials necessary to reach certain current densities for four studied stainless steels in carbonated, saturated $Ca(OH)_2$ solutions with 1% NaCl.

under 5×10^{-6} A/cm^2 (Fig. 2), data can be highly influenced by Reaction (1). Bearing in mind the E_{corr} values shown by reinforcements (Fig. 3b), 2205 and 2304 in carbonated solution with chlorides require very high anodic overpotentials to reach similar intensities to those considered in Fig. 5. However, it should be pointed that 2304 shows a somewhat worse behaviour than the higher-alloyed duplex. The strength of the corrosion cells needed for reaching 5×10^{-6} A/cm^2 is quite similar for 2001 and 304. 2001 requires as little higher polarizations to reach higher intensities and this difference seems to increase as the considered current value increases. This fact suggests a minor rate for the progress of the attack after its onset for the duplex 2001 type than in the austenitic type, which could be related to a less localized pitting attack in the duplex. It is well-known that the location of corrosion has always been considered a factor which clearly leads to increased dangerousness. The results obtained in carbonated solutions with 0.5% and 5% NaCl lead to similar conclusions.

Fig. 6 shows representative images of the morphology of the corrosive attack on austenitic 304 and duplex 2001 stainless steels after potentiodynamic tests. In non-carbonated media with identical chloride content, 304 and 2001 steels were polarized until very similar potential values, as show E_{pit} (Fig. 4) during the polarization test. This allows a meaningful comparison of their pit distribution. The austenitic stainless steel (Fig. 6a) shows very large pits when compared to those observed in lean duplex stainless (Fig. 6b), where pits are numerous but smaller. Moreover, pits in lean duplex always show irregular mouth shapes, in contrast to the circular pit mouths often observed in the tested austenitic material. Besides the pits, a more generalized attack in the corrugations and other especially susceptible regions can be detected on duplex stainless steel. This means that – although certain electrochemical parameters regarding corrosion susceptibility can be very similar for 2001 and 304 grades (Fig. 4) – the former material tends to develop the attack with a less dangerous morphology. The high ability shown by 2001 for reducing corrosion intensity during the reverse potential sweep (Fig. 2) is also coherent with a less localized attack where the autocatalytic effect caused by the corrosion products is usually more limited than inside deep pits or crevices.

At pH 9 (Fig. 6c and d), it can also be checked the tendency of lean duplex 2001 of distributing the attack in smaller, less dangerous pits than the austenitic 304. Moreover, 2001 has been submitted to higher polarization than 304 during corrosion tests (Fig. 5).

As it is well known, duplex stainless steels are formed by two phases (austenite and ferrite) with different corrosion resistances.

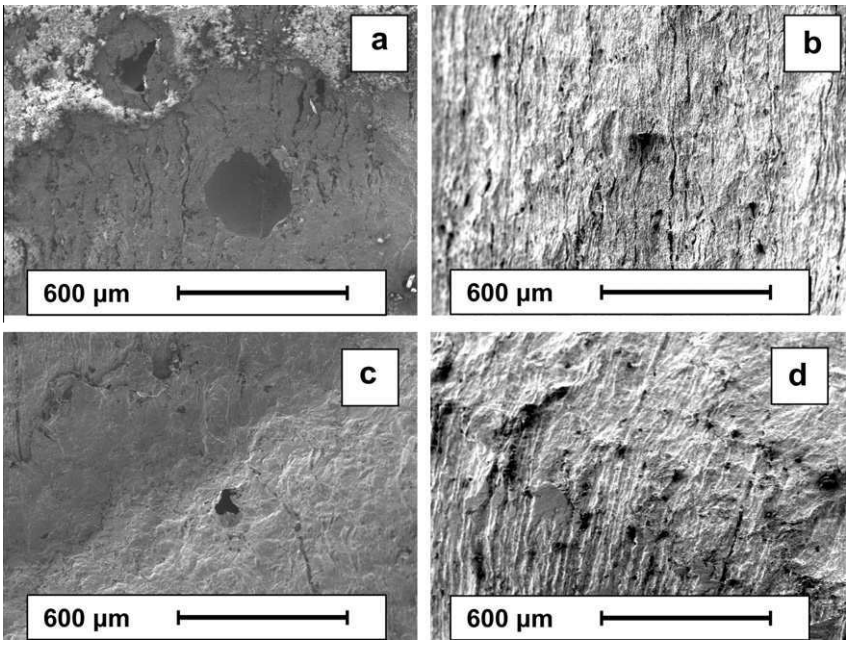

Fig. 6. Morphology of the attack after the polarization in solutions with chlorides: (a) austenitic 304 in non-carbonated medium, (b) duplex 2001 in non-carbonated medium austenitic (c) 304 in carbonated medium and (d) duplex 2001 in carbonated medium.

This means that corrosion starts in the weakest phase of the duplex stainless steel and preferential corrosion of one of the phases could probably take place. For instance, in chloride-containing neutral media, pits are reported to tend to appear in ferrite in 2001 [27,34] as well as in 2205 duplex [35]. However, higher corrosion resistance in either one or the other phase of the duplex depends on duplex composition. However, the use of parameters such as the pitting resistance equivalent number (PREN) calculated from the average chemical composition of both phases can be a too dangerous simplification to make theoretical estimations of the corrosion behaviour of duplex materials. This fact had been suggested previously by other authors [37]. Several studies attempt to explain the lower or higher corrosion resistance in the phases of duplex grades, calculating the PREN index for austenite and ferrite independently [27,36,37]. However, their success is limited by

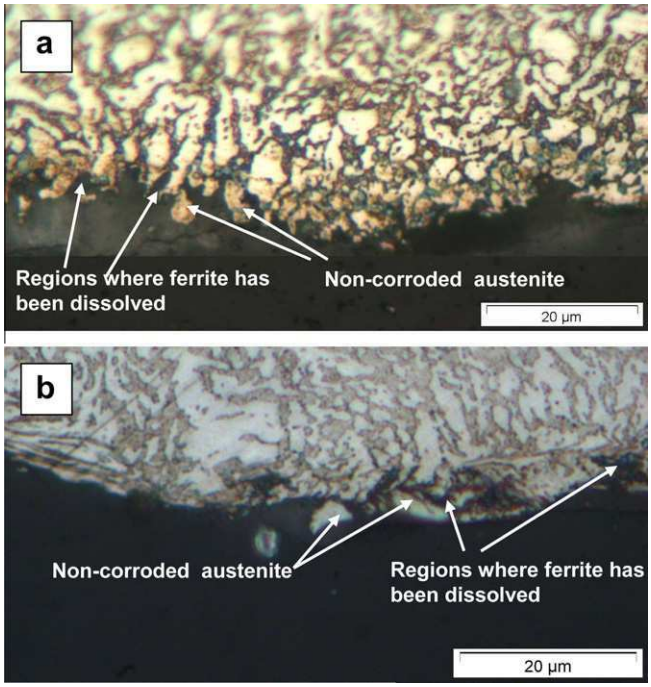

Fig. 7. Images showing the selective corrosion of the lean duplex 2304 after the polarization curves (a) in non-carbonated solution with chlorides and (b) in carbonated solution with chlorides. The metallographic attack has coloured ferrite phase in dark and austenite phase in light. (For interpretation of the references to color in this figure legend, the reader is referred to the web version of this article.)

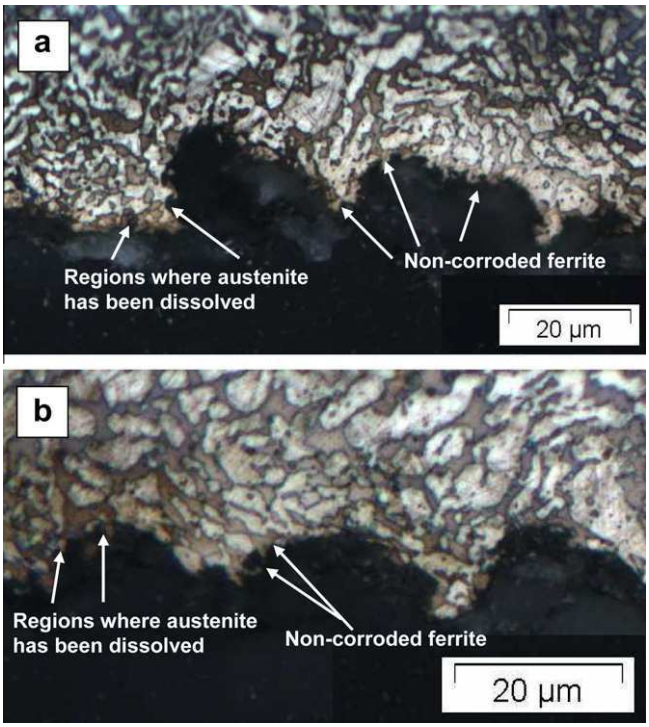

Fig. 8. Images showing the selective corrosion of the lean duplex 2001 after the polarization curves (a) in non-carbonated solution with chlorides and (b) in carbonated solution with chlorides. The metallographic attack has coloured ferrite phase in dark and austenite phase in light. (For interpretation of the references to color in this figure legend, the reader is referred to the web version of this article.)

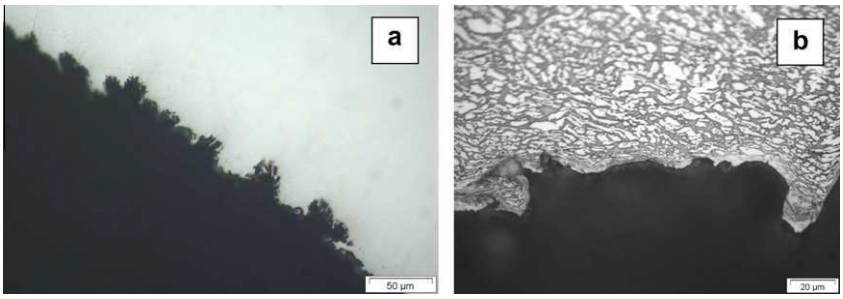

Fig. 9. Cross-sectional views of the morphology of the attack on lean duplex after polarization test in non-carbonated, chloride contaminated solutions (a) 2001 and (b) 2304.

Table 2
Grain size (µm) of the corrugated stainless steels considered in the study.

	2205	2304	2001	304L
Bulk material	4.9 ± 0.4	3.0 ± 0.2	3.6 ± 0.4	6.6 ± 0.7
Surface	2.3 ± 0.2	1.9 ± 0.1	2.3 ± 0.1	4.9 ± 0.9

the difficulty to know the exact composition of each phase, particularly the N content that has a very high weight in the PREN expression. Moreover, there are many factors besides the chemical compositions that influx corrosion behaviour which are not included in the calculation of the PREN index. For instance, for a given 2205 duplex in acid medium, the trend of selective corrosion of austenite or ferrite depends on the conditions of the aggressive environment [36,37]. This work evaluates and qualitatively explains the selective corrosion of the lean duplex from metallographic samples.

In duplex 2304, the extent of the attack after the polarization curves is limited. However, it has been detected a difference in the corrosion resistance of the phases that clearly determine the development of the corrosion process (Fig. 7). Cross-sectional views of the specimens tested in solutions with chlorides show that the ferrite (the continuous, dark-coloured phase) acts as the less corrosion-resistant phase. The progress of the attack is limited by the austenite (the discontinuous, light-coloured phase). This fact was verified at the different chloride contents considered in the study as it is independent from the carbonation or not of the $Ca(OH)_2$ solution. Bearing in mind the excellent behaviour of 2205 during the polarization test, the slightly worse behaviour of 2304 can be understood considering the different chemical composition of the ferrite in both duplex grades. The difference between 2205 and 2304 performances can be assumed to be due to their different Mo content (Table 1). Mo is a ferritizer element (i.e., it tends to be localized in the ferrite and therefore it mainly increases the corrosion resistance of this phase). The lower Mo content of 2304 explains why ferrite in this material corrodes during the tests (Fig. 7), while the whole material remains fully immune in 2205.

On the other hand, for 2001 duplex grade, chlorides are observed to cause the preferential corrosion of the austenite (discontinuous, light-coloured phase in Fig. 8) in non-carbonated and carbonated solutions. In 2001, not only Mo content is reduced, but also Cr and Ni contents are lower than in 2304 (Table 1). Cr and Ni also enhance corrosion resistance. Chromium is a ferritizer and Ni is an austenitizer, so both phases can be assumed to reduce their corrosion resistance in 2001 in comparison with 2304. However, results prove that the Ni-content reduction is much more meaningful than the Cr-content, as selective corrosion of austenite in 2001 has been detected. Moreover, Mn – which is an alloying element with detrimental effect on corrosion resistance – is added to 2001, but it is very low concentration in 2304. The role of Mn in phase stability is complex [38], but it is assumed to act as an austenitizer at these concentrations. The presence of Mn in the austenite contributes to justify that the different selective corrosion observed in 2001 and 2304.

Independently from which phase corrosion starts in, duplex microstructure has a very important influence on attack development in these materials. Stainless steels usually have lower tensile strength than carbon steel. Corrugated stainless steels must be appropriately processed to obtain similar mechanical properties to those in the defined by standards (EN 10080) for corrugated carbon steel. Thus, they can replace it as a structural material. Bars with small diameter are hardened by cold forming. Bars with higher diameter – as the studied stainless steels – must be hot-formed, and hardening is achieved through grain size reduction (Table 2). As can be seen from the experimental results, in the corrugations of hot-formed stainless steels, the grain is even smaller and more deformed than in the bulk material. Small grain size has been proven to reduce crack propagation rate in the fatigue test of corrugated stainless steel [39]. Small grain size in hot-formed reinforcements can also be easily assumed to limit the corrosion rate of duplex stainless steels, because – although the onset of the attack takes place in the weakest phase – its development can be easily slowed down by the most corrosion-resistant phase. On the other hand, as the duplex microstructure – together with the reduced grain size – seems to favour certain attack generalization (which obviously also depends on the medium composition), this fact can be related to the reduced tendency shown by 2001 in comparison to 304 for localizing the attack in pits (Fig. 6).

The selective corrosion of the phases and the deformed microstructure of the corrugations explain the irregular pit shape in lean duplex (Fig. 9a). When the pits appear in strongly deformed regions of the corrugation, they often grow in a semi-parallel way to the surface, following the characteristics of the local microstructure (Fig. 9b). The open shape of these pits can be related to their easy repassivation (Fig. 1a).

The very positive results obtained from the polarization studies of these new duplex grades in carbonated and non-carbonated, saturated $Ca(OH)_2$ solutions demonstrate the interest of going on studying these materials as reinforcements in structures exposed to very aggressive conditions. It would be interesting to definitively check the conclusions of this work about pitting resistance and corrosion mechanisms with long-term corrosion in concrete, because, though it is not very probable from the authors' point of view, factors that are different in concrete and in solution (such as the resistivity of the medium, the oxygen diffusion rate or possible chemical changes in the crevices of the concrete–metal interface) could affect these conclusions.

4. Conclusions

1. The onset of corrosion in duplex stainless steels is only conditioned by the corrosion resistance of the weakest phase. As grain size is very small, the development of the attack is also conditioned by the corrosion resistance of the other phase.

For 2304, ferrite preferentially corrodes in all studied alkaline solutions with chlorides. On the other hand, in 2001 duplex, austenite shows lower corrosion resistance than ferrite under the studied aggressive conditions.

2. Several electrochemical parameters obtained from polarization curves suggest that the lean duplex 2001 has a similar resistance to the corrosion onset than the more expensive austenitic 304 in carbonated and non-carbonated chloride contaminated media. Moreover, the duplex microstructure favours minor localization of the corrosion attack and seems to be able to decrease their progress rate.
3. The lean duplex 2304 has clearly better corrosion behaviour than the 304 grade in simulated concrete solutions, the former being economically advantageous. The corrosion resistance of corrugated 2304 in these media is intermediate between the austenitic grade and the 2205 duplex.

Acknowledgements

Authors wish to acknowledge the Spanish Ministry of Science and Innovation (through project BIA2007-66491-C02-02) for its financial support in this research.

References

[1] O. Klinghoffer, T. Frolung, B. Kofoed, A. Knudsen, F.M. Jensen, T. Skovsgaard, Practical and economical aspects of application of austenitic stainless steel, AISI 316, as reinforcement in concrete, in: J. Mietz, R. Polder, B. Elserner (Eds.), Corrosion of Reinforcement in Concrete, European Federation of Corrosion, London, 2000, pp. 121–133.
[2] J.T. Pérez-Quiroz, J. Terán, M.J. Herrera, M. Martínez, J. Genescá, Assessment of stainless steel reinforcement for concrete structures rehabilitation, J. Constr. Steel Res. 64 (2008) 1317–1324.
[3] A. Bautista, G. Blanco, F. Velasco, M.A. Martínez, Corrosion performance of welded stainless steels reinforcements in simulated pore solutions, Constr. Build. Mater. 21 (2007) 1267–1276.
[4] F. Velasco, G. Blanco, A. Bautista, M.A. Martínez, Effect of welding on local mechanical properties of stainless steels for concrete structures using universal hardness tests, Constr. Build. Mater. 23 (2009) 1883–1891.
[5] U. Nürberger (Ed.), Stainless Steel in Concrete. State of the Art Report. Publication n° 18, European Federation of Corrosion, 1996.
[6] A. Knudsen, F.M. Jensen, O. Klinghoffer, T. Skovsgaard, Cost-effective enhancement of durability of concrete structures by intelligent use of stainless steel reinforcement, Conference on Corrosion and Rehabilitation of Reinforced Concrete Structures, Florida, December 1998.
[7] A. Bautista, G. Blanco, F. Velasco, A. Gutiérrez, L. Soriano, F.J. Palomares, H. Takenouti, Changes in the passive layer of corrugated, low-Ni, austenitic stainless steel due to the exposure to simulated pore solutions, Corros. Sci. 51 (2009) 785–792.
[8] L. Veleva, A.A. Alpuche-Avilés, M.K. Graves-Brook, D.O. Wipf, Comparative cyclic voltammetry and surface analysis of passive films grown on stainless steel 316 in concrete pore model solutions, J. Electroanal. Chem. 538 (2005) 45–53.
[9] C.M. Abreu, M.J. Cristóbal, R. Losada, X.R. Nóvoa, G. Pena, M.C. Pérez, Comparative study of passive films of different stainless steels developed on alkaline medium, Electrochim. Acta 49 (2004) 3049–3056.
[10] L. Freire, M.J. Carmezim, M.G.S. Ferreira, M.F. Montemor, The passive behaviour of AISI 316 in alkaline media and the effect of pH: a combined electrochemical and analytical study, Electrochim. Acta 55 (2010) 6174–6181.
[11] P. Castro-Borges, O.T. de Rincón, E.I. Moreno, A.A. Torres-Acosta, M. Martínez-Madrid, A. Knudsen, Performance of a 60-year-old concrete pier with stainless steel reinforcement, Mater. Perform. 41 (2002) 50–55.
[12] G.N. Flint, R.N. Cox, The resistance of stainless steel partly embedded in concrete to corrosion by seawater, Mag. Concrete Res. 40 (1988) 13–27.
[13] M.C. García-Alonso, M.L. Escudero, J.M. Mirando, M.I. Vega, F. Capilla, M.J. Correia, M. Salta, A. Bennani, J.A. González, Corrosion behaviour of new stainless steels reinforcing bar embedded in concrete, Cement Concrete Res. 37 (2007) 1463–1471.
[14] P. Gu, S. Ellliot, J.J. Beaudoin, B. Arsenault, Corrosion resistance of stainless steel in chloride contaminated concrete, Cement Concrete Res. 26 (1996) 1151–1156.
[15] B.G. Callagham, The performance of a 12% chromium steel in concrete in severe marine environments, Corros. Sci. 35 (1993) 1535–1541.
[16] C.M. Abreu, M.J. Cristóbal, R. Losada, X.R. Nóvoa, G. Pena, M.C. Pérez, Long-term behaviour of AISI 304L passive layer in chloride containing medium, Electrochim. Acta 51 (2006) 1881–1890.
[17] C.M. Abreu, M.J. Cristóbal, R. Losada, X.R. Nóvoa, G. Pena, M.C. Pérez, High frequency impedance spectroscopy study of passive films formed on 316 stainless steel in alkaline medium, J. Electroanal. Chem. 572 (2004) 335–345.
[18] A. Bautista, G. Blanco, F. Velasco, A. Gutiérrez, S. Palacín, L. Soriano, H. Takenouti, Passivation of duplex stainless steels in solutions simulating chloride-contaminated concrete, Mater. Constr. 57 (288) (2007) 17–31.
[19] A. Bautista, G. Blanco, F. Velasco, Corrosion behaviour of low-nickel austenitic stainless steels reinforcements: a comparative study in simulated pore solutions, Cement Concrete Res. 36 (2006) 1922–1930.
[20] I.-U.-H. Toor, P.J. Hyun, H.S. Kwon, Development of high Mn–N duplex stainless steel for automobile structural components, Corros. Sci. 50 (2008) 404–410.
[21] T. Laitinen, L. Wegrelius, A. Bergquist, Mill exposure test of duplex stainless steel LDX 2101 in recycled fiber applications, 6th Stainless Steel Conference, Helsinki, Finland, 2008, pp. 599–604.
[22] J. Mietz, J. Rueckert, B. Isecke, Electrochemical investigations on austenitic and duplex stainless steels for use as ground anchor materials, Mater. Sci. Forum 247 (1997) 25–36.
[23] P.E. Hazlewood, P.M. Singh, J.S. Hsieh, Effect of black liquor oxidation on the stress corrosion cracking susceptibility of selected materials, Corrosion 62 (2006) 765–772.
[24] R. Merello, F.J. Botana, J. Botella, M.V. Matres, M. Marcos, Influence of chemical composition on the pitting corrosion resistance of non-standard low-Ni, high Mn–N duplex stainless steels, Corros. Sci. 45 (2003) 909–921.
[25] L. Zhang, Y. Jiang, B. Deng, W. Zhang, J. Xu, J. Li, Effect of aging on the corrosion resistance of 2101 lean duplex stainless steel, Mater. Charact. 60 (2009) 1522–1528.
[26] W. Fredriksson, K. Edström, C.-O.A. Olssom, XPS analysis of manganese in stainless steel passive films on 1.4432 and the lean duplex 1.4162, Corros. Sci. 52 (2010) 2505–2510.
[27] I.-U.-H. Toor, P.J. Hyun, H.S. Kwon, Development of high Mn–N duplex stainless steel for automobile structural components, Corros. Sci. 50 (2008) 404–410.
[28] M.F. Hassanein, Numerical modelling of concrete-filled lean duplex slender stainless steel tubular stub columns, J. Constr. Steel Res. 66 (2010) 1057–1068.
[29] M. Theofanous, L. Gardner, Experimental and numerical studies of lean duplex stainless steel beams, J. Constr. Steel Res. 66 (2010) 816–825.
[30] C.M. Abreu, M.J. Cristóbal, X.R. Nóvoa, G. Pena, M.C. Pérez, R.J. Rodríguez, Modifications of the stainless steels passive film induced by cerium implantation, Surf. Coat. Technol. 158–159 (2002) 582–587.
[31] L. Freire, X.R. Nóvoa, G. Pena, V. Vivier, On the corrosion mechanism of AISI 204Cu stainless steel in chlorinated alkaline media, Corros. Sci. 50 (2008) 3205–3212.
[32] B. Beverskog, I. Puigdomenech, Revised Pourbaix diagrams for chromium at 25–300 °C, Corros. Sci. 39 (1997) 43–57.
[33] L.J. Parrott, Carbonation, moisture and empty pores, Adv. Cem. Res. (1991/92) 111–118.
[34] L. Zhan, W. Zhang, Y. Jiang, B. Deng, D. Sun, J. Li, Influence of the annealing treatment on the corrosion resistance of lean duplex stainless steel 2001, Electrochim. Acta 54 (2009) 5387–5392.
[35] L.F. Garfias-Mesias, J.M. Sykes, C.D.S. Tuck, The effect of phase compositions on the pitting corrosion of 25 Cr duplex stainless steel in chloride solutions, Corros. Sci. 38 (1996) 1319–1330.
[36] I.-H. Lo, Y. Fu, C.-J. Lin, W.-T. Tsai, Effect of electrolyte composition on the active-to-passive transition behaviour of 2205 duplex stainless steel in H_2SO_4/HCl solutions, Corros. Sci. 48 (2006) 696–708.
[37] W.-T. Tsai, J.-R. Chen, Galvanic corrosion between the constituent phases in duplex stainless steel, Corros. Sci. 49 (2007) 3659–3668.
[38] K.H. Lo, C.H. Shek, J.K.L. Lai, Recent developments in stainless steels, Mater. Sci. Eng., R 65 (2009) 39–104.
[39] M. Histcherich, M. Anglada, A. Mateo, Comportamiento a fatiga de las barras corrugadas de acero inoxidable, in: J.A. Odriozola, J. Botella, C. Merino (Eds.), Avances en Ciencia y Tecnología del Acero Inoxidable-II, Seville, 2003, pp. 381–388.

5.2 PUBLICACION 2: P2

E.C. Paredes, A. Bautista, S.M. Alvarez, F. Velasco.

"*Influence of the forming process of corrugated stainless steels on their corrosion behaviour in simulated pore solutions*".

Corrosion Science, vol. 58, p. 52-61, 2012.

Corrosion Science 58 (2012) 52–61

Contents lists available at SciVerse ScienceDirect

Corrosion Science

journal homepage: www.elsevier.com/locate/corsci

Influence of the forming process of corrugated stainless steels on their corrosion behaviour in simulated pore solutions

E.C. Paredes, A. Bautista *, S.M. Alvarez, F. Velasco

Material Science and Engineering Department – I.A.A.B., Universidad Carlos III de Madrid, Avda. Universidad 30, Leganés, Madrid, Spain

ARTICLE INFO

Article history:
Received 25 October 2011
Accepted 21 January 2012
Available online 28 January 2012

Keywords:
A. Stainless steel
A. Steel reinforced concrete
B. Polarization
C. Effects of strain
C. Pitting corrosion
C. Hardening

ABSTRACT

Stainless steels are formed by either hot working (HW) or cold working (CW) when used as reinforcement for concrete structures. The influence of the forming process on the corrosion behaviour is analyzed in depth in the present work. CW and HW corrugated bars of austenitic AISI 304L and 316L, and duplex SAF 2205 grades are studied. The electrochemical behaviour of the corrugated surface and the core of these materials are characterized by Mott–Schottky analysis and polarization curves. Tests are carried out in both carbonated and non-carbonated $Ca(OH)_2$ solutions. The microstructure and local mechanical properties of these materials are also analysed by means of universal hardness (UH) measurements to complete available information. The results prove that the surface of corrugated bars is far more likely to suffer corrosion than the core of the same material. The corrosion probability and the morphology of the attack induced in corrugated surfaces by anodic polarization clearly differ in HW and CW bars.

1. Introduction

The corrosion resistance of stainless steel in mortars or concrete is much higher than that of the carbon steel traditionally used as reinforcement [1–4]. Simulations of chloride penetration into concrete exposed to periodic de-icing salts predict that the time until corrosion initiation may increase 100 years or more for concrete structures when stainless steel reinforcements replace carbon steel [5].

A problem initially posed by the use of stainless steel reinforcements was that these materials must meet the mechanic requirements offered by carbon steel in terms of yield strength, stiffness and ductility, so as carbon steel can be easily substituted as structural material [6]. Stainless steels are typically softer than carbon steel. A simple stainless steel cladding of carbon steel bars proves very sensitive to surface defects in the material [5]. From the viewpoint of corrosion, the most reliable option is the application of a specially-designed hardening treatment. Although this treatment makes the product somewhat more expensive, it provides stainless steels with the appropriate mechanic features. Reinforcements of different types of both cold-worked (CW) and hot-worked (HW) stainless steels can be currently found in market. CW is usually employed for bar diameters over 11–12 mm, while HW is more appropriate for higher-diameter bars.

Some studies analyse the influence of processing on the tensile results of corrugated stainless steels [7]. The presence of corrugations was observed to modify the tensile properties and the fatigue behaviour of stainless steel. Worse results are obtained when testing stainless steel bars with corrugations than when they are eliminated [8].

Regarding the corrosion behaviour of stainless steel in concrete, their performance was proven to depend on the pH and composition of the pore solution. As expected, chloride concentration leads to increase the risk of pitting corrosion in stainless steel [9–13]. Most authors also agree in the fact that higher alkalinity in the pore solution has a positively impact on the corrosion behaviour of stainless steel [10–13]. The influence of the alloying elements in base metal on the corrosion behaviour in simulated pore solutions was also studied [10–15], as well as the influence of scales on stainless-steel surface [5,11,16]. However, no deep study on the possible influence of the processing method, and thus, of the microstructure, on the corrosion behaviour of corrugated stainless steel could be found in literature.

Studies carried out in neutral and acidic conditions show up a likely relationship between mechanical hardening induced in stainless steels and their pitting behaviour [17,18]. Pit development in stainless steels is postulated to depend on metallurgical factors such as stresses, density of dislocations, and preferential orientation of the crystallographic planes. It has been proven that the influence of the forming process on pitting can change with the stainless steel composition and the pH and contaminants in the environment [19].

Pitting has also been previously related to the stoichiometric characteristics of the passive layers. The stoichiometry of passive layers on stainless steels has been previously evaluated using Mott–Schottky analysis [20]. This approach allows to obtain

* Corresponding author. Tel.: +34 916249914; fax: +34 916249430.
E-mail addresses: asuncion.bautista@uc3m.es, mbautist@ing.uc3m.es (A. Bautista).

0010-938X/$ - see front matter © 2012 Elsevier Ltd. All rights reserved.
doi:10.1016/j.corsci.2012.01.010

information about the type of stoichiometric deviation of the oxides that form the passive layer under different circumstances, as well as to quantify the amount of defects. Recent results prove that stoichiometry of the passive layers in stainless steels is modified by the pH [21,22], oxidation temperature or the formation potential [23]. The ability of the method for detecting changes in the passive layers due to the forming process has not been checked up to now. Hence, it is interesting to evaluate how the forming processes of stainless steel reinforcements can affect the characteristics of the passive layers and the corrosion behaviour in concrete.

There are some experimental evidences seem to prove that corrosion always appear on corrugations when the real surface of the stainless steel reinforcements is tested [10,12]. However, a great amount of the recently-published work on stainless steel corrosion performance in simulated pore solutions used polished sections of stainless steels embedded in resin [5,7,9,13,24–26], and sometimes the samples had been cut from stainless steels that had not been processed as corrugated bars [27–30]. In these cases, the possible influence of the forming method and the characteristic microstructure of the corrugations were not considered. Though corrosion tests were carried out on the real surface of the reinforcements in some studies [5,10,12,16], the possible influence of the forming process on the pitting resistance of the material and on the corrosion mechanism was not analysed.

The aim of the present paper is to use different techniques of obtain new information about how the forming process can affect the corrosion behaviour of stainless steels in simulated pore solutions. With this objective, results obtained with HW and CW bars of similar chemical composition are analyzed and compared with results obtained for samples of the core of the bars.

2. Experimental procedure

Three different stainless steel grades were considered in this study: AISI 304L, AISI 316L and SAF 2205. These grades were selected because of their current market importance. Their characteristics and corrosion performance were analysed when manufactured by both HW and CW. All the corrugated bars were processed by the Spanish manufacture company Roldán S.A. (ACERINOX Group). The diameters and chemical compositions of the six corrugated stainless steel grades are shown in Table 1.

The tensile properties of the corrugated stainless steels can be seen in Table 2. It is noteworthy mentioning that the yield strength of the HW corrugated bars double that of materials with the same composition processed by HW for other more traditional applications [31]. The usual information about the mechanical properties of the bars obtained from tensile tests was supplemented with the more localized studies carried out through universal hardness (UH) measurements. Results were obtained on cross-sectional, metalographically-prepared samples of the bars. Measurements were carried out on the corrugation and at the centre of the bars. Tests were performed at a load rate of 1 mm/min using a maximum load of 20 N. UH plastic hardness, indentation modulus, and mechanical work (together with the elastic and plastic parts of the indentation work) were measured. Microhardness was measured at the same time in each point. All results are the average of about 15 measurements. Some theoretical background about this characterization method can be found elsewhere [32].

Table 2
Tensile mechanical properties of the corrugated stainless steels considered in the study.

	AISI 304L		AISI 316L		SAF 2205	
	CW	HW	CW	HW	CW	HW
YS (MPa)	580	580	656	603	968	583
UTS (MPa)	747	780	822	800	1156	855
Elongation (%)	38	15	26	12	12	33

The microstructural study of stainless steels was carried out on cross sections of the corrugated bars. Metalographically-prepared specimens were chemically etched to reveal their microstructure. For austenitic stainless steels, *aqua regia* ($HCl + HNO_3$ solution) was used as a reagent agent, while the Bloech and Wedl reactive ($HCl + K_2S_2O_5$ solution) was used for duplex grades. Grain size in stainless steel was measured on the bulk of the bars and on the corrugation according to the ASTM E112 standard.

Electrochemical polarization studies were carried out on the corrugated surface of stainless steel reinforcing bars. A 2 cm-long surface area of the bars was immersed in the test solution. Neither the microstructure of the corrugated surface nor the usual industrial passivating treatment were modified. The influence of the industrial passivating treatment on the protecting nature of the passive layer had already been suggested in the bibliography [14]. The cross-section of the bars was also exposed to the solution, although it had been previously ground to 320 and passivated (50 s in 12% HNO_3 (w/w)). Experimental evidence demonstrates that the attack never localizes in the cross section, so the measurement of the length of the passive region obtained under these conditions always corresponds to that of the corrugated surface. No risk of differential aeration corrosion exists for corrugated stainless steels in alkaline media with this cell configuration.

Materials were polarized in eight different simulated pore solutions at room temperature. Fresh, saturated $Ca(OH)_2$ solutions ($pH \approx 12–13$) were used to simulate non-carbonated concrete. Solutions where the pH had been reduced to about nine by bubbling CO_2-enriched air were used to simulate carbonated concrete.

Table 1
Nominal diameter and chemical composition of the six corrugated stainless steels considered in the study.

	AISI 304L		AISI 316L		SAF 2205	
	CW	HW	CW	HW	CW	HW
Diameter (mm)	12	16	6	16	12	20
Chemical composition (% w/w)						
C	0.023	0.026	0.018	0.013	0.029	0.020
P	0.031	0.027	0.03	0.029	0.029	0.018
S	0.001	0.001	0.002	0.003	0.001	0.003
Si	0.361	0.298	0.365	0.351	0.387	0.374
Mn	1.448	1.420	1.441	1.782	1.721	1.665
Cr	18.30	18.37	16.97	16.76	22.49	22.17
Ni	8.675	8.740	11.21	11.17	4.721	4.710
Mo	0.275	0.275	2.081	2.504	3.221	3.500
N	0.0507	0.0549	0.0476	0.0443	0.1743	0.1778
Cu	0.487	0.506	0.497	0.257	0.237	0.093
Fe	Bal.	Bal.	Bal.	Bal.	Bal.	Bal.

At both pHs, tests were carried out in solutions without chlorides and with three different amounts of NaCl (0.5%, 1% or 5% (w/w)). Polarization curves were performed after 17 h of exposure of the reinforcements to the simulated pore solutions, as meaningful change in passive-layer composition was observed to take place during the first hours of immersion [14,15]. Saturated calomel electrode (SCE) was used as a reference electrode. A mesh of AISI 316 stainless steel that surrounds the working electrode acted as counter-electrode. The sweeping rate of the potential was 0.17 mV/s, following the advice of the ASTM G61 standard. The current limit for reversing the sign of the potential sweep was 10^{-4} A/cm^2. The multiplicity of measurements (3–4) assures the reliability of the results.

For checking the effect of the corrugations, polarization studies were repeated. In these cases, the corrugated bars had been machined to cylinders and the surface of the cylinders had been ground to 320.

The morphology of the attack after the corrosion tests as well as the influence of the microstructure were studied by optical microscopy.

The semiconducting properties of the passive layer were measured using Mott–Schottky analysis. To obtain these results, capacities were measured at 1 kHz. Cathodic polarization was applied. The polarization swept from +600 to −1300 mV *vs*. SCE, with 5 mV/s scanning rate. The usual electrochemically or thermally forced generation of the passive layer was not used, but the passive layers were left to modify spontaneously along 48 h in the medium of study. Hence, as-realist-as-possible working conditions were favoured.

The electrochemical cell configuration used in Mott–Schottky studies was similar to that used in polarization curves, as well as the specimens used to study the behaviour of the corrugated surface and the material at the core of the bars. The media considered also included non-carbonated and carbonated $Ca(OH)_2$-saturated solutions, yet always without chlorides. The number of measurement repetitions was four to assure the scientific relevance of the obtained results. Since this is a relatively new technique, carbon steel corrugated bars were included in this part of the study for comparison purposes.

3. Results and discussion

3.1. Local mechanic properties and micro-structural characterization

The results of the localized micro-hardness measurements corresponding to UH can be seen in Fig. 1. A clear parallelism can be observed between hardness and the results of tensile strength and yield strength obtained in more traditional tests (Table 2). The obtained UH results prove that the corrugations are always far harder than the core of the bars. Greater differences were observed between core and corrugation in HW grades than in CW ones. Small hardness difference was observed between HW and CW corrugations for the same type of stainless steel. On the other hand, the amount of plastic work (W_{plast}) is inversely related to hardness (Fig. 1b). Thus, corrugations (which are harder than cores) present lower W_{plast} values. The evolution of the other parameters obtained from UH measurements and non-plotted in the figure (indentation module, mechanical work and elastic work) confirm these trends.

Local differences regarding mechanical behaviour in the different areas of the corrugated bars can be explained by the differences observed between the microstructures of corrugations and cores. Corrugations always have smaller grain size than cores (Table 3).

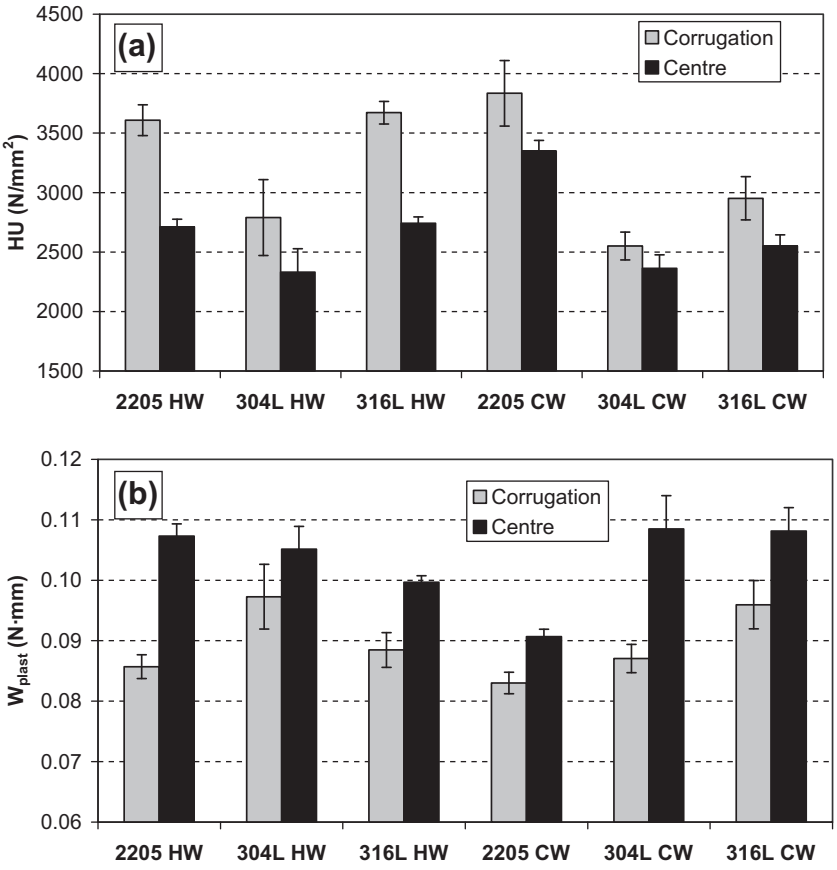

Fig. 1. Local mechanical properties measured on the corrugation and on the centre of the studied reinforcing stainless steels: (a) universal hardness (b) plastic work.

Table 3
Grain size on the corrugated surface and on the centre of the bar for the corrugated stainless steels considered in the study.

	AISI 304L		AISI 316L		SAF 2205	
	CW	HW	CW	HW	CW	HW
Grain size (μm)						
Corrugation	42 ± 2	4.9 ± 0.9	47 ± 4	2.9 ± 0.3	2.7 ± 0.2	1.8 ± 0.1
Centre	51 ± 3	6.6 ± 0.7	60 ± 4	3.6 ± 0.4	4.3 ± 0.4	3.9 ± 0.6

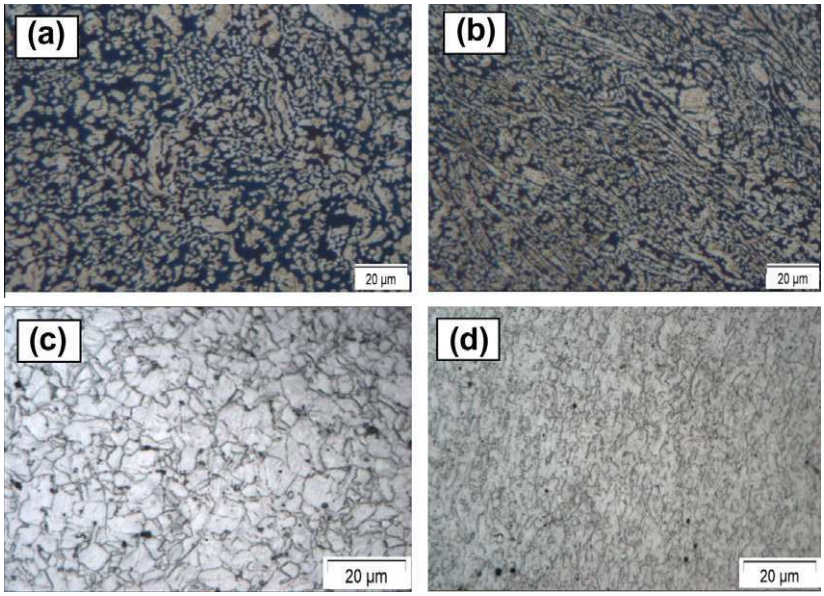

Fig. 2. Cross sectional views of the microstructure of the corrugated bars: (a) core of CW 2205 (b) outer region of CW 2205 (c) core of the HW 316L (d) outer region of the HW 316L.

This leads to lower hardness in the core than in the surface of the bars. HW grades have smaller grain size than CW. This smaller grain size explains the high yield strength of HW bars, in spite of being processed at high temperature (Table 2). Besides, a striking difference was observed between the grain sizes of austenitic and duplex bars. Because of their reduced grain size, the corrugated 2205 grades studied can be considered as microduplex (duplex with average austenite grain size between 5 and 16 μm) [33]. Microduplex stainless steels had been previously studied in the bibliography mainly because of their markedly superplastic behaviour at high temperatures [34].

Apart from the reduced grain size, deformation is another factor that contributes to the greater hardness measured in corrugations. Grain is more strained in the corrugations due to processing, which led to the accumulation of stresses in this area. This can be observed both in corrugated CW grades (Figs. 2a, b) and HW grades (Figs. 2c, d). The development of preferential texture in the corrugation (Figs. 2b, d) implies the formation of low atomic density planes in these regions. It has been suggested in literature that the lower binding energy of the atoms in this less close-packed plane can result in enhanced diffusion rate for the atoms [19]. This fact might modify the characteristics of the passive layer in the corrugations.

3.2. Semiconducting properties of passive layers

The application of the Mott–Schottky model to capacity (C) measurements of stainless steels informs about the semiconductive properties of oxides. The results presented in this work prove that the semi-conductive properties of passive layers on corrugated stainless steels are affected not only by base metal composition and medium features but also by material processing. The representation of C^{-2} *vs.* potential (E) obtained for the different stainless steels at frequencies dominated by the capacitive behaviour of the passive layer give rise to Mott–Schottky plots as those in Figs. 3 and 4. At both pHs, two regions where C^{-2} varies linearly with the potential can be distinguished for all stainless steels. The negative slope at lower E corresponds to an oxide film that behaves as a p-type semiconductor. A positive slope can be observed in the plots for medium E values, indicating that the passive layer also comprises an oxide films that behaves as an n-type semiconductor. Both regions are separated by a narrow E range where the two oxides are in flat-band conditions. This region of flat-band condition appears at lower potentials as pH in the medium increases. Moreover, the behaviour of other n-type semiconductor can be guessed at high anodic polarizations.

It is well-known that passive films on stainless steels usually comprise an inner layer rich in Cr-oxides and an outer layer rich in Fe oxides/hydroxides [35]. When the tests are carried out in carbon steel reinforcements, only the contribution of the n-types oxides appear on the plot (Fig. 5). This fact proves, as other authors have also assumed before [23,35,36–38], that the oxides with n-type behaviour are Fe oxides, while the p-type behaviour corresponds to the Cr oxide. The presence of different Fe-oxides in these alkaline conditions (Fe_3O_4, Fe_2O_3, etc.) [14] may explain the complex structure observed in the high E region of the plots.

The doping densities of the oxides was calculated using the Mott–Schottky equation [35] and assuming a value for the relative dielectric constant (ε_r) of the films of 12, as it has been previously done by other authors [37,39]. The results on the doping density

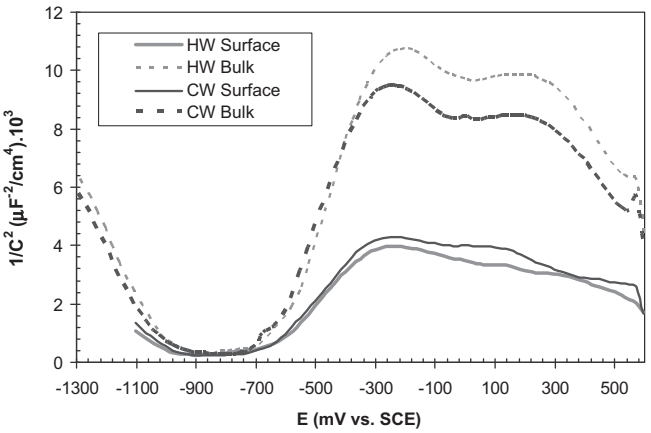

Fig. 3. Mott–Schottky plots for the passive layer formed on the corrugated surface and on the core of HW 2205 and CW 2205 in non-carbonated solutions.

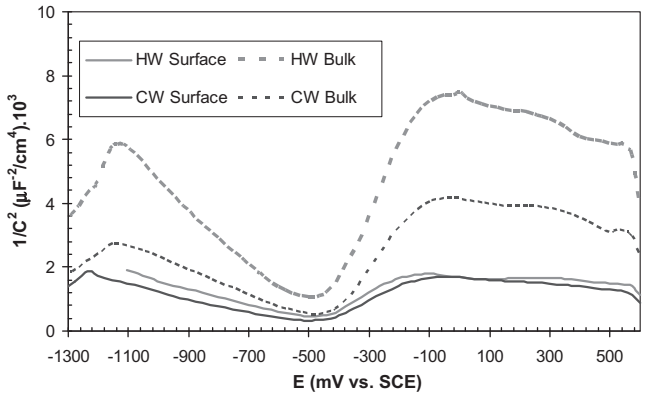

Fig. 4. Mott–Schottky plots for the passive layer formed on the corrugated surface and on the core of HW 2205 and CW 2205 in carbonated solutions.

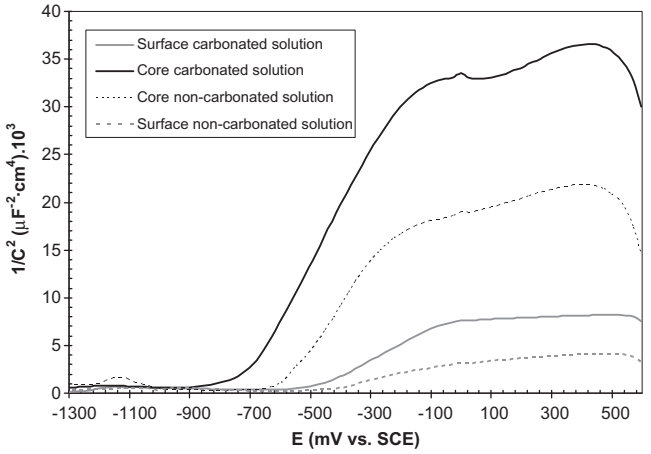

Fig. 5. Mott–Schottky plots corresponding to the passive layer on the corrugated surface and on specimens for the bulk of reinforcing black steel bars. The layers have spontaneously been formed in non-carbonated and carbonated solutions.

are shown in Table 4. In stainless steels, the density of donors in the structure of n-type semiconductive oxides is determined from the slope observed in medium *E*. This density of dopants corresponds to oxygen vacancies that act as donors (N_d). n-type semiconduction means that energy bands rise to the electrolyte [35]. That is, increased N_d would favour, from the viewpoint of energy, the diffusion of aggressive anions such as Cl^- from the exterior to the base metal and the diffusion of metallic cations in the opposite direction. Both processes would favour corrosion. Besides, increased N_d has also been experimentally proven to lead to increased probability of pitting nucleation in passive layers generated in stainless steel, although in conditions different from those in the present study [20,39].

For stainless steel bars, N_d is always lower for specimens manufactured from the core of the bars than for those specimens of the same corrugated materials (Table 4). This would indicate that the Fe oxides appearing on corrugations are less protective than those forming on the core material in stainless steels. The lack of stoichiometry in oxides on the corrugations might well be related to the higher atomic disorder in the base metal shown in UH results (Fig. 1). On the contrary, the black-oxide layer that appears on the surface of carbon-steel bars during processing show more protective semiconductive properties that the passive layer formed in specimens for the core of the bar. When the corrugated black steel bars are exposed to simulated pore solutions, N_d is lower than N_d for the bulk material in the same conditions.

At first sight the high N_d values detected for duplex 2205 may well seem somewhat striking when compared to those measured for CW austenitic grades, when duplex is a better-performing steel against corrosion [10]. In this case, influence from grain size (lower in duplex than in austenitic grades, as shown in Table 3) on oxide stoichiometry cannot be discarded. The higher Cr content in 2205 grades (Table 1), which provides passive layers with greater Cr_2O_3 [14], may also imply that Fe oxide stoichiometry in these grades becomes more conditioned by underlying Cr oxide stoichiometry than in austenitic grades.

In the studied stainless steel bars, the values of N_d show that the Fe oxides on the surface of HW grades have less oxygen vacancies than those on the surface of CW grades (Table 4). The greater oxide stoichiometry observed in HW grades may be related to the lower stresses and strains involved by this forming procedure.

N_d is also observed to decrease as pH becomes increasingly alkaline for the same material in both stainless and carbon steels (Table 4). These results are consistent with Thermodynamics, as the formation of (more stoichiometric) protective Fe oxides is more thermodynamically favoured by pH 12–13 than pH 9.

In the Cr oxide layer, stoichiometric deviations are cation vacancies that behave as acceptor dopants. Acceptor density (N_a) in Cr oxide was calculated from the slopes in the linear areas of the Mott–Schottky plots at low *E*. The penetration of aggressive ions with Cl^- is inhibited in p-type oxides [35]. It has been said that pitting corrosion decreases as N_a increases in the oxides [20]. Table 4 shows that greater N_a tends to be observed for passive layers on corrugations than on bar core. The passivation treatment applied to the outer side of the corrugated bar, which favours Cr_2O_3 formation [14], could explain the higher N_a values for the corrugations. Other clear tendencies observed for Cr oxide in Table 4 include that: (a) greater N_a is observed in carbonated than in non-carbonated solutions, and (b) among CW-processed bars, the 2205 grade has much higher N_a under all conditions than austenitic grades. This parallelism between N_d and N_a values in the passive layer is the expected in stainless steels with more than 15% Cr content [23,37]. The formation of Fe-oxides and Cr-oxides in the passive layer is obviously interrelated as well as that greater or lower stoichiometry in one of them definitely conditions the stoichiometry of the other.

The duplex structure in passive layers hinders the direct extrapolation of a relation between the conductivity of the passive layer in stainless steels and the susceptibility to pitting corrosion, because those factors that have a positive impact on the protective nature of Fe oxides affect the Cr oxides negatively. Previous works

Table 4
Doping densities from the Mott–Schottky plots in non-carbonated and carbonated solutions.

Doping densities (10^{20} at/cm^3)	Carbon steel		AISI 304L				AISI 316L				SAF 2205			
			CW		HW		CW		HW		CW		HW	
	Corrug.	Centre	Corrug.	Centre	Corrug.	Centre	Corrug.	Centre	Corrug.	Centre	Corrug.	Centre	Corrug.	Centre
N_d in non-carbonated	1.6 ± 0.8	11.2 ± 2.1	9.2 ± 0.9	4.5 ± 0.1	5.1 ± 0.0	2.9 ± 0.8	6.3 ± 0.7	4.1 ± 0.7	3.6 ± 0.9	3.3 ± 0.6	7.6 ± 0.9	3.9 ± 0.8	8.4 ± 1.1	3.6 ± 0.8
N_a in non-carbonated	–	–	6.3 ± 0.4	4.9 ± 0.2	3.0 ± 0.0	2.7 ± 0.3	3.9 ± 0.4	3.5 ± 0.9	3.1 ± 0.2	3.5 ± 0.9	14.6 ± 0.7	5.4 ± 0.8	12.4 ± 0.9	5.1 ± 1.9
N_d in carbonated	5.8 ± 1.9	10.9 ± 3.2	18.7 ± 3.4	9.2 ± 1.1	10.8 ± 0.2	7.2 ± 0.1	30.1 ± 3.1	11.7 ± 1.4	15.2 ± 0.6	8.9 ± 3.5	37.1 ± 7.2	8.9 ± 2.1	30.4 ± 5.3	6.3 ± 0.3
N_a in carbonated	–	–	24.5 ± 3.9	16.3 ± 3.3	16.1 ± 2.0	15.8 ± 2.8	54.6 ± 5.1	23.5 ± 5.9	29.5 ± 2.6	24.0 ± 7.6	48.9 ± 14.4	29.8 ± 0.5	37.0 ± 9.7	13.2 ± 2.8

have shown that increased N_d has prevailing negative effect for the corrosion behaviour of a specific type of stainless steel under some specific conditions [38]. However, systematic negligence of the role of Cr oxides might be a big mistake. Besides, it must be taken into account that —beyond oxide stoichiometry— the thickness, exact composition and concentration of the different oxides in each layer

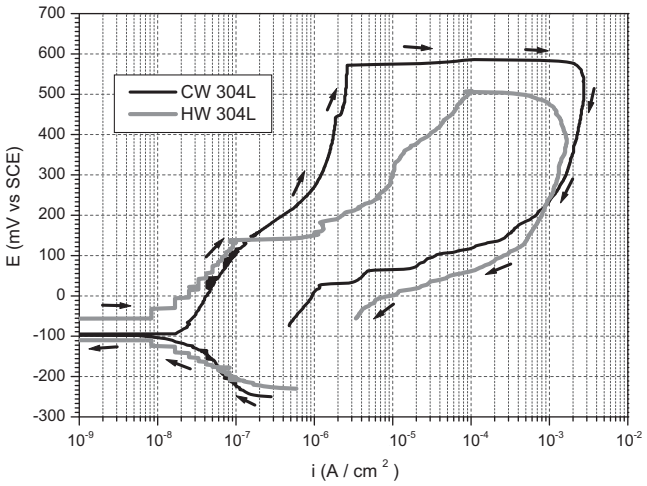

Fig. 6. Polarization curves for HW 304L and CW 304L in non-carbonated solution with 0.5% NaCl.

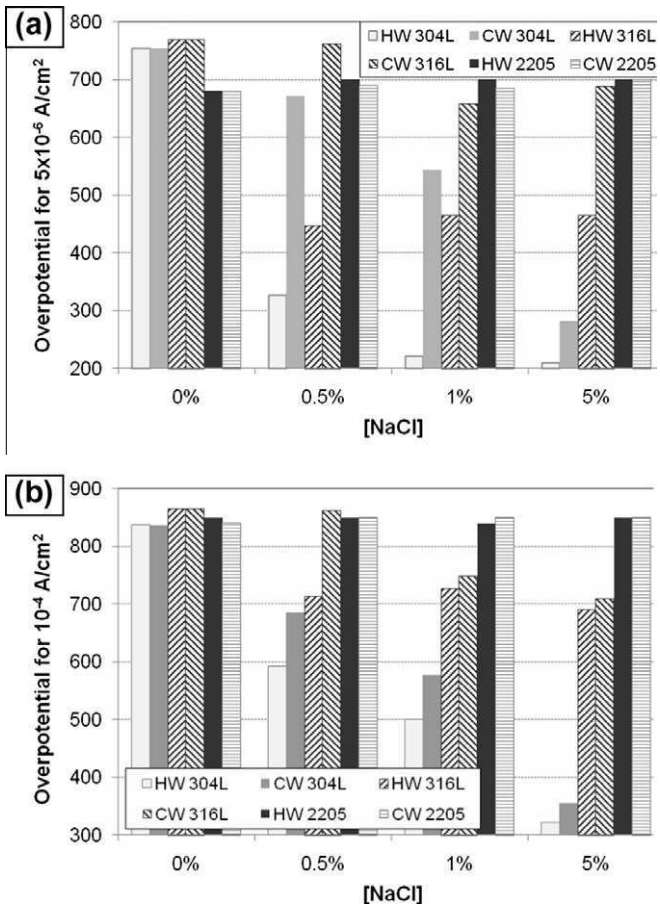

Fig. 7. Anodic overpotentials for the studied corrugated stainless steels in non-carbonated solutions: (a) for reaching 5×10^{-6} A/cm^2; (b) for reaching 10^{-4} A/cm^2.

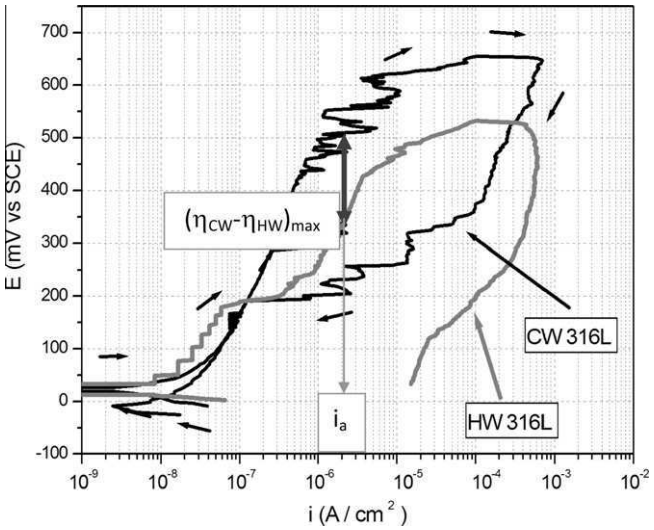

Fig. 8. Polarization curves for HW 316L and CW 316L in carbonated solutions with 0.5% NaCl.

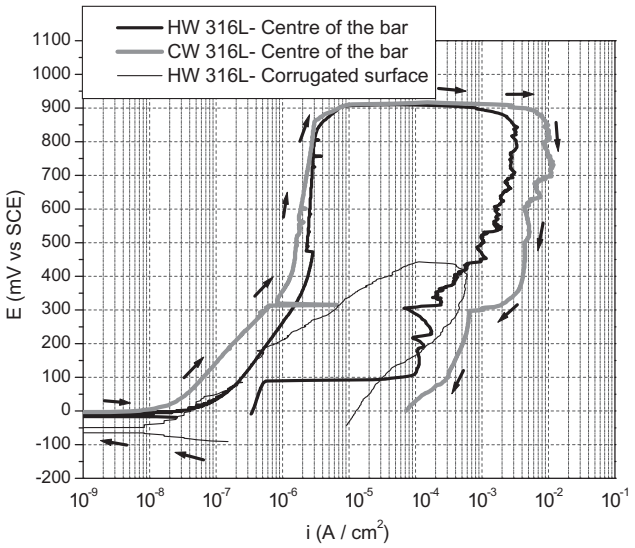

Fig. 9. Polarization curves for the cores of HW and CW 316L bars in carbonated solution with 1% NaCl. Curve corresponding to the corrugated surface of one of the materials in that media is included for comparison.

is a key factor when it comes to determine its corrosion behaviour, as previously mentioned [14]. These other factors may well mask the relation between defect density in the oxides forming the passive layer and its stability in corrosive media [36].

The obtained results of the Mott–Schottky analysis clearly prove that the stoichiometric features of the passive layers depend on stainless-steel microstructure and processing. As it has been commented, a big amount of the previous research on the corrosion behaviour of stainless steels in concrete is carried out with stainless steels processed in a different way or with different surface finishing from reinforcing bars. Mott–Schottky data suggest that the extrapolation from those results to the corrosion behaviour of corrugated stainless steels can be risky.

3.3. Behaviour to anodic polarization of corrugated surfaces

The polarization curves of corrugated austenitic steels in non-carbonated $Ca(OH)_2$-saturated solutions with different chloride content also show clear differences due to the forming process. As shown in Fig. 6, a well-defined passive area and a clear pitting potential (E_p) can be observed in the anodic polarization curves for CW austenitic grades (in the case of 304L in non-carbonated solutions containing 0.5% NaCl, E_p would be 560 mV *vs*. SCE). Once E_p is exceeded, current intensity increases very quickly in CW grades.

On the other hand, in HW austenitic grades, corrosion seems to begin at lower anodic overpotential, usually with scarcely defined E_p (in the case of HW 304L in non-carbonated solutions containing 0.5% NaCl may be around 140 mV *vs*. SCE). However, the increases in corrosion intensity after the onset of the attack are milder than in CW austenitic grades.

The influence of the type of forming on corrosion behaviour can be ascertained by observing the data corresponding to the corrugated bars of types 304L and 316L in chloride-containing solutions in Fig. 7. To reach current intensities around 5 μA/cm^2, which characterize active corrosion (Fig. 7a), higher anodic overpotentials are reported in CW than in HW grades for the same austenitic types. That is, corrosive attack is more likely to begin in HW than in CW grades in aggressive media. If polarization continues, the differences observed between the overpotentials needed to reach a specific anodic-current intensity decrease. This can be seen for the austenitic grades at 10^{-4} A/cm^2 (Fig. 7b) and becomes particularly clear at high chloride contents. The shape of the curves of CW and HW austenitic grades in low chloride concentrations suggests that the curves would intersect at anodic intensities higher than 10^{-4} A/cm^2. This points out that, although corrosion in CW grades requires more powerful corrosion cells to start than in HW grades with the same composition because their higher E_p, the attack in CW grades progresses more dangerously once it has started.

For non-carbonated solutions without chlorides, the six materials are completely corrosion-proof in the tests and the overpotentials represented in Fig. 7 correspond to reaction of decomposition of water. In these cases, the plotted overpotentials exhibit always similar values. However, the overpotentials of duplex grades at 5 μA/cm^2 are an exception, being lower than those of the austenitic grades in the same conditions. Due to the higher Cr content of the duplex stainless steels (Table 1), oxidation from Cr(III) to Cr(VI) [12] is observed to contribute to a great extent to the anodic polarization curve in this area.

Duplex 2205 grades, regardless of chloride content of the medium and the forming method, were immune to corrosion in the performed tests. All the polarization curves obtained for 2205 are rather similar. This can be checked in the similarity of the data corresponding to HW and CW 2205 grades in Fig. 7a, b.

The influence of the forming conditions in carbonated media observed in austenitic grades is similar to that observed at higher pH levels (Fig. 8), but carbonation has a detrimental effect on the

Table 5
Parameters obtained from the polarization curves in carbonated, saturated $Ca(OH)_2$ solutions with different chloride contents.

	AISI 304L			AISI 316L		
% NaCl	0.5	1	5	0.5	1	5
$\Delta(\eta_{CW}-\eta_{HW})_{max}$ (mV)	130	116	96	260	172	4
i_a (A/cm^2)	10^{-6}	6×10^{-8}	3×10^{-8}	1.3×10^{-6}	2×10^{-7}	1.3×10^{-7}

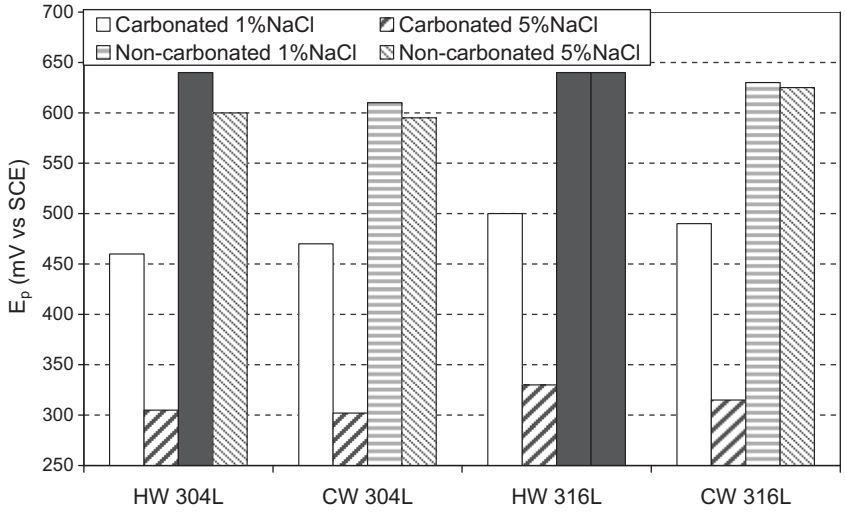

Fig. 10. E_p values obtained for the core of the bars in carbonated and non-carbonated solutions with chlorides. Black bars represent systems where water decomposition conditions are reached, and pitting does not takes place.

corrosion behaviour of austenitic stainless steels as it has been observed and justified previously [10,14]. The onset of corrosion occurs at lower anodic overpotentials for HW grades. However, when corrosion appears in CW grades, it progresses quicker than in HW. For corrugated CW austenitic steels, within a specific intensity interval, the anodic overpotential needed to reach a certain intensity (η_{CW}) is always higher than that needed by HW bars with the same composition (η_{HW}). Table 5 shows the maximum differences between η_{CW} and η_{HW} reported by polarization curves of corrugated 304L and 316L in carbonated solutions, as well as the anodic intensity (i_a) at which the difference $\eta_{CW} - \eta_{HW}$ becomes maximum for each type of stainless steel and Cl^- concentration in the medium. In Fig. 8 both parameters at plotted.

Table 5 shows that the lower the aggressiveness of the medium is, the greater the influence of the forming conditions on the shape of the polarization curves is. This has been concluded from the fact that the parameter used to quantify the influence of the forming process $(\eta_{CW} - \eta_{HW})_{max}$ decreases as chloride content increases. Another outstanding fact is that these maximum differences between the HW and CW curves for the same grade appear at progressively lower i_a depending on chloride content, this corroborating the fact that these processing-related differences could become less meaningful in highly aggressive media where highly powerful corrosion cells would appear.

In carbonated media the 2205 grade proves itself immune to corrosion under all studied conditions, regardless of its forming method.

3.4. Behaviour to anodic polarization of the bar cores

Different results are obtained when polarization curves are carried out in specimens machined from bar cores, whose microstructure clearly differs from that in bar surface (Table 2 and Fig. 3). An example of these differences between corrugated surface and core material is shown in Fig. 9. Corrosion resistance of bar cores is much greater than that of the corrugated surfaces of the same bars under the same conditions. Anodic polarization of both HW and CW bar cores always shows a clearly-defined passive area and much higher E_p than those detected for corrugated surface. Several researches show that pitting onset can be directly related to the hardening processes occurring in the outer part of the bars (Fig. 1) [17,40]. This difference of behaviour between bar core

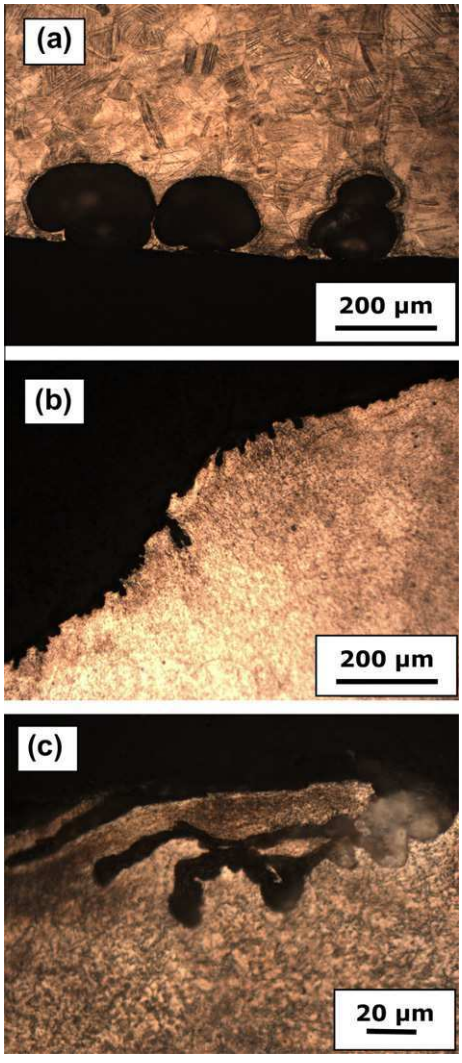

Fig. 11. Cross-sectional views of the morphology of the pits in corrugated surfaces after polarization in solutions with chlorides: (a) CW 304L; (b) HW 304L (predominant way of attack); (c) HW 304L (detail of the most strained region).

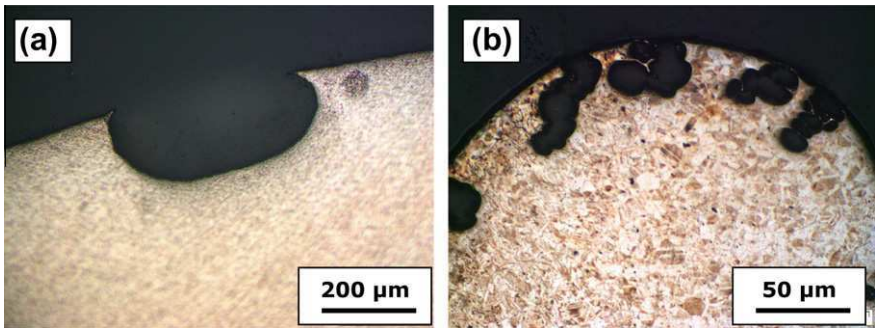

Fig. 12. Cross-sectional views of the morphology of the pits in specimens manufactured from the cores of the bars after polarization in solutions with chlorides: (a) HW 304L; (b) CW 304L.

and corrugation may also be related to the higher N_d values obtained for the passive layers formed in the corrugated surfaces of the cores of the same material under identical exposure conditions (Table 4). These data prove that the corrosion resistance of stainless steels in concrete may easily be overestimated when the specific features of the corrugations are not considered.

The E_p obtained from the polarization tests completed in the bar core of austenitic grades are shown in Fig. 10. It is important to highlight that the potentials corresponding to non-carbonated solution of the HW 304L containing 1% NaCl and the HW 316L with 1% and 5% NaCl (black bars in the figure) do not correspond (because of the shape of the curves) to pitting corrosion processes but to water decomposition. That is, the materials plotted in black bars are immune to corrosion in the carried out tests. If E_p values are compared for the same stainless steel and medium composition, it can be observed that differences in the corrosion behaviour of HW and CW bar cores are smaller than those due to forming process when the study is completed on bar surface. Unlike corrugations, the forming method bears little significance in the corrosion behaviour of bar cores. However, results suggest that HW cores tend to be slightly more corrosion resistant than CW cores.

The present results suggest that the stoichiometric features of the Cr oxide (N_a) may have a significant impact on pitting onset, while attack speed may be influenced to a greater extent by Fe-oxide stoichiometry (N_d). However, it seems rather obvious for stainless steels in alkaline media that no easily-recognisable relationship between the results of capacity and corrosion-behaviour studies can be obtained. It is due to the complex structure of the passive layers (formed by Cr and Fe oxides of changing nature and different thickness ratios depending on the base material and medium). The possible masking of the effect of stoichiometry on pitting behaviour by other characteristics of the passive layers should also be considered.

3.5. Study on attack morphology

The different shape of polarization curves depending on the microstructure of the corrugated bar corresponds to different attack morphologies. Thus, polarization of CW austenitic grades in media with chlorides, in both carbonated and non-carbonated solutions, gives rise to the appearance of globular pitting on the bar surface (Fig. 11a). Pits tend to appear in the most strained area of the corrugations, characterized by greater stress (Fig. 1).

The prevailing attack morphology in austenitic HW is very small pits (Fig. 11b), that are numerous and well-distributed on those areas with greater mechanic strains (Fig. 2d). This type of morphology explains the curve shape observed for HW grades (Figs. 6 and 8), where passive layer breakage does not lead to abruptly increasing intensity, unlike it occurs with CW grades. The morphological study of the attack confirms that for HW grades, where corrosion develops for lower anodic overpotentials, attack tends to adopt a less aggressive mechanism. The greatest danger of localized *vs.* generalised corrosion becomes particularly relevant when dealing with concrete reinforcements. The tensile stresses created in concrete by localized corrosion of the reinforcements are far more dangerous than stresses created by uniform corrosion. The pressures to cause cracking of the concrete cover under non-uniform corrosion conditions are proven to be much smaller than under uniform corrosion [41].

Another fact that can be drawn from the study of the morphology of the attack is that the shape of small pits in HW grades is often conditioned by microstructure deformation (Fig. 11c). It must also be pointed out that a few big pits, similar to those observed in CW grades, were also observed for HW austenitic grades after testing.

The pits caused by polarization tests in HW specimens machined from the bulk of austenitic bars clearly differ from those appearing on the surface of HW bars (Fig. 12a). After the polarization test, pits, when they appear, are large and exhibit globular shape. In samples manufactured from the core of CW austenitic grades, globular pits also appear, but in this case they develop in an interconnected way (Fig. 12b).

4. Conclusions

1. The forming process of the corrugations strongly modifies the microstructure of the stainless steels and it has an important effect on the characteristics of the passive layers and on the corrosion behaviour of the stainless steels.
2. The stoichiometry of the oxides that form the passive layers of the stainless-steel corrugated bars is higher in the bar core than in the corrugated surface.
3. In the studied simulated pore solutions, CW bars have less stoichoimetric passive layer than HW bars.
4. Cr and Fe oxides in the passive layer of stainless steels exhibit higher N_a and N_d, respectively, in carbonated than in non-carbonated media.
5. The core of the corrugated bars presents much lower pitting probability than bar surface. Besides, the morphology of the anodic polarization-induced attack is clearly different.
6. Less powerful corrosion cells are needed for corrosion onset in the corrugated surface of HW grades than in CW grades with identical composition.
7. If the attack of the corrugated surface starts in CW grades, it tends to develop in a more localised and faster manner than in the corrugated surface of HW grades.

Acknowledgement

The authors wish to acknowledge the Spanish Ministry of Science and Innovation (through project BIA2007-66491-C02-02) for its financial support in this research.

References

[1] L.G. Andion, P. Garcés, F. Cases, C.G. Andreu, J.L. Vázquez, Metallic corrosion of steels embedded in calcium aluminate cement mortars, Cem. Concr. Res. 31 (2001) 431–436.
[2] M.C. García-Alonso, M.L. Escudero, J.M. Miranda, M.I. Vega, F. Capilla, M.J. Correia, M. Salta, A. Bennani, J.A. González, Corrosion behaviour of new stainless steels reinforcing bars embedded in concrete, Cem. Concr. Res. 37 (2007) 1463–1471.
[3] M. Criado, D.M. Bastidas, S. Fajardo, A. Fernández-Jiménez, J.M. Bastidas, Corrosion behaviour of a new low-nickel stainless steel embedded in activated fly ash mortars, Cement Concr. Compos. 22 (2011) 644–652.
[4] U. Nürberger (Ed.), Stainless steel in concrete. State of the art report, Publication n° 18, Institute of Materials, London, 1996.
[5] M.F. Hurley, J.R. Scully, Threshold chloride concentration of selected corrosion-resistant rebar materials compared to carbon steel, Corrosion 62 (2006) 892–904.
[6] Guidance on the use of stainless steel reinforcement, Technical report N° 51, The Concrete Society, London, 1998.
[7] H. Castro, C. Rodríguez, F.J. Belzunce, A.F. Cantelli, Mechanical properties and corrosion behaviour of stainless steel reinforcing bars, in: T.R. Torralba (Ed.), New Developments on Metals, Vol. III, 2Color SL, Madrid, 2001, pp. 81–86.
[8] H. Castro, C. Rodriguez, F.J. Belzunce, A.F. Cantelli, Mechanical properties and corrosion behaviour of stainless steel reinforcing bars, J. Mater. Process. Technol. 143-144 (2003) 134–137.
[9] L. Freire, M.J. Carmezim, M.G.S. Ferreira, M.F. Montemor, The passive behaviour of AISI 316L in alkaline media and the effect of pH: A combined electrochemical and analytical study, Electrochim. Acta 55 (2010) 6174–6181.
[10] A. Bautista, G. Blanco, F. Velasco, Corrosion behaviour of low-nickel austenitic stainless steels reinforcements: A comparative study in simulated pore solutions, Cem. Concr. Res. 36 (2006) 1922–1930.
[11] M. Kouril, P. Novak, M. Bojko, Threshold chloride concentration for stainless steels activation in concrete pore solutions, Cem. Concr. Res. 40 (2010) 431–436.
[12] S.M. Alvarez, A. Bautista, F. Velasco, Corrosion behaviour of corrugated lean duplex stainless steels in simulated pore solutions, Corros. Sci. 53 (2011) 1748–1755.
[13] L. Bertolini, F. Bolzoni, T. Pastore, P. Pedeferri, Behaviour of stainless steel in simulated concrete pore solution, Br. Corros. J. 31 (1996) 218–222.
[14] A. Bautista, G. Blanco, F. Velasco, A. Gutiérrez, L. Soriano, F.J. Palomares, H. Takenouti, Changes in the passive layer of corrugated, low-Ni, austenitic stainless steel due to the exposure to simulated pore solutions, Corros. Sci. 51 (2009) 785–792.
[15] A. Bautista, G. Blanco, H. Takenouti, EIS study of passivation of austenitic and duplex stainless steels reinforcements in simulated pore solutions, Cement Concr. Compos. 28 (2006) 212–219.
[16] A. Bautista, G. Blanco, F. Velasco, M.A. Martínez, Corrosion performance of welded stainless steels reinforcements in simulated pore solutions, Constr. Build. Mater. 21 (2007) 1267–1276.
[17] K.R. Trethewey, M. Wenman, P. Chard-Tuckey, B. Roebuck, Correlation of meso- and micro-scale hardness measurements with pitting of plastically deformed Type 304L stainless steel, Corros. Sci. 50 (2008) 1132–1141.
[18] U. Kamachi Mudali, P. Shankar, S. Ningshen, R.K. Dayal, H.S. Khatak, B. Raj, On the pitting corrosion resistance of nitrogen alloyed cold worked austenitic stainless steels, Corros. Sci. 44 (2002) 2183–2198.
[19] A. Barbucci, G. Cerisola, P.L. Cabot, Effect of cold-working in the passive behavior of 304L stainless steel in sulfate media, J. Electrochem. Soc. 149 (2002) B534–B542.
[20] G. Bianchi, A. Cerquetti, F. Mazza, S. Torchio, Electronic properties of oxide films and pitting susceptibility of type 304L stainless steel, Corros. Sci. 12 (1972) 495–502.
[21] M.J. Carmezin, A.M. Simoes, M.F. Montemor, M. Da Cunha Belo, Capacitance behaviour of passive films on ferritic and austenitic stainless steel, Corros. Sci. 47 (2005) 581–591.
[22] A. Fattah-Alhosseini, M.A. Golozar, A. Saatchi, K. Raeissi, Effect of solution concentration on semiconducting properties of passive films formed on austenitic stainless steels, Corros. Sci. 52 (2010) 205–209.
[23] N.E. Hakiki, B. Maachi, F. Mechehoud, C. Pirri, A. Mehdaoui, J.L. Bubendorff, Structural and Semiconductive Investigation of Passive Films and Thermally Grown Oxides on Stainless Steels, Paper 58, 7th European Stainless Steel Conference, Como (Italy) September 2011.
[24] C.M. Abreu, M.J. Cristobal, R. Losada, X.R. Novoa, G. Pena, M.C. Pérez, Long-term behaviour of AISI 304L passive layer in chloride containing medium, Electrochim. Acta 51 (2006) 1881–1890.
[25] M. Abreu, M.J. Cristobal, R. Losada, X.R. Novoa, G. Pena, M.C. Pérez, The effect of Ni in the electrochemical properties of oxide layers grown on stainless steels, Electrochim. Acta 51 (2006) 2991–3000.
[26] L. Freire, X.R. Novoa, G. Pena, V. Vivier, On the corrosion mechanism of AISI 204Cu stainless steel in chlorinated alkaline media, Corros. Sci. 50 (2008) 3205–3212.
[27] M. Kouril, P. Novak, M. Bojko, Limitations of the linear polarization method to determine stainless steel corrosion rate in concrete environment, Cement Concr. Compos. 28 (2006) 220–225.
[28] L. Veleva, M.A. Alpuche-Avilés, M.K. Graves-Brook, D.O. Wipf, Voltammetry and surface analysis of AISI 316L stainless steel in chloride-containing simulated concrete pore environment, J. Electroanal. Chem. 578 (2005) 45–53.
[29] B. Elsener, D. Addari, S. Coray, A. Rossi, Nickel-free manganese bearing stainless steel in alkaline media – Electrochemistry and surface chemistry, Electrochim. Acta 45 (2011) 4489–4497.
[30] S. Fajardo, D.M. Bastidas, M. Criado, M. Romero, J.M. Bastidas, Corrosion behaviour of a new low-nickel stainless steel in saturated calcium hydroxide solution, Constr. Build. Mater. 25 (2011) 4190–4196.
[31] A. Iversen, B. Leffler, Aqueous corrosion of stainless steel, in: B. Cottis, M. Graham, R. Lindsay, S. Lyon, T. Richardson, D. Scantlebury, H. Stott (Eds.), Shreir's Corrosion, vol. 3, Elsevier, Amsterdam, 2010, pp. 1802–1878.
[32] F. Velasco, G. Blanco, A. Bautista, M.A. Martínez, Effect of welding on local mechanical properties of stainless steels for concrete structures using universal hardness tests, Constr. Build. Mater. 23 (2009) 1883–1891.
[33] G. Lothongkim, P. Wongpanya, S. Morito, T. Furuhara, T. Maki, Effect of nitrogen on corrosion behaviour of 28Cr-7Ni duplex stainless steels in air-saturated 3.5%wt% NaCl solution, Corros. Sci. 48 (2006) 137–153.
[34] N. Orhan, T.I. Kahn, M. Eroglu, Diffusion bonding of a microduplex stainless steel next term to Ti–6Al–4V, Scripta Mater. 45 (2001) 441–446.
[35] S. Fujimoto, H. Tsuchiya, Semiconductor property of passive films and corrosion behavior of Fe–Cr alloys, in: Y. Waseda, S. Suzuki (Eds.), Characterization of Corrosion Products on Steel Surfaces, Springer, Berlin Heidelberg, 2006, pp. 33–49.
[36] L.V. Taveira, M.F. Montemor, M. Da Cuhha Belo, M.G. Ferreira, L.F.P. Dick, Influence of incorporated Mo and Nb on the Mott–Schottky behaviour of anodic films formed on AISI 304L, Corros. Sci. 52 (2010) 2813–2818.
[37] N.E. Hakiki, S. Boudin, B. Rondot, M. Da Cunha Belo, The electronic structure of passive films formed on stainless steels, Corros. Sci. 37 (1995) 1809–1822.
[38] S. Ningshen, U. Kamachi Mudali, V.K. Mittal, H.S. Khatak, Semiconducting and passive films properties of nitrogen-containing type 316LN stainless steel, Corros. Sci. 49 (2007) 481–496.
[39] J.-B. Lee, S.-I. Yoon, Effect of nitrogen alloying on the semiconducting properties of passive films and metastable pitting susceptibility of 316L and 316LN stainless steels, Mater. Chem. Phys. 122 (2010) 194–199.
[40] L. Peguet, B. Malki, B. Baroux, Influence of cold working on the pitting corrosion resistance of stainless steel, Corros. Sci. 49 (2007) 1933–1948.
[41] B.S. Jang, B.H. Oh, Effects of non-uniform corrosion on the cracking and service life of reinforced concrete structures, Cem. Concr. Res. 40 (2010) 1441–1450.

5.3 PUBLICACION 3: P3

S.M. Alvarez, A. Bautista, F. Velasco.

"*Influence of process parameters on the corrosion resistance of corrugated austenitic and duplex stainless steels*".

Materials and technology (Materiali in tehnologije), vol. 47, p. 317–321, 2013.

UDK 669.14.018.8:620.19
Original scientific article/Izvirni znanstveni članek

ISSN 1580-2949
MTAEC9, 47(3)317(2013)

INFLUENCE OF PROCESS PARAMETERS ON THE CORROSION RESISTANCE OF CORRUGATED AUSTENITIC AND DUPLEX STAINLESS STEELS

VPLIV PROCESNIH PARAMETROV NA KOROZIJSKO ODPORNOST REBRASTIH AVSTENITNIH IN DUPLEKSNIH NERJAVNIH JEKEL

Sandra M. Alvarez, Asunción Bautista, Francisco Velasco

Universidad Carlos III de Madrid, Materials Sci. and Eng. Dept – IAAB, Avda. Universidad 30, Leganés, Madrid, Spain
asuncion.bautista@uc3m.es

Prejem rokopisa – received: 2012-09-06; sprejem za objavo – accepted for publication: 2012-11-13

The main objective of this work is to study the influence of the forming process on two corrugated, lean, duplex stainless steels (DSSs): UNS S32001 and UNS S32304. Both grades have been recently proposed as alternative materials to the austenitic UNS S30403 grade for manufacturing reinforcement bars to be embedded in concrete structures, exposed to corrosive environments. Hot-worked (HW) corrugated bars of both DSSs are analyzed and their corrosion behaviour is compared with that of the HW and cold-worked (CW) corrugated bars of S30403.
The corrosion performance is characterized through cyclic polarization curves in 8 different solutions that simulate those contained inside the pores of concrete in different circumstances.
The obtained results justify a great interest in the studied lean DSS grades with respect to their use as reinforcements. Moreover, it is proved that the corrugated surface of a bar is clearly less corrosion resistant than the centre of the bar. The processing method of producing reinforcements influences not only the pitting susceptibility but also the pitting morphology.

Keywords: corrosion, stainless steel, reinforcements, processing, lean duplex

Glavni cilj tega dela je študija vpliva postopka izdelave na dve rebrasti dupleksni nerjavni jekli brez molibdena (DSS): UNS S32001 in UNS S32304. Obe vrsti jekla sta bili predloženi kot nadomestni material za avstenitno jeklo UNS S30403 za izdelavo palic za ojačanje, ki se vgradijo v strukture iz betona, ki so izpostavljene korozivnemu okolju. Vroče izdelane (HW) rebraste palice obeh DSS so bile analizirane in njihovo korozijsko vedenje je primerjano z vroče (HW) in hladno izdelanimi (CW) rebrastimi palicami iz jekla S30403.
Korozijsko vedenje je ocenjeno z uporabo krivulj pri ciklični polarizaciji v 8 različnih raztopinah, ki simulirajo tekočine, ki so v porah betona v različnih okoliščinah.
Dobljeni rezultati potrjujejo veliko zanimanje za uporabo preučevanih jekel DSS z nizko vsebnostjo molibdena za ojačitev betona. Še več, dokazano je, da je rebrasta površina palic nedvomno bolj korozijsko odporna kot sredina palice. Metoda izdelave ojačitvenih palic vpliva poleg občutljivosti na jamičasto korozijo tudi na morfologijo korozijskih jamic.

Ključne besede: korozija, nerjavno jeklo, ojačitve, izdelava dupleksnega jekla z malo Mo

1 INTRODUCTION

The use of stainless-steel corrugated bars instead of carbon steel bars in those parts of reinforced concrete structures that are more exposed to corrosion is one of the most reliable strategies for assuring the durability of a structure.[1] Initially, austenitic grades were used with this objective.[2]

Duplex stainless steels (DSSs) have shown a good corrosion resistance in many media. With respect to the reinforced concrete exposed to aggressive environments, corrosion studies have shown advantages of the traditional UNS S32205 DSS reinforcements in comparison with the most common austenitic grades[3,4] and they started to be used for corrugated bars about ten years ago. Recently, two more economical DSSs have been proposed for their use in concrete,[5] not for replacing the S32205 reinforcements used in extremely aggressive conditions, but as an alternative to the corrugated bars of the austenitic UNS S30403 grade.

UNS S32304 DSS, considered in the present study, has a low Mo-content and it has been known for years. Since 2003 its use has been growing in desalinization industries, marine applications or production processes, replacing the austenitic UNS S31603 steel. UNS S32001 is the other DSS evaluated in this study. It is a very novel DSS grade, lower alloyed than S32304, with smaller Ni and Cr contents, i.e., cheaper.

There are scarce references about the corrosion behaviour of these lean DSS grades and most of the studies consider the environments very different form concrete. Special chemical characteristics of the solution inside concrete pores introduce factors that modify the protective ability of the passive layers on stainless steels. These characteristics are different from the ones shown by the materials that are exposed to the atmosphere or to other environments.[6] Most authors also agree that a higher alkalinity in a pore solution has a positive impact on the corrosion behaviour of stainless steel,[4–8] though the issue remains controversial.[9]

Moreover, to be used as reinforcements in concrete structures, the stainless steels must be hardened during the processing[10] and their surface must be formed into corrugations to assure a good adherence with the concrete. There are factors that many of the previous corrosion studies on stainless steels in simulated pore solutions have not considered, as they were carried out in stainless steels that were not formed as corrugated bars.[11–14] However, recent studies suggest that the forming process of corrugated bars can dramatically affect the corrosion behaviour of austenitic stainless steels in alkaline solutions with chlorides.[15]

2 EXPERIMENTAL WORK

Four different stainless-steel grades were considered in the study, two corrugated, lean, duplex stainless steels (DSSs): the UNS 32001 and UNS S32304 hot-worked (HW) corrugated bars and two austenitic UNS S30403, HW and cold-worked (CW) corrugated bars. The products were manufactured by Roldán S. A. (Acerinox Group, Spain). The diameters of the corrugated bars considered in the study as well as their chemical compositions can be seen in **Table 1**. The chemical compositions of the bars were experimentally determined with X-ray fluorescence (XRF), using a Spectre XEPOS equipment.

The corrosion behaviour of different places (core and surface) of the corrugated stainless steels was characterized with cyclic polarizations curves, using an EG&G 263A galvanostat- potentiostat from Princeton Applied Research. Electrochemical measurements were carried out in the solutions that simulate those contained in the concrete pores in different conditions. Saturated $Ca(OH)_2$ solutions (pH ≈ 13), simulating non-carbonated concrete, with four different NaCl contents in mass fractions were used: (0, 0.5, 1 and 5) %. The saturated $Ca(OH)_2$ solutions, whose pH values decreased to about 9 due to CO_2-bubbling, were used to simulate the behaviour in carbonated concrete. Chloride contents of (0, 0.5, 1 and 5) % were also considered for carbonated solutions.

The testing procedure was based on the ASTM G61 Standard. Cyclic polarization curves were carried out using a three-electrode cell. A saturated calomel electrode (SCE) was used as the reference electrode and a stainless-steel mesh as the counter-electrode. Samples of the corrugated stainless-steel bars acted as working electrodes. The measurements were carried out after a 48-h exposure of the stainless-steel samples to the testing solution to assure the correct stabilization of the corrosion potential (E_{corr}). The sweeping rate was 0.17 mV/s. The potential was reversed when the current densities reached a value of 10^{-4} A/cm^2.

To study the corrosion behaviour of a corrugated surface, samples 2 cm of the real surfaces of the bars were exposed to the corresponding testing media. The corrosion behaviour of the non-corrugated materials was analyzed exposing the samples from the centres of the bars to the testing solutions. For the samples from the centres of the bars, an Avesta cell was used to assure the absence of crevices that could interfere with the measurements.

An analysis of the morphology of the attack after the polarization curves was carried out with scanning electronic microscopy (SEM) using a Philips XL30 equipment.

3 RESULTS AND DISCUSSION

The polarization curves of the corrugated surfaces and the centres of the stainless-steel bars clearly exhibit different shapes, as can be seen in **Figure 1**, where the curves corresponding to the non-carbonated solutions with 5 % NaCl are shown. For the samples without corrugations (**Figure 1a**), the pitting potential (E_{pit}) is well defined and corresponds with very sharp current increases. On the other hand, in the tests carried out on the real surfaces of the bars (**Figure 1b**), the current increase after E_{pit} is less pronounced. It must be pointed out that on certain materials exposed to particular testing conditions, no corrosion occurred during the test. This is the case, for example, of the centre of the HW S32304 bar in a non-carbonated solution with 5 % NaCl (**Figure 1a**), where the current increase does not correspond to any corrosion phenomenon but it is due to the water decomposition through reaction 1:

$$4OH^- \rightarrow 2H_2O + O_2 + 4e^- \quad (1)$$

In the case of a sudden current increase and the absence of hysteresis during the reverse cycle, the potential value confirms that no corrosion has taken place during the test.

The $E_{pit} - E_{corr}$ distance is widely considered to be a reliable way of measuring the resistance to localized corrosion. The E_{corr} values of all the systems considered in this study are very similar. The E_{pit} values plotted in

Table 1: Diameters of corrugated bars and experimentally determined chemical compositions of the studied stainless steels
Tabela 1: Premer rebrastih palic in eksperimentalno določena kemijska sestava preiskovanih nerjavnih jekel

Stainless steel	Diameter *d*/mm	Main alloying elements, *w*/%								
		S	Si	Mn	Cr	Ni	Mo	N	C	Fe
CW S30403	10	0.001 0	0.361	1.45	18.30	8.68	0.27	0.050	0.023	Bal.
HW S30403	16	0.001 2	0.298	1.42	18.37	8.74	0.27	0.055	0.026	Bal.
HW S32001	16	0.001 0	0.681	4.14	19.98	1.78	0.24	0.124	0.025	Bal.
HW S32304	16	0.002 0	0.651	1.54	22.70	4.47	0.26	0.153	0.017	Bal.

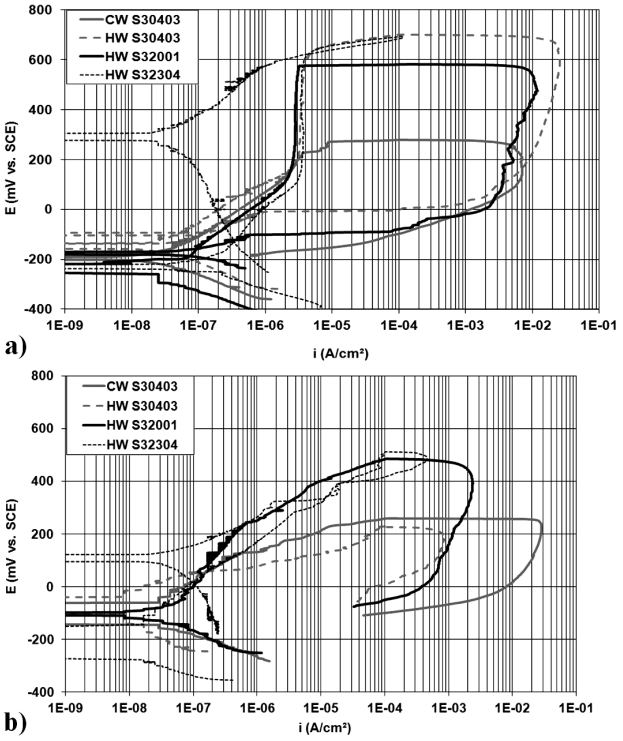

Figure 1: Polarization curves in non-carbonated $Ca(OH)_2$ solutions with 5 % NaCl: a) centres of the bars, b) corrugated surfaces

Slika 1: Polarizacijske krivulje v negazirani raztopini $Ca(OH)_2$ s 5 % NaCl: a) sredina palice, b) rebrasta površina

Figures 2 and **3** can be an adequate tool for comparing the corrosion behaviours of stainless steels in different conditions.

It is very interesting to find a significant decrease in the corrosion resistance of the bars due to the changes to the corrugations taking place during the forming process. **Figure 2** shows the difference between the E_{pit} values of the studied stainless steels in carbonated solutions, with the measurements carried out on the corrugated surfaces

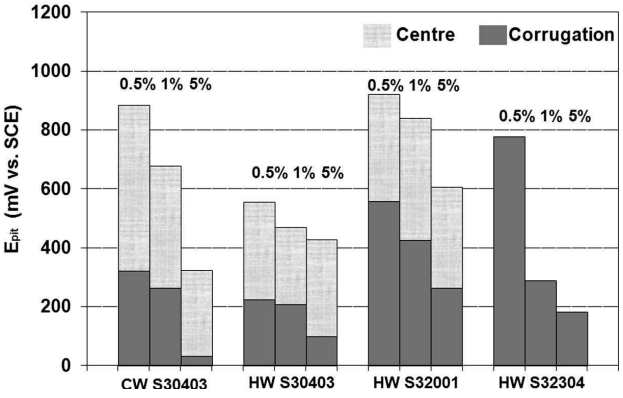

Figure 2: Differences between the E_{pit} measured in the centres of stainless-steel bars and on corrugated surfaces in carbonated $Ca(OH)_2$ solutions with different chloride contents

Slika 2: Razlika med izmerjenim E_{pit} v sredini palice iz nerjavnega jekla in na rebrasti površini v gazirani raztopini $Ca(OH)_2$ z različno vsebnostjo kloridov

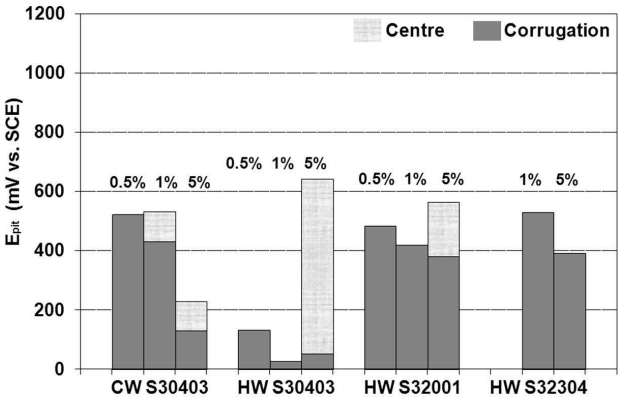

Figure 3: Differences between the E_{pit} measured for the centres of stainless-steel bars and for the corrugated surfaces in non-carbonated $Ca(OH)_2$ solutions with different chloride contents. Conditions without the plotted E_{pit} values correspond to tests where no corrosion takes place.

Slika 3: Razlika med izmerjeno E_{pit} za sredino nerjavne palice in za rebrasto površino v negazirani raztopini $Ca(OH)_2$ z različno vsebnostjo kloridov. Primeri brez prikazane E_{pit} ustrezajo preizkusom, kjer se korozija ni pojavila.

or in the centres of the bars. As in some cases the definition of E_{pit} is not easy, the potential, at which the anodic current reaches the value of 10^{-4} A/cm^2, has been chosen as the criterion for determining this parameter.

The marked difference between the E_{pit} values, corresponding to the corrugated surface and to the other regions of a bar, emphasises the effect of the process parameters. It would be risky to extrapolate the results of the stainless steels processed in the way different from that of the corrugated bars to the performance in concrete, though it has been often done in literature. These data confirm the trend observed in the recently published work on more traditional austenitic stainless steels.[15] The minor corrosion resistance of a corrugated surface of stainless steel has been explained with a more deformed microstructure and a higher stress concentration in the corrugation than found in the centre of the bar.[15] Different grain sizes and grain morphologies of the corrugations and of the centres of the bar were studied previously for the reinforced bars considered in our earlier work,[16] and the obtained results proved that the corrugations exhibit a highly deformed microstructure with a reduced grain size.

In the carbonated solutions without chlorides, no corrosion was detected for any of the studied stainless steels. Moreover, the centres of the HW S32304 bars proved to be immune to corrosion during the polarization tests carried out independently of the chloride content of the carbonated solution. However, during the polarization of the corrugated surfaces of HW S32304 in the presence of chlorides, current increases corresponding to a corrosive attack were detected, even with 0.5 % NaCl.

For the other three studied stainless-steel grades, a localized corrosion always occurred during the polarization tests in the carbonated solutions with chlorides.

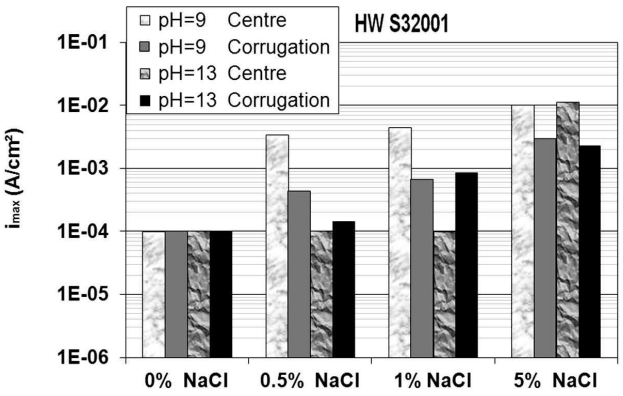

Figure 4: Differences between the i_{max} values obtained with the polarization curves for the centres and the corrugated surfaces of duplex HW S32001 bars in carbonated and non-carbonated $Ca(OH)_2$ solutions with different chloride contents

Slika 4: Razlike med vrednostmi i_{max}, dobljene iz polarizacijskih krivulj iz sredine in iz rebraste površine dupleksnih palic HW S32001 v gazirani in negazirani raztopini $Ca(OH)_2$ z različno vsebnostjo kloridov

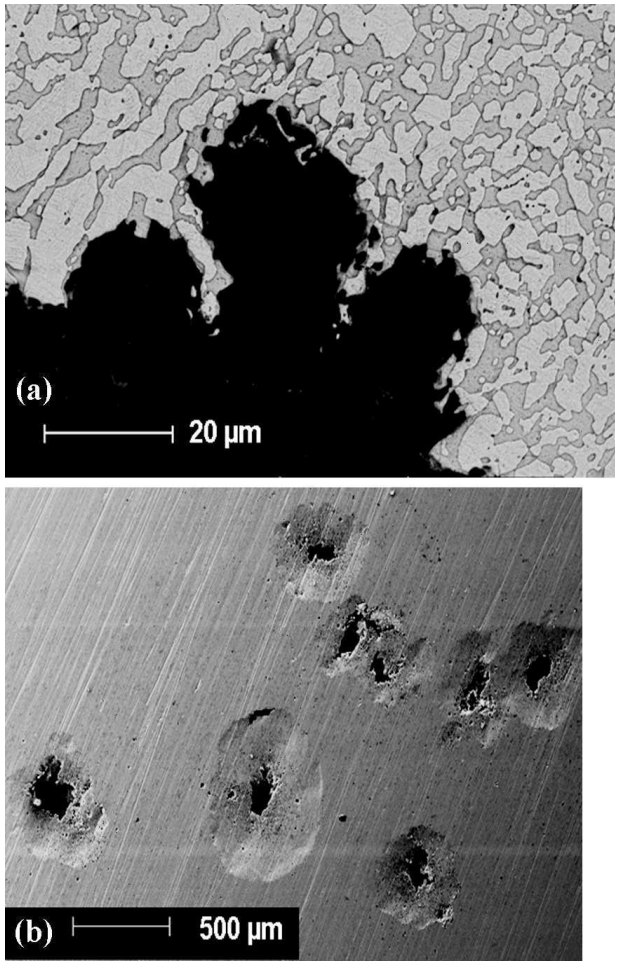

Figure 5: Images of different morphologies of the attacks that appear on the centre of a bar and on the corrugated surface. The pits after the polarization of HW S32001 in non-carbonated $Ca(OH)_2$ solutions with 5 % NaCl: a) corrugated surface, b) center of the bar.

Slika 5: Posnetki različnih morfologij napada, ki se pojavi v sredini palice in na rebrasti površini. Jamice po polarizaciji HW S32001 v negazirani raztopini $Ca(OH)_2$ s 5 % NaCl: a) rebrasta površina, b) sredina palice.

For all the materials the E_{pit} of the corrugated surface is much lower than the E_{pit} of the centre of a bar.

As expected, in all the cases an increase in the chloride content of the solution causes a decrease in the resistance to localized corrosion, i.e., a decrease in E_{pit}.

In **Figure 3**, the E_{pit} values detected in non-carbonated solutions are plotted. It can be seen that, at a higher pH, it is more difficult to cause corrosion during the test. In the solutions without chlorides, no corrosion occurs in any of the cases and the centre of HW S32304 is immune to the attacks in the testing media with chlorides, as reported for pH ≈ 9. Besides, no corrosion occurs during the polarization in the solutions with 0.5 % NaCl on the centres of the other studied bars. In the case of the 1 % NaCl testing solution, no corrosion was found on the centres of HW S30403 or HW S32001.

The corrugated surfaces of the bars prove again to be much more prone to corrosion. For this type of samples, the only condition where no pitting is detected is HW S32304 with 0.5 % NaCl. The important influence of the microstructural changes occurring in the surfaces of the corrugated bars during the forming process is again clearly proved.

If the results from **Figures 2** and **3** are used to compare the corrosion behaviours of different grades, it is demonstrated that HW S32304 is clearly more corrosion resistant than any of the studied austenitic grades. Despite the volatility of the prices in the market, it can be considered that a S32304 grade can cost about 9 % less than a S30403 grade. This result justifies the great interest in this DSS grade that is seen as an alternative for the traditional austenitic grade used in these applications, as S32304 has a better performance and it is somewhat more economical. The DSS S32001 grade can be estimated to be about 15 % cheaper than the austenitic S30403. The results of the corrosion tests carried out indicate that the corrosion resistance of both grades are quite similar, or that the corrosion resistance of the cheap, new DSS grade is even better.

In addition to E_{pit}, another interesting parameter, which can be obtained from the polarization curves, is the maximum intensity (i_{max}) reached during the measurements. All the curves are programmed to reverse the potential sweep when a current intensity of 10^{-4} A/cm^2 is reached. When no corrosion occurs, i_{max} is 10^{-4} A/cm^2, as the current quickly decreases when the applied potentials decrease. When pits are formed during the anodic polarization, the current still increases as the potentials start to decrease due to the important autocatalytic effect of the localized corrosion. The higher the i_{max}, the more dangerous is the pitting morphology. As an example, the values of this parameter for sixteen tested conditions of HW S32001 were plotted in **Figure 4**. If the conditions, under which no corrosion takes

place, are not considered (0 % NaCl and the centre of the bar for 0.5 and 1 % NaCl at pH ≈ 13), it can be seen that the samples from the centre of the bar, though less susceptible to corrosion than the corrugated surfaces, suffer from a more aggressive attack than when it occurs on the surface. The same conclusion is reached if the results for the other four studied materials are analyzed. It can also be seen in **Figure 4** that chlorides have an important influence on the increase of i_{max}.

An observation of the morphology of the pits after the polarization curves confirms the idea deduced from the i_{max} values. As it can be seen in **Figure 5**, the polarization causes small, shallow pits widely distributed on the most deformed regions of the surface of the corrugation. In the centre of the bar, polarizations cause scarce, but much bigger pits that can be much more dangerous.

4 CONCLUSIONS

The susceptibility to pitting corrosion on the corrugated surface of corrugated stainless steel is always much higher than in the centre of the bars of the same material. The forming process clearly decreases the corrosion resistance of stainless steel used as a reinforcement material in concrete structures.

The attack that appears on the corrugated surfaces of stainless steels during an anodic polarization is less localized and less dangerous than the attack that appears in the centres of the bars.

The new lean DSSs for reinforcing bars are very interesting options for substituting the traditional austenitic S30403 bars. S32304 clearly exhibits a better corrosion behaviour being also somewhat cheaper. S32001 is highly interesting from an economic point of view and its corrosion results are similar, even slightly better, than those of S30403.

5 REFERENCES

[1] U. Nürberger (Ed.), Stainless steel in concrete, State of the art report, Publication n° 18, Institute of Materials, London, 1996

[2] L. Bertolini, P. Pedeferri, Corrosion Reviews, 20 (**2002**), 129–152

[3] A. Bautista, G. Blanco, F. Velasco, A. Gutiérrez, S. Palacín, L. Soriano, H. Takenouti, Materiales de Construcción, 57 (**2007**), 17–32

[4] A. Bautista, G. Blanco, F. Velasco, Cement and Concrete Research, 36 (**2006**), 1922–1930

[5] S. M. Alvarez, A. Bautista, F. Velasco, Corrosion Science, 53 (**2011**), 1748–1755

[6] A. Bautista, G. Blanco, F. Velasco, A. Gutiérrez, L. Soriano, F. J. Palomares, H. Takenouti, Corrosion Science, 51 (**2009**), 85–792

[7] M. Kouril, P. Novak, M. Bojko, Cement Concrete Research, 40 (**2010**), 431–436

[8] L. Bertolini, F. Bolzoni, T. Pastore, P. Pedeferri, British Corrosion Journal, 31 (**1996**), 218–222

[9] L. Freire, M. J. Carmezim, M. G. S. Ferreira, M. F. Montemor, Electrochimica Acta, 55 (**2010**), 6174–6181

[10] Guidance on the use of stainless steel reinforcement, Technical report N° 51, The Concrete Society, London, 1998

[11] M. Kouril, P. Novak, M. Bojko, Cement Concrete Composites, 28 (**2006**), 220–225

[12] L. Veleva, M. A. Alpuche-Avilés, M. K. Graves-Brook, D. O. Wipf, Journal of Electroanalytical Chemistry, 578 (**2005**), 45–53

[13] B. Elsener, D. Addari, S. Coray, A. Rossi, Electrochimica Acta, 45 (**2011**), 4489–4497

[14] S. Fajardo, D. M. Bastidas, M. Criado, M. Romero, J. M. Bastidas, Construction and Building Materials, 25 (**2011**), 4190–4196

[15] E. C. Paredes, A. Bautista, S. M. Alvarez, F. Velasco, Corrosion Science, 58 (**2012**), 52–61

[16] S. M. Alvarez, A. Bautista, F. Velasco, S. Guzman, Proceedings of the 7th European Stainless Steel Conference, Como, Italy, 2011

5.4 PUBLICACION 4: P4

S.M. Alvarez, A. Bautista, F. Velasco.

"*Influence of strain-induced martensite in the anodic dissolution of austenitic stainless steels in acid medium*".

Corrosion Science, vol. 69, p. 130-138, 2013.

Corrosion Science 69 (2013) 130–138

Contents lists available at SciVerse ScienceDirect

Corrosion Science

journal homepage: www.elsevier.com/locate/corsci

Influence of strain-induced martensite in the anodic dissolution of austenitic stainless steels in acid medium

S.M. Alvarez, A. Bautista *, F. Velasco

Universidad Carlos III de Madrid, Materials Science and Engineering Department – IAAB, Avda. Universidad n° 30, Leganés, Madrid, Spain

ARTICLE INFO

Article history:
Received 20 September 2012
Accepted 17 November 2012
Available online 5 December 2012

Keywords:
A. Stainless steel
B. Electrochemical calculation
B. Polarization
B. Potentiostatic
B. SEM
C. Acid corrosion

ABSTRACT

The anodic dissolution of austenitic stainless steel bars in an acid medium (0.5 M HCl + 2 M H_2SO_4) under different polarizations is studied. The material comes from bars formed by hot working (HW) and by cold working (CW). UNS S30403 and S31603 grades are considered. The determining effect of alloying elements and working method are proved. The morphology of the attack at different anodic potentials is analyzed. The important influence of the amount and distribution of strain-induced martensite on corrosion is demonstrated. The effect of the martensite on the anodic polarization curves is quantified using specifically designed software.

1. Introduction

Austenitic stainless steels are materials of outstanding importance because they offer an excellent combination of corrosion resistance, mechanical properties and formability. The corrosion resistance of austenitic stainless steels is often limited by the precipitation of phases in their microstructure. Hence, it is important to know how changes in the microstructure during processing can determine the corrosion behavior of a certain stainless steels grade.

The sensitization risk of stainless steel by the formation of chromium-rich precipitates is a well-known phenomenon [1,2]. The influence on the corrosion behavior of precipitates formed in austenitic stainless steels after annealing treatments has been previously studied in depth [3,4]. For heat-treated stainless steels, the detrimental effect of additional precipitation of δ-ferrite in the microstructure [5] or high-temperature oxides on the surface [6] have also been studied.

In non-sensitized austenitic stainless steels, a single phase is expected. However, some alloying elements such as Ti [7] or S [8–10] can cause precipitates that favor nucleation of the pits and localized attack.

It is a known fact that austenitic stainless steels are metastable under low temperature conditions, and plastic deformation can induce the formation of a martensitic phase in their microstructure [11,12]. The formation of martensite in the austenitic microstructure can be caused by a severe forming process [13–15], surface treatments [15,16] or stresses during service conditions [11,17].

This precipitated martensitic phase modifies the mechanical behavior of the austenitic stainless steels [15,18] and its influence in problems such as hydrogen assisted fracture has been analyzed [19]. Moreover, strain-induced martensite can also affect the localized corrosion performance of austenitic stainless steels. For highly-deformed stainless steels, the processing clearly can change the corrosion behavior of austenitic stainless steels [20]. It has been published that strain-induced martensite can condition the development of the pits in alkaline medium [13]. A decrease in the length of the passive regions of the polarization curves of austenitic stainless steels in 3.5% NaCl neutral solutions due to strain-induced martensite has also been reported [16,21]. However, other authors have detected no change in the pitting potential in media with chlorides due to the formation of martensite in austenitic stainless steels [14].

In acid medium, the corrosion of stainless steels develops through a very different mechanism than in neutral or alkaline medium, and a generalized attack can take place instead of localized corrosion. The behavior of stainless steel in diluted acid is complex and it is well known that the active-to-passive transition can be very sensitive to small changes in the alloy composition [22]. At low pHs, the microstructure can also condition the development of the attack. The decrease in the corrosion resistance of austenitic stainless steels in acid media with chlorides with cold rolling has been related to changes in microstructure, such as martensite formation, but also to others, such as grain morphology or crystallographic texture, with the authors being unable to evaluate

* Corresponding author. Tel.: +34 916249914; fax: +34 916249430.
E-mail address: asuncion.bautista@uc3m.es (A. Bautista).

0010-938X/$ - see front matter © 2012 Elsevier Ltd. All rights reserved.
http://dx.doi.org/10.1016/j.corsci.2012.11.033

the contribution of each microstructural factor to the corrosion performance [23]. More recently, other researchers have found some relationship between the increase in the corrosion rate in acidic NaCl solutions and the martensite fraction in the microstructure of an austenitic stainless steel [14].

Anodic polarization curves in acid media are a useful method for studying the corrosion resistance of stainless steels and their active-to-passive transition. Traditionally, anodic curves in different H_2SO_4 solutions have been used to evaluate the sensitization degree of austenitic stainless steel after a heat-treatment [5,24] or other manufacturing procedures [25]. The most typical testing solution is 0.5 M H_2SO_4 + 0.01 M KSCN (ASTM Standard G-108). Nowadays, the procedure has been extended to other types of stainless steel or Ni-base alloys [24,26]. Additionally, some optimizations of the standard method have been suggested for austenitic stainless steel [27] and a modified method of polarization in 1 M HCl solution has been proposed [28] to study the effect of heat-treatments in duplex stainless steels (formed by austenite and ferrite in a relation of about 50–50).

Mixed H_2SO_4 + HCl solutions have been previously used as testing media to study the corrosion behavior of new, highly-alloyed austenitic stainless steels [29], and a single activation peak can be appreciated during the anodic polarization curves. However, for the S32205 duplex grade in mixed H_2SO_4 + HCl solutions, it has been found two activation peaks [30,31]. Each peak has been related to the selective anodic dissolution of the austenitic phase or the ferritic phase in the material. The peak that appears at the lower potential region during anodic polarization was associated with the preferential dissolution of ferrite, and its relative intensity increases as the concentration of H_2SO_4 in the solution does [30]. On the other hand, the peak appearing at higher potentials corresponds to the austenite dissolution, and its relative intensity increases as the concentration of HCl does [30].

This work studies the influence of the composition and processing method on the corrosion behavior at different anodic potentials in acid media for the two most common austenitic grades when they have been work-hardened. The influence of the presence of strain-induced martensite is analyzed and quantified. The testing medium is the same solution (2 M H_2SO_4 + 0.5 M HCl) considered optimal in the literature for promoting the selective anodic dissolution of the phases for the S32205 duplex grade with anodic polarizations [31].

2. Experimental

The two austenitic stainless steel grades that are most common in the market were considered in the study: UNS S30403 and UNS S31603. Samples were obtained from cold worked (CW) and hot worked (HW) bars for both grades. The products were manufactured by Roldán S.A. (Acerinox Group, Spain). The chemical composition of the bars can be seen in Table 1.

The tensile strength (*TS*) of the bars as well as their grain size can be found in Table 2. The grain size of stainless steel bars was measured according to ASTM E112 Standard.

Table 2
TS and grain size of the stainless steel bars.

Stainless steel	*TS* (MPa)	Grain size (μm)
CW S31603	734	28
HW S31603	800	3.6
CW S30403	747	51
HW S30403	780	6.6

The cores of the four austenitic stainless steel bars considered in this study were characterized by X-ray Diffraction (XRD) to detect to the possible presence of martensite in their microstructures. λCu radiation was used for the measurements. The XRD was performed in step scan mode, with a step size of 0.02° and a time per step of 5 s. The angular interval was between 40° and 95°.

The amount of magnetic phase in the microstructure of the austenitic bars was quantified using the magnetic induction method, according to the ISO 17655.

Electrochemical corrosion tests were carried out using a three electrode configuration. A saturated calomel electrode (SCE) was used as reference electrode while a stainless steel mesh was used as counter-electrode. The transverse section of the material to be tested (polished to 0.3 μm) acted as working electrode. 2 M H_2SO_4 + 0.5 M HCl solution was used for testing. All tests were carried out in an Avesta cell to avoid any risk of crevice.

Anodic polarizations were performed starting from −550 mV to 400 mV *vs*. SCE at a sweep rate of 1 mV/s. The anodic polarization curves for each material were repeated 5–7 times to assure the reliability of the results.

The deconvolution of the peaks in the anodic polarization curves was carried out by specifically programmed software. The software was developed using the Graphical User Interface (GUI) builder tool and under Matlab language (Matlab version R2010b). The software used generalized extreme value (GEV) functions to obtain curves that fit the experimental data. The GEV distribution is defined by the Eq. (1):

$$F(x;\mu,\sigma,\xi) = \exp\left\{-\left[1+\xi\left(\frac{x-\mu}{\sigma}\right)\right]^{-1/\xi}\right\} \quad (1)$$

where x are the potential values and F are the current density values. μ is the location parameter (depending on the potentials at which the current peak appears), σ is the scale parameter (related to the area of the peak) and ξ is the shape parameter (that allows to simulate the characteristic asymmetry of the activation peaks). The theoretical background and physical applications of GEV can be easily found in literature [32,33]. The engineering application and limits of the GEV have been previously discussed [34].

The software generates two GEV curves whose addition can be fitted to the *E*–*i* measured function in the activation region of the polarization curve.

The fitting also allowed to obtain values of the charge density involved in the different phenomena occurring during the anodic polarization, in addition to other relevant parameters, such as the maximum current density (i_{max}) of each phenomenon and the potential (E_{max}) at which the corresponding i_{max} takes place.

Table 1
Chemical composition of the studied stainless steel bars.

Stainless steel	Chemical composition (%)								
	C	S	Si	Mn	Cr	Ni	Mo	N	Fe
CW S31603	0.025	0.003	0.350	1.40	17.05	10.12	2.11	0.042	Bal.
HW S31603	0.013	0.003	0.310	1.78	16.76	11.17	2.50	0.044	Bal
CW S30403	0.023	0.001	0.361	1.45	18.30	8.68	0.27	0.050	Bal.
HW S30403	0.026	0.001	0.298	1.42	18.37	8.74	0.27	0.055	Bal.

Potentiostatic tests were carried out for all of the steels at different anodic potentials to check the influence of the polarization on the morphology of the attack. Potentials values inside the activation region of the anodic polarization curves were chosen. The length of the potentiostatic tests was 4 h.

Sections perpendicular to the surface tested in the potentiostatic tests were metallographically prepared in order to observe the morphology of the attack. *Aqua regia* (HNO_3 + HCl solution) was used to etch the microstructure of austenitic grades. The observations were carried out through scanning electron microscopy (SEM).

3. Results and discussion

Representative anodic polarization curves of the four studied austenitic stainless steels are plotted in Fig. 1. In this acid media, as expected, the curves exhibit an activation region where high current densities are recorded. For the CW S31603, the curve apparently has the shape of a single peak, while for the other three studied materials, more complex shapes can be observed. Other authors have blamed notches in the working electrode for the double peak in the curve of austenitic stainless steels [5]. The experimental set-up used in this work discards this interpretation for the present results. The complex shape could be related to the anodic dissolution of different phases, as has been proved for duplex stainless steels [30,31,35].

Bearing in mind their composition (Table 1), it could be expected that the studied bars comprise pure austenitic microstructures. However, due to their final applications, the bars have been processed in a way that their mechanical properties (Table 2) are higher than those of other typical components of S30403 or S31603. A heavy working process can cause the formation of martensite, hence XRD spectra are carried out to check this point. The results can be seen in Fig. 2. The four big peaks characteristic of the austenite are clearly visible for all the materials. Moreover, for HW S31603, HW S30403 and CW S30403, small peaks compatible with the presence of martensite in their microstructure can be observed.

The magnetic measurements (Fig. 3) confirm the presence of a magnetic phase for all the studied materials except CW S31603. The strain-induced martensite is magnetic, unlike austenite. The results in Fig. 3 are coherent with the XRD spectra in Fig. 2: CW S30403 (the bar with the more intense martensite XRD-peaks) is the one with highest amount of strain-induced martensite; then the HW S30403, and the HW S31603 is the bar with lowest amount of martensite. For CW S31603, no martensite has been detected with both techniques. It is known that plastic deformation can induce the formation of martensite in austenitic stainless steels such as S30403 or S31603. The tendency to form strain-induced martensite depends on the stacking fault energy (*SFE*) of the austenitic material. *SFE* changes with temperature and chemical composition of the stainless steel [11]. The lower typical *SFE* value of S30403 ($\approx$18 mJ/m^2) compared to that of S31603 ($\approx$50 mJ/m^2) [36] is coherent with the experimental finding that S30403 bars processed in similar way to S31603 bars are more prone to the precipitation of strain-induced martensite (Figs. 2 and 3). This difference between the *SFE* values can be explained bearing in mind the composition of the alloys. It has recently been proved that Mo hinders the martensite formation [12], and this element is present in S31603 but not in S30403 (Table 1). Moreover, S31603 grades are also Ni-richer than S30403 grades (Table 1) and Ni greatly favors the stability of austenite [12].

The influence of the type of forming process on the amount of formed martensite can be difficult to predict. CW bars have larger grain size than HW bars (Table 2) and most authors who have studied this topic agree that an increase in the grain size enhances the martensitic transformation [12]. On the other hand, it was expected that the amount of martensite should be lower when the working process takes place at a higher temperature [12] and obviously HW occurs at a higher temperature than does CW. Bearing this in mind, those criteria CW bars of a given composition should have more strain induced martensite than HW bars. This occurs for S30403, but not for S31603 (Figs. 2 and 3). Another important parameter that determines the precipitation of martensite is obviously the amount of strain. The high *TS* of HW S31603 (Table 2) suggests that this bar may have been submitted to a heavier formation process.

Potentiostatic tests are carried out at meaningful anodic potentials within the activation region with the aim of indentifying the phenomena that cause the different peaks on the curves in Fig. 1. SEM images of the CW S30403 samples polarized at different anodic potential can be seen in Fig. 4. At anodic potentials close to corrosion potential (E_{corr}), it is clear that a selective anodic dissolution takes place (Fig. 4a). The electrochemical dissolution affects alternate bands inside the grains and occurs in austenitic grains with different orientations (Fig. 4b). There are a limited number of grains whose surfaces remain immune to the attack. Bearing in mind previous results on the microstructure of this bar (Figs. 2 and 3) and the reported influence on martensite on pit morphology in basic medium [13], it seems logical to assume that the strain induced martensite is the phase that dissolves in this condition.

When the applied anodic potential increases, the morphology of the attack clearly changes (Fig. 4c). The conditions also become

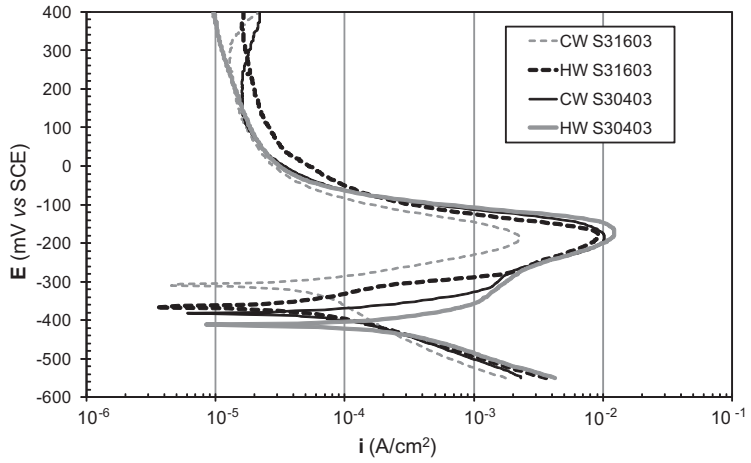

Fig. 1. Anodic polarization curves of the four studied austenitic stainless steel bars in 0.5 M HCl + 2 M H_2SO_4.

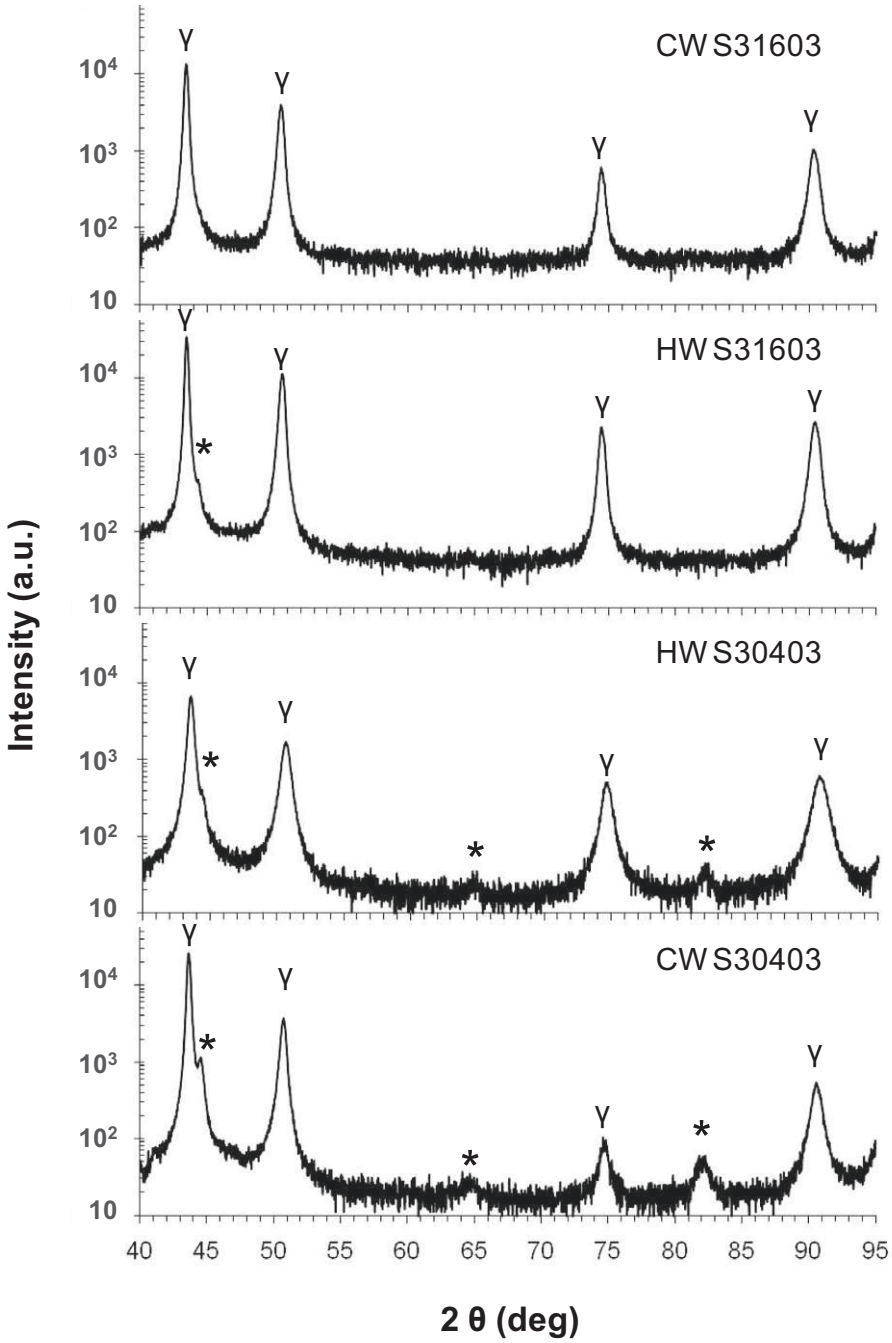

Fig. 2. XRD spectra of the studied austenitic stainless steel bars. Peaks marked with (*) correspond to martensite phase; peaks marked with (γ) correspond to the austenite phase.

aggressive for the austenite and all of the metallic material is dissolved. A generalized attack takes place with quite a ripple morphology that has no apparent relationship with the microstructure of the bar.

When the potentiostatic tests are carried out in the other CW grade studied, the S31603, where no strain-induced martensite had been previously detected with the two techniques used (Figs. 2 and 3), and apparently a single peak appeared in the activation region (Fig. 1); the morphology of the attack is that shown in Fig. 5. The attack at polarizations close to E_{corr} (Fig. 5a) seems to proceed through a mechanism similar to the attack at higher polarizations inside the activation region (Fig. 5b). The attack morphology is similar to that observed in Fig. 4c, and coincides with that expected for a pure austenitic stainless steel in acid media. However, a very detailed SEM study has revealed that images such as those in Fig. 5c can be observed during the polarization at small anodic overpotentials. A low-intensity, selective anodic dissolution can be guessed at very rare points of the tested material. Disregarding the intensity of the attack, its morphology could resemble that observed in Fig. 4a and b. This fact would indicate that some martensite could be present in the microstructure of CW S31603, although in an amount that is below the detections limits of the XRD and the magnetic measurements used.

In Fig. 6, the different morphology of the attack after polarization of HW S30403 at two different anodic overpotentials can be observed, corresponding with the two peaks observed in activation

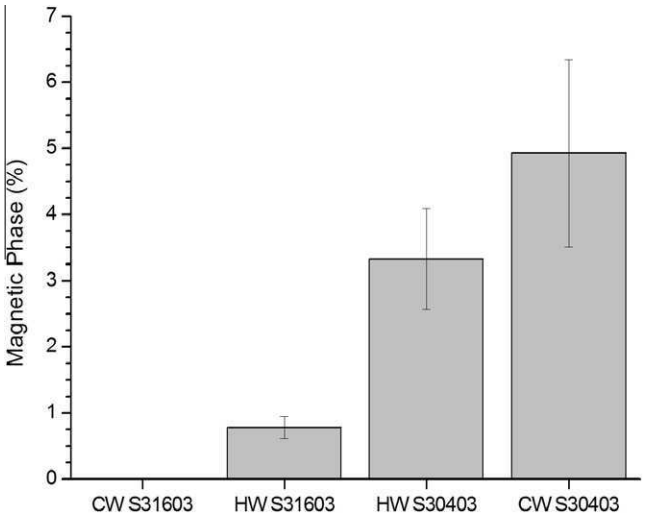

Fig. 3. Quantification of the amount of magnetic phase in the stainless steel bars obtained with a ferritometre.

region during the polarization curve of the stainless steel (Fig. 1). It has been exhaustively checked that, at low overpotentials, the tested surface exhibits smaller-sized waves with a more irregular shape (Fig. 6a) than at high polarizations. At high overpotentials (Fig. 6b), the morphology of the surface resembles those observed when the CW grades suffer general attack (Figs. 4c and 5b); that is to say, in this potential region the materials undergo a anodic dissolution process without any evident influence of the microstructure. The phenomenon shown in Fig. 6a, unlike that in Fig. 6b, seems to be microstructure dependant. The shape of the polarized surface seems to be related with the grain shape and size. The highly-reduced grain size of the HW grades (Table 2) does not allow to observe morphologies of the selective attack as those in Figs. 4a, 4b and 5c. The morphology of the tested surface suggests that the selective anodic dissolution of some grains takes place, whose presence is abundant throughout the microstructure. It seems logical to assume that this selective anodic dissolution is related to the presence of strain-induced martensite.

The images obtained after the potentiostatic tests of HW S31603 are shown in Fig. 7. The most noteworthy fact shown is the trend of the attack to proceed as pits, in spite of the pH of the medium, which is expected to promote general attack. For these bars a reduced, but detectable, amount of strain-induced martensite has been found (Figs. 2 and 3). This low corrosion-resistant phase can be unevenly distributed in certain grains inside the microstructure of the HW S31603 bar. The relations between the working direction and orientation of the grains can explain the uneven distribution of strain induced martensite inside the austentite grains. The formation of martensite bands has proved to be favored in the direction parallel to hot-rolling [21], and in this case, this probably occurs, although the small grain size of the studied HW grades (Table 2) does not allow this point to be easily checked. In Fig. 7a, it can be seen that the attack penetrates through several points of the surface while other regions remain unattacked. At higher anodic overpotential (Fig. 7b), the entire surface dissolves with the morphology observed for other bars at high potentials inside the activation region. However, what is remarkable is the additional presence of numerous pits whose profile seems to be clearly related to the grain shape. Selective grain dissolution is occurring. The higher localization of the strain-induced martensite in HW S31603 bars could explain the progress of localized attack, even at potentials where the austenite is also dissolving.

In Fig. 8, some representative examples of the current density evolution with time during the potentiostatic tests are shown. As expected, there exists certain proportionality among the current densities registered during the potentiostatic test and those registered at those potentials in the potentiodynamic curves for the same materials. When the potentiostatic tests are carried out inside the region where the general corrosion is the predominant

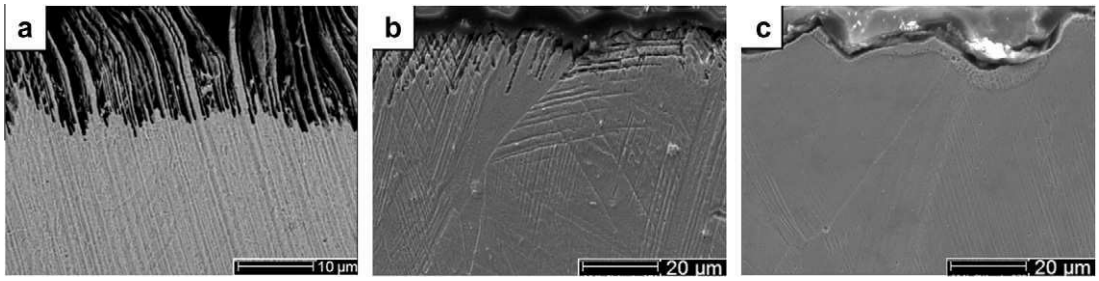

Fig. 4. Cross-sectional view of the CW S30403 austenitic stainless steel samples after potentiostatic tests: (a) at −272 mV *vs.* SCE at high magnifications; (b) at −272 mV *vs.* SCE; (c) at −184 mV *vs.* SCE.

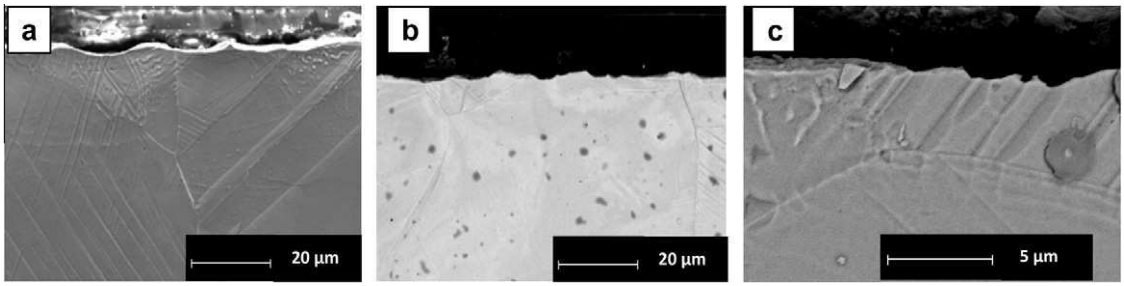

Fig. 5. Cross-sectional view of the CW S31603 austenitic stainless steel samples after potentiostatic tests: (a) at −230 mV *vs.* SCE; (b) at −185 mV *vs.* SCE; (c) detailed view of the selective attack that occurs in few points of the surface at −230 mV *vs.* SCE.

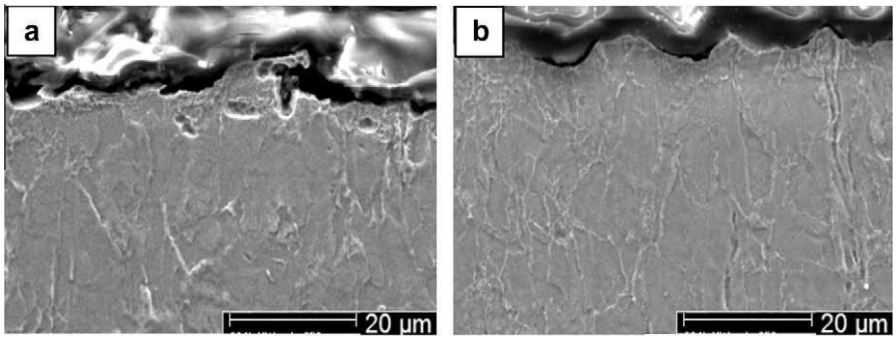

Fig. 6. Cross sectional view of HW S30403 austenitic stainless steel samples after potentiostatic tests: (a) at −350 mV *vs.* SCE; (b) at −172 mV *vs.* SCE.

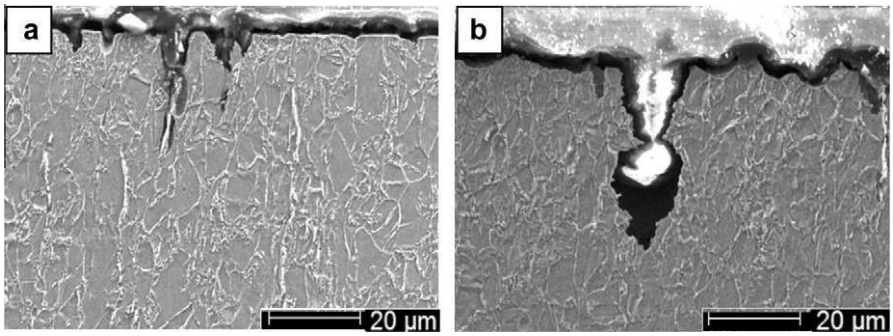

Fig. 7. Cross-sectional view of the HW S31603 austenitic stainless steel samples after potentiostatic tests: (a) at −250 mV *vs.* SCE; (b) at −190 mV *vs.* SCE.

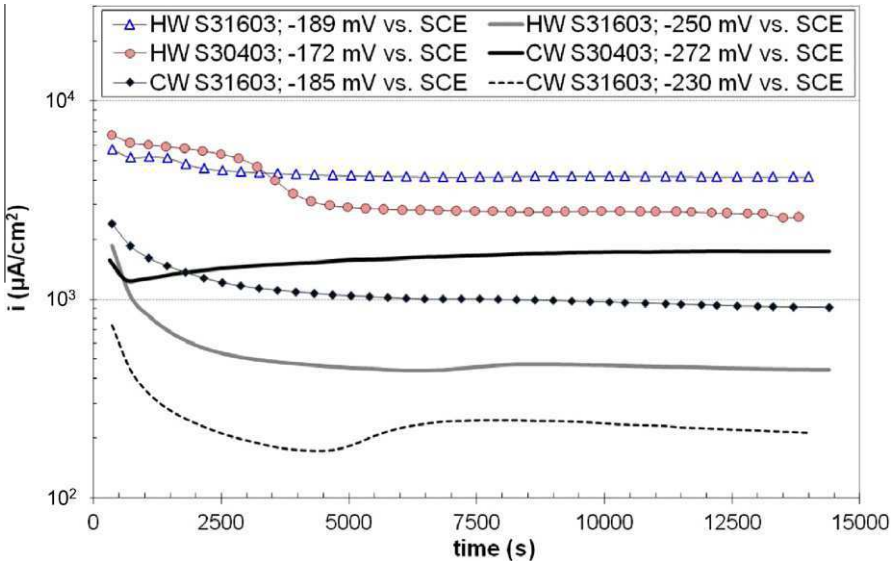

Fig. 8. Examples of the current density evolution during the potentiostatic tests of the stainless steel samples.

mechanism of attack (curves plotted using thin lines and symbols), the current densities tend to be higher at the beginning but they exhibit a pseudo-asymptotic behavior after a time.

On the other hand, if the potentiostatic tests are carried out at anodic overpotentials closer to E_{corr} (examples are plotted in Fig. 8 using thick lines without symbols), the shape of the curves depends on the working process. For CW bars, it can be observed that the current densities initially decrease, but after reaching a minimum, the current density tends to increase again to higher values. This trend could be related to the development of a localized attack. The auto-catalytic effect of the localized corrosion due to concentration cells that appear in the crevices caused by the attack is a well-known phenomenon. The minimum is clearly appreciated after short testing times for HW S30403 polarized at −272 mV *vs.* SCE. The high intensity of the localized attack at this potential for this material (Fig. 4a and b) explains this clearly observed trend. In materials where the trend to localized corrosion at small anodic overpotentials can be hardly guessed, as CW S31603 (Fig. 5c), the minimum in the current density is also hardly detectable.

For HW bars, as it can be seen in the curve of HW S31603 at −250 mV *vs.* SCE (Fig. 8), the current very sallow minimum perhaps could be guessed, but the small grain size of the tests HW bars

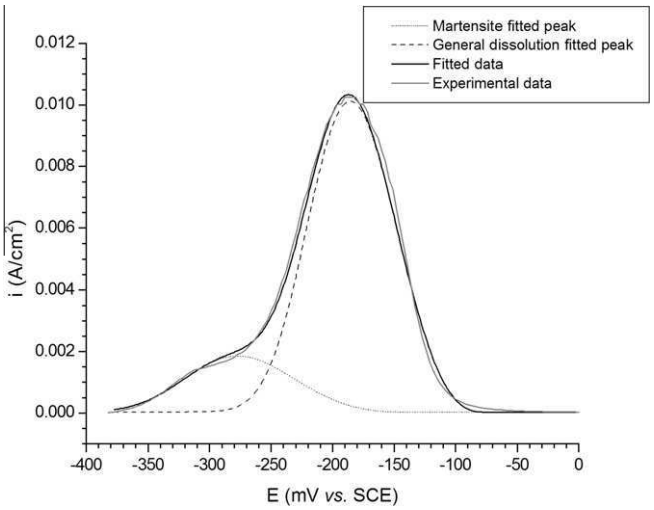

Fig. 9. Example of the deconvolution of the anodic activation region that appears during the polarization curves for austenitic CW S30403 using the software.

conditions the distribution of strain induced martensite and the shape of the potentiostatic curve.

The contribution of both selective anodic dissolution of martensite and general dissolution of the material to the shape of curves such as those in Fig. 1 are calculated using specifically designed software. An example of the fittings carried out can be seen in Fig. 9. The results of the fitting are plotted – as well as other parameters of the curves – in Figs. 10–12. For each type of stainless steel bar, about 5 experimental curves have been simulated. The error bars in Figs. 10–12 came from the small dispersion in the experimental curves that affects fitting results.

In Fig. 10, the charge density circulated during the anodic polarization curves is assigned at each phenomenon that occurs in the activation region. The charge density corresponding to total activation region is also plotted. The charge density values are obtained from the area under the corresponding curves, in simulations such as those in Fig. 9. This parameter can be considered as the most accurate way of evaluating the relative intensity of both types of attack in the different materials. The total activation region implies charge densities higher but close to those caused by the general dissolution of the material of the bars. It can be seen that the selective dissolution of the martensite implies charge densities lower than the general attack of the surface. This is due to the smaller amount of surface that reacts during this type of attack than during the corrosion at higher potentials. The ratio of the areas of the martensite corrosion peak and general corrosion peak ranges between 0.18 and 0.27. These values are much higher than those that could be predicted from the simple amount of martensite in the microstructure of each material (Fig. 3). The higher corrosion rate of the martensite in comparison with austenite is responsible for the meaningful contribution of this precipitated phase to the corrosion process in spite of its reduced presence in the microstructure.

It can be seen that the three types of charge densities plotted in Fig. 10 are higher for S30403 grades than for S31603 grades. This result is probably influenced by the martensite content in the microstructure (Fig. 3). However, it is important to point out that the distribution of martensite in the microstructure, not only its amount, should influence the corrosion process. For HW S30403, the charge densities are slighter higher than for CW S30403, although the former has less strain-induced martensite. HW S31603 has charge density values lower than those of CW S30403, but closer than those that the simple difference between the amounts of martensite in their microstructures would lead us to assume. HW grades, with a much smaller grain size than CW grades seem to be more prone to develop more aggressive attacks.

In Fig. 11, the maximum current densities of the peaks (i_{max}) are plotted. The i_{max} values are sometimes used for evaluating the dissolution of the stainless steel in acid media due to its easy calculation [37]. The analysis of the i_{max} values confirms the trends observed in Fig. 1, but it proves to be less sensitive to detect differences among the materials: the i_{max} for HW S31603, CW S30403 and HW S30403 are similar, but meaningful differences can be found if the area of the peaks is analyzed (Fig. 10). The areas of the peaks clearly exhibit a direct proportionality with the amount of species dissolved through the different mechanisms during the anodic polarizations, while the relationship between the magnitude of the anodic dissolution and i_{max} can be partly masked when complex phenomena occurs, as in this case.

The passivation intensities (i_{pass}) reflect no differences among the studied materials (Fig. 11). No information about differences in the quality of the passive layer after it has been anodically formed can be deduced from this parameter, which has proved to be independent from strain-induced martensite.

In Fig. 12 it can be seen that the E_{corr} of the bar decreases as the amount of martensite in the bar increases (Figs. 2 and 3). The same phenomenon can be observed for the E_{max} corresponding to the martensite peak (Fig. 12). Both potentials (E_{corr} and $E_{max\text{-}martensite}$) tend to decrease their values as the area of the martensite peak increases (Fig. 10), that is to say, as more strain induced martensite is

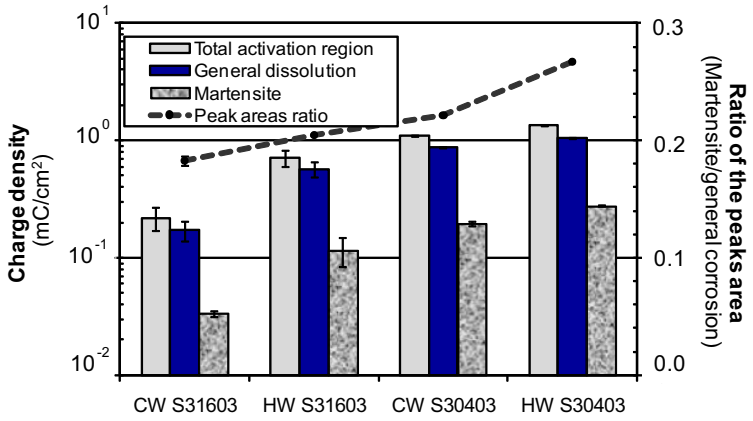

Fig. 10. Charge density values obtained from the fitting of the curves for the different phenomena occurring in the active region of the anodic polarization curves of the austenitic stainless steels.

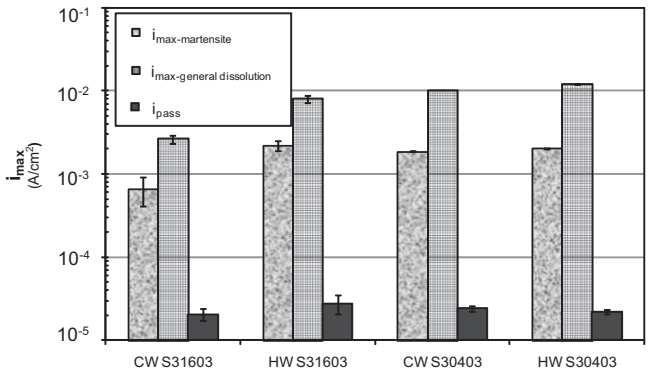

Fig. 11. Current density values obtained from the analysis of the activation region in the anodic polarization curves of the studied stainless steels.

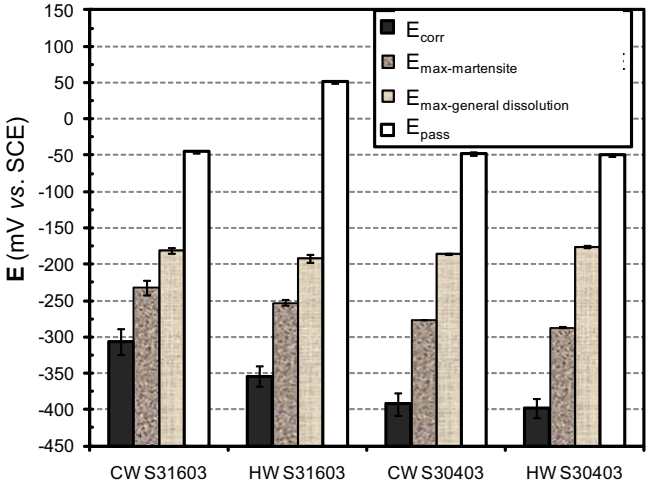

Fig. 12. Potential values obtained from the analysis of the activation region in the anodic polarization curves of the studied stainless steels.

precipitated in the bars, the peak corresponding to their selective anodic dissolution expands to more negative potentials and higher intensities. These facts confirm that the value E_{corr} depends on the electrochemical characteristics and relative abundance of the less corrosion resistant phase in the stainless steels. As E_{corr} is a mixed potential whose value is governed by the fastest equilibrium, these results suggest that the attack of the strain-induced martensite is the faster anodic process that takes place in these media in absence of polarizations. These results also suggest that in more-concentrated acid medium, where the cathodic semireaction would be shifted to higher potential values, the equilibrium could be established at higher E_{corr} values, where the general attack would be the fastest anodic process.

Moreover, it can also be seen in Fig. 12 that the value of $E_{max\text{-}general\ corrosion}$ remains constant for all the materials studied, independently of the composition and working process. The E_{pass} values are also similar for all the studied material, except for the HW S31603. This suggests that the E_{pass} value is not very sensitive to the changes in the composition of the allying elements of strain-induced martensite, whenever the anodic dissolution does not mainly proceed by a localized mechanism. When there is meaningful amount of martensite, but unevenly distributed in the microstructure, as occurs in HW S31603, the localized attack progresses not only at potentials close to E_{corr}, but during all the activation region of the curve (Fig. 8). In these cases, the morphology of the pits hinders the passivation and shifts E_{pass} to higher values.

4. Conclusions

1. The presence of small amounts of strain-induced martensite strongly conditions the anodic dissolution behavior of heavily-worked stainless steels in acid media.
2. The martensite selectively corrodes at potentials lower than those the general anodic dissolution of the microstructure occurs.
3. Specifically designed software has allowed to obtain quantitative information about the contributions of the selective anodic dissolution of the martensite and the general corrosion of the material to the attack in the activation region of the anodic polarization curves.
4. S30403 grades suffer the selective anodic dissolution of the martensite to a higher extent than S31603 grades, due to their chemical composition.
5. The influence of the martensite on the corrosion behavior depends not only on its amount but also on its distribution. HW bars, – which have much smaller grain size than CW bars to obtain similar mechanical properties – can develop more aggressive ways of attacks.

Acknowledgements

The authors would like to thank Rubén Martín for his help with the design of the software used in this research. The authors would also like to express their thanks to the Spanish Science and Innovation Ministry for financial support (BIA-2007-66491-C02-02).

References

[1] R. Singh, S.G. Chowdhury, B.R. Kumar, S.K. Das, P.K. De, I. Chattoraj, The importance of grain size relative to grain boundary character on the sensitization of metastable austenitic stainless steel, Scr. Mater. 57 (2007) 185–188.
[2] N. Parvathavarthini, R.K. Dayal, Time–temperature-sensitization diagrams and critical cooling rates of different nitrogen containing austenitic stainless steels, J. Nucl. Mater. 399 (2010) 62–67.
[3] R. Jones, V. Randle, Sensitisation behaviour of grain boundary engineered austenitic stainless steel, Mater. Sci. Eng. A 527 (2010) 4275–4280.
[4] C. Garcia, M.P. de Tiedra, Y. Blanco, O. Martin, F. Martin, Intergranular corrosion of welded joints of austenitic stainless steels studied by using an electrochemical minicell, Corros. Sci. 50 (2008) 2390–2397.
[5] P. De Tiedra, O. Martín, M. López, M. San-Juan, Use of EPR test to study the degree of sentitization in resistance spot welding joints of AISI 304 austenitic stainless steel, Corros. Sci. 53 (2011) 1563–1570.
[6] A. Bautista, G. Blanco, F. Velasco, M.A. Martínez, Corrosion performance of welded stainless steels reinforcements in simulated pore solutions, Constr. Build. Mater. 21 (2007) 1267–1276.
[7] A. Bautista, G. Blanco, F. Velasco, Corrosion behaviour of low-nickel austenitic stainless steels reinforcements: a comparative study in simulated pore solutions, Cem. Concr. Res. 36 (2006) 1922–1930.
[8] P. Schmuki, H. Hildebrand, A. Friedrich, S. Virtanen, The composition of the boundary region of MnS inclusions in stainless steel and its relevance in triggering pitting corrosion, Corros. Sci. 47 (2005) 1239–1250.
[9] L. Freire, X.R. Novoa, G. Pena, V. Vivier, On the corrosion mechanism of AISI 204Cu stainless steel in chlorinated alkaline media, Corros. Sci. 50 (2008) 3205–3212.
[10] N. Parvathavarthini, R.K. Gupta, A.V. Kumar, S. Ramya, U.K. Mudali, Interpretation of electrochemical potentiokinetic reactivation data in the presence of sulphide/oxysulphide inclusions in 316LN stainless steel, Corros. Sci. 53 (2011) 3202–3214.
[11] W. Hübner, Phase transformations in austenitic stainless steels during low temperature tribological stressing, Tribol. Int. 34 (2001) 231–236.
[12] S. Das, S. Tarafder, P.C. Chakraborti, Estimation of deformation induced martensite in austenitic stainless steels, Mater. Sci. Eng. A 529 (2011) 9–20.
[13] R.D. Moser, P.M. Singh, L.F. Kahn, K.E. Kurtis, Chloride-induced corrosion resistance of high-strength stainless steels in simulated alkaline and carbonated concrete pore solutions, Corros. Sci. 57 (2012) 241–253.
[14] A.S. Hamada, L.P. Karjalainen, M.C. Somani, Electrochemical corrosion behavior of a novel submicron-grained austenitic stainless steel in an acid NaCl solution, Mater. Sci. Eng. A 431 (2006) 211–217.
[15] I. Altenberger, B. Scholtes, U. Martin, H. Oettel, Cyclic deformation and near surface microstructures of shot peened or deep rolled austenitic stainless steel AISI 304, Mater. Sci. Eng. A 264 (1999) 1–16.

[16] B.K. Mordyuk, G.I. Propopenko, M.A. Vasylyev, M.O. Iefimov, Effect of the structure evaluation induced by ultrasonic peening on the corrosion behavior of AISI-321 stainless steel, Mater. Sci. Eng. A 458 (2007) 253–261.
[17] H. Chen, X.Z. Guo, W.Y. Chu, K.W. Gao, Y.B. Wang, Y.J. Su, L.J. Qiao, Martensite caused by passive film-induced stress during stress corrosion cracking in type 304 stainless steel, Mater. Sci. Eng. A 358 (2003) 122–127.
[18] K. Spencer, J.D. Embury, K.T. Conlon, M. Véron, Y. Bréchet, Strengthening via the formation of strain-induced martensite in stainless steels, Mater. Sci. Eng. A 387–389 (2004) 873–881.
[19] M. Martin, S. Weber, C. Izawa, S. Wagner, A. Pundt, W. Theisen, Influence of machining-induced martensite on hydrogen-assisted fracture of AISI type 304 austenitic stainless steel, Int. J. Hydrogen Energy 36 (2011) 11195–11206.
[20] E.C. Paredes, A. Bautista, S.M. Alvarez, F. Velasco, Influence of the forming process of corrugated stainless steels on their corrosion behaviour in simulated pore solutions, Corros. Sci. 58 (2012) 52–61.
[21] I.T. Hong, C.H. Koo, Antibacterial properties, corrosion resistance and mechanical properties of Cu-modified SUS 304 stainless steel, Mater. Sci. Eng. A 393 (2005) 213–222.
[22] A. Pardo, M.C. Merino, M. Carboneras, F. Viejo, R. Arrabal, J. Muñoz, Influence of Cu and Sn content in the corrosión of AISI 304 and 316 stainless steel in H_2SO_4, Corros. Sci. 48 (2006) 1075–1092.
[23] A. Barbucci, M. Delucchi, M. Panizza, M. Sacco, G. Cerisola, Electrochemical and corrosion behaviour of cold rolled AISI 301 in 1 M H_2SO_4, J. Alloys Compd. 317–318 (2001) 607–611.
[24] V. Cihal, R. Stefec, On the development of the electrochemical potetiokinetic method, Electrochim. Acta 46 (2001) 3867–3877.
[25] A. Bautista, F. Velasco, S. Guzmán, D. de la Fuente, F. Cayuela, M. Morcillo, Corrosion behavior of powder metallurgical stainless steels after two years of exposure in atmosphere, Corros. Eng. Sci. Technol. 41 (2006) 284–290.
[26] V. Cihal, S. Lasek, M. Blahetova, E. Kalabisova, Z. Krhutova, Trends in elelectrochemical polarization potentiondynamic reactivation methods-EPR, Chem. Biochem. Eng. Q. 21 (2007) 47–54.
[27] O. Martín, P. De Tiedra, C. García, F. Martín, M. López, Comparative study between large-scale and small-scale electrochemical potentiokinetic reactivation performed on AISI 316L austenitic stainless steel, Corros. Sci. 54 (2012) 119–126.
[28] C.-J. Park, H.-S. Kwon, Effects of aging at 475 °C on corrosion properties of tungsten-containing duplex stainless steels, Corros. Sci. 44 (2002) 2817–2830.
[29] S. Zor, M. Soncu, L. Çapan, Corrosion behavior of G-X CrNiMoNb 18-10 austenitic stainless steel in acidic solutions, J. Alloys Compd. 480 (2009) 885–888.
[30] I.-H. Lo, Y. Fu, C.-J. Lin, W.-T. Tsai, Effect of the electrolite compostion on the active-to-passive trasition behavior of 2205 duplex stainless steel in H_2SO_4/HCl solutions, Corros. Sci. 48 (2006) 696–708.
[31] W.-T. Tsai, J.-R. Chen, Galvanic corrosion between the constituent phases in duplex stainless steel, Corros. Sci. 49 (2007) 3659–3668.
[32] J. Swait, Choice set generation within the generalized extreme value family of discrete choice models, Transport. Res. B-Meth. 35 (2001) 643–666.
[33] M. Clusel, E. Bertin, Global fluctuations in physical systems: a subtle interplay between sum and extreme value statistics, Int. J. Mod. Phys. B 22 (2008) 3311–3368.
[34] J.D. Holmes, W.W. Moriarty, Application of the generalized Pareto distribution to extreme value analysis in wind engineering, J. Wind Eng. Ind. Aerodyn. 83 (1999) 1–10.
[35] S.-J. Pan, Y.-J. Shih, J.-R. Chen, J.-K. Chang, W.-T. Tsai, Selective micro-etching of duplex stainless steel for preparing manganese oxide supercapacitor electrode, J. Power Sources 187 (2009) 2161–2167.
[36] S.S. Tavares, M.R. da Silva, J.M. Pardal, H.F.G. Abreu, A.M. Gomes, Microstructural changes produced by plastic deformation in the UNS S31803 duplex stainless steel, J. Mater. Process. Technol. 180 (2006) 318–322.
[37] M. Romero, V. Matres, Comparative evaluation on uniform corrosion resistance behaviour of ferritic stainless steels: experimental studies of electrochemical test, in: 7th European Stainless Steel Conference, Paper No. 5, Como, Italy, September 2011.

5.5 PUBLICACION 5: P5

A. Bautista, S.M. Alvarez, F. Velasco.

"*Selective corrosion of duplex stainless steel bars in acid. Part 1: effect of the composition, microstructure and anodic polarizations*".

Materials and Corrosion, aceptado. DOI: 10.1002/maco.201307419.

Selective corrosion of duplex stainless steel bars in acid
Part 1: Effect of the composition, microstructure and anodic polarizations

A. Bautista*, S. M. Alvarez and F. Velasco

The selective corrosion of the phases comprised in four duplex stainless steels (DSS) is studied in acid media ($H_2SO_4 + HCl$ solutions). The work considers traditional UNS S32205 grade as well as other economical-advantageous grades (UNS S32001 and UNS S32304). The samples of the lean DSS come from bars formed by hot working (HW), while those of the S32205 come both from HW bars and bars obtained by cold working. The amount of strain-induced martensite in the austenitic phase of DSS that the processing has induced is highly dependent on the DSS composition. The change in the relative corrosion resistance of the different phases comprised in the microstructure with the potential is considered. The influence of the composition of the DSS is discussed. It has been checked that, at potentials close to the corrosion potential (E_{corr}), the corrosion of the ferritic phase is more favored than that of the austenite. Increasing potentials in the anodic activation region tends to favor the selective corrosion of the austenite. The trend to selective dissolution is less marked for the least alloyed DSS. The strain-induced martensite in the austenitic phase exhibits a corrosion resistance clearly higher than that of the ferrite at E_{corr} or potentials close to E_{corr}. The possible influence of TiN precipitates in the corrosion development is also analyzed.

1 Introduction

Duplex stainless steels (DSS) are materials of outstanding importance because of their combination of corrosion resistance and mechanical properties. These grades tend to generate highly protective passive layers in many environments [1]. DSS are progressively coping new applications in structural components, for example, in the automobile industry [2] or in construction [3,4]. Their microstructure tends to hinder the progress of the localized attack [5]. New compositions appear continuously in the market [6–8]. The volatility on the Ni prize has been an important drawback for the commercialization of stainless steel for years. The low-Ni content of DSS in comparison to the Ni concentration of traditional austenitic grades makes DSS very interesting from the economic point of view, especially when lean DSS are considered. Lean DSS exhibit higher corrosion resistance than usual austenitic and ferritic grades against chloride induced corrosion and chloride induced stress corrosion cracking [9]. Moreover, they are clearly less susceptible to crevice corrosion [9].

Additionally to the traditional DSS UNS S32205 grade, two more economical DSS grades are included in the study: UNS S32304 and UNS S32001. S32304 DSS has low Mo-content. Its use has grown up in desalinization industries, marine applications or production processes since 2003, thus displacing austenitic UNS S31603. It has also been proposed as an alternative for UNS S30404 reinforcing bars in concrete [5]. S32001 is lower alloyed than S32304, containing less Ni and Cr (i.e., cheaper). It has been suggested that its corrosion performance is lower than other highly alloyed DSS grades, but similar to that of traditional austenitic UNS S30400, in alkaline solutions with chlorides [5].

The influence of precipitates formed after annealing treatments in DSS on the corrosion behavior has been previously studied in depth [10–12], but microstructure-dependant corrosion phenomena can also appear in absence of precipitates. Moreover, DSS are formed by ferrite and austenite phases in a ratio about 50/50, which has been proved to be the optimum ratio to enhance corrosion performance in acid media [13]. When non-annealed DSS are exposed to a corrosive medium, the attack is expected to start in the least corrosion-resistant phase of the DSS, so preferential corrosion of one of the phases could often take place.

A. Bautista, S. M. Alvarez, F. Velasco
Department of Materials Science and Engineering, Universidad Carlos III de Madrid, IAAB, Avda. Universidad No. 30, Leganés, Madrid, (Spain)
E-mail: asuncion.bautista@uc3m.es

The distribution of the elements that enhance corrosion resistance in the phases is a key factor. Cr and Mo tend to concentrate in the ferrite, while Ni and N tend to concentrate in the austenite [7], but their accurate distribution changes not only with the DSS grade but also with specific processing of the material [14].

Many corrosion studies with DSS are focused on localized corrosion resistance. It has sometimes been assumed that the ferritic phase is more resistant to the chloride attack than the austenitic phase [13]. However, it has been reported that, for DSS in chloride-containing neutral or alkaline media, pits tend to appear in ferrite [4,5][15–17] or in austenite [5,7,18], depending on the composition of the DSS and on the composition of the aggressive medium. Moreover, the grain boundary between ferrite and austenite can also act as a preferential region for pit nucleation [19].

When DSS are exposed to an acid medium and tend to corrode in a generalized way, the effect of the biphasic structure could also be expected. However, the studies about the effect of the microstructure of DSS in the development of the attack in acid are limited. The selective corrosion of S32750 DSS in diluted HCl solution has been already reported [12]. For a given S32205 DSS in acid medium, the trend towards the selective corrosion of austenite or ferrite depends on the conditions of the aggressive environment [20] and galvanic effects between the constituent phases in DSS have been measured [21].

Anodic polarization curves in acid media are a useful method to study corrosion resistance of stainless steels and their active-to-passive transition. Traditionally, anodic curves in H_2SO_4-based solutions have been used to evaluate the sensitization degree of austenitic stainless steels after heat-treatment [22]. The traditional testing solution was 0.5 M H_2SO_4 + 0.01 M KSCN [23]. Subsequently, the procedure was extended to DSS [24]. Moreover, modifications have also been proposed for the acid solutions in the anodic polarization tests. HCl has been used as depassivator. Other authors have tested heat-treated 25% Cr DSS in pure 1 M HCl solution [25].

Anodic polarization curves in mixed H_2SO_4 + HCl solutions have been previously used for studying the sensitization of DSS with 22 or 25% Cr [26–29]. Some authors have pointed out that two activation peaks can be found for S32205 DSS grade [20,21]. The presence of a double peak in the activation region has also been found in austenitic grades with strain-induced martensite [30] and in ferritic grades [31]. In DSS, the double structure of the activation peak has been previously related to the selective corrosion of each phase in the material [20,21]. The selective dissolution of the phases in this media has already been used for fabrication of electrodes with high surface area, useful for supercapacitor applications [32].

This work delves further into the knowledge related to the corrosion resistance of austenite and ferrite of DSS in acid medium. The study also considers new factors as the possible influence of the forming process in the relative corrosion resistance of the phases of DSS. It is an interesting point because recently it has been proved that mechanical stresses caused by the forming process can also modify the development of corrosion for austenitic stainless steels [30,33]. Totally new information about the influence of the alloying level of the DSS and about the influence of the strain-induced martensite is obtained.

2 Experimental

The influence of the composition and processing on the corrosion behavior of DSS at different anodic potentials in acid media was studied. Three different DSS grades were considered: the traditional UNS S32205, and the lean UNS S32304 and UNS S32001 grades. All the DSS were supplied by Roldán S.A. (Acerinox group, Spain) as corrugated bars (typically used in construction). The studied DSS were obtained from hot worked (HW) bars, but cold worked (CW) UNS S32205 bars were also considered. The tensile strength of the bars, their diameter and their chemical composition can be found in Table 1.

A typical three electrode configuration cell was used for the potentiodynamic tests: a saturated calomel electrode (SCE) was used as reference electrode, a stainless steel mesh as counter-electrode and the DSS samples as working electrode. Transverse sections of the core of the bars, polished to 0.3 μm, were submitted to potentiodynamic tests. An Avesta cell was used to avoid crevice corrosion during anodic polarization. Polarizations were performed starting from −550 to 400 mV *versus* SCE at a sweep rate of 1 mV/s [18,19]. A 2 M H_2SO_4 + 0.5 M HCl solution was always used for testing [18,19,32]. The polarization curves for each material were repeated four to six times.

Samples were also potentiostically tested. Potentiostatic tests were carried out on all steels at different anodic potentials to check the influence of the polarization on the morphology of the attack. The configuration of the cell and the testing solution were the same as those used for the potentiodynamic testing. The length of the potentiostatic tests was 4 or 7 h, depending on the intensity of the current at the testing potential. Moreover, DSS samples were exposed to the testing solution at their corrosion potential (E_{corr}).

Table 1. Chemical composition (w/w), diameter, and tensile strength of the four studied DSS

Duplex stainless steel	Diameter (mm)	Main alloying elements (%)										Tensile strength (MPa)
		S	C	Ti	Si	Mn	Cr	Ni	Mo	N	Cu	
HW S32001	16	<0.002	0.025	0.012	0.75	4.39	20.58	1.74	0.22	0.124	0.07	825
HW S32304	16	<0.002	0.017	0.046	0.57	1.67	23.66	4.32	0.24	0.153	0.19	769
HW S32205	20	0.003	0.020	0.048	0.37	1.67	22.17	4.71	3.5	0.177	0.09	855
CW S32205	14	0.001	0.018	0.044	0.39	1.82	22.31	4.92	3.41	0.184	0.04	1132

Non-corroded samples, samples corroded in the potentiostatic tests and samples of materials exposed to E_{corr} were studied by optical microscopy and scanning electron microscopy (SEM) with semiquantitative energy-dispersive X-ray spectroscopy (EDS). Sections perpendicular to the tested surface and sections parallel to the testing surface were metallographically prepared, to observe the morphology of the attack. The Bloech and Weld reagent was used for coloring the microstructure.

The phases on DSS were characterized by X-ray diffraction (XRD). λCu radiation was used for the measurements. The XRD measurements were performed in step scan mode, with a step size of 0.02 ° and a time per step of 5 s. The angular interval was between 40 ° and 95 °.

The amount of ferrite and austenite was quantified using image analysis (IA) methods because in this technique (unlike others based on magnetic properties [34]), the possible precipitation of martensite in the austenite does not increase the signal of the ferrite. After an adequate metallographic preparation of the samples, a good contrast between the intensity of ferrite and austenite was achieved. Eighteen high-quality micrographs were taken for each DSS with optical microscopy, always at the same magnification. The amount of ferrite and austenite has been quantified using the software from Image-Pro Plus. Edge enhancement was the only required feature during the image processing.

3 Results and discussion

The microstructure of the DSS bars is shown in Fig. 1. The discontinuous austenite phase surrounded by the continuous ferrite phase, as is characteristic of DSS, can be seen. It can also be checked that, in the images corresponding to regions close to the surface of the bars, the processing has made the grain size smaller than in the center of the bars. The amount of phases has been estimated by IA (Table 2). The studied S32205 steels are somewhat more ferrite-richer than the lean DSS. The distribution of the main alloying elements in the phases has been evaluated by EDS and results are included in Table 2. It can be checked that alphagenous elements, as Cr, Si, and Mo, tend to concentrate in ferrite, while gammagenous elements, as Ni and Mn, concentrate in austenite. However, the relatively small differences found between the concentration of the elements in ferrite and austenite should be pointed out. This fact can possibly be related to the small grain size of the studied DSS. The most marked difference found is for the Mo concentration in the S32205 grades.

Precipitates as the one marked with a black circle in Fig. 1e can be found in the microstructure of all the DSS. They have been identified with EDS as TiN. The number and size of TiN precipitates are more reduced in S32001 bars than in the other DSS grades, probably because of the lower Ti and/or N content of S32001 (Table 1). TiN precipitates are considered relatively harmless for the corrosion behavior of stainless steels, though they have been blamed on a small decrease on the pitting resistance of pure austenitic stainless steels in alkaline media [35].

Moreover, a careful examination of the austenite in all the images in Fig. 1 reveals the presence of strain-induced

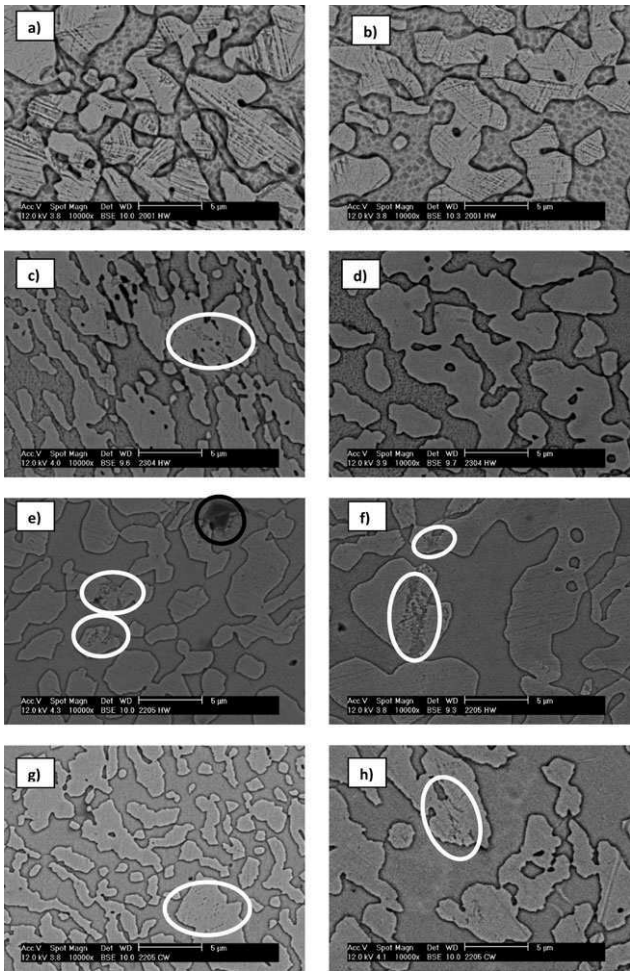

Figure 1. SEM images of the microstructure of cross-sections of DSS bars: (a) HW S32001 close to surface; (b) HW S32001 center of the bar; (c) HW S32304 close to surface; (d) HW S32304 center of the bar; (e) HW S32205 close to surface; (f) HW S2205 center of the bar; (g) CW S32205 close to surface; (h) CW S32205 center of the bar

martensite. It is known that austenite is metastable at low-temperature conditions, and plastic deformation can induce its partial transformation to martensite [36,37]. In materials different to HW S32001 (where the martensite can be easily seen inside

Table 2. Amount of ferrite and austenite measured with image analysis

		Amount of phase	Si	Mn	Cr	Ni	Mo
HW S32001	α	51 ± 1	0.8	4.2	20.6	1.7	0.3
	γ	49 ± 1	0.7	4.6	20.6	1.8	0.2
HW S32304	α	52 ± 1	0.6	1.6	25.0	4.0	0.3
	γ	48 ± 1	0.5	1.8	22.2	4.7	0.1
HW S32205	α	66 ± 3	0.4	1.6	22.7	4.2	4.3
	γ	34 ± 3	0.3	1.7	21.1	5.7	1.9
CW S32205	α	64 ± 2	0.4	1.7	22.6	4.4	4.3
	γ	36 ± 2	0.4	2.0	21.8	5.8	1.8

Compositions (% by wt) of austenite and ferrite, measured with EDS, for the studied DSS.

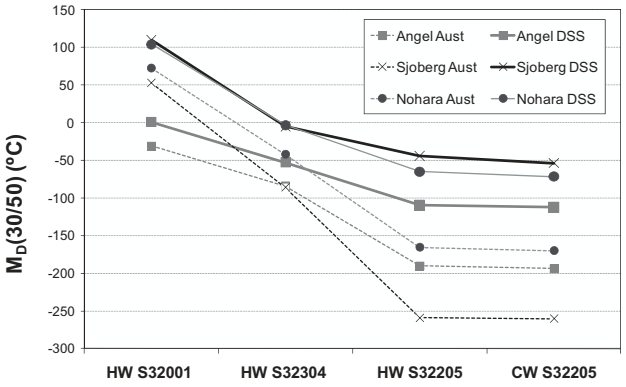

Figure 2. M_D(30/50) calculated with different approaches, using the composition of DSS (Table 1) and the measured for austenite (Table 2)

most of the austenite grains), the presence of martensite in the images has been marked with white ellipses.

The effect of martensite on the corrosion behavior of pure austenitic stainless steels in different conditions has been already studied. It is generally accepted that strain-induced martensite decreases the corrosion resistance of pure austenitic stainless steels [17,30,38]. Martensite formation in the austenitic phase of DSS under plastic deformation has also been proved by other authors [39]. However, the corrosion behavior has not been studied enough. There are some results regarding the behavior of UNS S31803 in neutral NaCl that suggest that martensite does not affect the pitting resistance [40]. Hence, it is relevant to analyze the formation of martensite in DSS depending on their composition and, especially, to determine the possible influence of martensite in their corrosion behavior.

After a careful analysis of different sections of the bars, it can be concluded that for the same material, the presence of martensite is higher in regions close to the surface than in the center of the bars. This is easy to understand bearing in mind that the surfaces have always suffered a heavier plastic deformation. However, in this case, the nature of the bar can be considered the parameter that determines the main differences in the amount of martensite.

The SEM observations inform that the amount of martensite is very high inside the austenite of HW S32001 bars, it is reduced for CW S32205, being in an intermediate amount for the other grades studied. Different parameters have been proposed in the literature for estimating the susceptibility to the formation of

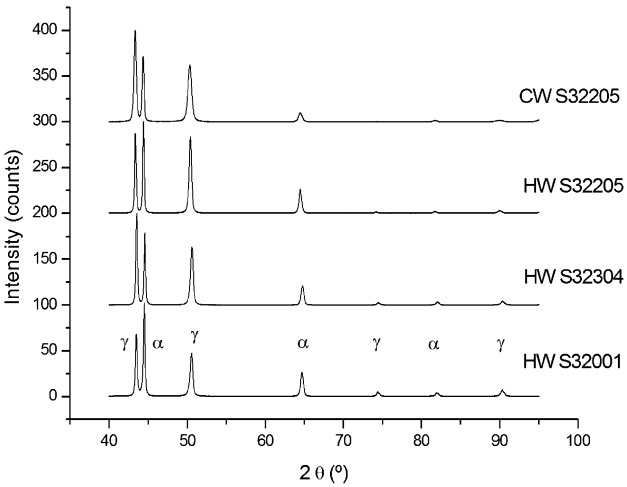

Figure 3. XRD of cross-sections of the DSS bars, where the peaks corresponding to the austenite (γ) and ferrite (α) are marked

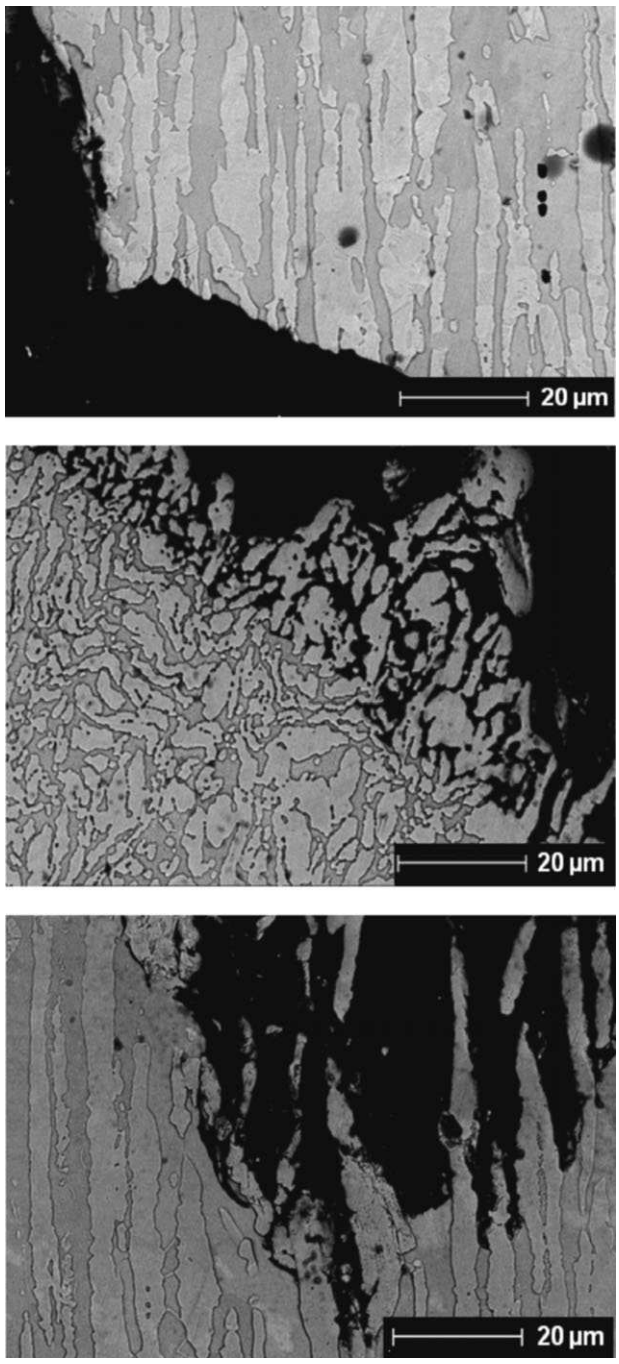

Figure 4. Morphology of the attack developed at E_{corr} in the acid solution: (a) longitudinal view of the HW S32001 after 2 days of exposure; (b) cross-sectional view of surface of HW S32304 bar after 4 days of exposure; (c) longitudinal view of the HW S32205 bar after 12 days of exposure

strain-induced martensite depending on the composition, martensitic deformation temperature ($M_D(30/50)$) being one of the most important. $M_D(30/50)$ measures the temperature at which 50% of martensite is produced after 30% of true deformation in tensile conditions. Higher values of this parameter imply an easier formation of martensite. There are different expressions proposed to calculate $M_D(30/50)$. It is true that all these expressions have been proposed for pure austenitic stainless steels and when they are applied to DSS some inaccuracies can appear. However, they can be useful in a qualitative way for suggesting trends. In this work, the different expressions for $M_D(30/50)$ proposed by *Angel* [41], *Sjöberg* [42] and *Nohara* et al. [43] have been calculated using two approaches. On one hand, the usual procedure of considering composition data of the DSS (Table 1) has been used. On the other hand, the composition of the austenite has been used (Table 2). For N, whose concentration cannot be obtained by EDS, a maximum solubility of 0.05% in the ferrite has been assumed [7,16,22], and then, the global amount of nitrogen has been distributed in both phases (bearing in mind the phase volume calculated from IA). Carbon levels are so low that equal composition has been assumed in both phases [44]. With those data, Fig. 2 shows $M_D(30/50)$ for the four studied steels. Independently from the numeric value obtained, all the data in Fig. 2 suggest that the tendency of forming martensite decreases as follows: S32001 > S32304 > S32205. Hence, the chemical composition of the DSS can be able to explain, at least partially, the differences in the amount of martensite found in the different bars. The lean DSS, because of their composition, are more prone to form martensite when they are strained. The differences detected in the SEM study between the CW S32205 and the HW S32205 can be unexpected at first sight, specially bearing in mind the expected influence of the deformation temperature in the amount of martensite demonstrated for pure austenitic steel [45]. The results of the SEM observation are conclusive, so the higher amount on martensite in the HW S32205 must be due to the level of the stresses during working process and the considerable difference existing between the bars diameter (Table 1).

Another relevant point that can be deduced from the results in Fig. 2 is the fact that when the approximate composition of the austenite is used, instead of the composition of all the DSS, the influence of decreasing the alloying degree of the material on the tendency to form martensite under strains is higher. This is essentially due to the marked gammagenous character of the N. The results are consistent with microstructures in Fig. 1, where very marked differences among the amount of martensite in the materials are found. Moreover, these results suggest the interest of trying to estimate the composition of the martensite before

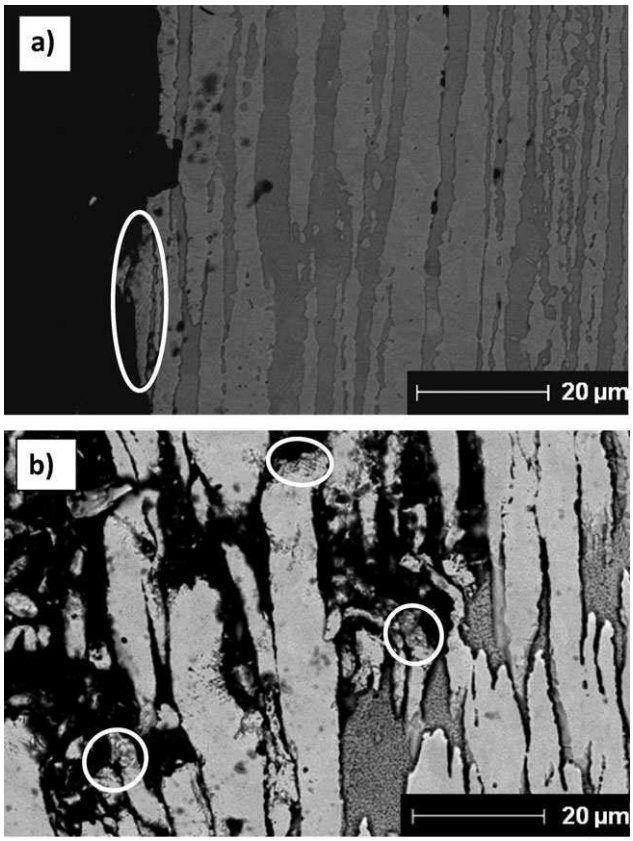

Figure 5. SEM details about the corrosion resistance of the strain-induced martensite in the solution at E_{corr}: (a) HW S32001 and (b) HW S32304

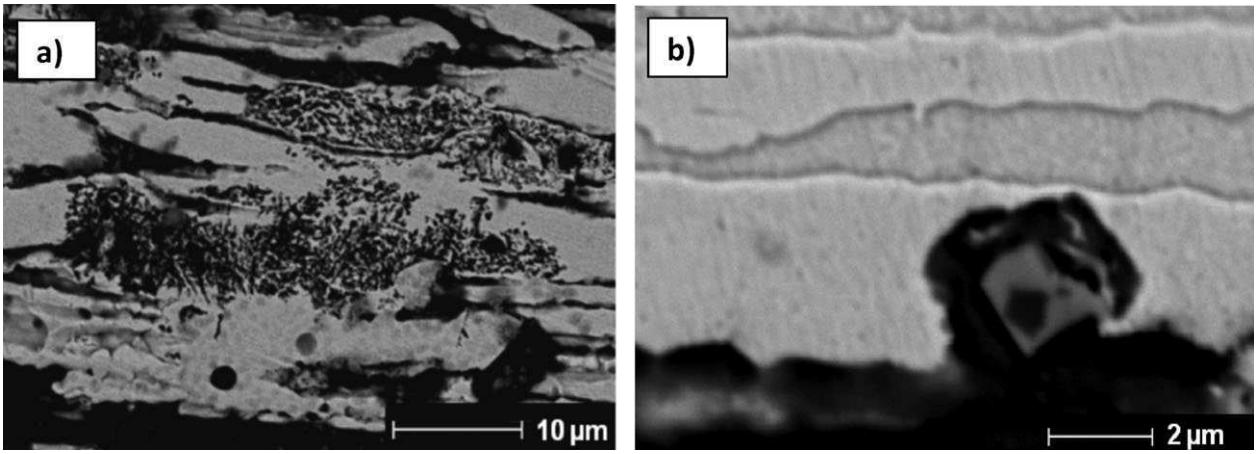

Figure 6. SEM images showing partially dissolution of phases after several days of exposure at E_{corr}: (a) dissolved martensite in HW S32304 and (b) partially dissolved TiN in HW S32205

calculating this type of parameter, instead of directly using the composition of the steel as direct extrapolation of the method used for pure austenitic stainless steels. The inconsistencies of the results obtained using the composition of the DSS have already been discussed by other authors [46].

The XRD results of the bars can be seen in Fig. 3. Though it is impossible to obtain quantitative information about the phases, interesting complementary information can be obtained from XRD measurement, bearing in mind that other critical factors as grain size and grain orientation are quite similar. Martensite has a body centered cubic structure, as ferrite, and the martensite peaks overlap with ferrite peaks in a XRD pattern. Hence, the precipitation of martensite in the austenite should cause a decrease in the intensity of the austenite peaks and an increase in the intensity of the ferrite peaks. It can be observed that for HW S32001 the relative intensity of the peaks corresponding to the ferrite is higher than that of those corresponding to the austenite, in spite that the amount of ferrite in its microstructure is not very high (Table 2). For CW S32205, the opposite trend can be observed: the relative height of the peaks corresponding to the body centered cubic phases is smaller than those of austenite (Fig. 3), their amount of ferrite being quite high (Table 2), so the contribution of martensite to the spectrum must be negligible in this case. The ratio between the peak heights corresponding to the different phases is intermediate for HW S32304 and HW S32205.

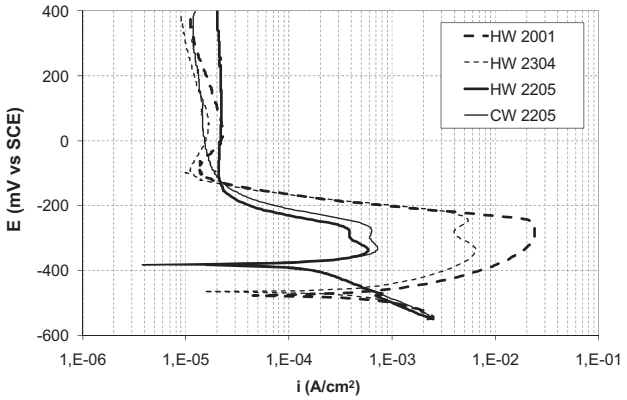

Figure 7. Examples of polarization curves corresponding to the core of the DSS bars in the acid medium

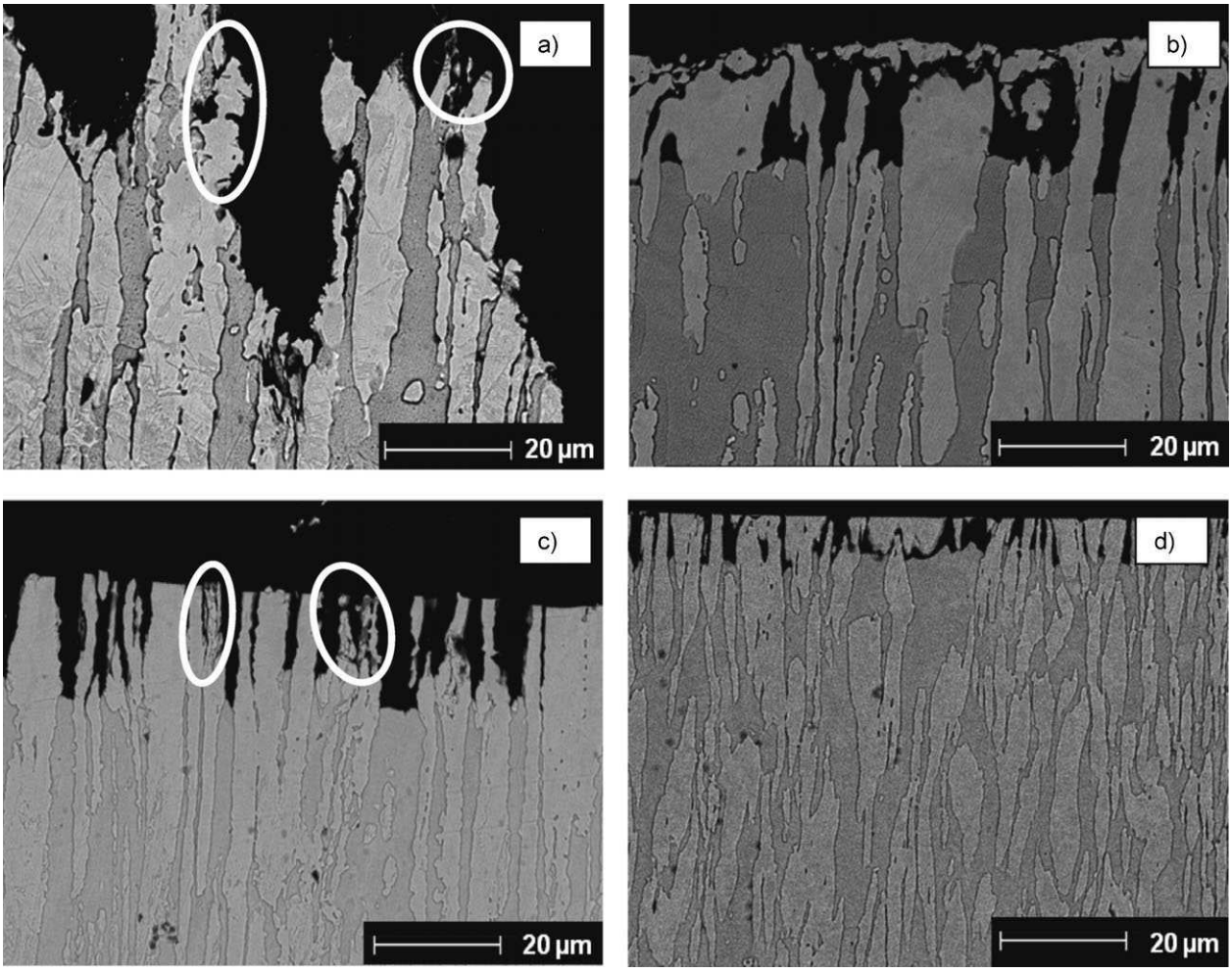

Figure 8. SEM images of the morphology of the attack in the cores of the bars after potentiostatic tests at low anodic overpotentials: (a) HW S32001 at −325 mV *versus* SCE for 4 h; (b) HW S32304 at −344 mV *versus* SCE at 4 h; (c) HW S32205 at −330 mV *versus* SCE for 7 h; (d) CW S32205 at −355 mV *versus* SCE for 7 h

Hence, XRD results are consistent with the conclusions about the amount of martensite depending on the bar drawn after the SEM study.

In Fig. 4, how the microstructure of DSS determines the corrosion attack development can be seen. When the samples are exposed to the $HCl + H_2SO_4$ testing solution for different time periods, it can be observed that, for all the DSS, the main mechanism of attack is the ferrite dissolution (the phase seen as the least bright in the images). This phenomenon has been clearly observed for S32304 and S32205 grades (Fig. 4b and c). For the lowest alloyed S32001 grade (Fig. 4a), the corrosion behavior of ferrite and austenite is very similar, though a slightly higher corrosion resistance of the austenite can be guessed.

Moreover, information about the corrosion behavior of strain-induced martensite can also be obtained from this SEM study. In Fig. 4c, marked with white ellipses, the martensite can be seen. This image proves that the martensite in HW S32205 is more corrosion resistant than the ferrite. Uncorroded martensite can be observed in spite of the length of the exposure.

Results in Fig. 5 give the same information about the resistance of martensite for less alloyed materials. When S32001 and S32304 are exposed for a short time in the acid medium, uncorroded martensite (marked with white ellipses) can be observed while the ferrite has been dissolved. These results prove that the martensite of the studied DSS is more corrosion resistant than the ferrite at E_{corr}. Hence, the attack at this pH would be mainly controlled by the dissolution rate of the ferrite (especially for S32304 and S32205), in spite of the formation of martensite during the working process. From a practical point of view, these results suggest that no relevant detrimental effect can be expected from the precipitation of martensite during processing, unlike that demonstrated for pure austenitic stainless steels [17,30,38].

On the other hand, when exposure to the solution is extended, and ferrite has completely disappeared from the region, martensite can start to dissolve preferentially. This phenomenon can be clearly observed in the image in Fig. 6a, corresponding to S32304 grade. This result proves that martensite is less corrosion resistant than austenite, as expected [30].

After days of exposure at E_{corr}, TiN also tends to dissolve as it is shown in Fig. 6b. Hence, they are clearly more stable than ferrite, but less than austenite, at least for the studied S32304 and S32205 grades. For S32001, the number of TiN precipitates is very

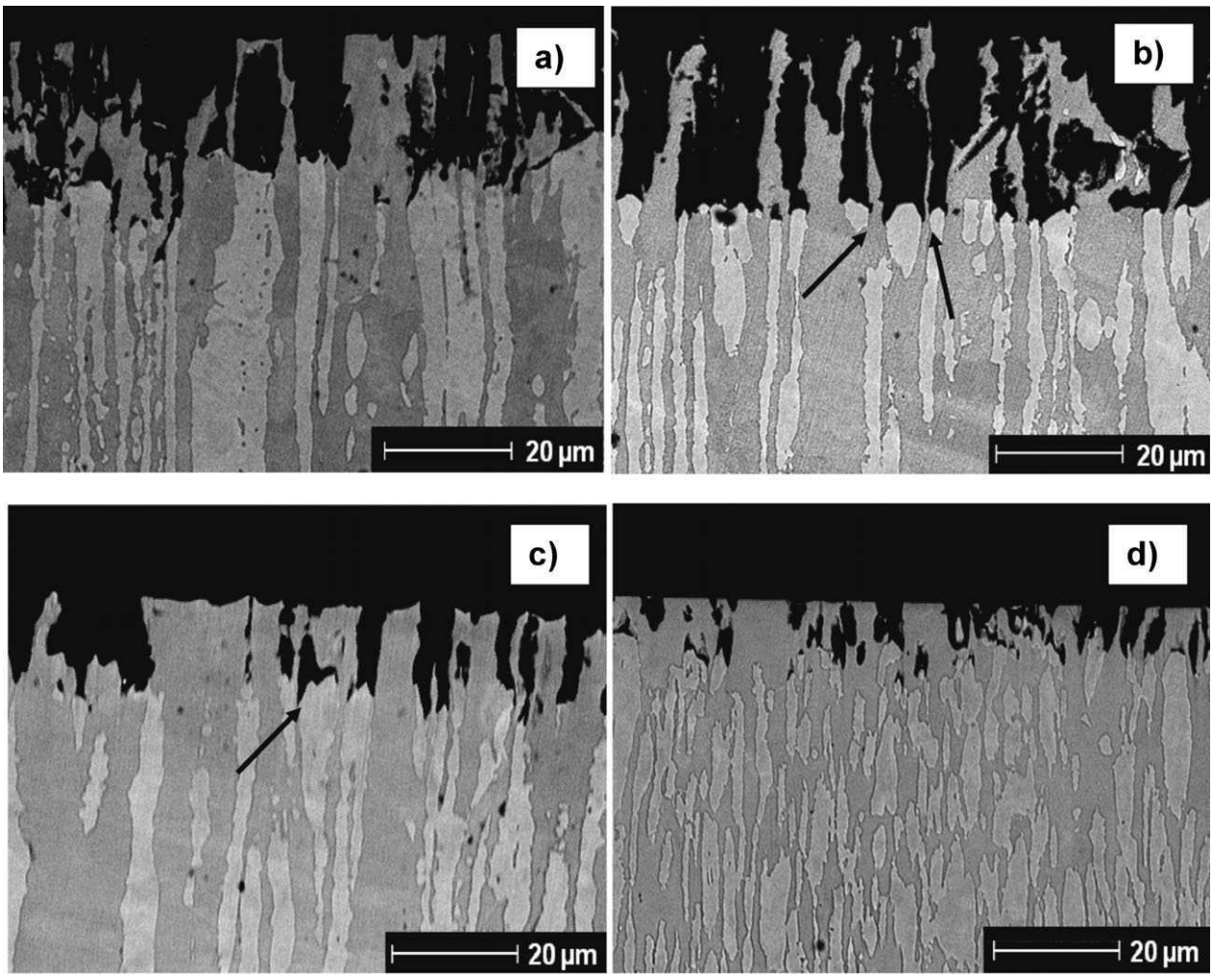

Figure 9. SEM images of the morphology of the attack in the cores of the bars after potentiostatic tests at high anodic overpotentials inside the activation region: (a) HW S32001 at −200 mV *versus* SCE for 4 h; (b) HW S32304 at −244 mV *versus* SCE at 4 h; (c) HW S32205 at −295 mV *versus* SCE for 7 h; (d) CW S32205 at −250 mV *versus* SCE for 7 h

low because of its Ti content (Table 1), but a lower dissolution rate of TiN than that of both ferrite and austenite can be guessed after the study. From a practical point of view, it can be concluded that TiN precipitates in DSS are never the most corrosion-prone phase where the attack in acid media would start in, though in the long term, TiN can have a higher trend to dissolution than the austenite in S32304 and S32205 grades.

Representative anodic polarization curves of samples of the center of the DSS bars are plotted in Fig. 7. At anodic potentials over E_{corr}, the typical activation region of stainless steels in acid can be observed, before the current density decreases because of the passive layer that is generated by the anodic polarization. A double-structure for the activation peak can be clearly identified in most of the cases, but not for HW S32201. For non-strained S32205, other authors have blamed the complex shape of the peak on selective corrosion of the ferrite and austenite [20,21,32].

Potentiostatic tests have been carried out at different potentials in the activation region. The morphology of the attack at different anodic overpotentials informs about how the corrosion would be affected by changes in the medium that could increase E_{corr} (e.g., a decrease in the pH will favor the cathodic reduction semireaction of H_2 evolution and the E_{corr} will be shifted to more anodic values). Strong acid media can be found in many industrial processes, but it also appears inside crevices and pits, due to acid hydrolysis of the corrosion processes. Hence, localized corrosion processes often develop in very acid local media [47] in spite of the pH of the surrounding environment.

The images in Fig. 8 correspond to the attack occurring at potentials where the maximum of the less anodic component of the activation peak could be approximately guessed. For all the DSS, a phenomenon similar to that observed at E_{corr} can be observed, but it takes place at a higher dissolution rate. Ferrite corrodes selectively in these conditions, and the trend of the austenite to be also dissolved can be seen for the S32001. Austenite dissolution is negligible in these conditions for the most alloyed grades. Martensite (marked with white ellipses in Fig. 8a and c) proves again to have higher corrosion resistance than ferrite. It is also clear that martensite stability at these polarizations is slightly lower than that of pure austenite, as some dissolution of the martensite can be guessed.

In Fig. 9, the morphology of the attack at high anodic polarizations can be seen (but always at values under the passivation potential, E_{pass}). In the upper part of the activation region, a selective corrosion of austenite is observed for all the DSS, while ferrite remains almost unattacked, especially for S32205 grades. The austenite dissolves preferentially at these

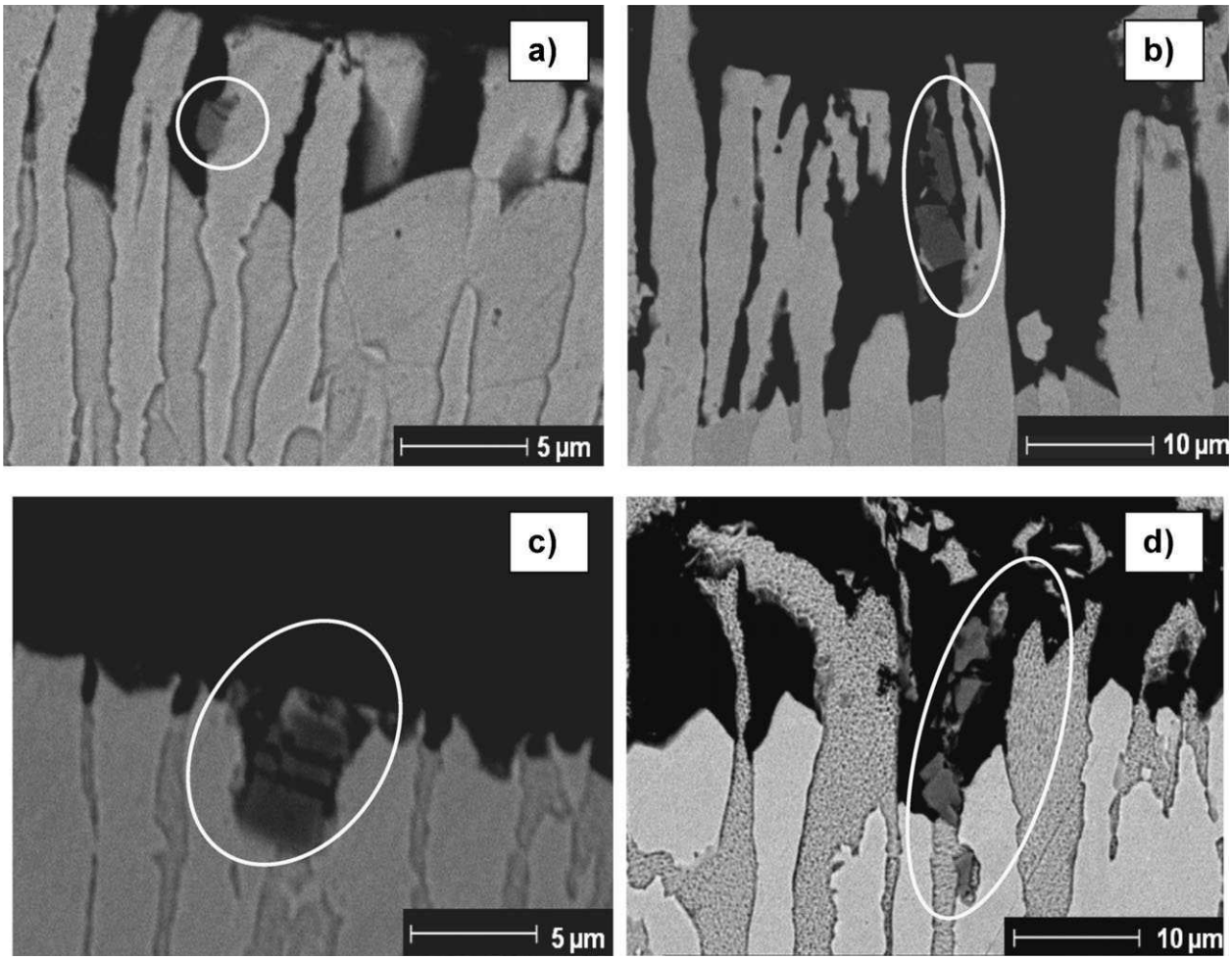

Figure 10. SEM images showing the stability of TiN precipitates under polarizations: (a) CW S32205 at −355 mV *versus* SCE for 4 h; (b) HW S32304 at −344 mV *versus* SCE for 7 h; (c) CW S32205 at −295 mV *versus* SCE for 4 h; (d) HW S32304 at −244 mV *versus* SCE for 7 h

potential ranges also for the S32001 (Fig. 9a). The potentiostatic tests prove that the selective corrosion also occurs for S32001, in spite of the fact that the double structure of the activation peak cannot be visually detected in the polarization curve (Fig. 7). These results confirm that, for all the studied grades, the peak at lowest potentials is associated with the preferential dissolution of the ferrite phase while the austenite preferentially corrodes at higher potentials. This occurs independently from the changes in the corrosion resistance of the phases caused by the different chemical composition of the studied grades.

Non-corroded martensite cannot be observed in regions in contact with the solution at high anodic polarization under E_{pass} (Fig. 9). This phase completely dissolves in the conditions that austenite does and no small difference in the corrosion rate of martensite and austenite can be noticed at polarization corresponding to the upper region of the activation peak.

At these polarizations, sometimes a galvanic effect between the phases can be detected during the SEM observations. For HW S32304 and HW S32205 (Fig. 9b and c), black arrows mark the regions where the austenite corrodes at a higher rate at grain boundaries. This is due to the galvanic microcouple formed between austenite and the contiguous ferrite grains that have a more noble behavior in these conditions. For CW S32205 (Fig. 9d), the phenomenon is less visible because of the lower grain size, but it can also be guessed. Other cases of galvanic corrosion in acid medium between austenitic and ferritic phases for S32205 DSS have been previously discussed by other authors [21,25]. However, no galvanic coupling is observed for the least alloyed DSS (Fig. 9a). This agrees with the high overlapping of austenite and ferrite peaks in the anodic polarization curve for the HW S32001 grade and the small differences found in the concentrations of N and other alloying elements that determine the corrosion behavior between ferrite and austenite (Table 2).

SEM images of the effect of the polarization on TiN can be seen in Fig. 10. After exposure, no trend to dissolution is observed for the precipitates, neither at potentials where ferrite preferentially dissolves (Fig. 10a and b) nor at potentials where dissolution of the austenite takes place (Fig. 10c and d). It seems that in these conditions, TiN dissolution is more sensitive to time exposure than to anodic polarization.

4 Conclusions

From the results obtained for the four DSS studied, the following conclusion can be drawn:

- Lean DSS are more prone to strain-induced martensite precipitation during the working process than S32205. The differences of the amount of martensite with the alloying degree seem to be higher than those foreseen using the global composition of the DSS.
- The different phases present in strained DSS corrodes selectively depending on the exposure conditions. The trend to selective dissolution is less marked for the least alloyed DSS.
- Selective dissolution of the ferrite is always detected at E_{corr} or at potentials slightly over E_{corr} in the selected testing solution. An increase of the potential causes a selective corrosion of the austenite, so the austenite would be the dissolved phase in more acid media than the testing solution.
- In absence of polarizations, strain-induced martensite in the austenite phase exhibit a corrosion resistance clearly higher than that of the ferrite, but somewhat lower than that of the austenite. Hence, it can be assumed that the detrimental effect of the precipitation of martensite in DSS in these conditions is not very important.
- At potentials where austenite dissolves, martensite has not been observed.
- TiN precipitates in DSS are never the most corrosion-prone phase where the attack in acid media would start, though in the long term, TiN can have a higher trend to dissolution than the austenite in S32304 and S32205 grades.
- The anodic polarization in the activation region does not seem to meaningfully increase the dissolution rate of TiN.

Acknowledgements: The present work was funded by the Spanish Ministry of Education and Science and MINECO through the Projects reference BIA2007-66491-C02-02 and MAT2011-29182-C02-02.

5 References

[1] B. Elsener, D. Addari, S. Coray, A. Rossi, *Mater. Corros.* **2011**, *62*, 111.
[2] I.-U.-H. Toor, P. J. Hyun, H. S. Kwon, *Corros. Sci.* **2008**, *50*, 404.
[3] M. Theofanus, L. Garner, *J. Constr. Steel Res.* **2010**, *66*, 816.
[4] L. Bertolini, M. Gastaldi, *Mater. Corros.* **2011**, *62*, 120.
[5] S. M. Alvarez, A. Bautista, F. Velasco, *Corros. Sci.* **2011**, *53*, 1748.
[6] K. H. Lo, C. H. Shek, J. K. L. Lai, *Mater. Sci. Eng. R* **2009**, *65*, 39.
[7] R. Merello, F. J. Botana, J. Botella, M. Marcos, *Mater. Corros.* **2004**, *55*, 95.
[8] J. Li, Z. Ma, X. H. Xiao, J. Zhao, L. Jiang, *Mater. Des.* **2011**, *32*, 2199.
[9] A. Burkert, J. Lehmann, A. Burkert, J. Mietz, P. Gümpel, *Mater. Corros*[Q2]. **2013**, *64*, doi: 10.1002/maco201307057
[10] L. Q. Guo, M. Li, X. L. Shi, Y. Yan, X. Y. Li, L. J. Qiao, *Corros. Sci.* **2011**, *53*, 3733.
[11] H. Tan, Z. Wang, Y. Jiang, D. Han, J. Hong, L. Chen, L. Jiang, J. Li, *Corros. Sci.* **2011**, *53*, 2191.
[12] V. M. Linton, N. J. Laycock, S. J. Thomsem, A. Klumplers, *Eng. Fail. Anal.* **2004**, *11*, 243.
[13] J. H. Potgieter, P. A. Olumbi, L. Cornish, C. N. Machio, E.-S. M. Sherif, *Corros. Sci.* **2008**, *50*, 2572.
[14] W. Zhang, J. Hu, *Mater. Charact.* **2013**, *79*, 37.
[15] L. Zhang, Y. Jiang, B. Deng, W. Zhang, J. Xu, J. Li, *Mater. Charact.* **2009**, *60*, 1522.
[16] L. F. Garfias-Mesias, J. M. Sykes, C. D. S. Tuck, *Corros. Sci.* **1996**, *38*, 1319.
[17] R. D. Moser, P. M. Singh, L. F. Kahn, K. E. Kurtis, *Corros. Sci.* **2012**, *57*, 241.
[18] H. Luo, C. F. Dong, X. G. Li, K. Xiao, *Electrochim. Acta* **2012**, *64*, 211.

[19] L. Zhang, W. Zhang, Y. Jiang, B. Deng, D. Sun, J. Li, *Electrochim. Acta* **2009**, *54*, 5897.
[20] I.-H. Lo, Y. Fu, C.-J. Lin, W.-T. Tsai, *Corros. Sci.* **2006**, *48*, 696.
[21] W.-T. Tsai, J.-R. Chen, *Corros. Sci.* **2007**, *49*, 3659.
[22] V. Cihal, R. Stefec, *Electrochim. Acta* **2001**, *46*, 3867.
[23] A. Bautista, G. Blanco, F. Velasco, M. A. Martínez, *Constr. Build. Mater.* **2007**, *21*, 1267.
[24] J. R. Scully, R. G. Kelly, *Corrosion* **1986**, *42*, 537.
[25] C.-J. Park, H.-S. Kwon, *Corros. Sci.* **2002**, *44*, 2817.
[26] C. Duret-Thual, M. Bonis, J. L. Crolet, *Mater. Corros.* **2001**, *52*, 37.
[27] T. Amadou, C. Braham, H. Sidhom, *Metall. Mater. Trans. A* **2004**, *35A*, 3499.
[28] B. Deng, Y. Jiang, J. Xu, T. Sun, J. Gai, L. Zhang, W. Zhang, J. Li, *Corros. Sci.* **2010**, *52*, 969.
[29] J. Gong, Y. M. Jiang, B. Deng, J. L. Xu, J. P. Hu, J. Li, *Electrochim. Acta* **2010**, *55*, 5077.
[30] S. M. Alvarez, A. Bautista, F. Velasco, *Corros. Sci.* **2013**, *59*, 130.
[31] M. Romero, V. Matres, presented at *7th European Stainless Steel Conference*, Como, Italy, September 21–23, **2011**, Paper no. 5.
[32] S.-J. Pan, Y.-J. Shih, J.-R. Chen, J.-K. Chang, W.-T. Tsai, *J. Power Sour.* **2009**, *187*, 2161.
[33] E. C. Paredes, A. Bautista, S. M. Alvarez, F. Velasco, *Corros. Sci.* **2012**, *58*, 52.
[34] S. S. M. Tavares, J. M. Neto, M. R. da Silva, I. F. Vasconcenlos, H. F. G. de Abreu, *Mater. Character.* **2008**, *59*, 901.
[35] A. Bautista, G. Blanco, F. Velasco, *Cement Concrete Res.* **2006**, *36*, 1922.
[36] W. Hübner, *Tribol. Int.* **2001**, *34*, 231.
[37] S. Das, S. Tarafder, P. C. Chakraborti, *Mater. Sci. Eng. A* **2011**, *529*, 9.
[38] A. S. Hamada, L. P. Karjalainen, M. C. Somani, *Mater. Sci. Eng. A* **2006**, *431*, 211.
[39] S. S. Tavares, M. R. da Silva, J. M. Pardal, H. F. G. Abreu, A. M. Gomes, *J. Mater. Process. Tech.* **2006**, *180*, 318.
[40] V. S. Moura, L. D. Lima, J. M. Pardal, A. Y. Kina, R. R. Corte, S. S. M. Tavares, *Mater. Character.* **2008**, *59*, 1127.
[41] T. Angel, *J. Iron Steel Inst.* **1954**, *177*, 165.
[42] J. Sjöberg, *Wire* **1973**, *23*, 155.
[43] K. Nohara, Y. Ono, N. Ohashi, presented at *Proc. 1. JIM Int. Symp. New Aspects of Martensitic Transformation*, Kobe, Japan, May 10–12, **1976**, p. 315.
[44] D. H. Kang, H. W. Lee, *Corros. Sci.* **2013**, *74*, 396.
[45] H. Mirzadeh, A. Najafizadeh, *Mater. Character.* **2008**, *59*, 1650.
[46] J. Y. Choi, J. H. Ji, S. W. Hwang, K.-T. Park, *Mater. Sci. Eng. A* **2011**, *528*, 6012.
[47] J. A. González, E. Otero, S. Feliu, A. Bautista, E. Ramírez, P. Rodríguez, W. López, *Mag. Concrete Res.* **1988**, *50*, 189.

(Received: September 25, 2013) W7419
(Accepted: October 26, 2013)

Keywords: acid corrosion
duplex stainless steel
polarization
selective corrosion
SEM
strain-induced martensite

Q1: Author: A running head short title was not supplied; please check if this one is suitable and, if not, please supply a short title of up to 45 characters that can be used instead.
Q2: Author: Please provide the first page number for this reference.

5.6 PUBLICACION 6: P6

A. Bautista, S.M. Alvarez, F. Velasco.

"*Selective corrosion of duplex stainless steel bars in acid. Part 2: effect of the surface strain and numerical analysis*".

Materials and Corrosion, aceptado. DOI: 10.1002/maco.201307420.

Selective corrosion of duplex stainless steel bars in acid. Part 2: Effect of the surface strain and numerical analysis

A. Bautista*, S. M. Alvarez and F. Velasco

In the second part of this study, the effect of the strain level on the selective corrosion of the phases comprised in four different heavily strained duplex stainless steel (DSS) bars is analyzed. The corrosion behavior of the surface of bars with variable strain levels is analyzed and compared to the results of the less strained core of the same bars. For lean DSS bars (UNS S32304 and S32001 grades), an increase on the corrosion rate caused by the strains has been detected for the surface. For these DSS without Mo, ferrite has proved to be more sensitive to decrease on the corrosion resistance caused by the strain than austenite. In these cases, the strains expand the region of active corrosion toward higher potentials. On the other hand, when the grains are heavily strained parallel to the surface, if the most corrosion resistant phase has good corrosion behavior in the medium (UNS S32205 grades), the corrosion rate can be effectively slowed down, in spite of the microstructural defects.

1 Introduction

The strains caused by machining or working of stainless steels are very common and they often cause inevitable microstructural changes. The relationship between plastic strain and stress corrosion cracking is a well-known phenomenon [1,2], but strains can also favor the development of corrosion through other mechanisms.

Due to the practical relevance of the topic, there are several published studies about the interplay of the microstructure and electrochemical phenomena for pure austenitic stainless steels [3]. It has been published that, for austenitic grades in chloride medium, the strains decrease the pitting corrosion resistance. Some authors have published that the decrease was significant if the strain level was up to 10%, but over 10% the effect was weaker [4]. In media with chlorides, it has been demonstrated that for reductions over 50%, the beneficial effect of texture in the pitting resistance prevails over the detrimental effect of the stresses or induced martensite [3]. The existing relationship between corrosion behavior in acid media and strains has also been studied for traditional austenitic grades [3]. Nowadays, duplex stainless steels (DSS) are materials of fast growing importance for manufacturing components exposed to corrosive environments.

Chemical composition is usually the first parameter used to foresee their corrosion resistance. However, it is also necessary to know in depth how the processing strain and the associated microstructural changes can affect their durability. There are already some studies about how the microstructural transformations during the working process can affect the corrosion behavior of DSS when there is a risk of localized corrosion. Potentiodynamic anodic polarization tests in a neutral solution with chlorides have revealed that the pitting corrosion resistance of DSS can decrease noticeably with increasing pre-strained level [5,6]. End-users and manufacturers have been advised to take steps to assess the effect of specific plastic strains on corrosion resistance [6]. However, there is limited published information about the influence of the working process in the corrosion behavior of DSS in acid medium.

For decades, anodic polarization curves in acid have been used to study the resistance against intergranular attack of austenitic stainless steels. Tests have usually been carried out in H_2SO_4 solutions with different additions of depassivator compounds [7]. Nowadays, the procedure has been extended to other types of corrosion-resistant metallic materials, as Ni-base alloys [8] or DSS. The area of the peak defined in the activation region has always been considered a key parameter for evaluating the corrosion behavior of stainless steels in these tests. For DSS, the anodic polarizations in acid have mainly been used to evaluate the effect of heat inputs in the formation of precipitates [9], but they have proved to be useful for studying the effects of stresses and strains in the active-passive transition [5].

The present work deepens in the effect of the working on the corrosion behavior of DSS. The studied samples come from bars whose surfaces have been heavily strained. The straining process suffered by the surface of the bars has always been heavier than that of the cores. These bars also exhibit a variable level of strain depending on the region of the surface considered. The material

A. Bautista, S. M. Alvarez, F. Velasco
Materials Science and Engineering Department – IAAB, Universidad Carlos III de Madrid, Avda. Universidad n° 30, Leganés, Madrid (Spain)
E-mail: asuncion.bautista@uc3m.es

of the lean DSS comes from hot worked (HW) formed bars, while that of the S32205 comes from HW bars, but also from bars that were subjected to cold working (CW). Corrugated bars, as those used in reinforced concrete structures, have been used to obtain the testing samples with these straining characteristics. The study of materials processed in this way allows obtaining interesting information about the topic studied.

The measurements are carried out in acid media. Acids are very corrosive environments often present in many industrial processes. Moreover, the results of this study could also be considered relevant for extrapolations to corrosion behavior in other media, even in concrete. Though concrete is an alkaline environment, once localized corrosion has started, the acid hydrolysis of the corrosion products causes a marked decrease of the pH inside the pits and the characteristic crevices of the concrete–reinforcement interface. pH values of about 1 have been measured inside corroding reinforced specimens, through crevices or macropores [10]. In general, independently from the pH where the component is exposed, a strong acid medium is always expected inside pits or crevices once the corrosion has started.

In the first part of this work [11], results about the corrosion behavior of the different phases present in the cores (the least strained region) of the DSS bars have been presented. It has been checked that ferrite dissolution tends to occur at E_{corr} or at potentials slightly over E_{corr}. At higher anodic overpotentials inside the activation region, the selective corrosion of austenite takes place. Moreover, it has been demonstrated that in absence of high polarizations, strain-induced martensite in the austenite phase exhibits a corrosion resistance clearly higher than that of the ferrite, but somewhat lower than that of the austenite.

2 Experimental

The chemical composition and other relevant characteristics of the four DSS bars studied can be found in the experimental chapter of the first part of the present study [11].

Localized studies of the mechanical properties of the bars were carried out through universal hardness (UH) measurements. Results were obtained in cross-sectional, metallographically prepared samples. Measurements were carried out at the surface and at the center of the bars. Tests were performed at a load rate of 1 mm/min using a maximum load of 20 N. All the given results are the average of about 15 measurements. Some theoretical background about this characterization method can be found elsewhere [12].

A typical three-electrode configuration cell was used for the potentiodynamic tests: a saturated calomel electrode (SCE) was used as reference electrode, a stainless steel mesh as counter-electrode and the DSS samples as working electrode. The working electrodes were 2-cm long samples from the bars whose transverse section was polished to 0.3 μm. Other details about studied DSS samples whose results are also analyzed in the present article can be found in the first part of the work [11]. Polarizations were performed starting from −550 to 400 mV *versus* SCE at a sweep rate of 1 mV/s [13,14]. 2 M H_2SO_4 + 0.5 M HCl solution was always used for testing [13,15,16]. The polarizations curves for each material were repeated up to six times.

The deconvolution of the activation peak in the anodic polarization curve was carried out by software specifically designed in the laboratory. The software was developed using the GUI builder tool and under Matlab language. It uses generalized extreme value functions to obtain curves that fit the experimental data. It allows to obtain values of the charge density involved in the different phenomena occurring during the anodic polarization, besides other relevant parameters, as the maximum current density (i_{max}) of each phenomenon and the potential (E_{max}) at the corresponding i_{max} takes place. More information about the fitting procedure can be found in a previous publication by the authors [17].

Samples of the heavily strained DSS bars were also potentiostatically tested. Potentiostatic tests were carried out for all steels at different anodic potentials to check the influence of polarization on the morphology of the attack. The configuration of the cell and the testing solution were the same as those used for the potentiodynamic testing. The length of the potentiostatic tests was 4 or 7 h, depending on the intensity of the current of the studied DSS at the testing potential. Sections of the potentiostatically corroded materials were metallographically prepared using the Bloech and Weld reagent, and then they were studied by scanning electron microscopy (SEM).

3 Results and discussion

The mechanical characteristics of the surfaces of the bars are different from that of the bulk materials, because the former have suffered a heavier working process. Results in Fig. 1 inform about the magnitude of these differences. The UH of the surface is always higher than the UH of the bulk of the DSS bars. These differences are due to the high amount of dislocations and defects in the microstructure near the surface, but also, as it has already be shown for these materials [11], to the higher amount of strain-induced martensite and the reduced grain-size in the regions close to the surface.

In Fig. 2, representative anodic polarization curves corresponding to the surface of the DSS bars in acid media are plotted.

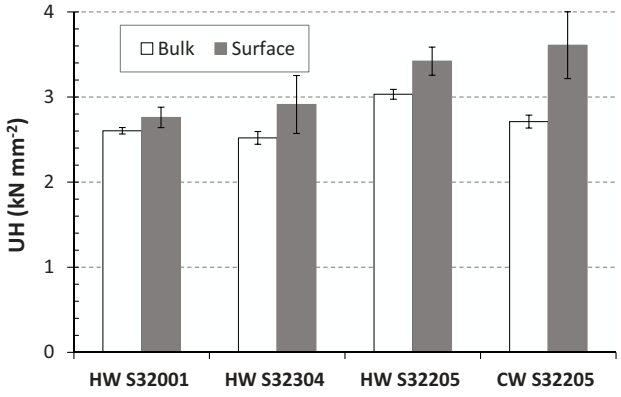

Figure 1. Local mechanical properties measured in cross sections of the bars, in the center and close to heavily strained surface

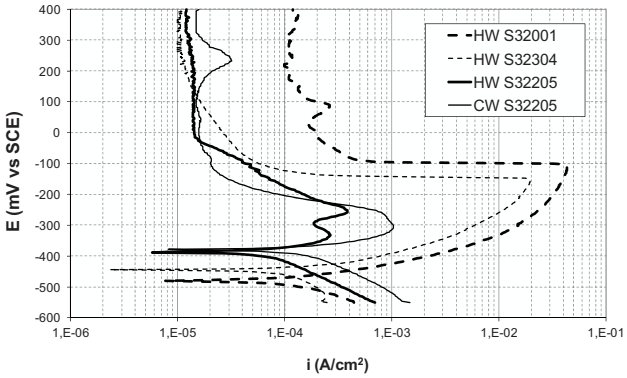

Figure 2. Anodic polarization curves corresponding to the strained surface of the bars in acid medium

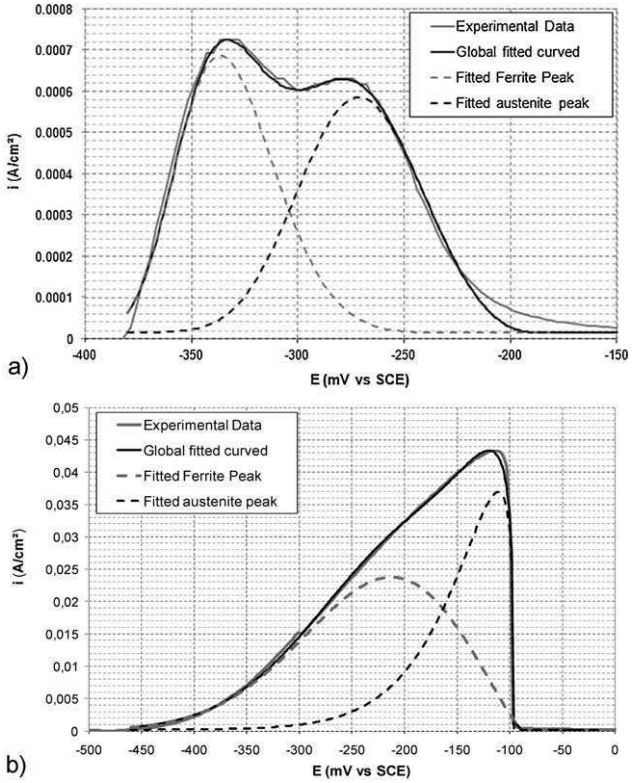

Figure 3. Examples of the deconvolution of the anodic activation region that appears during the polarization curves. (a) Bulk of the CW S32205 bar; (b) surface of the HW S32001 bar

If these curves are compared to those of the bulk of the same DSS bars, important differences can be found. For example, the clearly visible double structure of the activation peak of the HW S32304 disappears. The influence of the microstructure must explain the changes in the polarization curves when the real surface of the bars is considered. The analysis of the polarization curves can help to understand how the working process can modify the corrosion resistance of the phases comprised in the DSS microstructure.

Using an adequate fitting procedure, the deconvolution of the active region of the curve can be carried out. An example of the procedure can be seen in Fig. 3. Following the same mathematical procedure used for non-DSS with different phases in their microstructure [17], two peaks have proved to be enough to reproduce the corrosion behavior in the active region of the DSS bars. In Fig. 3a, the results of the simulation of the polarization behavior of the bulk of the CW S32205 bar can be seen, a curve where the double-structure of the activation region is obvious. In Fig. 3b, an example of the fitting achieved for the curve of the surface of HW S32001 is shown. In this case, the double structure of the region is not visible, but the shape of the peak cannot be fitted by a single peak. Two peaks suggest the presence of two phases whose relative corrosion intensities change meaningfully with polarization. It is true that the asymmetry of the peak at the highest anodic overpotentials tends to increase in the curves where there is no visible double structure in the active region (bulk and surface of HW S32001 and surface of HW S32304) but this point will be explained after the microstructural observations.

Bearing in mind the careful study carried out about the effect of polarization in the corrosion behavior of the bulk materials of the bars [11] and the results of other researchers in quite similar materials [13,15], the physical meaning of the peaks for the bulk material can be easily suspected. The peak that appears at low anodic overpotentials should correspond to the preferential corrosion of ferrite, while the peak at high anodic overpotentials should correspond to the preferential corrosion of the austenite. After the observation of images as those in Fig. 4, corresponding to potentiostatic tests of the surface of both S32205 bars, the results are confirmed. It should be remembered that the double structure of the activation region is clearly visible in the polarization curves for these DSS bars (Fig. 2). In Fig. 4a and b, the selective corrosion that occurs during potentiostatic tests carried out inside the region of the peak that appear at low anodic polarizations can be seen. Selective corrosion of the ferrite (the least bright phase in the SEM images) is observed, both for CW S32205 and HW S32205. Figure 4c and d shows that, for CW S32205 and HW S2205, austenite dissolves and ferrite remains unattacked at higher polarizations inside the activation region. From the present experiments, the relationship between the double structure of the peak and notches as has been suggested by other authors can be discarded [18].

In Fig. 5, the results of the potentiostatic tests in surfaces that did not show a visible double structure of the activation region during the potentiodynamic tests (Fig. 2) can be seen. When the surface of HW S32304 and HW S32001 bars suffer low anodic polarizations, the expected phenomenon is again observed: ferrite corrodes preferentially than austenite. This mechanism of attack has been checked in the entire surface of the bars at these polarization conditions. Ferrite preferentially dissolves at these potentials, independently of the variable strain level of the surface. However, when the samples of the surface are polarized at higher anodic potentials, an interesting fact is detected. Bearing in mind the results of the four bulk materials [11] or those corresponding to surfaces shown in Fig. 4c and d, a selective corrosion of the austenite could have been expected. However, it is easy to see regions in the surfaces of the S32001 and S32304 where a clear preferential corrosion of the ferrite exists (Fig. 6a). At the same time, regions of the surface of these two lean DSS

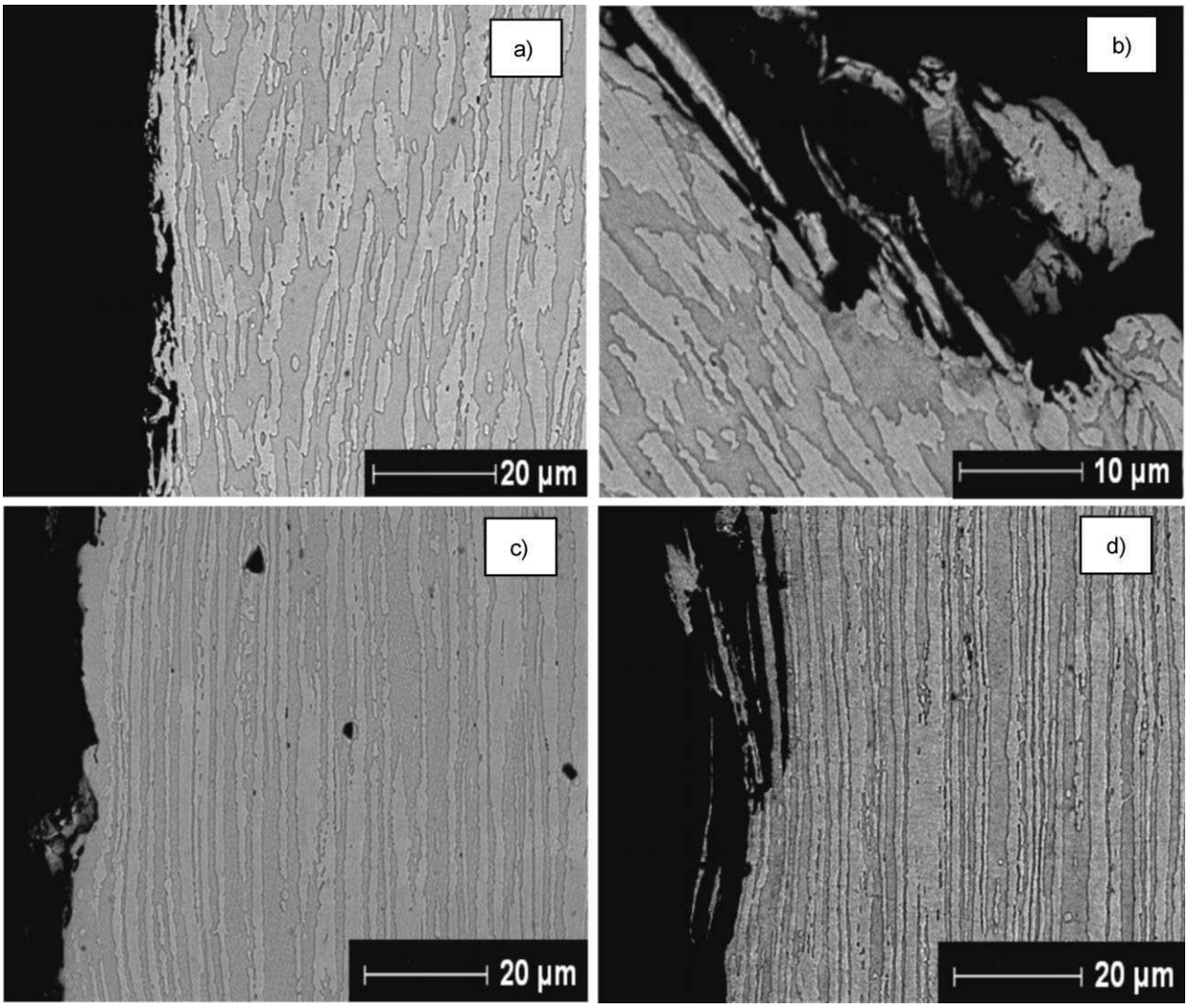

Figure 4. SEM images of the selective corrosion of the phases in DSS at anodic polarizations: (a) HW S32205 at −330 mV *vs.* SCE; (b) CW S32205 −330 mV *vs.* SCE; (c) HW S32205 at −230 mV *vs.* SCE; (d) CW S32205 at −250 mV *vs.* SCE

where austenite preferentially corrodes also exist. It has been checked that austenite is dissolved in the least strained regions of the surface and ferrite dissolves in the most strained regions. The fact of having tested materials with a variable degree of strain has allowed checking that the relative corrosion rate of the phases changes when the strain increases. So preferential corrosion of the ferrite takes place at potentials in the upper section of the activation region, which appears on very heavily strained surfaces. In Fig. 6b, obtained after testing at high anodic overpotentials, it can be seen in the same image how, close to the surface (white arrow), ferrite preferentially dissolves, but when the attack progresses up to more inner regions (that have not suffered such high working stresses, black arrow), the austenite is the phase that dissolves.

The change in the relative corrosion resistance of the phases due to the strain level can also be checked for the S32304 DSS in the example of Fig. 7. In this case, the polarization is relatively high, but closer to the corrosion potential (E_{corr}) than the examples in Fig. 6, and the same phenomenon is detected. The three SEM images correspond to tests carried out at the same anodic overpotential. Figure 7a and b shows the selective corrosion of the ferrite that takes place in the surface of the bar or in the region of the cross section close to the surface of the bar when they are exposed to acid medium. However, Fig. 7c, corresponding to attacks suffered by the bulk material, confirms that selective corrosion of the austenite takes place in the least strained region at the same polarization that selective corrosion ferrite occurs in more strained regions of the same bar.

The mixed phenomena occurring in the surface of S32001 and S32304 at high anodic polarizations inside the active regions explains why the ferrite peak expands the potential range upwards where it selectively and markedly overlaps the austenite peak (Fig. 3b). It is well known that the microstructural changes caused by the strain tend to reduce the corrosion resistance of the metals. These results suggest that ferrite is more sensitive to the strains than austenite and hence the corrosion resistance of the ferritic phase in DSS decreases to a higher extent. This experimental evidence can be understood bearing in mind the crystallographic

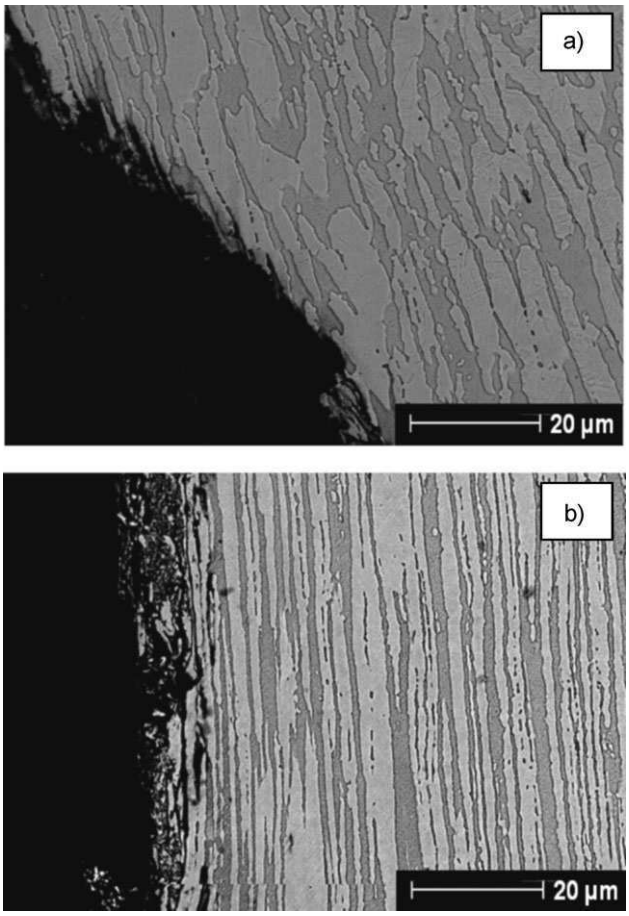

Figure 5. SEM images showing the selective corrosion of ferrite in the strained surface of lean DSS at low anodic overpotentials: (a) HW S32001 at −400 mV *vs.* SCE; (b) HW S32304 at −344 mV *vs.* SCE

characteristics of both phases. The body centered cubic structure of the ferrite is less ductile than the face centered cubic structure of the austenite. Austenitic microstructure has more slip planes, which probably leads to less microstructural defects appearing during the working process. As a first approach, it can be assumed that the higher the number of microstructural defects, the lower the corrosion resistance.

The double structure that can be visually detected for S32205 grades (Fig. 2) suggest that the ferrite in the most alloyed DSS is less sensitive to the decrease in the corrosion resistance caused by straining. The working procedure of CW S32205 causes more marked differences in the mechanical properties between the surface and the center of the bar (Fig. 1), but no selective corrosion of ferrite is detected at high anodic polarization (Fig. 4d). This phenomenon can be explained bearing in mind the Mo content of S32205 grades. The Mo concentrates preferentially in the ferrite [11] and it meaningfully increases the corrosion resistance in acid media [19].

It is true that, besides ferrite and austenite, a variable amount of martensite has been detected in these materials [11]. Images of the behavior of the martensite in the surface of the bars at low anodic overpotentials can be seen in Fig. 8 (inside white ellipses). It is again proved that martensite is more corrosion-resistant than ferrite at low anodic polarizations and that it exhibits a corrosion behavior close to austenite. It is true that, besides the uncorroded martensite in the white ellipses, some attack of the martensite can also be guessed in Fig. 8b. These results confirm that the martensite has a range of potentials where corrosion takes place wider than that of austenite and that martensite dissolves at a very slow rate at potentials close to the E_{corr} where the corrosion rate of austenite is not meaningful (Fig. 8).

Due to the huge magnitude of the overlapping detected in the SEM study for conditions where martensite and austenite dissolves, only two peaks have been considered for the fitting of the activation region (Fig. 3). Including a third peak in an attempt to distinguish between the behavior of the austenite and martensite would imply a big risk. The authors have chosen to assume, as a more rigorous option, that information regarding to martensite dissolution is included in the austenite contribution to the curve. Moreover, it is clear that the austenite peaks become clearly asymmetrical and develop a tail toward low potentials in the curves of samples where more martensite has been detected in the microstructure [11]. So, this tail (seen in Fig. 3b) must be related to the contribution of martensite to the so-called austenite peak.

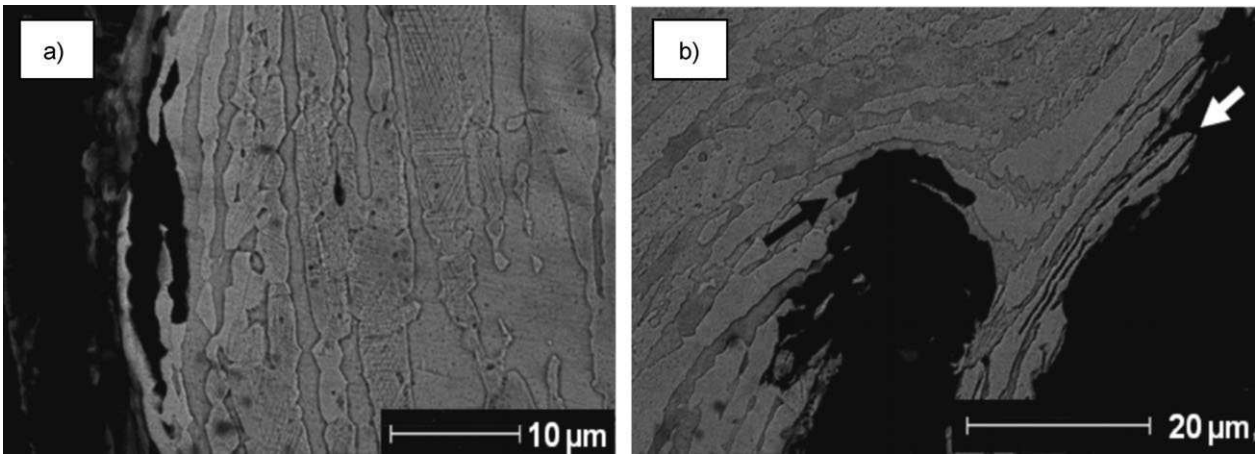

Figure 6. SEM images of the attack on the most strained regions of surface of HW S32001 bar after being polarized at −110 mV *vs.* SCE for 4 h[Q2]

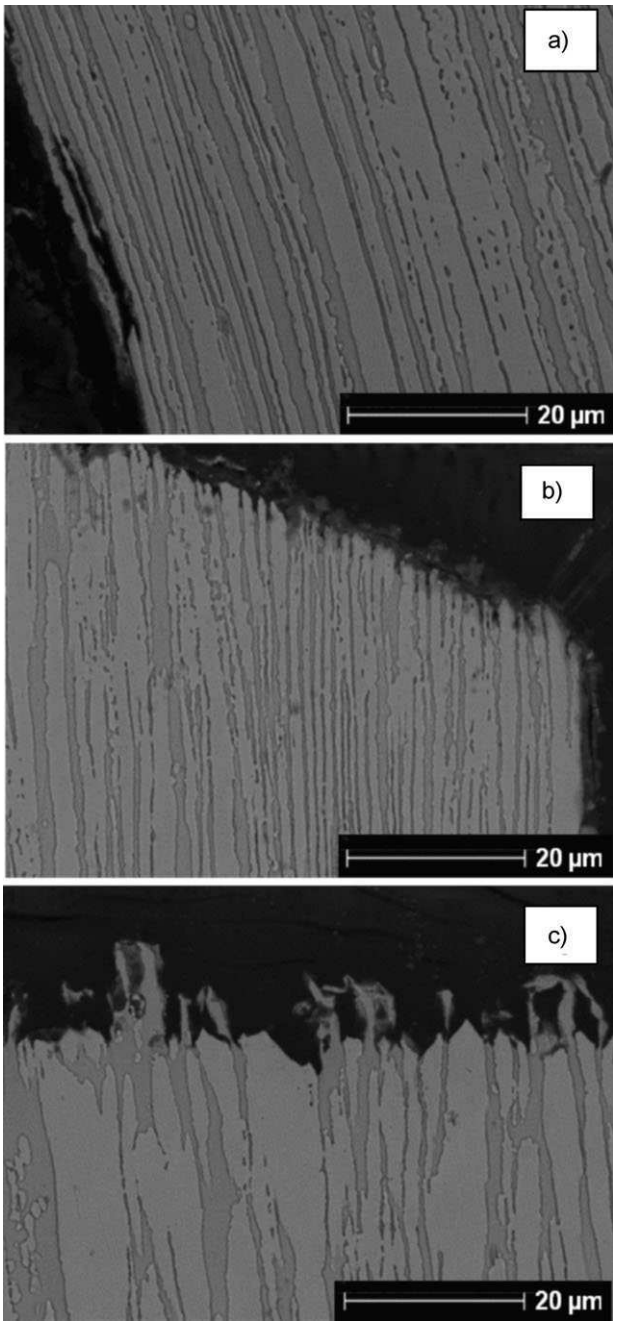

Figure 7. Morphology of the attack in different regions of the HW S32304 bar after being polarized at −225 mV *vs.* SCE for 4 h

The designed fitting procedure carried out allows to obtain relevant numerical parameters about the corrosion behavior of the phases comprised in DSS in different conditions (Figs. 9–11). The error bars plotted in these figures correspond to the experimental dispersion found among the different anodic polarization curves fitted to obtain the data.

In Fig. 9, the charge densities corresponding to each peak in the activation region of the polarization curves after mathematical deconvolution can be seen. The charge density of the peaks corresponds to the number of electrons transferred during the active corrosion of the different phases during the potentiodynamic tests. As expected, both lean DSS exhibit higher charge density values for both phases than S32205 grades. It can be concluded that the lower the alloying degree, the worse the corrosion behavior of all the phases. This is due to the fact that, in spite of the alphagenous or gammagenous character of the alloying element that determines the differences among grades, they are distributed, in fact, in a more or less unbalanced way, between ferrite and austenite [11], so the alloying elements affect the corrosion resistance of both phases.

The ratio between the charge densities of the peaks is also plotted in Fig. 9 and it can be used as an indicator of the relative corrosion resistance of the phases. In Fig. 9a, it can be seen that, for S32205 and S32304 grades, the ferrite has a higher contribution to the region of active corrosion than the austenite. The lower Mo content of S32304 grade could have caused a relative increase of the corrosion rate of the ferrite (Mo is an alphagenous element). However, bearing in mind that the corrosion of the martensite is included in the austenite contribution and the higher trend of S32304 to form martensite than that of S32205 [11], it can be concluded that the corrosion of martensite has balanced the effect of the absence of Mo in the charge density ratio of the phases. On the other hand, for HW S32001 bar (a low Ni, high Mn DSS grade), a higher contribution of the austenite to the active corrosion region is found. In this case, the effect of the high amounts of strain-induced martensite as well as the lower content in gammagenous corrosion-resistant alloying elements [11] can easily explain this fact.

It could be shocking that, for both HW and CW S32205 surfaces (Fig. 9b), the charge densities associated to the corrosion of austenite and ferrite exhibit lower values than for samples of the bulk material (Fig. 9a). This fact can be explained bearing in mind the high anisotropy of the grains (lengthened in the direction parallel to the exposed surface) and the way corrosion progresses in DSS. For DSS, the corrosive attack starts in the least corrosion resistant phase and, if there is a meaningful difference between the corrosion resistance of ferrite and austenite, the most corrosion resistant phase hinders the progress of the attack. When cross-sections from the bars are studied, the attack penetrates in the same direction as the grains are elongated, as can be seen in Figs. 7b, c and 8b and in Ref. [11]. If the attack proceeds in this way, the most corrosion resistant phase is barely effective to slow down the corrosive attack that easily deepens in the material through the least corrosion resistant phase. Moreover, when the least corrosion resistant phase is dissolved, the real surface of the most-corrosion resistant phase exposed to the attack is higher, so its dissolution rate can be somewhat increased. On the other hand, if the grains are elongated parallel to the surface exposed to the attack, the corrosion rate can be effectively slowed down. The effectiveness of this protection mechanism lies in the existence of a phase with good corrosion behavior in the medium and in the small susceptibility to lose it because of plastic strains. Once the less corrosion resistant phase has been dissolved and has disappeared from the exposed surface, the attack rate is reduced. This argument explains the reason why a reduced corrosion rate can be observed for the surface of both S32205 bars (Fig. 9b). Hence, the interplay among microstructure, chemical composition, and

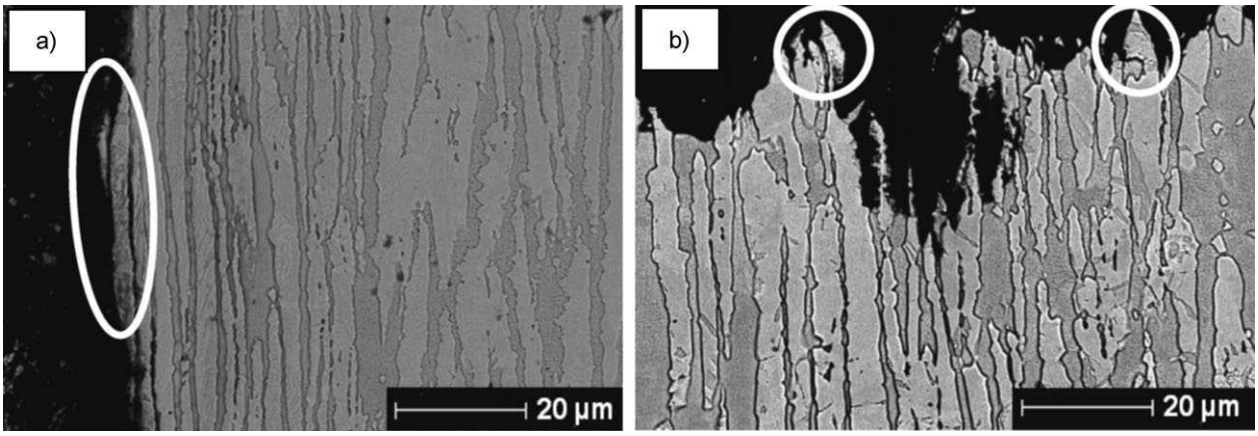

Figure 8. Images of the stability of the martensite in HW S32001 after being polarized at −400 mV *vs.* SCE for 4 h: (a) surface; (b) bulk material

strains can lead to very different results as regards the corrosion behavior of DSS.

When the charge density results of the surface of the bars are calculated for no-Mo DSS (Fig. 9b), it can be observed that ferrite increases meaningfully its contribution to the active region. The increase in the charge associated to ferrite corrosion is coherent with the observations about the selective corrosion of the phases on the surface at high polarizations (Figs. 6 and 7). The increase in the charge density corresponding to the austenite must be understood bearing in mind not only a certain increase of the corrosion rate of the austenite due to the strain, but the higher amount of strain-induced martensite in the surface [11].

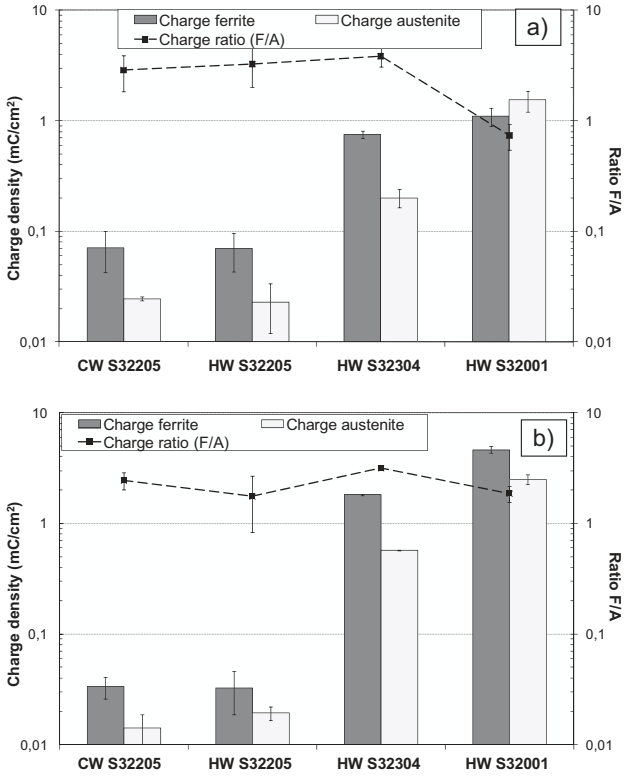

Figure 9. Charge densities corresponding to the activation peaks of the anodic polarization curves of the DSS: (a) samples from the bulk of the bars; (b) samples from the surface of the bars

Comparing the ratio between the charge densities of ferrite and austenite, it can be seen that its values are approximately the same for samples of the bulk DSS bars (Fig. 9a) and those of the strained surfaces (Fig. 9b), except for HW S32001 DSS. The constant value for HW and CW S32205 can be explained considering that the strains do not increase the corrosion rate of these materials. For HW S32304 a pronounced gradient on the martensite concentration can be guessed from the bulk to the surface [11]. Of course, a contribution to the increase on the area of the austenite + martensite peak due to an increase in the corrosion rate of the austenite cannot be discarded because of more microstructural defects in this phase. Anyway, the effect of the higher amount of martensite in the surface of HW S32304 compensates the effect of the higher corrosion susceptibility of the ferrite, making the ratio between the charge densities of the phases similar for the bulk of the bar and for the surface. For HW S32001, in tests carried out on the surface, the relative charge density of the ferrite increases meaningfully, surpassing that of the austenite. In this case, the increase on the contribution of the austenite + martensite peak is lower when bulk material and surface are compared. HW S32001 shows a high amount of strain-induced martensite distributed on the entire material of the bar [11]. This occurs because the chemical composition of this grade makes its austenite more unstable under processing stresses [11].

Other supplementary data obtained from the analysis of anodic polarization curves are plotted in Figs. 10 and 11. In Fig. 10, representative potential values are plotted. It can be seen that E_{corr} is sensitive to DSS compositions. Its value decreases with the decreasing alloying degree, becoming more active. However, E_{corr} values seem to be quite independent from the strain level of the samples.

The E_{max} corresponding to the active corrosion of both the ferrite and the austenite exhibit relatively similar values for all the bulk studied DSS (Fig. 10a). When comparing samples from the surface of the bars (Fig. 10b) to samples of the core, the E_{max} of ferrite and austenite peak does not meaningfully change their values for both S32205 bars, but they are highly shifted to more

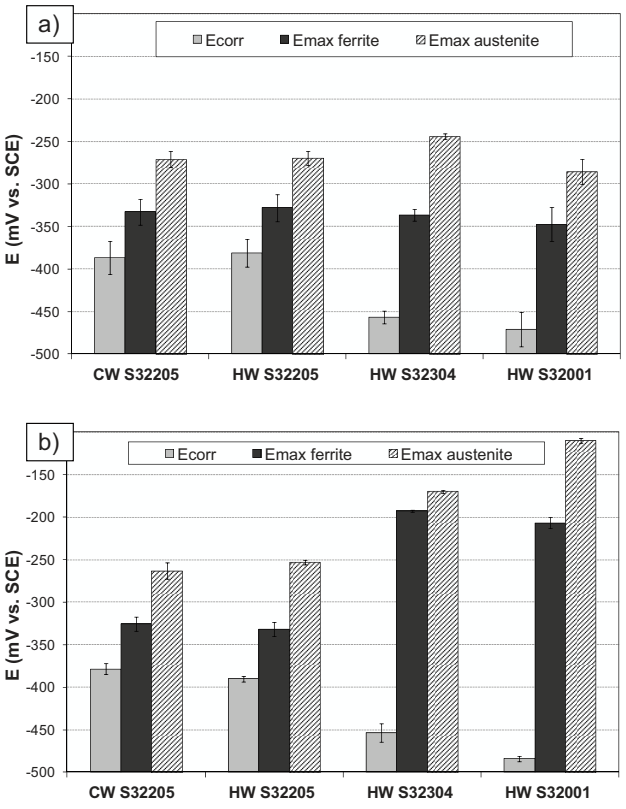

Figure 10. Potential values obtained from the analysis of the anodic polarization curves of the DSS: (a) samples from the bulk of the bars; (b) samples from the surface of the bars

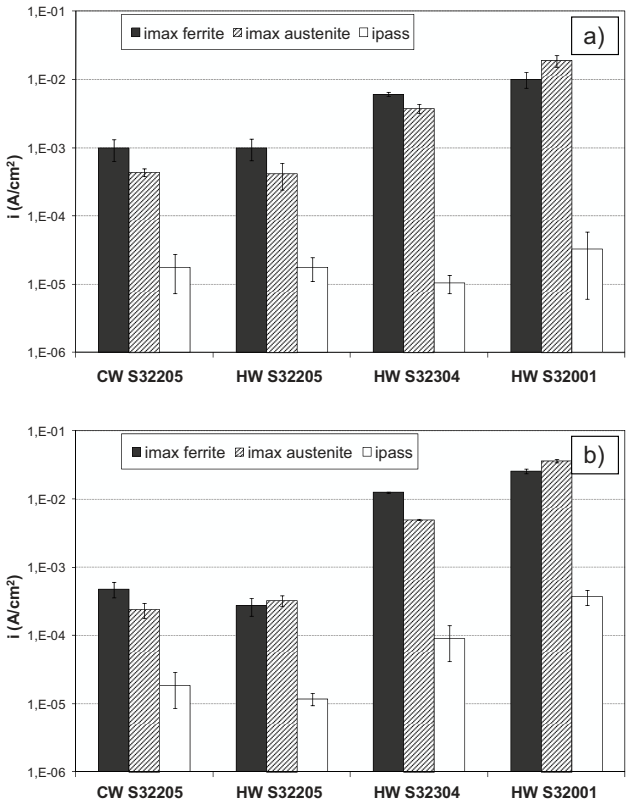

Figure 11. Current density values obtained from the analysis of the anodic polarization curves of the DSS: (a) samples from the bulk of the bars; (b) samples from the surface of the bars

anodic values for lean DSS. This means that the increase in the charge density of the peaks due to strains is associated with an expansion of their region of active corrosion toward higher potentials. The increase of E_{max} of austenite and the trend of martensite to dissolve slowly at potentials slightly over E_{corr}, explain the asymmetry of peaks such as those of the austenite + martensite contribution in Fig. 3b.

Moreover, when, the i_{max} of the phases are compared for a given bar for samples obtained from bulk materials (Fig. 11a) or for strained surfaces (Fig. 11b), it can be seen that S32205 bars exhibit lower values when specimens of the strained surface are considered. However, for HW S32304 and HW S32201, the observed trend is just the opposite. The same trend has been previously observed for the charge density in Fig. 9, and it has already been discussed in depth. However, it must be pointed out that i_{max} values are a much less sensitive indicator of the effect of the stresses on the corrosion behavior than the charge density. When the strain increases, the main effect related to the corrosion behavior of each phase is the growth of the peaks corresponding to active corrosion toward higher potentials (Fig. 10). The influence of the chemical composition of the DSS on i_{max} (Fig. 11) can also be explained bearing in mind the same arguments used to explain the trend in Fig. 9.

The passivation current density (i_{pass}) is the current density measured in the passive region, when a protective passive layer has been formed by anodic polarization. Obtained i_{pass} values are plotted in Fig. 11 and they can be related with the quality (isolating ability) of the passive layer formed in the different samples. No meaningful differences can be observed in Fig. 11a, so the chemical composition of the DSS is not a key parameter for determining the i_{pass} values. More interesting results can be observed when i_{pass} values in Fig. 11a are compared to those in Fig. 11b. For lean DSS, the i_{pass} of the surface is clearly higher than that of the bulk materials. This fact has not previously been observed for similar materials when they have been tested at much less aggressive, higher pHs [20]. Previous results have concluded that the nature of the passive film in stainless steels can depend on the pre-strained level of the base material. Other authors have also found that i_{pass} increases with the strain level for certain DSS grades [5]. It has been published that less protective, less stoichiometric passive layers are formed on strained surfaces [21]. In this case, the same conclusion can be reached for HW S32304 and S32001 bars. In the studied conditions, the strains in the surface of the lean DSS bars must favor the generation of less stoichiometric oxides with lower isolating ability. It would explain the higher i_{pass} values for surfaces than those for the bar cores. Moreover, it has been published that deformations up to 50% increases i_{pass} because the process is governed by tensile stresses, but at higher reductions, the passivation process is taken over by the texture of the material and the i_{pass} is reduced [5]. Results presented in this paper show that the values of deformation that limit the predominance of the texture effect over the effect of the amount of defects are highly dependent on the chemical composition of the material. For both

S32205 bars, no increase in the i_{pass} is detected when the surface is compared with the core.

4 Conclusions

From the results presented in this work, the following conclusions can be drawn:

- For lean DSS bars, an increase in the corrosion rate caused by strains has been detected. In no-molybdenum DSS, ferrite has proved to be more sensitive to decrease in the corrosion resistance caused by strains than austenite.
- In DSS, when the strains have negative effects on the corrosion behavior, the active region corresponding to the corroding phase tends to increase toward higher potentials.
- When the grains are heavily strained parallel to the surface, if the most corrosion resistant phase has good corrosion behavior in the medium as occurs with the S32205 grade, the corrosion rate can be effectively slowed down, in spite of the microstructural defects.
- In heavily strained surfaces of lean DSS bars, the passive layers need higher anodic polarizations to be formed and are less isolating than those formed in lesser strained surfaces of the same materials.

Acknowledgements: The present work was funded by the Spanish Ministry of Science and Innovation and MINECO through the Projects reference BIA2007-66491-C02-02 and MAT2011-29182-C02-02.

5 References

[1] S. G. Acharyya, A. Khandelwal, V. Kain, A. Kumar, I. Samajdar, *Mater. Charact.* **2012**, *12*, 68.
[2] K. Klyk-Spyra, M. Sosanska, *Mater. Charact.* **2006**, *56*, 384.
[3] B. Ravi Kumar, R. Singh, B. Mahato, P. K. De, N. R. Bandyopadhyay, D. K. Bhattachacharya, *Mater. Charact.* **2005**, *54*, 141.
[4] G. Lu, H. Cheng, C. Xu, Z. He, *Chin. J. Chem. Eng.* **2008**, *16*, 314.
[5] J. Yang, Q. Wang, K. Guan, *Int. J. Pres. Vessels Piping*[Q3] **2013**. http://dx.doi.org/10.1016/j.ijpvp.2013.04.025
[6] N. C. Renton, A. M. Elhoud, W. F. Deans, *J. Mater. Eng. Perform.* **2011**, *20*, 436.
[7] V. Cihal, R. Stefec, *Electrochim. Acta* **2001**, *46*, 3867.
[8] V. Cihal, S. Lasek, M. Blahetova, E. Kalabisova, Z. Krhutova, *Chem. Biochem. Eng. Q.* **2007**, *21*, 47.
[9] M. Martins, L. C. Casteletti, *Mater. Charact.* **2009**, *60*, 150.
[10] J. A. González, E. Otero, S. Feliu, A. Bautista, E. Ramírez, P. Rodríguez, W. López, *Mag. Concrete Res.* **1988**, *50*, 189.
[11] A. Bautista, S. M. Alvarez, F. Velasco, *Mater. Corros.*[Q4] **2013**. DOI: 10.1002/maco.201307419
[12] F. Velasco, G. Blanco, A. Bautista, M. A. Martínez, *Constr. Build. Mater.* **2009**, *23*, 1883.
[13] H. Luo, C. F. Dong, X. G. Li, K. Xiao, *Electrochim. Acta* **2012**, *64*, 211.
[14] L. Zhang, W. Zhang, Y. Jiang, B. Deng, D. Sun, J. Li, *Electrochim. Acta* **2009**, *54*, 5897.
[15] W.-T. Tsai, J.-R. Chen, *Corros. Sci.* **2007**, *49*, 3659.
[16] S.-J. Pan, Y.-J. Shih, J.-R. Chen, J.-K. Chang, W.-T. Tsai, *J. Power Sources* **2009**, *187*, 2161.
[17] S. M. Alvarez, A. Bautista, F. Velasco, *Corros. Sci.* **2013**, *59*, 130.
[18] P. De Tiedra, O. Martín, M. López, M. San-Juan, *Corros. Sci.* **2011**, *53*, 1563.
[19] J. R. Davis (Ed.), *Stainless Steels ASM Specialty Handbook*, ASM International, Materials Park, OH **1994**.
[20] S. M. Alvarez, A. Bautista, F. Velasco, *Corros. Sci.* **2011**, *53*, 1748.
[21] E. C. Paredes, A. Bautista, S. M. Alvarez, F. Velasco, *Corros. Sci.* **2012**, *58*, 52.

(Received: September 25, 2013) W7420
(Accepted: October 26, 2013)

Keywords: acid corrosion
duplex stainless steel
polarization
SEM
selective corrosion
strain-induced martensite

Q1: Author: A running head short title was not supplied; please check if this one is suitable and, if not, please supply a short title that can be used instead.
Q2: Author: Please mention part labels in the caption of Figures 6 and 7.
Q3: Author: Please provide the volume number and first page number for this reference.
Q4: Author: Please provide the volume number and first page number for this reference.

5.7 PUBLICACION 7: P7

A. Bautista, S.M. Alvarez, E.C. Paredes, F. Velasco.

"*Corrosion performance of stainless steels corrugated bars after 9 years of exposure. Part I: Non-carbonated, chloride-contaminated mortar*".

Enviado a Corrosion Science.

Corrosion performance of corrugated stainless steels after 9 years of exposure. Part I: Non-carbonated, chloride-contaminated mortars

A. Bautista[1], S.M. Alvarez, E.C. Paredes, F. Velasco
Materials Science and Engineering Department - IAAB.
Universidad Carlos III de Madrid.
Avda. Universidad nº 30. 28911 - Leganés, Madrid (Spain)

Abstract

Mortar samples reinforced with 5 different corrugated stainless steels were tested for 9 years in 2 different conditions: partial immersion (PI) in 3.5% NaCl, and chloride addition to the mortar and exposure to high relative humidity (HRH). The monitoring during the exposures was carried out with corrosion potential (E_{corr}) and electrochemical impedance spectroscopy (EIS) measurements. After 8 years, the reinforced mortar samples were anodically polarized to obtain more information about the pitting resistance of the passive layers formed under the different conditions. The exposure was extended for 1 year more to study the progress or repassivation of the pits. The PI is the most aggressive testing condition and it causes low-intensity corrosion in S20430 austenitic stainless steel after 7 years of exposure. The S32205 duplex stainless steel shows excellent behaviour.

Keywords: A. Stainless steel; A. Steel reinforced mortar; B. EIS; B. Polarization; C. Passivity; C. Pitting corrosion.

1. Introduction

The high alkalinity of concrete creates an environment that protects steel against corrosion. However, the life expectancy of concrete structures is affected by corrosion of steel reinforcements, because of an aggressive attack of chloride ions or as a result of carbonation [1,2]. The presence of chloride in the environment increases the risk of

[1] Corresponding author. Tel: +34 91 624 9914. Fax: +34 91 624 9430. E-mail address: mbautist@ing.uc3m.es (A. Bautista).

pitting corrosion in these steels. When chloride levels are extremely high, the passive layer of the steel can be destroyed in large areas of the reinforcement and general corrosion takes place [3].

Stainless steels are more corrosion resistant to chloride than traditional carbon steel reinforcements [4]. The study of the corrosion behaviour of stainless steel reinforcements, to replace carbon steel reinforcements in highly aggressive environments, has been a subject of research in recent years [5-7]. Most studies of the corrosion behaviour of stainless steel are based on the use of solutions simulating those found in concrete pores. Almont all authors agree that the high alkalinity of simulated pore solutions improves the corrosion behaviour of stainless steel in chloride-contaminated environments [8-13].

Although some authors have studied the importance of the forming process in the corrosion behaviour of corrugated stainless steel bars [13,14], most published studies deal with the influence of alloying elements in simulated solutions. Traditionally, the UNS S30400 and S31600 austenitic stainless steel grades have been analysed [12,15]. Some researchers detect no difference between the pitting corrosion resistance of both materials in solution tests [10,16,17]. However, others conclude that there is a slightly better behaviour of S31600 grade [18,19].

The low-alloyed, austenitic UNS S20430 stainless steel has been proposed as an economic alternative to traditional stainless steels for use in reinforced concrete structures, due to its corrosion performance [20]. Results in simulated pore solutions have shown slightly less pitting corrosion resistance than UNS S30400 steel [21,22]. The analysis of the passive layer in alkaline environments has revealed that its composition is slightly less protective than that of traditional austenitic steels [18].

Duplex stainless steels have appeared in the market as a noteworthy option for concrete structures [11,14,23,24]. The preliminary studies in simulated solutions suggest excellent corrosion behaviour of UNS S32205 duplex grade [8,18].

There are scant studies on the corrosion behaviour of corrugated stainless steels embedded in concrete or mortar, especially when compared to the large number of studies published using simulated pore solutions. There are a few old studies performed on mortar and concrete, but focused on less interesting steel grades than those used

today, or on steels not processed as corrugated reinforcements [25,26]. More recent studies only cover a limited time period (1.5-3 years) [6,23,27,28].

Nevertheless, concrete and mortar studies are very important for confirming the durability of corrugated stainless steels, because there are four key aspects in the early stages and in the development of the corrosion process that simulated pore solutions are not able to reproduce:

a) The crevices present in the rebar/mortar interface, which can play an important role in the corrosion mechanism [29].
b) The presence of a dense, lime-rich layer of hydration products in the steel- concrete interface [30], which can hinder the attack.
c) The difficulty for oxygen diffusion, much greater in mortar than in solution. The oxygen diffusion often limits the corrosion rate [31], which is a key factor that often restricts or inhibits the attack in immersed structures.
d) The resistivity of the concrete, which depends on the porosity and the water saturation level of the pores, can be much higher than the resistivity of the testing solutions. There is a correlation between concrete resistivity, the corrosion initiation period and the corrosion propagation [1,32-34]. In aerial structures, the concrete resistivity can often control the corrosion rate when the environment is dry. When there is humidity in the air, concrete is able to absorb it facilitating the corrosion attack. It this case, oxygen gains access to the reinforcement, since the diffusion distance through the aqueous layer is small and the environment resistivity is low [35].

The main objective of this study is to analyse the corrosion behaviour of different grades of corrugated stainless steel embedded in mortar, which have been exposed to highly aggressive environments. The electrochemical behaviour has been monitored for 8 years, using non-destructive techniques such as electrochemical impedance spectroscopy (EIS) and corrosion potential measurements (E_{corr}). In addition, at the end of the exposition period, anodic polarization tests were performed to determine the probability of pitting corrosion in the steels that were still in a passive state. The samples were left another additional year in order to analyse the evolution of the attack provoked with these polarization tests.

2. Experimental

Five different corrugated stainless steels were considered in the study. The chemical composition of the stainless steels, their diameter and their tensile strength are shown in **Table 1**. Traditional carbon steel corrugated bars were also included for reference.

Table 1. Chemical composition (w/w), diameter and tensile strength of the four studied DSS.

Stainless Steel			⌀	Main Alloying Elements (%)										Tensile Strength (MPa)
UNS	AISI	EN	(mm)	S	C	Ti	Si	Mn	Cr	Ni	Mo	N	Cu	
S20430	204Cu	1.4597	5	0.002	0.049	0.003	0.23	8.26	16.12	1.89	0.015	0.130	2.65	918
S30400	304	1.4301	8	0.002	0.063	0.004	0.31	1.42	18.33	8.12	0.297	0.050	0.32	1035
S31603	316L	1.4404	10	0.006	0.021	0.003	0.21	1.67	17.05	10.25	2.171	0.47	0.32	805
S31635	316Ti	1.4571	12	0.001	0.029	0.251	0.45	1.21	16.68	11.25	2.232	0.020	0.41	860
S32205	2205	1.4462	12	0.001	0.029	0.027	0.39	1.72	22.49	4.72	3.221	0.174	0.24	1156

The corrugated bars were partly embedded in mortar with a cement/sand/water ratio of 1/3/0.6 (w/w). Ordinary Portland cement was used for preparing the mortar. Half of the samples were manufactured with 3% $CaCl_2$, weighed in relation to the amount of cement. This chloride concentration is slightly higher than those sometimes used to test the behaviour of carbon steel [36] or galvanized steel [37] in mortar, and it is inside the range of those used to test some stainless steels [28].

Cylindrical mortar samples were used to minimize inhomogeneities in the electrical signal distribution during the EIS monitoring (**Figure 1**). The thickness of the mortar cover was always 1.5 cm, independently of the diameter of the bar (**Table 1**). The length from the end of the corrugated bar to the bottom of the mortar sample was also 1.5 cm. The surface of the bars exposed to the mortar-air interface was isolated to avoid interference in the study (mainly carbonation). The exposed length of the bar in mortar was always 3 cm. All cross-sections of the bars embedded in mortar were previously polished to 320# and passivated with HNO_3 in the laboratory, in order to reproduce the process carried out on the corrugated surfaces of the bars in industry.

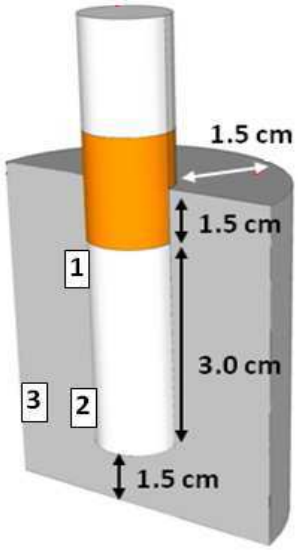

Figure 1. Scheme of the reinforced mortar specimens manufactured for the study. The regions where the chloride content was measured have been marked as 1-3.

After their manufacture, the reinforced mortar samples were cured for 30 days at approximately 90-95% relative humidity (RH). Then, they began their exposure period under two different conditions. The samples manufactured with chlorides were exposed at 90-95% RH (condition labelled as HRHCl). The samples without chlorides were partially immersed (PI) in 3.5% (w/w) NaCl solution and at 90-95% RH. In this case, the level of the solution was maintained at the same height as the middle of the length of the bars exposed in the mortar. Curing processes and exposures were always carried out at room temperature.

The electrochemical monitoring of the corrosion behaviour during the 8-year exposure period was carried out using E_{corr} and EIS measurements. To obtain the E_{corr} values, a saturated calomel electrode (SCE) was used. For the EIS measurements, a three-electrode configuration was used. The surface of corrugated bar exposed to the mortar acted as working electrode, the reference electrode was a SCE and the counter-electrode was a copper cylinder, with a diameter slightly larger than that of the mortar sample. To assure good contact between the mortar and the counter-electrode, a wet pad was used. The EIS spectra were acquired using a perturbation signal of 10 mV of amplitude, from 10^{2} to 10^{-3} Hz.

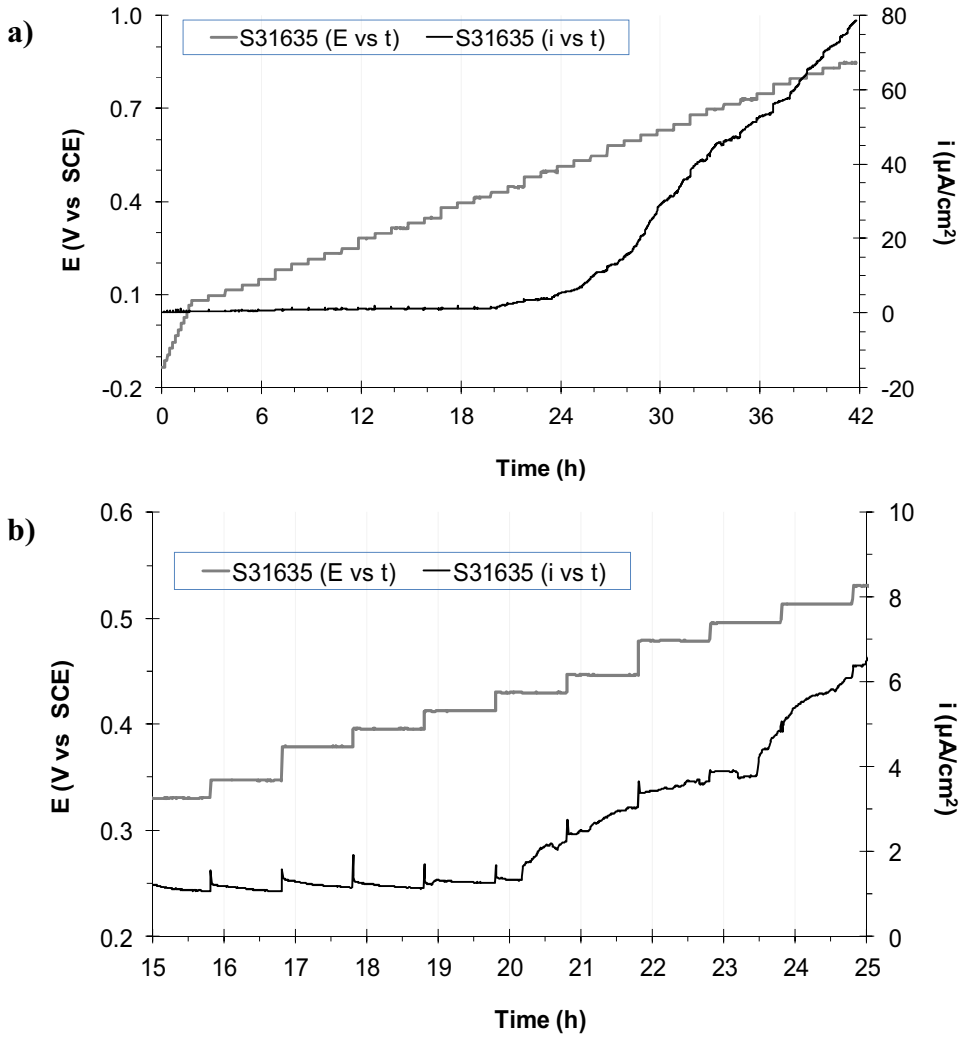

Figure 2. Example of the potential steps applied to the mortar samples at the end of the exposure and the obtained current response: a) Test carried out for a sample reinforced with S31635 after PI; b) Detail of the data shown in figure 2a.

After the 8-year exposure period, the reinforced mortar samples were submitted to anodic polarization tests. The tests started from the E_{corr} and were based on short potentiostatic steps of 10 min. When a potential of about 100 mV vs SCE is reached, the length of the steps increased to 1 h. The increase of the length of the steps is due to greater difficulties of stabilization of the current signal at increasing anodic overpotentials. All the steps (short and long) increased the potential by 20 mV. The polarization steps finished at 900 mV vs SCE. An example of the signal applied to obtain the polarization curves in mortar and of the obtained current response can be seen

in **Figure 2a**. In **Figure 2b**, a detail of both signals is shown, where the shape of the current transients caused by the increasing potential steps can be seen.

The current value plotted on the polarization curves used in this study corresponds to the stabilization value of the current after each potential step. The analysis procedure of the transitories was based on the potential-step method, where the contribution of the ohmic drop through the mortar can easily be distinguished from the electrochemical response of the reinforcements [38]. The length chosen for the potential steps allows us to obtain more reliable results than the traditional polarization curves carried out at a much higher sweeping rate, as the stabilization of the current after the pulses is slower as polarizations increases.

After the polarization tests, the samples remained for 1 year in PI or HRH to allow progress or possible repassivation of the provoked pits. Then, the samples were broken and the morphology and localization of the attack were studied by scanning electron microscopy (SEM).

Moreover, the total chloride content of the mortar after the 9-year exposure was measured in 3 different regions of the samples. The localization of the studied regions is marked in **Figure 1**. The quantification of the total chloride content was carried out by X-ray fluorescence (XRF) spectrometry [39]. The obtained value is the average of at least 5 measurements in each region of the samples.

3. Results and Discussion

The E_{corr} values monitored for the corrugated bars in mortar are shown in **Figures 3** and **4**. The ASTM C876 standard suggests a criterion for determining the probability of corrosion for non-coated reinforcements that has been included in the figures. Factors than can sometimes limit the reliability of the information from E_{corr} about the corrosion performance [32] can be ruled out in this case, due to the characteristics of the experimental design.

In **Figure 3**, it can be seen that, after only 3 months under PI conditions, carbon steel shows quite low E_{corr} values. A review paper has stated that these values (< -426 mV vs.

SCE) are typical of a severe corrosion attack [40], and in our laboratory it has been checked that these samples were completely cracked after 6-8 months of testing. On the other hand, the E_{corr} of the stainless steel bars (under PI) tends to remain in the region where the risk of corrosion is lower than 10%, with some random values in the region with an uncertain risk of corrosion. However, for the low-alloyed austenitic S20430 grade, a meaningful evolution of the E_{corr} can be observed. During the last year of exposure, the E_{corr} of this material exhibits values corresponding to a high risk of corrosion. Though this relationship between E_{corr} and corrosion condition has not been specifically validated for stainless steels, these results suggest an excellent performance all the tested stainless steel but S20430 (especially bearing in mind that the resistivity of the mortar cannot mask the attack because of its wetness).

The E_{corr} evolution of the corrugated bars embedded in mortar with chloride additions and exposed at HRHCl can be seen in **Figure 4.** Under these conditions, the observed trends of the passive/active state are quite similar to those found at PI (**Figure 3**) for carbon steel and for all the tested stainless steels, except S20430. Carbon steel actively corrodes since the first monitoring measurement carried out, and all the tested stainless steels, including S20430, seem to be able to keep their passivity.

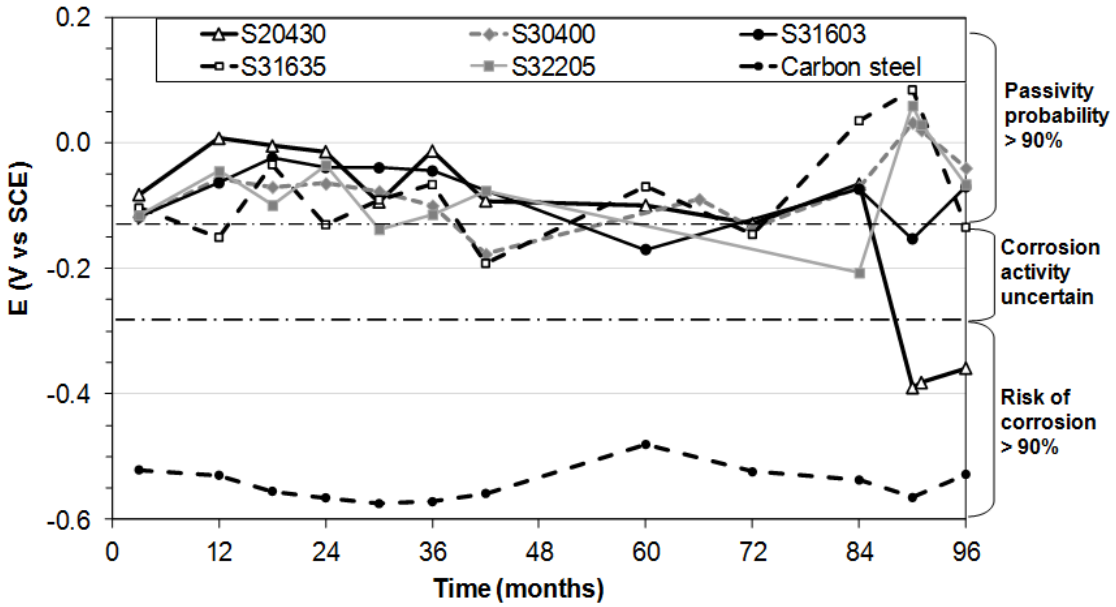

Figure 3. E_{corr} evolution of the PI mortar samples during the 8-year exposure. The evaluation of the corrosion risk following the standardized criteria has been included.

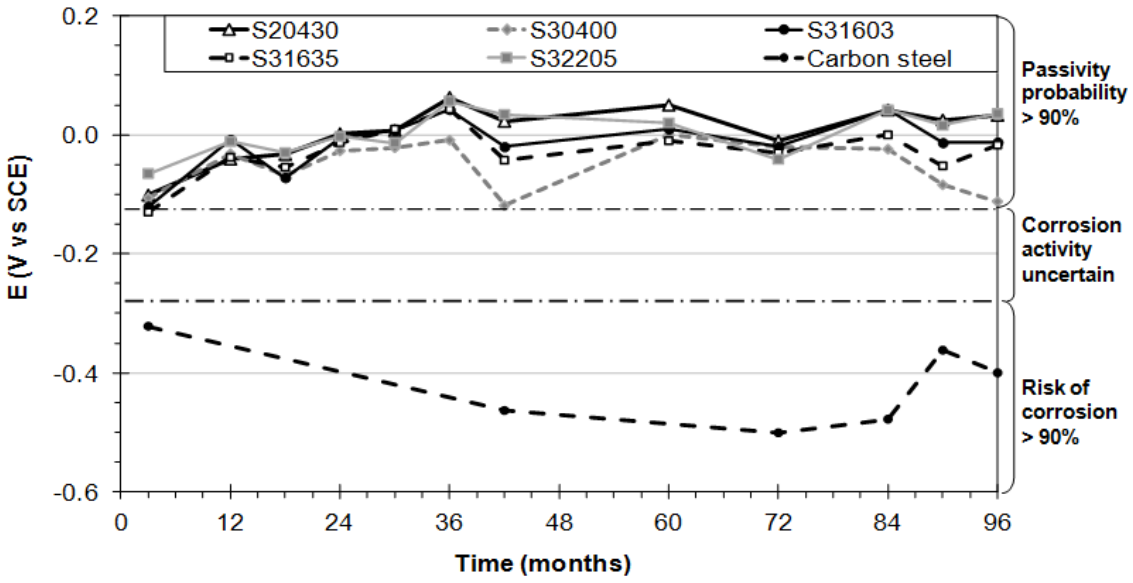

Figure 4. E_{corr} evolution of the samples exposed to HRHCl (mortar with chloride additions and exposed at high RH). The evaluation of the corrosion risk following the standardized criteria has been included.

In HRHCl, the low-Ni austenitic stainless steel exhibits E_{corr} typical of the passive state during a period of 8 years, showing a better corrosion performance than in PI. In addition, S32205, S30400, S31603 and S31635 in HRHCl do not show any E_{corr} value in the uncertain corrosion range, unlike that observed in PI. These results are coherent with the fact that the PI in chloride media is an especially aggressive condition if the chloride concentration has reached a critical value on the surface of the reinforcement. The existence of an aerated region close to a submerged region (where the oxygen access is more hindered) favours the formation of an active corrosion cell and fosters the attack. Besides, the data plotted in **Figure 5** regarding the chloride concentration at the end of the exposure contribute to understanding the different behaviour observed between PI and HRHCl exposures.

In **Figure 5**, it can be seen that the chloride concentration in samples where the depassivating ion has been added during the mortar manufacturing (HRHCl) remains constant in all the regions of the samples. This chloride level (in relation to the mortar weight) can be comparable, for example, to those found (in relation to the concrete weight) at 7-8 cm from the surface of non-submerged region of a structure exposed for 60 years in a tropical marine environment [41].

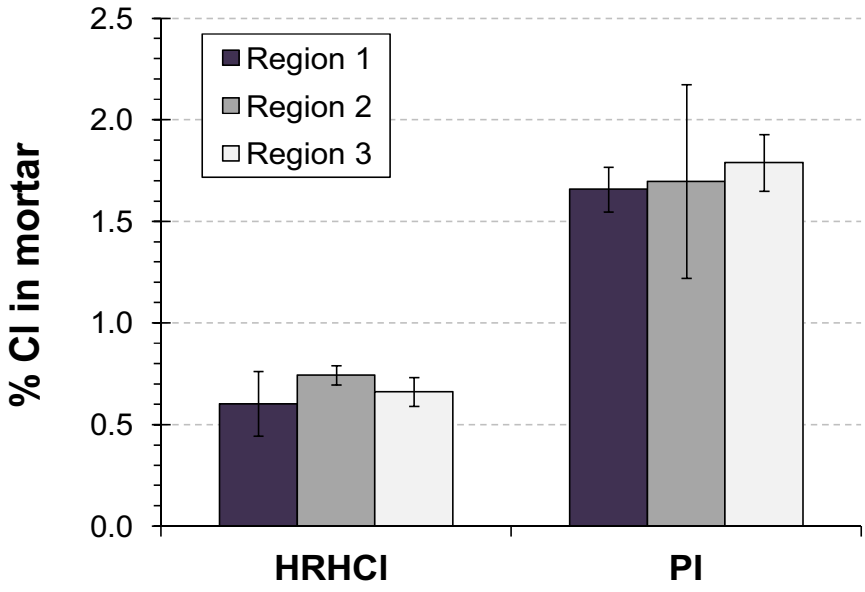

Figure 5. Chloride concentration (% by wt. to mortar) after 9 years exposure.

The concentration of ions in the PI exposed samples reaches also similar values in the these regions after 9 year of exposure (**Figure 5**). Although the chlorides penetrate from the outer solution (PI exposure). The diffusion and the length of the exposure eliminate the possibility of formation of chloride concentration cells between the submerged and non-submerged-region of the PI samples. Anyway, the extremely high aggressivity of the PI conditions is supported by the higher level of chlorides, and the formation of the aeration cells between submerged and non-submerged areas. Good behaviour by the bars in such a corrosive exposure condition is a reliable guarantee of the durability of the bars in practice, which supports previous conclusions of published solution and short-term tests.

With the aim of obtaining more complete information about the corrosion performance of the samples during the exposure, they have been monitored by EIS. Representative examples of the shape of the spectra corresponding to reinforcing stainless steels can be seen in **Figure 6a and b**. An excellent quality of the fitting is achieved using a two-time constant cascade model (**Figure 6c**). Previous EIS studies in simulated pore solutions have demonstrated that the spectrum of passive stainless steels is formed by two, very overlapped, time constants [12,18,24].

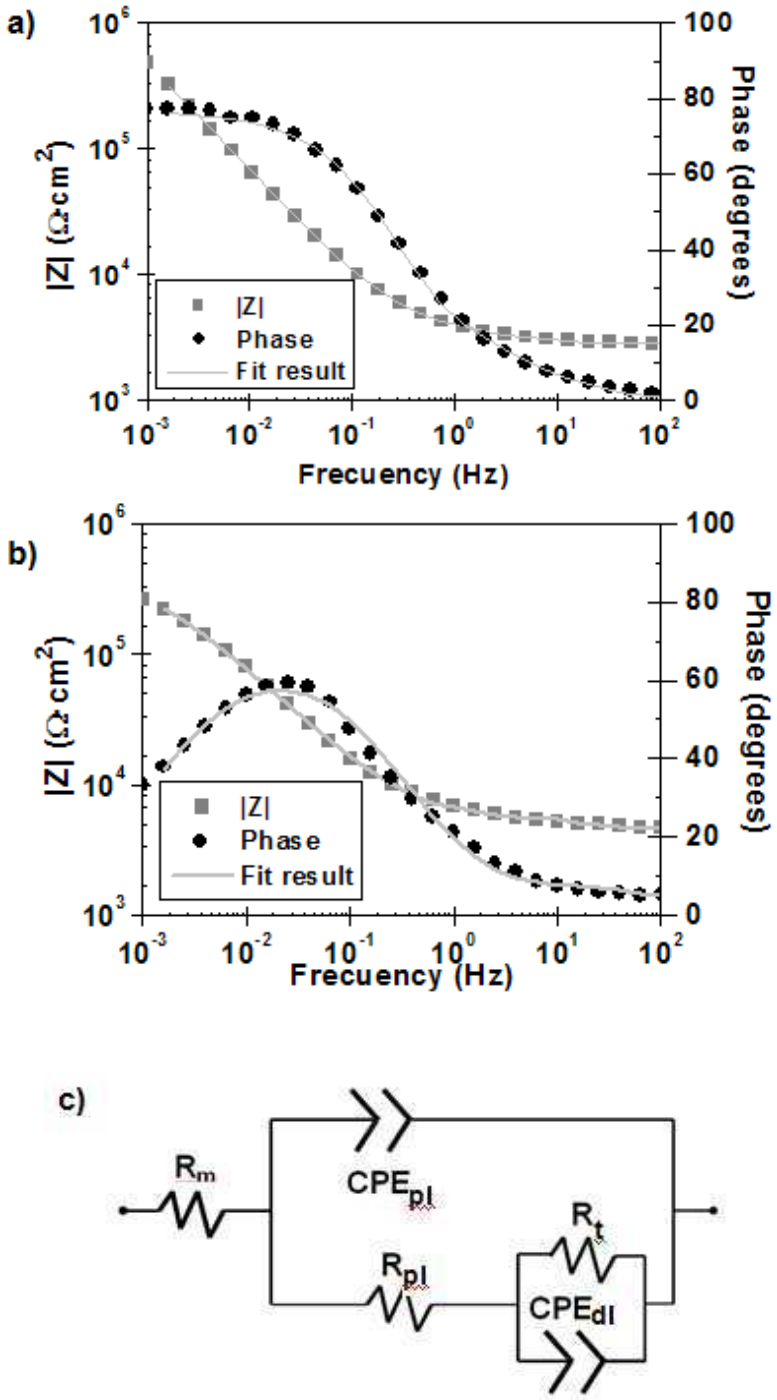

Figure 6. Example of the experimental EIS spectra and fitting results corresponding to stainless steel reinforcements: a) System whose E_{corr} is in the passive region (S32205 after 3 months in PI); b) System whose E_{corr} is in the active region (S20430 after 8 years in PI); c) The equivalent circuit used to fit the experimental results.

The work carried out in this study proves that this model is also valid when stainless steel corrugated bars are embedded in mortar. Furthermore, the equivalent circuit is still

useful when the E_{corr} of the stainless steel reinforcements decreases to the region of high corrosion risk, as during the last period of PI of S20430, though this stainless steel had never exhibited such low E_{corr} values during the simulated pore solution tests in a spontaneous way. Other research groups have also chosen this equivalent circuit to simulate the electrochemical behaviour of active and passive stainless steel in solution and in mortar [6,42].

The resistive behaviour obtained at high frequencies in the EIS spectra corresponds to the mortar resistance (R_m). Mortar or concrete are electrolytes with moderate conductivity, so R_m is an important parameter that can control the corrosion rate, as has been mentioned in the introduction. In **Figure 7**, the R_m values obtained from the simulation of the EIS data can be seen. For samples PI in 3.5% NaCl, R_m increases at the beginning of the exposure due to chemical processes in the mortar that increase its density, and, hence, its electrical resistance. These processes determine the increases of R_m values during the first two years (**Figure 7a**). Then, as the exposure extends, the migration of chloride ions inside the mortar from the solution prevails, and the R_m decreases. This effect is clearly visible from the third year of exposure. Other authors have observed somewhat similar trends for PI samples in a low-quality mortar [6]: R_m increasing due to mortar curing during the first 4 months and then decreasing due to chloride penetration. A certain stabilization of R_m can be guessed during the last year of exposure. This could be explained considering the fact that the chloride concentration inside the pore solution is high and the diffusion process from the external solution is hindered on very slowing down.

When the mortar samples are manufactured with chlorides and no entry of new-chlorides takes place during the exposure, R_m tends to increase during the first 3 years, and later, its value remains stable (**Figure 7b**). The increase in the R_m value is explained not only by the reduction of the pore volume during the mortar curing, but also because of the well-known fact that part of the added chlorides can be retained in the products formed during the curing, so they cannot contribute to increasing the conductivity of the pore solution. If the R_m values corresponding to both tested exposure conditions are compared (**Figures 7a** and **7b**), lower R_m values can be observed for the samples manufactured with chlorides, but for long exposure times. This agrees with the higher chloride level in PI than in HRHCl mortars (Figure 5).

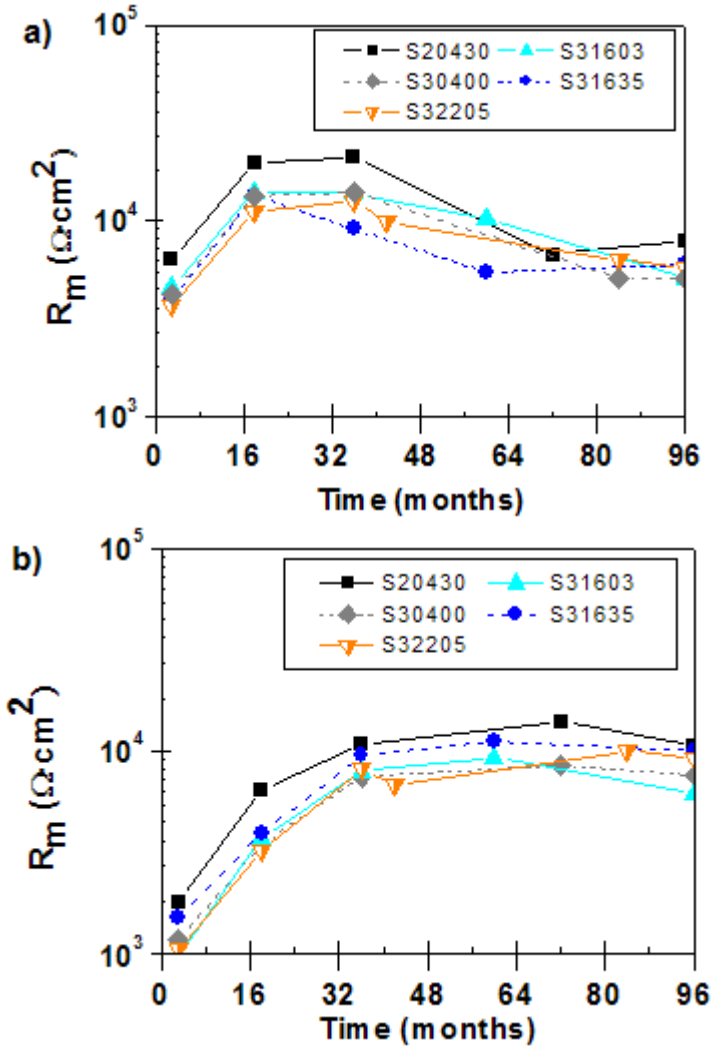

Figure 7. Time evolution of R_m: a) PI; b) HRHCl.

Previous EIS studies of corrugated stainless steel in alkaline solutions [18] and in mortar [6] have identified the first time constant at intermediate frequencies (**Figure 6**) with electrochemical characteristics of the passive layer. The R_{pl} values and the C_{pl} and n_{pl} corresponding to CPE_{pl} that have been obtained from the simulation of the EIS spectra can be seen in **Figures 8** and **9.**

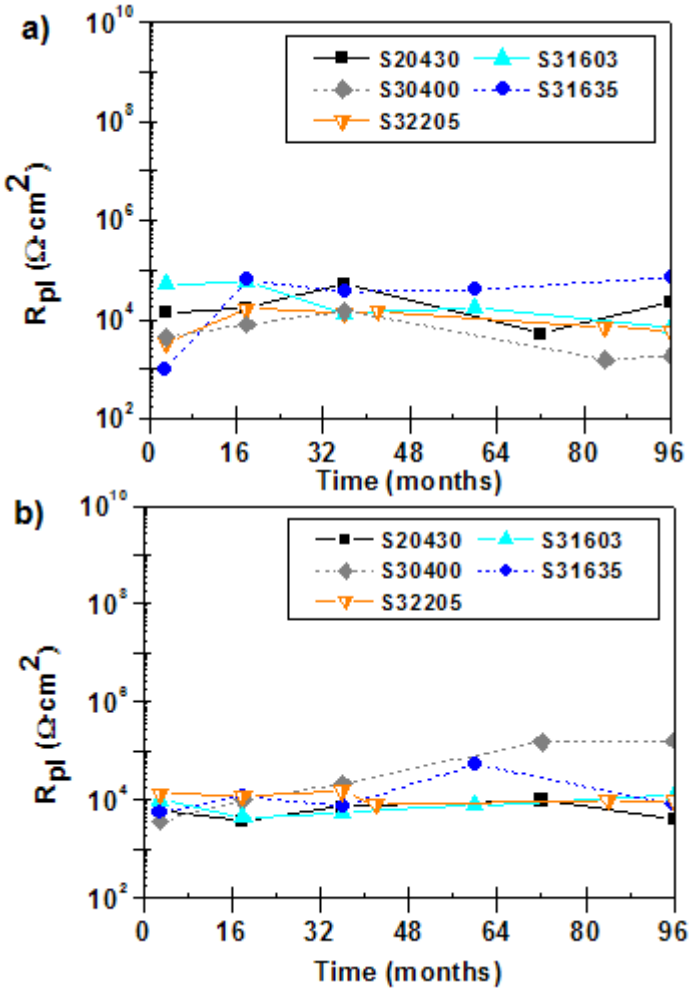

Figure 8. Time evolution of R_{pl}: a) PI; b) HRHCl.

In the solution tests, during the first hours, an increase in R_{pl} value has been reported due to the changes in the oxidation state on the oxides in the passive layer due to the exposure to the alkaline medium [18]. For the same type of reinforcements embedded in mortar, this trend can hardly be guessed (**Figure 8**). The oscillation in R_{pl} values can probably be related to the uncertainty that implies obtaining data from spectra with such overlapped constants. Hence, it can be assumed that, after a certain time, the chemical composition and structure of the passive film reach an equilibrium with the medium, with this process taking less than 3 months. The R_{pl} values increase about one order of magnitude in solution during the first day of exposure [18]. Now, the R_{pl} values measured in mortar during the long-term exposure are about 1 order of magnitude higher than those measured in solution after 1 day, so the transformation of the passive layer in the previous solutions tests was incomplete.

The C_{pl} values (**Figure 9**) are similar to those previously measured in solution for these bars [18]. In certain cases, a slight trend of n_{pl} to decrease its value with time could be guessed. This would correspond to an increase in the dispersion with frequency of the capacitive behaviour of CPE_{pl} that could reflect an increase of inhomogeneities in the passive layer with time. The testing conditions in mortar do not seem to introduce any relevant influence in the R_{pl} and C_{pl} values, though the more frequent oscillations in the values in **Figures 8a** and **9a** can be related to the higher aggressivity of the PI exposure.

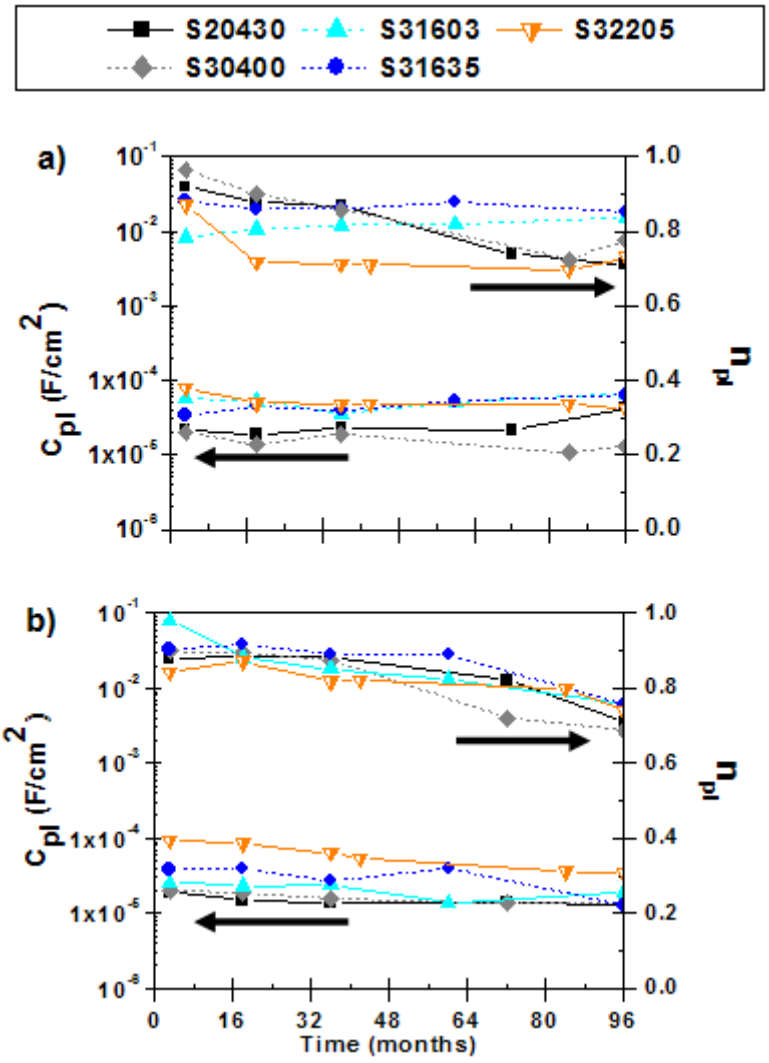

Figure 9. Time evolution of the C_{pl} and n_{pl} parameters that define CPE_{pl}: a) PI; b) HRHCl.

The low-frequency time constant is often identified with the corrosion process. In this case, R_t would be the charge transfer resistance of the electrochemical reaction. The R_t values obtained from the EIS measurements are shown in **Figure 10**. R_t values tend to

increase during the first period of exposure. This trend has already been detected in short-term solution tests [18,19], but it should be borne in mind that, during 18 h solution tests, R_t does not reach 10^7 Ω·cm^2. After years in mortar, R_t can be as high as 10^9 Ω·cm^2. That is to say, there is an improvement of the passive behaviour of the stainless steels during the first year of exposure to aggressive environments. This process is faster during the PI test than during the HRHCl test, perhaps because of the low-chloride concentration close to the reinforcements during the first months of exposure in the PI.

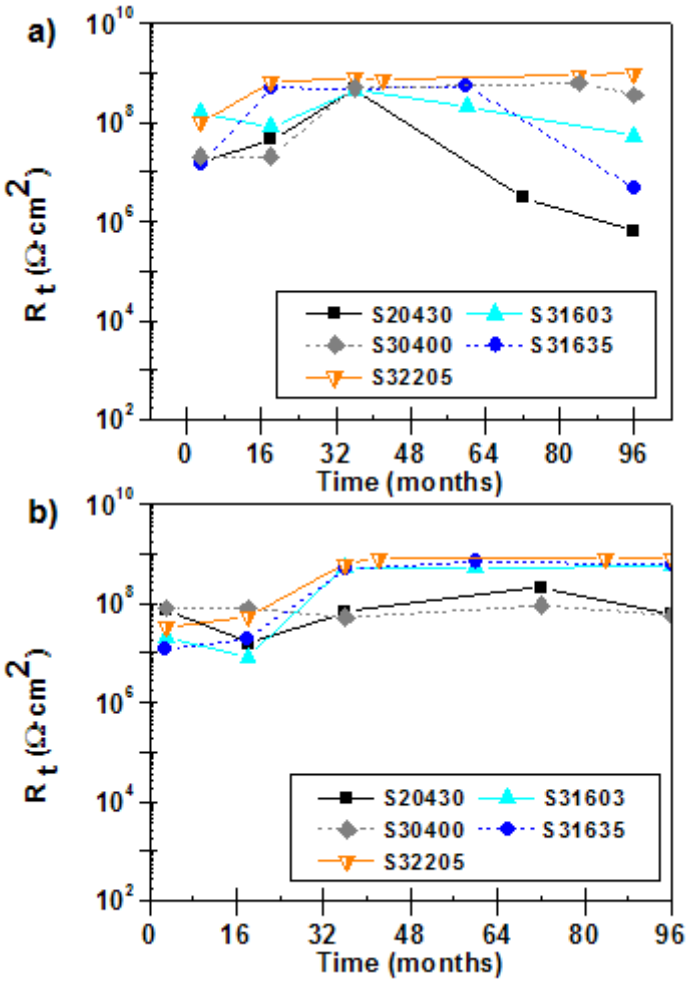

Figure 10. Time evolution of R_t: a) PI; b) HRHCl.

On the other hand, at the end of the PI exposure, a decrease of R_t values can be observed for some stainless steel grades (**Figure 10a**). Low-nickel austenitic stainless

steel grade S20430, with E_{corr} values in the high corrosion risk zone (**Figure 3**), exhibits a meaningful decrease of R_t. This information seems to confirm the corrosion attack on this grade under these conditions. On the other hand, S31635 also shows a meaningful decrease of its R_t value (**Figure 10a**), when its E_{corr} is only in the upper area of the uncertain corrosion region. It is difficult to obtain reliable conclusions about these results, but certain dissolution of TiN precipitates (abundant in this material) can explain the phenomenon. It has been previously demonstrated that preferential TiN dissolution occurs at high potentials in simulated pore solutions [21]. The unusually high E_{corr} of PI S31635 samples after 6-7 years of exposure can correspond to a TiN dissolution process (**Figure 3**). The decrease on R_t could be the consequence of a lower corrosion resistance of the surface of the reinforcement due to the surface irregularities (cavities) caused by the dissolution of the precipitates.

As has been reported for the same reinforcements in solution tests [18] and for different passive stainless steel bars in mortar [6], the R_t values (**Figure 10**) are significantly higher than R_{pl} (**Figure 8**). That is to say, the charge transfer is the rate-limiting step for passive reinforcements. This fact allows us to identify R_t also with the polarization resistance in the Stern-Geary equation [43] and calculate corrosion intensities, i_{corr}. Though a B about 52 mV has been traditionally proposed for passive steel in concrete [44], recent studies have calculated a higher value, about 75 mV, for this parameter [45]. Assuming B=75 mV (which is the most conservative hypothesis), the i_{corr} from studied stainless steels with E_{corr} in the passive region and region with uncertain risk of corrosion (**Figures 3** and **4**) would range from about 7 to nearly 0.07 nA/cm^2. Those i_{corr} are quite similar or lower than others determined for passive S30400 in concrete specimens using other electrochemical methods (about 0.01-0.1 μA/cm^2) [23,28]. The uncertainty in the determination of the corrosion rate of passive systems is unavoidable, but it is obvious that the measured i_{corr} values are able to comply with any durability requirement of reinforced structures.

Corrugated S20430 stainless steel in PI mortar exhibits E_{corr} typical of active corrosion at the end of the exposure (**Figure 3**). For active steel in concrete, values of B for 15 to 26 mV have been reported in the literature [44,45]. Assuming again the most conservative hypothesis, with B=26 mV, the i_{corr} of the S20430 steel would always be below 0.04 μA/cm^2. This corrosion rate is obviously very low and it hardly represents a meaningful risk for the durability of the structure [29]. For comparison, studies of

carbon steel reinforcements in similar conditions carried out in our laboratory give corrosion rates that can oscillate approximately between 0.3 and more than 3 μA/cm^2, that to say 1 or 2 order of magnitude higher. Moreover, for carbon steel in chloride contaminated concrete slabs, i_{corr} between 0.3-1 μA/cm^2 have been measured [28]. Hence, the S20430 probably suffers a corrosion attack of very low-intensity during the last year of the PI test.

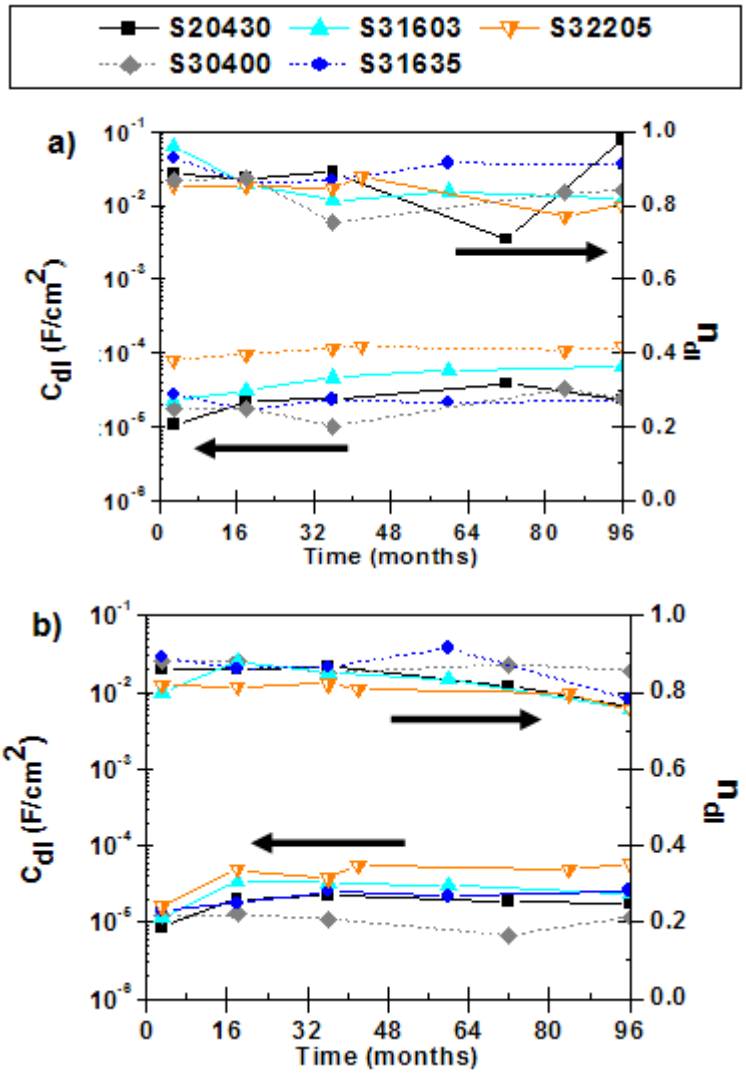

Figure 11. Time evolution of the C_{dl} and n_{dl} parameters that define CPE_{dl}: a) PI; b) HRHCl.

The values obtained from the simulation of the EIS spectra for the CPE_{dl} are plotted in **Figure 11**. It can be checked that values are typical of the double-layer capacitance,

confirming the hypothesis that the low-frequency time constant corresponds to the charge-transfer process. No meaningful change is detected with time during the exposures, not even for S20430 or S31635.

At the end of the 8-year exposure of the stainless steel reinforced samples, they were submitted to anodic polarization tests to obtain information about the quality of the passive layer under these conditions and how the pitting resistance of the stainless steel has been modified. From experiments such as those shown in **Figure 2**, data similar to the typical polarization curves can be obtained (**Figure 12**). The anodic polarization causes a pitting attack on the corrugated surface of some of the stainless steels bars.

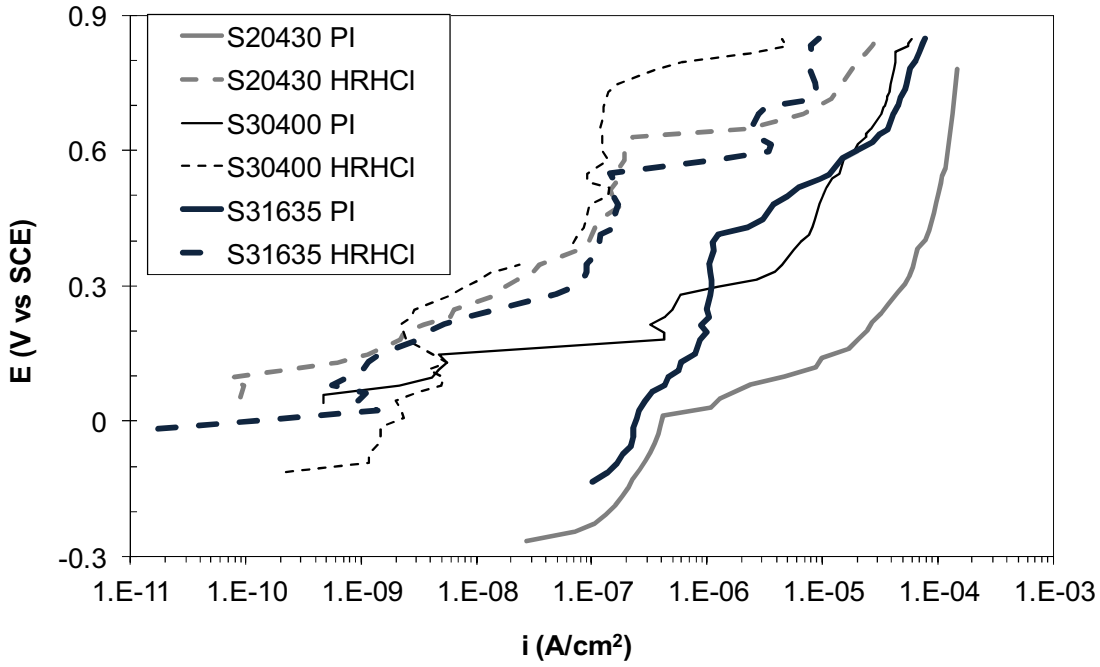

Figure 12. Example of the results of the results of the potential step tests when they are plotted as standard polarization curves in an Evans diagram.

A comparative analysis of the results of the mortar samples in the anodic polarization tests of the exposed specimens is shown in **Figure 13**. The anodic polarizations needed to reach a current density of 2 x 10^{-6} A/cm^2 are plotted. As has been previously justified, this value is typical of the corrosion rate for carbon steel reinforcements under the exposure conditions considered in the study, and it is also inside the range of the usual

current densities used to define the pitting potential or to compare the corrosion behaviour of stainless steel reinforcements [11,21,28].

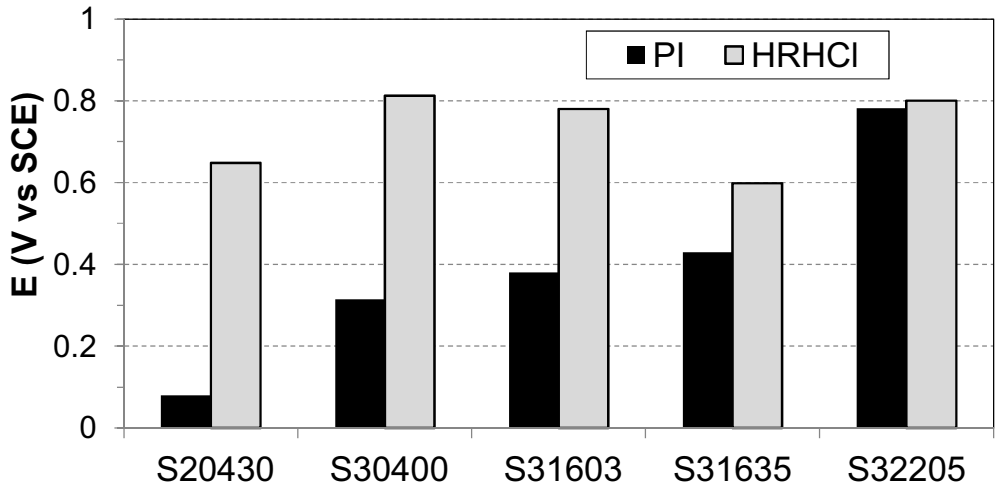

Figure 13. Potentials needed for the reinforced samples after the 8-year exposure to reach anodic current values of 2 x 10^{-6} A/cm^2.

In spite of small differences detected by EIS for most of the stainless steels in both testing conditions, after polarization tests, it is clear that PI samples are much more prone to develop pitting corrosion than the HRHCl samples. The length of the passive region of samples exposed to HRHCl seems to be able to guarantee the durability of reinforced structures in chloride contaminated environments, even when low-cost, low-alloyed grades as S20430 are considered (**Figure 13**). The good results for this material previously obtained in simulated pore solutions with chlorides are confirmed [21]. The potentials plotted in **Figure 13** for S30400, S31603 and S32205 in HRHCl seem to correspond to the oxygen evolution reaction, not to pitting corrosion. This hypothesis is based on two facts: a) the high value of the potential where the current increase takes place (at the limit of the region of the thermodynamic stability of water); and b) the similar potential value detected for the three materials with such different alloying elements (**Table 1**).

The behaviour exhibited by the S31635 (**Figure 13**) can be noteworthy, as can be considered comparable with that of the less alloyed, much cheaper S20430 grade. In this case, the length of the passive region is again limited by the presence of TiN

precipitates, as has been seen in previous studies in alkaline chloride contaminated solution [21]. The limited pitting resistance of S31635 grade is also coherent with the EIS results of the present study (**Figure 10a**).

On the other hand, in the polarization tests, all the austenitic corrugated stainless steel bars have proved to be quite sensitive to the aggressive conditions (high chloride concentration, aeration cells) created by the PI (**Figure 13**). After the PI exposure, the polarization test can cause pitting in all the grades except S32205. The excellent behaviour of this grade suggested in solution tests [13,21] is again confirmed. Such a high corrosion resistance can be understood bearing in mind the protective nature of the passive layer formed on this grade in alkaline media, as has been proved by XPS studies [18]. The differences found between S30400 and S31603 can hardly justify the economic differences existing between both materials (the presence of Mo in S31603 makes it rather more expensive than the S30400). For highly aggressive conditions, the S32205 is a much more interesting option than S31603, somewhat cheaper and much more corrosion-resistant (**Figure 13**). These results should be kept in mind when a stainless steel grade is selected for structures exposed to extremely aggressive conditions and long service life is expected.

The use of S20430 in aggressive environments can be risky in the long term and it pits in PI absence of external polarization (**Figure 3**). Though the R_t measured at E_{corr} are quite high (**Figure 10a**), the current density can easily become dangerous in the presence of anodic polarizations (**Figure 13**). The possible limitations for the use of S20430 are coherent with the results of shorter-test experiments carried out by other authors, also carried in PI mortar samples [6].

After polarizations, the tested samples remained in PI or HRHCl to allow pit development or repassivation. Then, the mortar samples were broken to allow the visual observation of the reinforcements. No pits were observed in S32205 samples in both exposure conditions, neither in S30400 and S31603 after HRHCl exposure, which is coherent with the hypothesis that in these systems the current increase in polarization tests is due to oxygen evolution. In addition, the corrosive attack in S31635 (where the polarization had caused corrosion, as suggests results in **Figure 13**) cannot be confirmed after SEM observations. These data suggest a certain ability of the S31635

grade to repassivate or highly limit the attack rate when it is exposed to mortars with a chloride contaminations, such as those of the samples tested at HRH (**Figure 5**).

Visible localized attack is clearly observed in the other stainless steel tested reinforcements. In the samples where the corrosion starts, before the polarization tests (S20430 in PI), the attack appears as very numerous, large and irregular pits (**Figure 14a**).

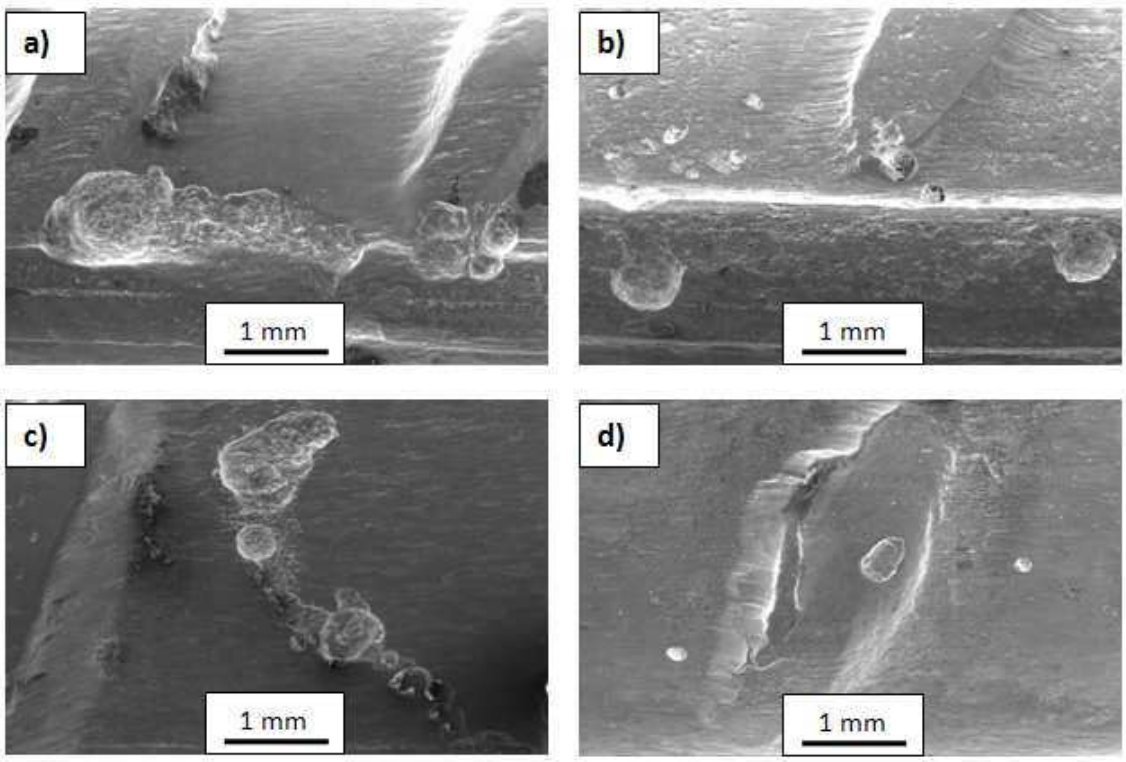

Figure 14. Images of the morphology of corrosive attack caused by the anodic polarization in the embedded reinforcements. a) S20430 after PI; b) S30400 after PI; c) S31603 after PI; d) S20430 after HRHCl.

On S30400 exposed at PI, numerous rounded pits can be observed, most of them with a location clearly related with the most strained regions of the surface of the bar (**Figure 14b**). The influence of the forming process in the corrosion behaviour of stainless steels has been demonstrated in simulated pore solutions tests [13]. The cold working of the reinforcements cause microstructural changes that can affect the corrosion behaviour of the stainless steels [46] and these changes are more pronounced in the corrugations than in other regions of the surface [47].

In S31603 and S31635 bars exposed to PI, the attack morphology is different, as can be seen in the examples in **Figure 14c**. The pits are irregular and quite shallow, and their location does not seem to be related to the corrugations or other more strained areas on the surface of the bars. This corrosion morphology seems less dangerous than that observed for non-Mo austenitic reinforcements. However, the difference could not be due to chemical composition of the stainless steels. The lower strain level of these bars in comparison with the tested S30400 can easily explain this fact (the lower tensile strengths of the S31603 and S31635 bars in **Table 1** correspond to a less heavy forming process).

After the HRHCl exposure, the only bar with visible signs of attack is the S20430. Anyway, the intensity of the attack is low in this environment, compared to that observed in other grades after PI and polarization. A few isolated, rounded pits have been detected (**Figure 14d**) after provoking the attack by anodic polarizations. Pits tend to appear and they are larger in most strained regions, but SEM observations proved that a few small pits also appear in the non-corrugated region of the surface. This trend can be related to the strain level in the bar, which is between that of the S30400 and those of the S31603 and S31605 bars (**Table 1**).

4. Conclusions

The results presented in this study allow us to draw the following conclusions:

1. It has been confirmed with long-term mortar tests that traditional austenitic and duplex corrugated stainless steels are an excellent option to assure the durability of reinforced structures in chloride contaminated media.
2. The PI exposure in 3.5% NaCl causes a very low-intensity corrosive attack in S20430 samples after 7 years of exposure.
3. The S32205 has proved its excellent behaviour in highly chloride-contaminated mortar, even under PI conditions and high polarizations, confirming that it is a better option for structures exposed to highly aggressive conditions.
4. The difference between the corrosion behaviour of S31603 and S30400 in chloride contaminated mortar does not seem to be able to justify their difference in price for their use as reinforcements.

5. It has been confirmed that the presence of Ti as an alloying element in austenitic grades can have a certain detrimental effect on the corrosion behaviour in mortar.
6. Once provoked, the morphology and localization of the attack seems to be conditioned by the strain level of the bar.

Acknowledgements

The present work was funded by the Spanish Ministry of Science and Innovation through the Project reference BIA2007-66491-C02-02. The authors acknowledge the help of Eng. Rubén Martin with EIS spectra.

References

[1] K.Y. Ann, J.H. Ahn, J.S. Ryou, The importance of chloride content at the concrete surface in assessing the time to corrosion of steel in concrete structures, Constr. Build. Mater. 23 (2009) 239-245.

[2] H.A. Elfergani, R. Pullin, K.M. Holford, Damage assessment of corrosion in prestressed concrete by acoustic emission, Constr. Build. Mater. 40 (2013) 925-933.

[3] K. Hornbostel, C.K. Larsen, M.R. Geiker, Relationship between concrete resistivity and corrosion rate – A literature review, Cem. Concrete Comp. 39 (2013) 60-72.

[4] L.G. Andión, P. Garcés, F. Cases, C.G. Andreu, J.L. Vázquez, Metallic corrosion of steels embedded in calcium aluminated mortars, Cem. Concrete Res. 31 (2001) 1263-1269.

[5] J.T. Pérez-Quiroz, J. Terán, M.J. Herrera, M. Martínez, J. Genesca, Assessment of stainless steel reinforcement for concrete structures rehabilitation, J. Constr. Steel Res. 64 (2008) 1317-1324.

[6] M. Serdar, L. Valek Žulj, D. Bjegović, Long-term corrosion behavior of stainless reinforcing steel in mortar exposed to chloride environment, Corros. Sci. 69 (2013) 149-157.

[7] G.S. Duffó, S.B. Farina, C.M. Giordano, Characterization of solid embeddable reference electrodes for corrosion monitoring in reinforced concrete structures, Electrochim. Acta 54 (2009) 1010-1020.

[8] R.D. Moser, P.M. Singh, L.F. Kahn, K.E. Kurtis, Chloride-induced corrosion resistance of high-strength stainless steels in simulated alkaline and carbonated concrete pore solutions, Corros. Sci. 57 (2012) 241-253.

[9] L. Freire, M.J. Carmezim, M.G.S. Ferreira, M.F. Montemor, The passive behavior of AISI 316 in alkaline media and the effect of pH: A combined electrochemical and analytical study, Electrochim. Acta 55 (2010) 6174-6181.

[10] M. Kouřil, P. Novák, M. Bojko, Threshold chloride concentration for stainless steels activation in concrete pore solutions, Cem. Concrete Res. 40 (2010) 431-436.

[11] S.M. Alvarez, A. Bautista, F. Velasco, Corrosion behaviour of corrugated lean duplex stainless steels in simulated concrete pore solutions, Corros. Sci. 53 (2011) 1748-1755.

[12] L. Freire, M.J. Carmezim, M.G.S. Ferreira, M.F. Montemor, The electrochemical behavior of stainless steel AISI 304 in alkaline solutions with different pH in the presence of chlorides, Electrochim. Acta 56 (2011) 5280-5289.

[13] E.C. Paredes, A. Bautista, S.M. Alvarez, F. Velasco, Influence of the forming process of corrugated stainless steels on their corrosion behaviour in simulated pore solutions, Corros. Sci. 58 (2012) 52-61.

[14] S.M. Alvarez, A. Bautista, F. Velasco, Influence of process parameters on the corrosion resistance of corrugated austenitic and duplex stainless steel, Mater. Tehnol. 47 (2013) 317-321.

[15] M.F. Hurley, J.R. Scully, Threshold chloride concentrations of selected corrosion - resistant rebar materials compared to carbon steel, Corrosion 62 (2006) 892-904.

[16] J.M. Deus, L. Freire, M.F. Montemor, X.R. Nóvoa, The corrosion potential of stainless steel rebars in concrete: Temperature effect, Corros. Sci. 65 (2012) 556-560.

[17] L. Freire, M.A. Catarino, M.I. Godinho, M.J. Ferreira, M.G.S. Ferreira, A.M.P. Simões, M.F. Montemor, Electrochemical and analytical investigation of passive films formed on stainless steels in alkaline media, Cem. Concrete Comp. 34 (2012) 1075-1081.

[18] A. Bautista, G. Blanco, F. Velasco, A. Gutiérrez, L. Soriano, F.J. Palomares, H. Takenouti, Changes in the passive layer of corrugated, low Ni, austenitic stainless steel due to the exposure to simulated pore solutions, Corros. Sci. 51 (2009) 785 -792.

[19] A. Bautista, G. Blanco, H. Takenouti, EIS study of passivation of austenitic and duplex stainless steels reinforcements in simulated pore solutions, Cem. Concrete Comp. 28 (2006) 212-219.

[20] S. Fajardo, D.M. Bastidas, M. Criado, M. Romero, J.M. Bastidas, Corrosion behaviour of a new low-nickel stainless steel in saturated calcium hydroxide solution, Constr. Build. Mater. 25 (2011) 4190-4196.

[21] A. Bautista, G. Blanco, F. Velasco, Corrosion behaviour of low-nickel austenitic stainless steels reinforcements: A comparative study in simulated pore solutions, Cem. Concrete Res. 36, pp. 1922-1930 (2006).

[22] L. Freire, X.R. Novoa, G. Pena, V. Vivier, On the corrosion mechanism of AISI 204Cu stainless steel in chlorinated alkaline media, Corros. Sci. 50 (2008) 3205-3212.

[23] L. Bertolini, M. Gastaldi, Corrosion resistance of low-nickel duplex stainless steel rebars, Mater. Corros. (2011) 120-129.

[24] H. Luo, C.F. Dong, X.G. Li, K. Xiao, The electrochemical behaviour of 2205 duplex stainless steel in alkaline solutions with different pH in the presence of chloride, Electrochim. Acta 64 (2012) 211-220.

[25] G.N. Flint, R.N. Cox, The resistance of stainless steel partly embedded in concrete to corrosion by seawater, Mag. Concrete Res. 40 (1988) 13-19.

[26] B.G. Callaghan, The performance of a 12% chromium steel in concrete in severe marina environments, Corros. Sci. 35 (1993) 1535-1541.

[27] M.C. García-Alonso, M.L. Escudero, J.M. Miranda, M.I. Vega, F. Capilla, M.J. Correia, M. Salta, A. Bennani, J.A. González, Corrosion behaviour of new stainless steels reinforcing bars embedded in concrete, Cem. Concrete Res. 37 (2007) 1463-1471.

[28] M.C. García-Alonso, J.A. González, J. Miranda, M.L. Escudero, M.J. Correia, M. Salta, A. Bennani, Corrosion behaviour of innovative stainless steels in mortar, Cem. Concrete Res. 37 (2007) 1562-1569.

[29] J.A. González, E. Otero, S. Feliu , A. Bautista, E. Ramírez, P. Rodríguez, W. López, Some considerations on the effect of chloride ions on the corrosion of steel reinforcements embedded in concrete structures, Mag. Concrete Res. 50 (3) (1998) 189-199.

[30] C.L. Page, Mechanism of corrosion protection in reinforced concrete marine structures, Nature 258 (1975) 514-515.

[31] B. Huet, V. L'hostis, G. Santarini, D. Feron, H. Idrissi, Steel corrosion in concrete: Deterministic modeling of cathodic reaction as a function of water saturation degree, Corros. Sci. 40 (2007) 1878-1932.

[32] J.A. González, J.M. Miranda, S. Feliu, Considerations on reproducibility of potential and corrosion rate measurements in reinforced concrete, Corros. Sci. 46 (2004) 2467– 2485.

[33] O. Sengul, O.E. Gjørv, Electrical resistivity measurements for quality control during concrete construction, ACI Mater. J. 105 (2008) 541–547.

[34] R.B. Polder, Critical chloride content for reinforced concrete and its relationship to concrete resistivity, Mater. Corros. 60 (2009) 623–630.

[35] J.A. González, W. López, P. Rodríguez, Mecanismos de corrosión en el hormigón armado y factores que controlan su cinética, Rev. Metal. Madrid 28 (1992) 297-305.

[36] D.M. Bastidas, A. Fernández-Jiménez, A. Palomo, J.A. González, A study on the passive state stability of steel embedded in activated fly ash mortars, Corros. Sci. 50 (2008) 1058-1065.

[37] I. Fayala, L. Dhouibi, X.R. Nóvoa, M. Ben Ouezdou, Effect of inhibitors on the corrosion of galvanized steel and on mortar properties, Cem. Concrete Comp. 35 (2013) 181-189.

[38] V. Feliu, J.A. González, C Andrade, S. Feliu, Equivalent circuit for modelling the steel-concrete interface. I. Experimental evidence and theoretical predictions, Corros. Sci. 40 (1998) 975-993.

[39] R.K. Dhir, M.R. Jones, H.E.H. Ahmed. Determination of total and soluble chlorides in concrete. Cem. Concrete Res. 20 (1990) 579-590.

[40] H.-W. Sing, V. Saraswathy, Corrosion monitoring of reinforcing concrete structures – A review, Int. J. Electrochem. Sci. 2 (2007) 1-28.

[41] P. Castro-Borges, O. Troconis de Rincón, E.I. Moreno, A.A. Torres-Acosta, M. Martínez-Madrid, Performance of a 60-years old concrete pier with stainless steel reinforcement, Mater. Perform. 41 (2002) 50-55.

[42] L. Valek, S. Martinez, D. Mikulic, I. Brnardic, The inhibition activity of ascorbic acid towards corrosion of steel in alkaline media containing chloride ions, Corros. Sci. 50 (2008) 2705-2709.

[43] M. Stern, A. Geary, Electrochemical polarization. I. A theoretical analysis of the shape of the polarization curves. J. Electrochem. Soc. 104 (1957) 56-58.

[44] C. Andrade, J.A. González, Quantitative measurements of corrosion rate of reinforcing steels embedded in concrete using polarization resistance measurements, Werkst. Korros. 29 (1978) 515–519.

[45] A. Poursaee, Potentiostatic transient technique, a simple approach to estimate the corrosion current density and Stern–Geary constant of reinforcing steel in concrete, Cem. Concrete Res. 40 (2010) 1451-1458.

[46] S.M. Alvarez, A. Bautista, F. Velasco, Influence of strain-induced martensite in the anodic dissolution of austenitic stainless steels in acid medium, Corros. Sci. 69 (2013) 130-138.

[47] A. Bautista, S.M. Alvarez, F. Velasco, Selective corrosion of duplex stainless steel bars in acid. Part 2: Effect of the surface strain and numerical analysis, Mater. Corros. *(in press)* DOI: 10.1002/maco.201307420.

5.8 PUBLICACION 8: P8

A. Bautista, S.M. Alvarez, E.C. Paredes, F. Velasco, S. Guzmán.

"*Corrosion performance of stainless steels corrugated bars after 9 years of exposure. Part II: carbonated mortars with and without chlorides*".

Enviado a Corrosion Science.

Corrosion performance of corrugated stainless steels after 9 years of exposure. Part II: carbonated mortars with and without chlorides

A. Bautista[1], S.M. Alvarez, E.C. Paredes, F. Velasco, S. Guzman
Materials Science and Engineering Department. IAAB.
Universidad Carlos III de Madrid.
Avda. Universidad nº 30. 28911 - Leganés, Madrid (Spain)

Abstract

The corrosion behaviour of the same 5 corrugated stainless steels studied in non-carbonated conditions in Part I of this work was evaluated in carbonated mortars. The tests were carried out in 3 different exposure conditions: at high relative humidity (HRH9); partially immersed in 3.5% NaCl (PI9); and with $CaCl_2$ added during mortar mixing and exposed to high relative humidity (HRH9Cl). Corrosion potential (E_{corr}) measurements and electrochemical impedance spectroscopy (EIS) were used to monitorize the behaviour during the first 8 years of exposure. Then, anodic polarization tests were carried out and the exposure was extended for another additional year. Stainless steels behave excellently in carbonated conditions without chlorides, but some grades can suffer localized corrosion if they are submitted to high anodic polarizations. In comparison with non-carbonated conditions, it has been seen that carbonation hinders the entry of chlorides and limits the rate of attack progress, but decreases the resistance of the stainless steel to the onset and process of pitting corrosion.

Keywords: A. Stainless steel; A. Steel reinforced mortar; B. EIS; B. Polarization; C. Passivity; C. Pitting corrosion.

[1] Corresponding author. Tel: +34 91 624 9914. Fax: +34 91 624 9430.
E-mail address: mbautist@ing.uc3m.es (A. Bautista).

1. Introduction

Corrosion of reinforcements often limits the durability of reinforced concrete structures. The corrosion of steel bars is caused by chlorides and/or CO_2 from the environment. The carbonation of concrete is associated to the CO_2 penetration through the pores. Initially, the concrete is highly alkaline (pH ≈ 12-14) due to the presence of $Ca(OH)_2$ and often of other hydroxides in the pore solution. The CO_2 that comes from the atmosphere, in presence of water, reacts with the $Ca(OH)_2$. As $Ca(OH)_2$ is consumed, the alkalinity of the solution inside the pores decreases. A CO_3^{2-}/HCO_3^- buffer is often formed, and the pH of the solution decreases to pH values of about 9. At these pHs, carbon steel bars suffer uniform corrosion, because the passive layer that protects the steel at a higher pH is dissolved.

The carbonation process progresses from the surface of the concrete, advancing usually as a quite uniform front. The carbonation rate depends on the diffusion of the gases in the concrete porous network. The penetration rate of the carbonation front is affected by the environmental conditions such as the CO_2 concentration [1] and the humidity [1,2], but also on concrete characteristics, such as the size of the aggregates [3], the water/cement ratio [4] or the composition of the cement [5-7].

It has been foreseen that the increasing generation of CO_2 emissions will increase the carbonation rate of concrete structures [8]. A reduction in service lifespan due to carbonation of 15-20 years has been calculated for concrete structures constructed in 2030, in areas with moderate humidity and high temperatures [1]. Hence, carbonation resistant conditions should be especially kept in mind nowadays while designing reinforced structures.

Substitution of the traditional carbon steel bars by stainless steel bars in the most exposed regions of the concrete structure [9] is an alternative increasingly in use to avoid damages caused by corrosion. A long-term study has analyzed the behavior of different stainless steel corrugated bars in non-carbonated mortars with chlorides and their susceptibility to pitting corrosion [10], offering reliable results about the in-service behavior of these materials. But it is also interesting to know in depth the behavior of stainless steel corrugated bars in carbonated concretes. The nature of the passive layers formed on stainless steel at pH 9 is different from that formed at more alkaline pHs [11]. Passive layers of less protective nature are formed in carbonated than in non-carbonated solutions

[12]. However, previous studies in solutions that simulate those contained in the pores of the concrete have proved that no corrosion takes place in stainless steels in carbonated solutions without chlorides [13-15], suggesting that they can be an excellent option to assure the durability of structures with a high-risk of carbonation.

Moreover, it is interesting to know the response of stainless steels in highly aggressive environments resulting from the simultaneous effect of chlorides and carbonation. This circumstance is not very usual in coastal areas, where low-CO_2 concentrations and high humidity are typical [4], but it can easily appear in other environments, for example, where the use of de-icing salts is common or where contaminated sand is used as aggregate.

The effect of carbonation and chlorides in the corrosion behavior of carbon steel in reinforcements has been studied in solution [16], showing a great dependence not only on the chloride content, but also on the concentration of the CO_3^{2-}/HCO_3^- buffer. Although a common way to express critical chloride threshold to initiate corrosion in reinforced structures is the $[Cl^-]/[OH^-]$ ratio [17], some authors [18,19] have proved that the inhibiting effect of hydroxide ions becomes weaker with decreasing pH. Hence, the carbonation of chloride contaminated structures is an especially dangerous situation if carbon steel reinforcements are used in the most exposed parts.

Results of stainless steels in carbonated simulated pore solutions with chlorides have also been published. These results show that stainless steels are susceptible to pitting corrosion under these conditions, depending on their resistance to localized corrosion and the morphology of the attack on the composition of the stainless steels [1013-15] and on the processing method of the corrugated bars [20,21]. It has been reported that the thickness of the passive layer formed on stainless steel in carbonated solution decreases as the chloride concentration increases, thus leading to a reduction in the corrosion resistance [22].

Anyway, it has been proved for carbon steels that the critical chloride concentrations that cause corrosion are different when they are obtained from solution tests than when they are obtained using concrete samples [17]. The main reasons for this difference have been mentioned in the first part of this work [10]. However, it should be mentioned that there is no significant difference in the critical chloride concentrations obtained in mortar and in concrete tests [17]. Up to now, results of two years have been published about the

behavior of a couple of stainless steels in activated fly-ash mortar that considered the dual effect of chlorides and carbonation [23], but long-term results of corrugated steel in carbonated mortars (with and without chlorides) can offer very interesting, complementary information.

2. Experimental

Five different corrugated stainless steels were considered in the study. The chemical compositions of the stainless steels are shown in **Table 1**. More data about the corrugated bars can be found in [10]. Traditional carbon steel corrugated bars were included in some parts of the study as reference.

Table 1. Chemical composition (w/w) of the five studied DSS.

UNS Stainless Steel	Main Alloying Elements (%)									
	S	C	Ti	Si	Mn	Cr	Ni	Mo	N	Cu
S20430	0.002	0.049	0.003	0.23	8.26	16.12	1.89	0.015	0.130	2.65
S30400	0.002	0.063	0.004	0.31	1.42	18.33	8.12	0.297	0.050	0.32
S31603	0.006	0.021	0.003	0.21	1.67	17.05	10.25	2.171	0.47	0.32
S31635	0.001	0.029	0.251	0.45	1.21	16.68	11.25	2.232	0.020	0.41
S32205	0.001	0.029	0.027	0.39	1.72	22.49	4.72	3.221	0.174	0.24

The corrugated bars were partly embedded in mortar with a cement/sand/water ratio of 1/3/0.6 (w/w). Ordinary Portland cement was used to prepare the mortar. Part of the samples was manufactured with 3% $CaCl_2$ (1.9% Cl), weighed in relation to the cement amount. As a reference, it can be considered that, in European countries and in North America, it has become common practice to limit the tolerable chloride content to around 0.4% of the weight of cement [24].

Cylindrical mortar samples were used, the thickness of the mortar cover always being 1.5 cm. The length of the bar exposed to the mortar was always 3 cm. All cross-sections of the bars embedded in mortar were previously polished to 320# and passivated with HNO_3 in the laboratory, in order to reproduce the process carried out on the corrugated surfaces of the bars in the industry. Ti-activated electrodes [25] where embedded close to the

corrugated bars to allow the monitoring of the carbonation front in a subsequent step. Other details about the samples can be found in the first part of the work [10].

After their manufacturing, the reinforced mortar samples were cured for 30 days at high relative humidity (HRH), about 90-95%, and then the mortar was carbonated. The carbonation process was carried out in a chamber where 10% CO_2 enriched air was injected. The potential of the Ti-electrode was monitored periodically using a saturated calomel electrode (SCE) placed in the outer part of the sample. The carbonation of each sample was determined individually by a change in the potential that corresponds to a change in the pH, thus avoiding possible effects of the placement in the chamber on the advance of the carbonation front [26].

After carbonation, the samples were divided into 3 groups and exposed to different aggressive conditions:

- HRH9: Half of the samples manufactured without chlorides where exposed at HRH.
- PI9: The other half of the samples manufactured without chlorides were partially immersed (PI) in 3.5% (w/w) NaCl solution and at HRH. In this case, the level of the solution was kept coinciding with the middle of the length of the bars exposed to the mortar.
- HRH9Cl: The samples manufactured with chlorides were exposed to HRH.

The electrochemical monitoring of the corrosion behaviour during the 8-year exposure period was carried out using corrosion potential (E_{corr}) and electrochemical impedance spectroscopy (EIS) measurements. To obtain the E_{corr} values, a SCE was used. For the EIS measurements, a three-electrode configuration was used. The surface of corrugated bar exposed to the mortar acted as a working electrode, the reference electrode was a SCE and the counter-electrode was a copper cylinder, with a diameter slightly higher than that of the mortar sample. To assure a good contact between the mortar and the counter-electrode, a wet pad was used. The EIS spectra were acquired using a perturbation signal of 10 mV of amplitude, from 10^3 to 10^{-3} Hz.

After the 8-year exposure period, the reinforced mortar samples were submitted to anodic polarization tests. The tests started from the E_{corr} and they were based on short potentiostatic steps of 10 min. When a potential of about 100 mV vs SCE was reached, the length of the steps increased up to 1 h. The increase in the length of the steps is due to higher difficulties of stabilization of the current signal at increasing anodic overpotentials. All the steps (short and long) increased the potential in 20 mV. The polarization steps finished at 900 mV vs. SCE. The current value plotted in the polarization curves used in this work corresponds to the stabilization value of the current after each potential step. More details about this type of tests can be found in [10].

After the polarization tests, the samples were kept for 1 additional year under the exposure conditions to allow the progress or the possible repassivation of the provoked pits. Then, the samples were broken and the morphology and localization of the attack of the bars were studied by scanning electron microscopy (SEM).

The total chloride content of the mortar after the 9-year exposure was measured in three different regions of the samples. The position of the studied regions is similar to that pointed out in [10]. The quantification of the total chloride content was carried out by X-ray fluorescence spectrometry (XRF) [27]. The given values of Cl^- concentration are the average of 6 measurements in each region of different samples.

3. Results and Discussion

The E_{corr} corresponding to the corrugated bars in carbonated mortar for the 3 different exposure conditions are shown in **Figures 1-3**. The criterion suggested by ASTM C876 standard for determining the probability of corrosion for carbon steel reinforcements has also been included in the figures.

In **Figure 1**, it can be seen that the E_{corr} of the stainless steel bars exposed to HRH9 exhibit values characteristics of the passive state with an occasional value in the border limit with the region of uncertain corrosion activity. These results suggest that all the stainless steel reinforcements remain passive in carbonated mortar when no chlorides are

present. These results are coherent with the predictions drawn from the polarization tests of the bars [13]: no corrosion appears in any of the grades considered in this study during anodic polarizations in pH 9 solutions when no chlorides have been added.

The results of stainless steels are completely different to those of carbon steel in the HRH9 condition (**Figure 1**). As expected, carbon steel bars show E_{corr} typical of the active corrosion in carbonated mortar without chlorides during the entire exposure.

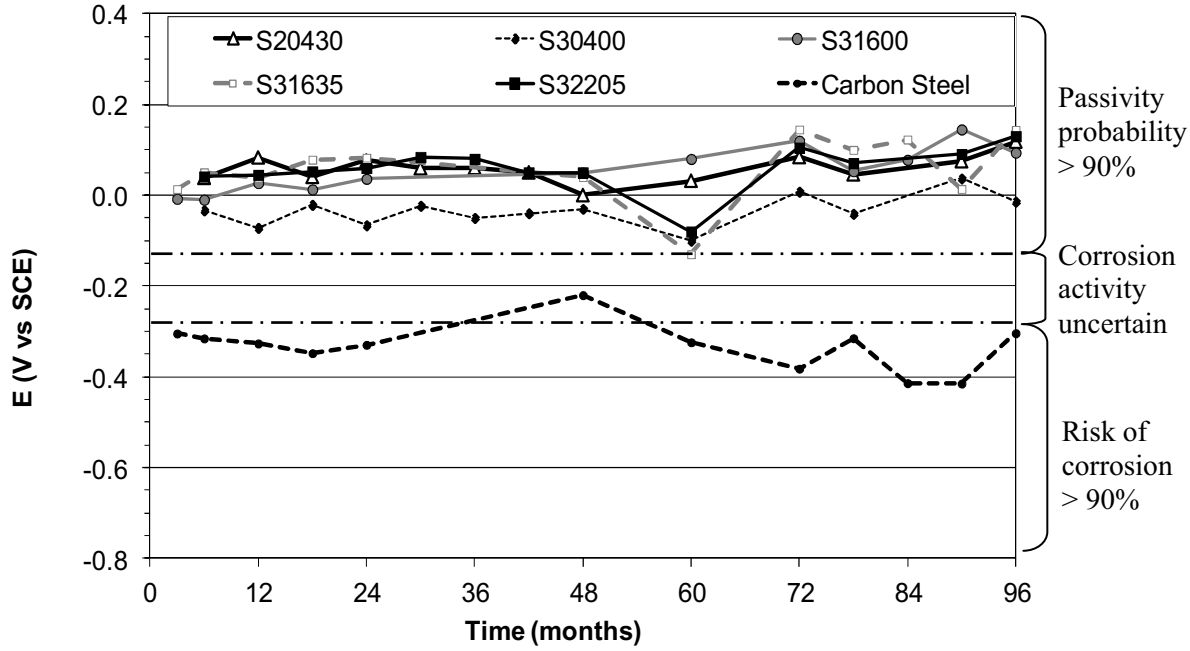

Figure 1. E_{corr} of the reinforced mortar samples exposed in HRH9 condition.

When the reinforced carbonated mortar samples are partially submerged in NaCl solution (PI9 condition), the E_{corr} of the low-Ni austenitic S20430 shows a different trend (**Figure 2**). For this grade, the E_{corr} suffers a meaningful decrease after 3 years of exposure. In comparison to HRH9, in PI9 conditions, there is a penetration with time of chloride ions from the solution to the reinforcements. Moreover, cells that favor the corrosion process can appear between the submerged and the non-submerged part of the sample. Aeration cells are formed due to the different O_2 access (much more limited in the submerged region), thus favoring the location of the anodes on the submerged surface of the bar. Other concentration cells could also appear (i.e.: Cl^-), fostering the corrosion in the submerged part of the bar.

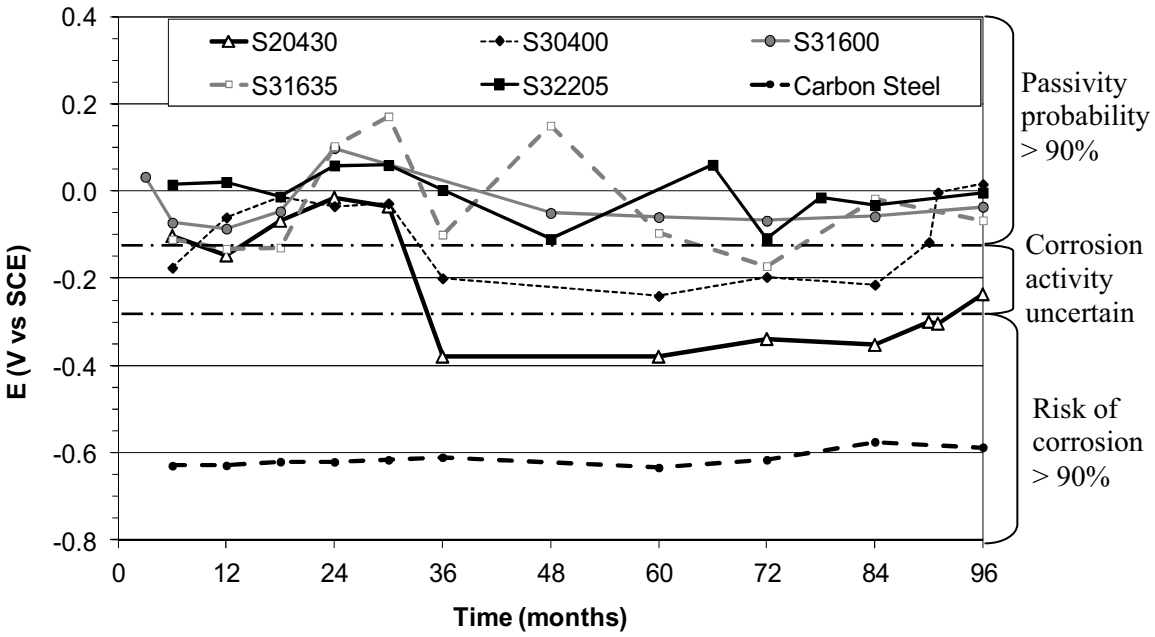

Figure 2. E_{corr} of the reinforced mortar samples exposed in PI9 condition.

In non-carbonated conditions [10], the partially immersed exposure has proved to be especially aggressive, provoking a low-intensity corrosive attack of low-Ni austenitic S20430 after 7 years of exposition. When the mortar is carbonated (**Figure 2**), the results of E_{corr} in partial immersion in NaCl could suggest an even higher aggressivity. The low-Ni S20430 exhibits E_{corr} values typical of active corrosion only after 3 years of exposure.

In **Figure 2**, it can also be seen that he traditional austenitic S30400 has E_{corr} in the uncertain activity region during several years, though the E_{corr} recovers values characteristic of passivity at the end of the exposure. On the other hand, considering the E_{corr} results, the presence of Mo in stainless steels (as S31603 or the duplex microstructure of S32205) seems to completely guarantee the stability of the passivity in PI9 conditions.

The limited corrosion resistance of S20430 in PI9 is coherent with the results of the polarization tests previously carried out in carbonated solutions with chlorides [13] where the limited length of the passive region was shown. The E_{corr} behavior during the long-term PI9 exposure of the other austenitic stainless steels and of the duplex stainless steel is also coherent with the results of polarization tests in carbonated solutions with chlorides [13,28] where longer passive regions were detected. Moreover, the different

protective nature of their passive films formed in carbonated conditions on the studied stainless steels grades and analyzed by X-Ray photoelectron spectroscopy (XPS) can also justify the E_{corr} trends observed in **Figure 2** (i.e. chromium-rich oxides for S32205 and iron-rich oxides also comprising of poorly protective Mn oxide for S20430) [12].

On the other hand, the E_{corr} of the carbon steel bars in PI9 are always typical of an active corrosion (**Figure 2**). But it must be pointed out that the E_{corr} values are, in this case, much more negative than those measured for the carbon steel in HRH9 (**Figure 1**). The foreseen decrease in the mortar electrical resistance due to the presence of chlorides in the PI9 is not enough to explain this difference. The E_{corr} measured in the PI9 are even lower than those measured for carbon steel in non-carbonated partially immersed samples (PI in [10]). The low E_{corr} measured in PI9 suggest an increased corrosion activity of the carbon steel due to the presence of chlorides since the first months of the exposure, in comparison to the values measured in HRH9.

When the chlorides are added during the manufacturing of the samples (HRH9Cl condition), the stainless steel reinforcements show E_{corr} values (**Figure 3**) similar to those observed for the HRH9 condition (**Figure 1**). It is worth remembering that an identical amount of chlorides added during manufacturing has previously been proved to be unable to cause pitting in stainless steels when the mortar was not carbonated (condition HRH in [10]). These results demonstrate that the foreseen decrease on the pitting resistance due to carbonation is not enough, for this chloride concentration, to break the passivity of the stainless steel reinforcements.

The E_{corr} of the carbon steel samples in HRH9 condition (**Figure 3**) are typical of the active state, with values lower than those found for the same material in absence of chlorides (HRH, **Figure 1**), but somewhat higher than those detected in the PI9 condition (**Figure 2**).

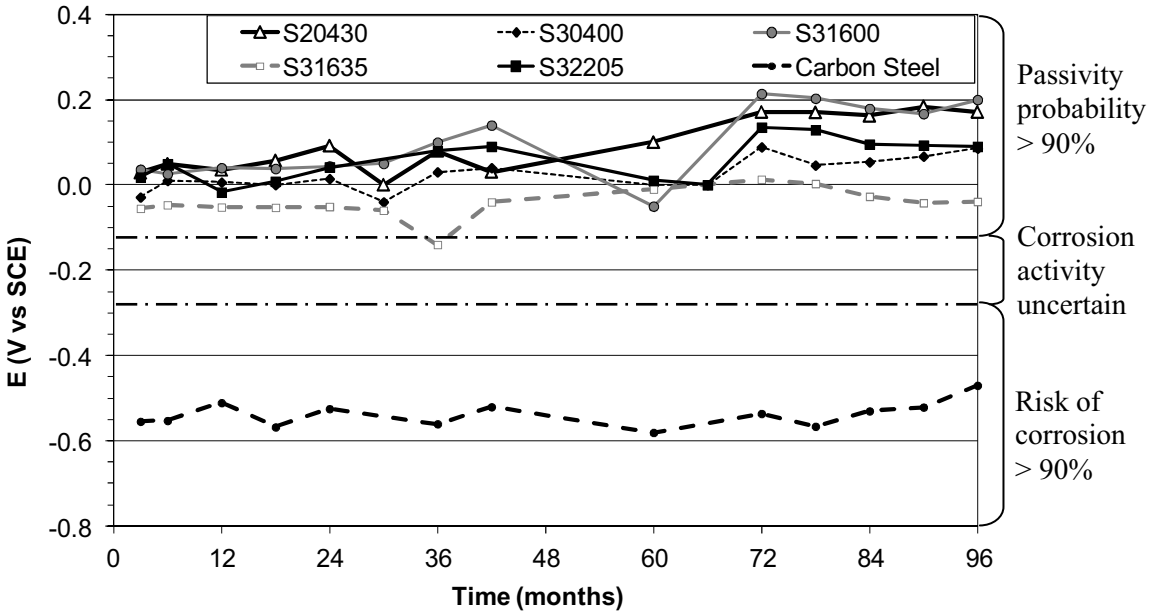

Figure 3. E_{corr} of the reinforced mortar samples exposed in HRH9Cl condition.

The total chloride content of the samples has been calculated after 9 years of exposure using XRF. Material from three different regions of the samples has been analyzed: Region 1 - mortar close to the upper part of the bar (in PI9 condition, from the aerated region); Region 2 - mortar close to the lower part of the bar (in PI9 condition, from the submerged region); Region 3 - mortar from the outer surface of the samples (in PI9 condition, from the submerged region). The localization of these regions in the sample is plotted in Figure 1 in [10].

Obviously, no chlorides are detected in any region of the samples after the HRH9 exposure. Results of chloride concentrations after PI9 and HRH9Cl are plotted in **Figure 4**. Bearing in mind the error bars (associated with the variability of the Cl^- amount in equivalent regions of different samples), it can be assumed that, for a given exposure condition, the chloride contents are quite similar all over the mortar samples after 9 years. Though the chlorides penetrate into the mortar from the NaCl solution and Cl^- concentration gradients must have existed at the beginning of the exposure, the duration of the tests has been long enough to homogenize the Cl^- concentration by diffusion [29]. The influence of possible Cl^- concentration cells formed on the surface of the bars in PI9 can be disregarded for long-term exposures of this kind of samples.

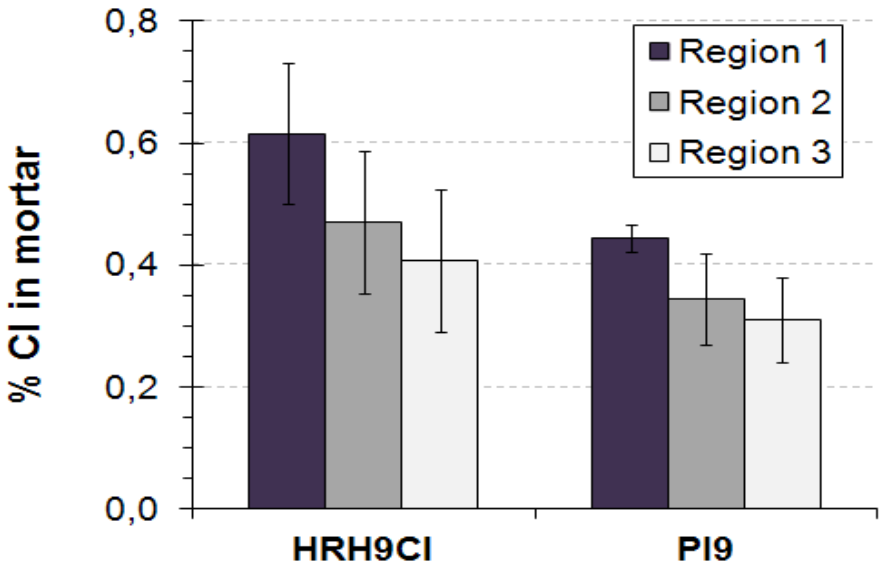

Figure 4. Chloride concentration (% by wt. to mortar) after 9 years of exposure.

The average Cl^- concentration of the mortars in the HRH9 could be considered slightly higher than that of the mortars in PI9, but the differences are quite close to the experimental variability of the data to be sure about their exact relevance. Moreover, chlorides added during the manufacturing of the mortar (as in HRH9) probably have a higher bonded fraction of these ions. It is well known that, during curing, some chlorides become physically and chemically bonded to the hydration products of the cement. When chlorides are bound, they represent a lower risk for the pitting corrosion, though they can play a certain role in pitting initiation [30]. Moreover, calcium chloride (HRH9) leads to more bonded chlorides than sodium chloride (PI9) [17,31]. Thus, it could be assumed that it is possible that, in spite of the values shown in **Figure 4**, Cl^- can be present in a more corrosive way in PI9 than in HRH9. The well-known importance of O_2 concentration cells is confirmed as a key to explain the aggressivity of the PI9 exposure.

Chloride concentrations determined for HRH9 are similar to those measured for HRH in [10], as expected. However, the amount of chlorides detected in non-carbonated samples after 9 years of partial immersion in 3.5% NaCl [10] is (about 5 times) higher than when the samples are carbonated. These results confirm that carbonates precipitate inside the pores due to $Ca(OH)_2$ reaction with CO_2, reducing the permeability of the mortar [32], and informs that this phenomenon is able to limit the amount of chlorides that penetrate. It is demonstrated that the carbonated mortar has a higher ability to limit the penetration.

Anyway, the fact that the S20430 decreases its E_{corr} to the region of corrosion before in the PI9 than in partial immersion without carbonation (PI) stresses the high importance that a decrease on the pH of the concrete might have on the durability of some stainless steel reinforcements where there are chlorides in the medium.

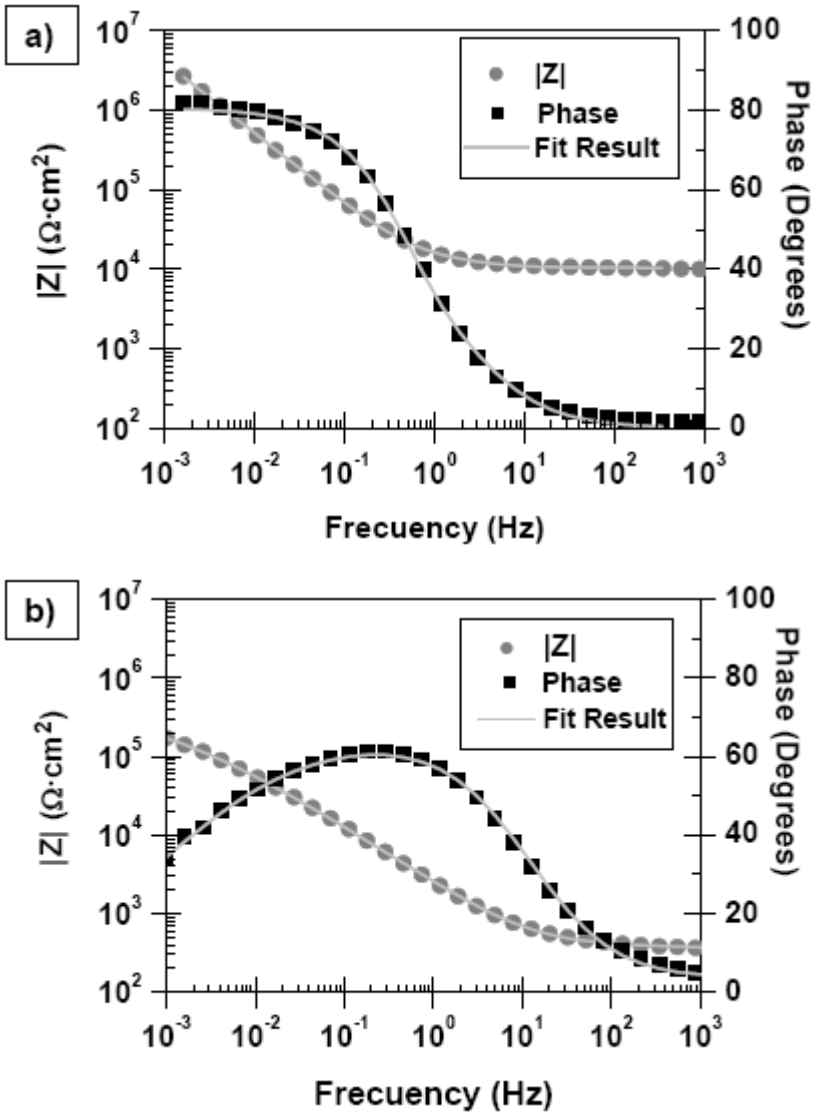

Figure 5. Experimental data and fitted curve of the EIS spectra corresponding to stainless steel bars in carbonated mortars after 60 months of exposure: a) S31603 in HRH9; b) S20430 in PI9.

As E_{corr} values offer only probabilistic information, and that information has been extensively checked for carbon steel reinforcements but not for stainless steels, it has been considered necessary to match these data with those obtained from EIS studies. In

Figure 5, two examples of the EIS spectra obtained for the stainless steel reinforced carbonated samples can be seen. In **Figure 5a,** the spectrum of a sample whose E_{corr} is in the passive region can be seen, while in **Figure 5b** the spectrum of a sample whose E_{corr} is in the active region appears. The fitted data obtained from the simulation of both examples are also included in the figure. The equivalent circuit previously used to simulate the behaviour of stainless steel reinforced non-carbonated mortars [10] has also proved to be adequate to simulate the EIS spectra of the carbonated samples. The equivalent circuit consists in a resistance that reproduces the resistive behaviour of the mortar (R_m) in series with two time-constants in cascade (Figure 6c in [10]). The medium-frequencies time-constant is formed by a resistance (R_{pl}) and a constant phase element (CPE_{pl}) that simulates the electrochemical behaviour of the passive layer. The low-frequency time-constant is constituted by the charge transfer resistant (R_t) in parallel with the constant phase element corresponding to the capacitive behaviour of the double layer (CPE_{dl}).

The R_m is an interesting parameter as it often determines the corrosion rate of carbon steel reinforced concrete structures. Obtained R_m values depend on the testing conditions, but they are independent from the nature of the reinforcement (if no cracking of the cover takes place, as occurs with stainless steel reinforcements). In **Figure 6**, the evolution with time of average R_m values for all the tested samples are plotted for each exposure condition. The HRH9 condition causes the highest R_m values. The presence of Cl^- in solution inside the pores of the samples in HRH9Cl conditions explain the decrease of the R_m values in comparison with those determined for HRH9. The partial immersion in NaCl assures the saturation of the pores with electrolyte, at least in the lower part of the samples. These facts explain the lower R_m values determined for PI9. Anyway, a lower level of bounded chlorides in PI9 than in HRH9Cl and differences in the curing process can also contribute to this difference.

If the R_m values in **Figure 6** are compared to those determined for the same parameter in non-carbonated mortars (Figure 7 in [10]), it can be seen that the initial increase in the R_m observed for the non-carbonated mortars can not be observed in these cases. This fact is due to the higher curing level of the carbonated mortars when they are exposed to the testing environments (the carbonation process lasted a few weeks). R_m in HRH9 is higher than R_m determined for non-carbonated mortar exposed in the same condition (HRH in

[10]) due to the precipitation of carbonates inside the pores. R_m values determined for PI9 are lower than R_m determined for PI in [10], that is to say, carbonation decreases the mortar resistance when the samples are partially immersed in NaCl. However, the chloride amount penetrated from the solution to the mortar surface is higher in non-carbonated conditions (compare results in **Figure 4** with those on Figure 5 in [10]). The fraction of bounded chlorides in carbonated mortars should be lower than in non-carbonated mortars to explain this fact.

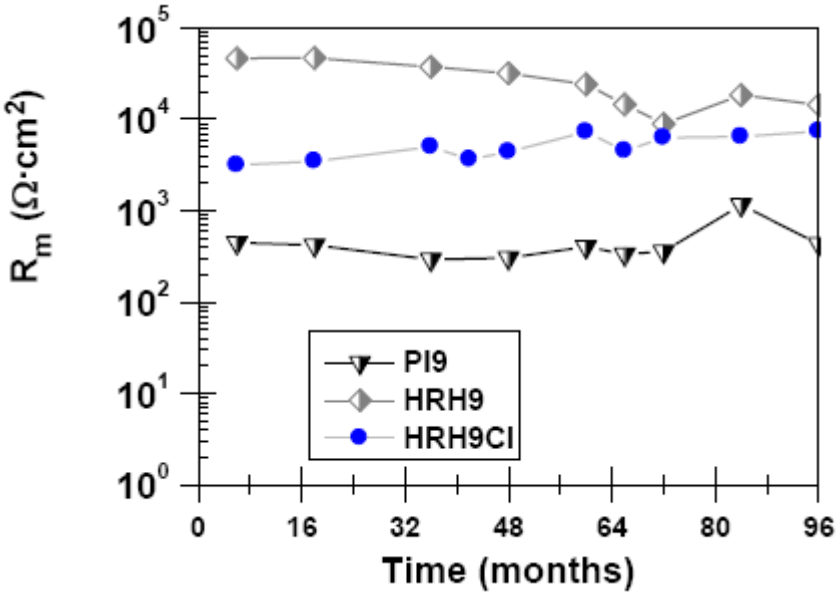

Figure 6. Average R_m values obtained from the EIS spectra for the stainless steel reinforced mortar samples in the different exposure conditions.

The R_t values from the EIS spectra are plotted in **Figures 7-9** for the different exposure conditions. In **Figure 7**, it can be seen that for HRH9, R_t exhibit high values, the order of magnitude of which is similar to that of passive stainless steels in non-carbonated mortars (Figure 10 in [10]). These values confirm the passive state suggested by the E_{corr} (**Figure 1**).

In **Figure 8**, it can be seen that the R_t of the S20430 in PI9 decreases nearly two orders of magnitude when its E_{corr} passes from the passivity region to the corrosion region (**Figure 2**). The pitting of low-Ni stainless steel in carbonated alkali activated fly ash mortars with

chlorides has been reported by other authors [23], confirming the limitations that this grade can have for its use in extremely aggressive conditions.

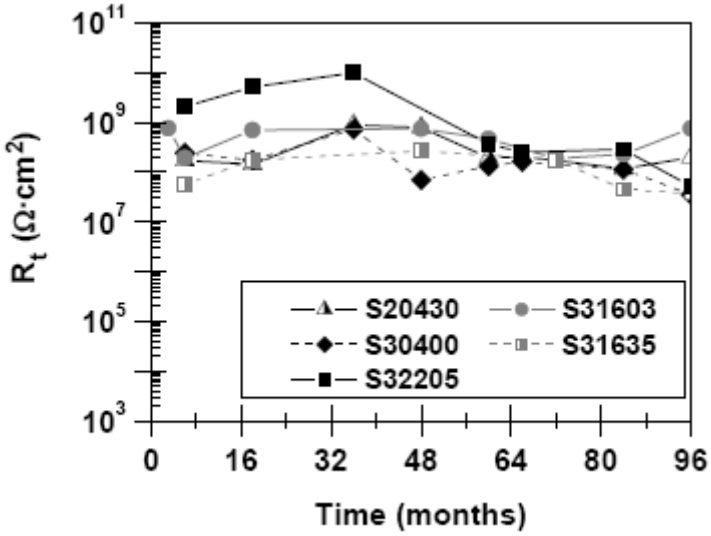

Figure 7. R_t values obtained from the EIS spectra of the stainless steels in HRH9 condition.

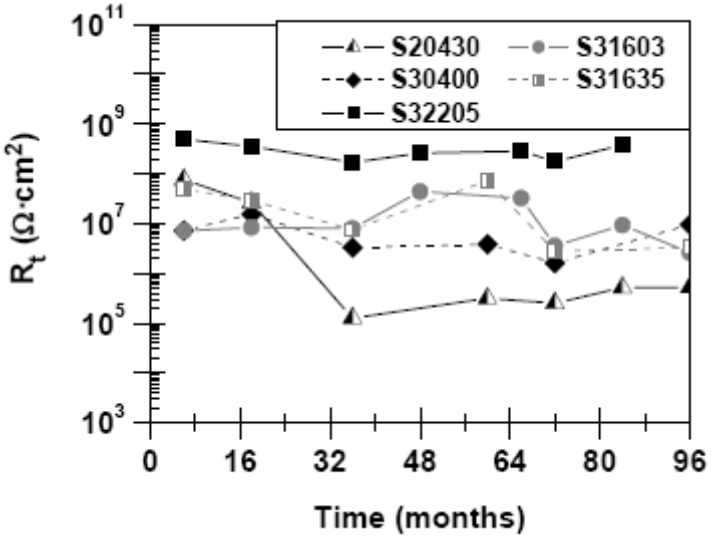

Figure 8. R_t values obtained from the EIS spectra of the stainless steels in PI9 condition.

S30400 stainless steel, whose E_{corr} remained for long periods in the region of uncertain corrosion activity in PI9 (**Figure 2**), exhibits R_t values (**Figure 8**) slightly lower than those usual for passive stainless steel reinforcements. In the period when the E_{corr} was in the region of uncertain activity, the calculated R_t are below 10^7 Ω·cm^2. Identifying R_t

with the polarization resistance in the Stern-Geary equation implies i_{corr} of the order of nA, that is to say, the S30400 can be considered at passive state, in spite of the ambiguous value of its E_{corr} if it is interpreted following the criterion defined in ASTM C876 for carbon steel. Anyway, the behaviour of S30400 in PI9 seems to be coherent with the results of the polarization tests, where this grade exhibits a pitting resistance in chloride-containing carbonated solutions lower than that of more alloyed/more expensive grades as S31603 or S32205 [12].

For the other stainless steels, the EIS simulation of the spectra obtained from samples in PI9 gives R_t values (**Figure 8**) typical of the passive state, as their E_{corr} have suggested (**Figure 2**). The S32205 stands out because of its high R_t value (admitting the uncertainty that implies the extrapolation of the experimental data to very low frequencies needed to obtain such high resistance values).

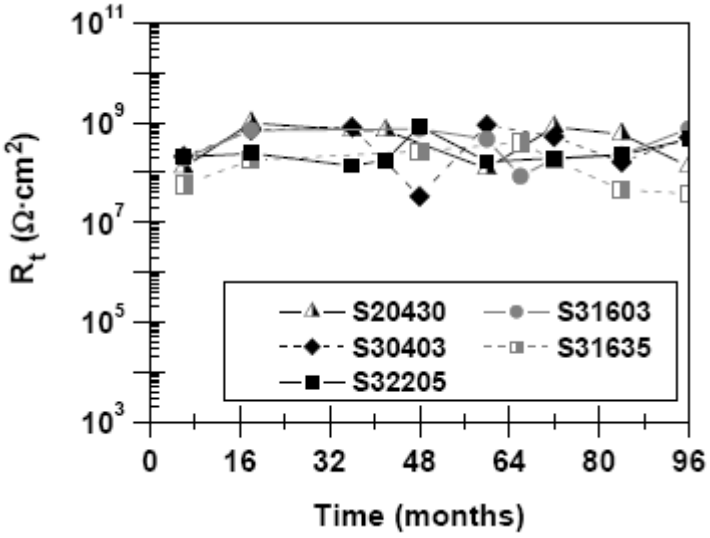

Figure 9. R_t values obtained from the EIS spectra of the stainless steels in HRH9Cl condition.

Comparing the results obtained in our laboratory for the R_t corresponding to S20430 in PI9 with those of the same material in non-carbonated mortar in partial immersion in 3.5% NaCl [10], it can be deduced that the low-intensity attack the S20430 tend to suffer in partial immersion exposures starts before when the mortar is carbonated. This occurs because much lower Cl^- concentration is needed to break the passivity at lower pHs.

Moreover, when the attack starts, it seems to progress at higher rates in carbonated mortars.

In HRH9Cl conditions (**Figure 9**), the R_t values are high, confirming the information about the passive state that can be deduced from the E_{corr} (**Figure 3**). If values in **Figure 9** are compared with those in **Figure 7**, no meaningful differences in R_t can be found due to addition of chlorides during mixing.

Table 2 - EIS parameters obtained for samples exposed in HRH9, different from those plotted in figures 6 and 7.

Steel Type	Exposition time (months)	C_{pl} ($\mu F/cm^2$)	n_{pl}	R_{pl} ($k\Omega \cdot cm^2$)	C_{dl} ($\mu F/cm^2$)	n_{dl}
S20430	6	6.0	0.76	19	8.2	0.74
	18	4.5	0.76	11	9.4	0.74
	36	5.0	0.76	8.1	10	0.74
	60	4.3	0.77	11	10	0.75
	66	8.0	0.77	9.5	8.4	0.74
	96	11	0.76	19	11	0.75
S30400	6	8.0	0.83	40	8.9	0.81
	18	8.5	0.84	30	9.4	0.82
	36	10	0.86	25	9.6	0.83
	60	6.6	0.85	12	14	0.85
	96	11	0.85	3.8	26	0.85
S31603	6	10	0.98	9.4	18	0.86
	18	13	0.91	13	13	0.89
	48	14	0.90	22	9.9	0.89
	60	15	0.90	20	8.2	0.89
	72	12	0.90	6.6	12	0.89
	96	13	0.89	10	9.4	0.88
S31635	6	4.9	0.86	5.8	31	0.87
	18	18	0.89	26	16	0.87
	48	16	0.88	19	16	0.86
	60	19	0.85	9.5	30	0.82
	72	7.8	0.79	8.9	22	0.86
	96	16.	0.84	9.2	25	0.86
S32205	6	5.6	0.80	40	11	0.78
	18	4.8	0.79	30	11	0.77
	36	6.9	0.79	23	9.9	0.77
	60	12	0.58	4.6	49	0.70
	66	9.3	0.78	28	8.0	0.75
	96	7.0	0.75	12	11	0.73

The values corresponding to other parameters obtained from the simulation of the EIS spectra can be seen in **Tables 2-4**. C_{pl} and n_{pl} are, respectively, the capacitance and the parameter that quantifies the deviation of the ideal behaviour for CPE_{pl}. C_{dl} and n_{dl} are the same parameters corresponding to CPE_{dl}. The data in the tables confirm that the corrosion rate is controlled by a low-frequency time constant (R_t is orders of magnitude higher than R_{pl}), so the estimations of i_{corr} made before using the Stren-Geary equation are correct.

Table 3 - EIS parameters obtained for samples exposed in PI9, different from those plotted in figures 6 and 8.

Steel Type	Exposition time (months)	C_{pl} ($\mu F/cm^2$)	n_{pl}	R_{pl} ($k\Omega \cdot cm^2$)	C_{dl} ($\mu F/cm^2$)	n_{dl}
S20430	6	19	0.89	1.1	18	0.88
	18	13	0.85	0.7	18	0.84
	36	53	0.79	0.3	66	0.77
	60	80	0.64	0.2	32	0.87
	72	70	0.68	0.5	19	0.89
	96	82	0.70	0.6	22	0.93
S30400	6	28	0.83	0.6	33	0.83
	18	17	0.87	0.3	24	0.87
	36	38	0.83	0.2	37	0.81
	60	30	0.85	0.2	43	0.84
	72	34	0.83	0.5	33	0.81
	96	28	0.87	0.1	26	0.87
S31603	6	26	0.89	0.3	27	0.87
	18	34	0.92	0.6	14	0.83
	36	37	0.79	0.1	35	0.78
	72	31	0.82	0.2	42	0.81
	96	58	0.83	6.7	16	0.98
S31635	6	29	0.89	4.0	13	0.89
	18	22	0.87	1.8	14	0.86
	36	37	0.83	2.5	12	0.82
	60	19	0.84	1.1	14	0.83
	72	22	0.80	0.4	18	0.78
	96	11	0.98	0.2	47	0.78
S32205	6	59	0.83	3.7	53	0.87
	18	46	0.81	1.1	54	0.78
	36	53	0.82	0.9	55	0.84
	66	75	0.82	2.2	40	0.83
	72	66	0.79	1.8	51	0.77
	84	31	0.77	3.0	62	0.80

In **Tables 2-4**, it is also shown that C_{dl} is about 10^{-5} A/cm^2, so it is in the range of values usually assumed for C_{dl}. It is not easy to see any meaningful evolution in the values of the

different parameters with time in any condition. However, it is clear that R_{pl} shows lower values in PI9 conditions, intermediate values in HRH9Cl and higher values in HRH9. That is to say, the presence of chlorides decreases the resistance of the passive layer, and this decrease is more marked when the samples are partially immersed. Moreover, carbonated samples with chlorides show lower R_{pl} values than non-carbonated samples with chlorides. The exposure conditions seem to be more determining for R_{pl} than the compositions of stainless steels.

Table 4 - EIS parameters obtained for samples exposed in HRH9Cl, different from those plotted in figures 6 and 9.

Steel Type	Exposition time (months)	C_{pl} ($\mu F/cm^2$)	n_{pl}	R_{pl} ($k\Omega \cdot cm^2$)	C_{dl} ($\mu F/cm^2$)	n_{dl}
S20430	6	14	0.83	3.0	22	0.84
	18	15	0.86	5.0	22	0.86
	36	12	0.81	8.1	18	0.82
	60	8.4	0.77	9.3	14	0.78
	72	8.9	0.77	11	15	0.80
	96	9.9	0.78	15	12	0.78
S30400	6	8.0	0.87	7.4	13	0.87
	18	11	0.88	12	14	0.89
	36	8.7	0.87	18	13	0.89
	60	6.9	0.84	17	12	0.87
	72	6.4	0.84	15	13	0.87
	96	6.3	0.84	16	14	0.88
S31603	6	19	0.86	16	11	0.86
	18	18	0.87	13	12	0.87
	36	9.4	0.84	6.9	14	0.84
	60	9.5	0.80	12	11	0.81
	72	10	0.81	9.6	12	0.80
	96	8.8	0.79	11	11	0.79
S31635	6	22	0.87	5.6	16	0.86
	18	12	0.86	2.6	25	0.86
	36	19	0.70	2.1	43	0.74
	60	14	0.79	6.8	12	0.78
	72	10	0.79	3.9	18	0.79
	96	15	0.79	13	12	0.78
S32205	6	39	0.83	1.8	60	0.83
	18	45	0.84	3.4	58	0.85
	36	34	0.83	4.1	50	0.83
	60	37	0.83	3.0	62	0.83
	72	29	0.77	2.7	49	0.79
	96	31	0.80	4.7	45	0.81

The mortar samples were submitted to anodic polarization tests to obtain more information about their relative corrosion resistance. Some examples of the obtained results, plotted as Evans diagrams, are shown in **Figure 10**. The influence of the media and the stainless steel composition are reflected in the current density values where the potential increases. Samples are anodically polarized up to 900 mV vs. SCE. As water decomposition in carbonated mortars takes place at higher potentials than in non-carbonated mortars (higher than 900 mV vs. SCE), no meaningful current increases take place in systems whose behaviour is very good (curve of S30400 in HRH9 in **Figure 10**). So, all detected current increases found in **Figure 10** correspond to the development of a corrosive attack.

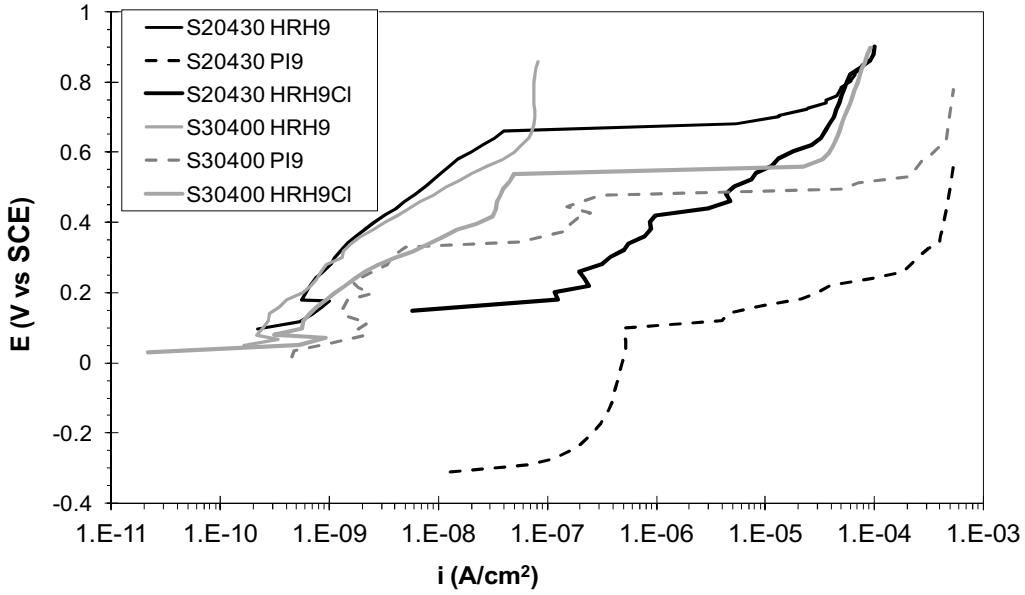

Figure 10. Examples of the results obtained from the polarization tests in carbonated mortars.

It must be pointed out that in the anodic polarization of the S20430 in HRH9Cl no passive region appears in the curve (**Figure 10**), though the system exhibits a E_{corr} characteristic of the passive state (**Figure 3**), and the R_t values measured without polarization confirm the passivity (**Figure 9**). Thus, the corrosion rate of the stainless steel at E_{corr} is negligible, but a small anodic polarization is able to break the passive state.

As has been done before [10], the potential values necessary to reach anodic current densities of $2 \cdot 10^{-6}$ A/cm^2 are used to compare the probability that the different systems have to reach a dangerous corrosion rate. These values are obtained from curves as those in the examples in **Figure 10** and plotted in **Figure 11**. Some conditions have not been included in the graph, because at the end of the experiments, when the morphology of the attack was analyzed, it was seen that corrosion was caused under the isolating tape that covers the bar in the mortar air-interface. As the polarization caused corrosion in a crevice created by the experimental set-up, those results were not taken into account for the study.

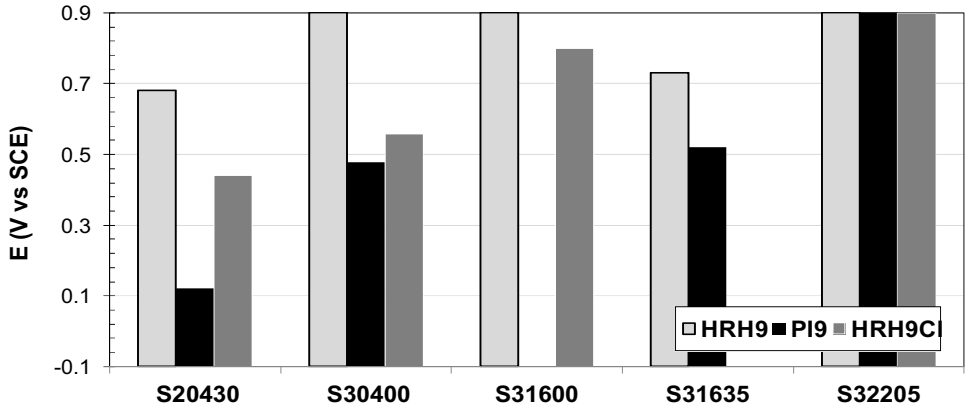

Figure 11. Anodic potential values needed not reach current densities of 2 x 10^{-6} A/cm^{-2}.

The duplex S32205 does not corrode under polarizations in any of the conditions, confirming the exceptional results of this material as reinforcement seen with non-carbonated mortar samples [10]. For the austenitic stainless steels, the PI9 confirm to be the most aggressive condition of the 3 considered in this article. The polarization results inform that the S20430 grade, that corrodes at a very low rate at E_{corr}, can easily reach very dangerous corrosion rates under moderate anodic polarizations. Thus, the use of this grade can be risky in extremely aggressive environments.

All the tested stainless steels seem to be able to guarantee the durability of carbonated structures when no chlorides are present. Only S20430 and S31635 corrode under polarization in HRH9, but at quite high anodic overpotentials.

If the results in **Figure 11** are compared to similar ones obtained for non-carbonated mortar samples (Figure 13 in [10]), it can be seen that, when similar amounts of chlorides are added during the manufacturing of the samples and then the samples are exposed at relative humidity of 90-95%, the corrosion resistance of a given stainless steel is clearly better in non-carbonated mortars. However, when carbonated and non-carbonated mortars are partially immersed in NaCl solution, the higher chloride concentration diffused in non-carbonated samples (compare results in Figure 4 with those in Figure 5 in [10]) makes it easy to reach dangerous corrosion rates for the stainless steels embedded in non-carbonated mortars.

After the anodic polarization, the caused attack was allowed to evolve for 1 additional year under the exposure conditions. Then, the samples were broken and the position and morphology of the attack in the stainless steel bars were studied. In **Figure 12**, examples of the attack developed in S20430 can be seen. S20430 in absence of chlorides and when the corrosion is provoked by anodic polarization in carbonated mortars corrodes in a localized way (**Figure 12a**). Round pits are observed on the surface of the material, but pits with less geometrical shape appear on the regions of the surface with a most strained microstructure. The relationship between high-strained microstructures of austenitic stainless steel corrugated bars and their corrosion behaviour has been analyzed in depth in previous papers based on solution tests [20,33]. A similar morphology of the attack is observed on the surface of S20430 after PI9 and HRH9Cl conditions (**Figure 12b**). The main influence of the presence of chlorides in the medium is an increase in the intensity of the damage.

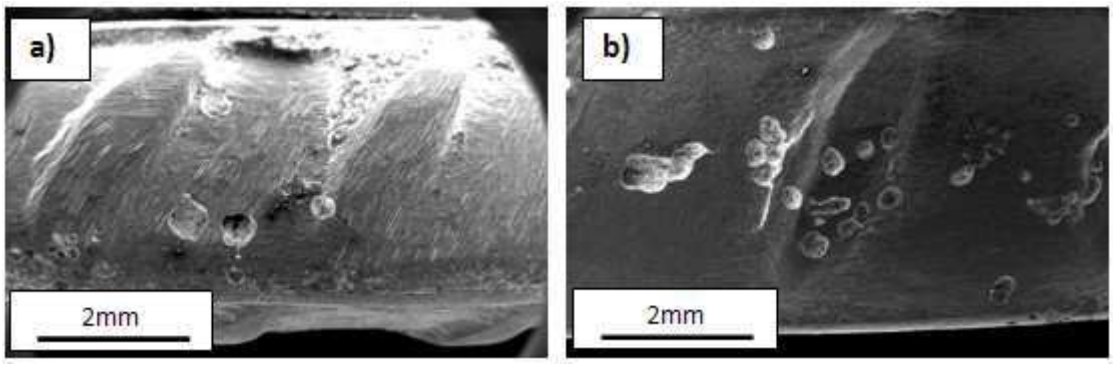

Figure 12. SEM images of the morphology of the attack on S20430 corrugated bars: a) In HRH9; b) In HRH9Cl$^-$.

In **Figure 13**, examples of the morphology of the attack observed in other more alloyed stainless steels are shown. As it has been reported for non-carbonated media [10], S30400 (**Figure 13a**) tends to develop big pits always located on the corrugations and in the most strained region of the bar. This behaviour has been related with the high deformation level of this corrugated material [10]. In austenitic grades with Mo, as in **Figure 13b**, localized attack with a low-penetrating shape has been observed. This is the same morphology of attack observed for these grades in non-carbonated mortars [10]. However, in carbonated mortars, a certain relationship between the localization of the attack and the most strained region of the surface has been detected. This relationship has not been previously observed for these materials in non-carbonated mortars [10].

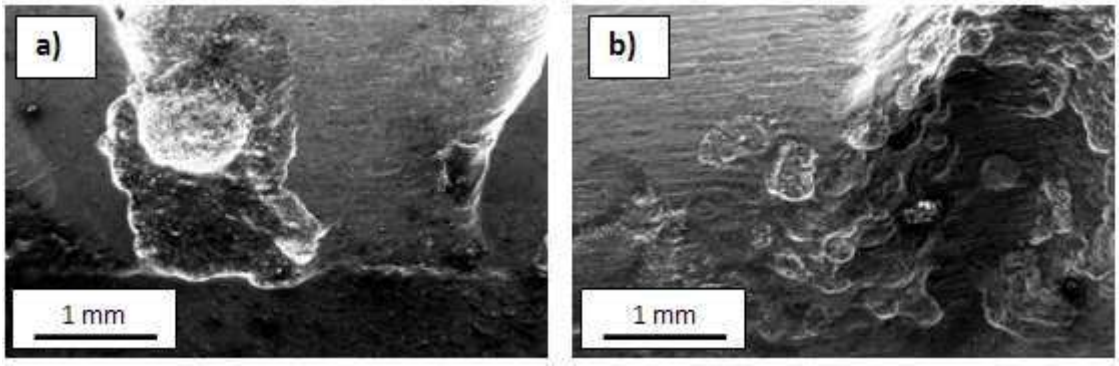

Figure 13. SEM images of the morphology of the attack on traditional austenitic grades embedded in carbonated mortar: a) S30400 in HRH9Cl; b) S31635 in PI9.

4. Conclusions

1. Low-Ni, austenitic S20430 is especially prone to suffer a low-intensity corrosive attack in carbonated mortars with chlorides whose rate can easily increase under moderate anodic polarizations.
2. Corrosion on S20430 reinforcements progress faster in carbonated mortars than in non-carbonated ones when they are partially immersed in 3.5% NaCl despite of the lower amount of diffused chlorides in the former.
3. Duplex S32205 is immune to corrosion in the carbonated mortar with chlorides, even in partial immersion conditions and under high anodic polarizations.

4. Austenitic stainless steel reinforcements could suffer localized corrosion in carbonated mortar with chlorides when they are submitted to high anodic polarizations.
5. When similar amounts of chlorides are added during the manufacturing of the samples, and then the samples are exposed to a relative humidity of 90-95%, the resistance to the pitting onset of the given stainless steel is clearly higher in non-carbonated mortars.

Acknowledgements

The present work was funded by the Spanish Ministry of Science and Innovation through the Project reference BIA2007-66491-C02-0

References

[1] S. Talukdar, N. Banthia, Carbonation in concrete infrastructure in the context of global climate change: Development of a service lifespan model, Constr. Build. Mater. 40 (2013) 775-782.

[2] P. Dangla, W. Dridi, Rebar corrosion in carbonated concrete exposed to variable humidity conditions. Interpretation of Tuutti's curve, Corros. Sci. 51 (2009) 1747-1756.

[3] Q. Huang, Z. Jiang, W. Zhang, X. Gu, X. Dou, Numerical analysis of the effect of coarse aggregate distribution on concrete carbonation, Constr. Build. Mater. 37 (2012) 27-35.

[4] S.-H. Han, W.-S. Park, E.-I. Yang, Evaluation of concrete durability due to carbonation in harbor concrete structures, Constr. Build. Mater. 48 (2013) 1045-1049.

[5] P.F. Marques, C. Chastre, A. Nunes, Carbonation service life modelling of RC structures for concrete with Portland and blended cements, Cem. Concrete Comp. 37 (2013) 171-184.

[6] E. Zornoza, P. Garcés, J. Mozó, M.V. Borrachero, J. Payá, Accelerated carbonation pf cement pastes partially subtituted with fluid catalytic cracking catalyst residue (FC3R), Cem. Concrete Comp. 31 (2009) 134-138.

[7] F. Pacheco Torgal, S. Miraldo, J.A. Labrincha, J. De Brito, An overview on concrete carbonation in the context of eco-efficient construction: Evaluation, use of SCMs and/or RAC, Constr. Build. Mater. 36 (2012) 141-150.

[8] S. Talukdar, N. Banthia, J. Grace, S. Cohen, Carbonation in concrete infrastructure in the context of global climate change: Part II - Canadian urban simulations, Cem. Concrete Comp. 34 (2012) 931-935.

[9] D.V. Val, M.G. Stewart, Life-cycle cost analysis of reinforced concrete structures in marine environments, Struct. Saf. (2003) 343-362

[10] A. Bautista, S.M. Alvarez, E.C. Paredes, F. Velasco, Corrosion performance of corrugated stainless steels after 9 years of exposure. Part I: non-carbonated, chloride contaminated mortar, Corros. Sci. (submitted).

[11] L. Freire, M.J. Carmezim, M.G.S. Ferreira, M.F. Montemor, The passive behaviour of AISI 316 in alkaline media and the effect of pH: A combined electrochemical and analytical study, Electrochim. Acta 55 (2010) 6174-6181.

[12] A. Bautista, G. Blanco, F. Velasco, A. Gutiérrez, L. Soriano, F.J. Palomares, H. Takenouti, Changes in the passive layer of corrugated, low Ni, austenitic stainless steel due to the exposure to simulated pore solutions, Corros. Sci. 51 (2009) 785-792.

[13] A. Bautista, G. Blanco, F. Velasco, Corrosion behaviour of low-nickel austenitic stainless steels reinforcements: A comparative study in simulated pore solutions, Cem. Concrete Res. 36 (2006) 1922–1930.

[14] S.M. Alvarez, A. Bautista, F. Velasco, Influence of process parameters on the corrosion resistance of corrugated austenitic and duplex stainless steel, Mater. Tehnol. 47 (2013) 317-321.

[15] S.M. Alvarez, A. Bautista, F. Velasco, Corrosion behaviour of corrugated lean duplex stainless steels in simulated concrete pore solutions, Corros. Sci. 53 (2011) 1748–1755.

[16] M. Moreno, W. Morris, M.G. Alvarez, G.S. Duffó, Corrosion of reinforcing steel in simulated concrete pore solutions: Effect of carbonation and chloride content, Corros. Sci. 46 (2004) 2681-2699.

[17] U. Angst, B. Elsener, C.K. Larsen, O. Vennesland, Critical chloride in reinforced concrete - A review, Cem. Concrete Res. 39 (2009) 1122-1138.

[18] V.K. Gouda, Corrosion inhibition of reinforcing steel. I. Immersed in alkaline solutions, Br. Corros. J. 5 (1970) 204-208.

[19] L. Li, A.A. Sagüés, Chloride concentration threshold of reinforcing steel in alkaline solutions - open-circuit immersion tests, Corrosion 57 (2001) 19-28.

[20] E.C. Paredes, A. Bautista, S.M. Alvarez, F. Velasco, Influence of the forming process of corrugated stainless steels on their corrosion behaviour in simulated pore solutions, Corros. Sci. 58 (2012) 52-61.

[21] R.D. Moser, P.M. Singh, L.F. Kahn, K.E. Kurtis, Chloride-induced corrosion resistance of high-strength stainless steels in simulated alkaline and carbonated concrete pore solutions, Corros. Sci. 57 (2012) 241-253.

[22] S. Fajardo, D.M. Bastidas, M.P. Ryan, M. Criado, D.S. McPhail, R.J.H. Morris, J.M. Bastidas, Low energy SIMS characterization on passive oxide films formed on a low-nickel stainless steel in alkaline media, Appl. Surf. Sci. 288 (2014) 423-429.

[23] C. Monticelli, M. Criado, S. Fajardo, J.M. Bastidas, M. Abbottoni, A. Balbo Corrosion behaviour of a Low Ni austenitic stainless steel in carbonated chloride-polluted alkali-activated fly ash mortar, Cem. Concrete Res. 55 (2014) 49-58.

[24] RILEM, Draft recommendation for repair strategies for concrete structures damaged by reinforcement corrosion, Mater. Struct. 27 (1994) 415-438.

[25] P. Castro, A.A. Sagües, E.I. Moreno, L. Maldona, J. Genescá, Characterization of activated titanium solid reference electrodes for corrosion testing of steel in concrete, Corrosion 52 (1996) 609-617.

[26] K. Kinoshita, M.J. Madou, Electrochemical measurements on Pt, Ir, and Ti oxides as pH probes, J. Electrochem. Soc. 131 (1984) 1089-1094.

[27] R.K. Dhir, M.R. Jones, H.E.H. Ahmed, Determination of total and soluble chlorides in concrete. Cem. Concrete Res. 20 (1990) 579-590.

[28] A. Bautista, G. Blanco, F. Velasco, A. Gutiérrez, S. Palacín, L. Soriano, H. Takenouti, Passivation of duplex stainless steels in solutions simulating chloride-contaminated concrete, Mater. Construcc. 57 (2007) 17-32.

[29] E. Zornoza, J. Payá, P. Garcés, Chloride-induced corrosion of steel embedded in mortars containing fly ash and spent cracking catalyst, Corros. Sci. 50 (2008) 1567-1575.

[30] C.K. Glass, N.R. Buenfeld, The presentation of the chloride threshold level for corrosion of steel in concrete, Corros. Sci. 39 (1997) 1001-1013.

[31] C. Arya, N.R. Buenfeld, J.B. Newman, Factor influencing the chloride binding in concrete, Cem. Concrete Res. 20 (1990) 291-300.

[32] H.-W. Song, S.-J. Kwon, Permeability characteristics of carbonated concrete considering capillary pore structure, Cem. Concrete Res. 37 (2007) 909-915.

[33] S.M. Alvarez, A. Bautista, F. Velasco, Influence of strain-induced martensite in the anodic dissolution of austenitic stainless steels in acid medium, Corros. Sci. 69 (2013) 130-138.

Capítulo VI

Otros Trabajos de Investigación

6.1 BARRAS CORRUGADAS DE ACERO INOXIDABLE SOLDADAS EMBEBIDAS EN MORTERO

En esta parte de la investigación se pretende estudiar el comportamiento frente a la corrosión de los aceros inoxidables soldados y embebidos en mortero. Para ello se ha realizando un seguimiento periódico del E_{corr} durante 8 años y se ha evaluando después su probabilidad de corrosión mediante ensayos de polarización anódica, similares a los utilizados en las **P7** y **P8**. Se han estudiado armaduras de inoxidables soldadas frente a sí mismas y frente a acero al carbono. Los óxidos generados durante la soldadura se han limpiado mediante chorreado con arena o mediante un decapante químico. Las armaduras se han embebido en mortero, sin carbonatar y carbonatado, siempre con $CaCl_2$ adicionado durante el amasado. Se han expuesto las probetas armadas durante 9 años al 90-95% de HR.

En las Figuras 6.1 y 6.2, se puede ver que la mayoría de los valores del E_{corr} correspondientes a las barras de acero inoxidable corrugadas que han sido soldadas frente a sí mismas tienden a permanecer en la región en la que el riesgo de corrosión es inferior al 10%, según el criterio propuesto por la norma ASTM C876 [1]. Estos resultados sugieren un buen comportamiento para la mayoría de los aceros inoxidables soldados ensayados, a pesar de los riesgos que, según ensayos previos en disolución, puede implicar la soldadura en estas aplicaciones [2].

Sólo se puede apreciar un comportamiento diferente del grado austenítico de baja aleación S20430 soldado frente a sí mismo cuando el mortero, además de contener cloruros, está carbonatado. Cuando los óxidos de soldadura se han eliminado mediante chorreado en arena, se observa una caída significativa del E_{corr} a los 5 años de exposición (Figura 6.2a), reduciéndose el valor de esta parámetro hasta valores correspondientes a un alto riesgo de corrosión. Este comportamiento podría ser indicativo de la nucleación de picaduras que no han sido capaces de repasivarse después de 5 años en condiciones tan agresivas. Además, en este mismo acero inoxidable, cuando se ha soldado frente a sí mismo y el proceso de limpieza de los óxidos de la soldadura se ha llevado a cabo con un decapado, la caída del E_{corr} ocurre sólo a los 6 meses de exposición (Figura 6.2b). Esta menor eficacia de la limpieza con decapante parece coincidir con incapacidad de este método para eliminar todos los óxidos generados durante el proceso de soldadura [2].

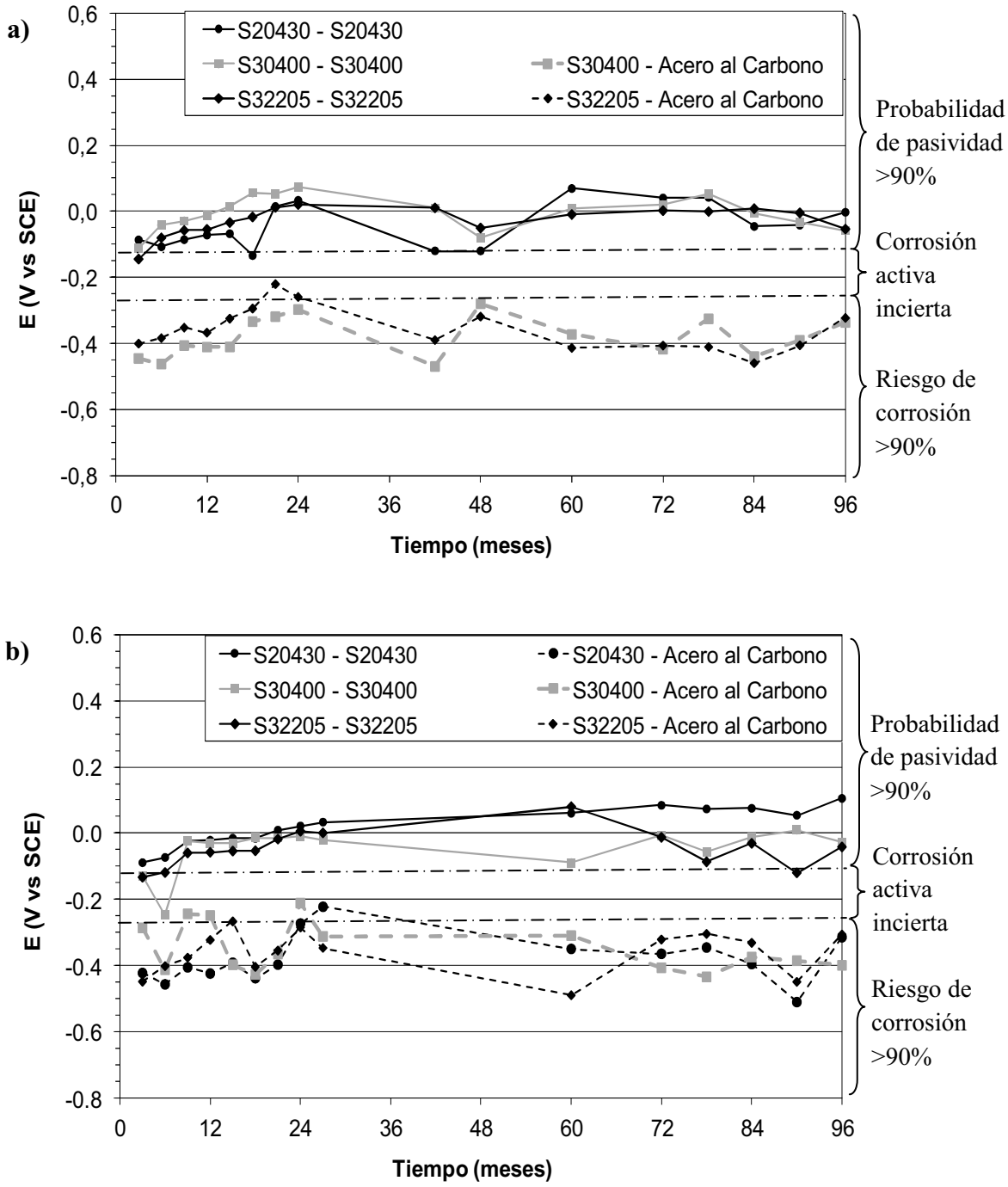

Figura 6.1. Evolución del E_{corr} de los aceros inoxidables corrugados soldados y embebidos en morteros sin carbonatar. Limpieza de los óxidos de soldadura mediante: a) chorreado con arena y b) decapado químico.

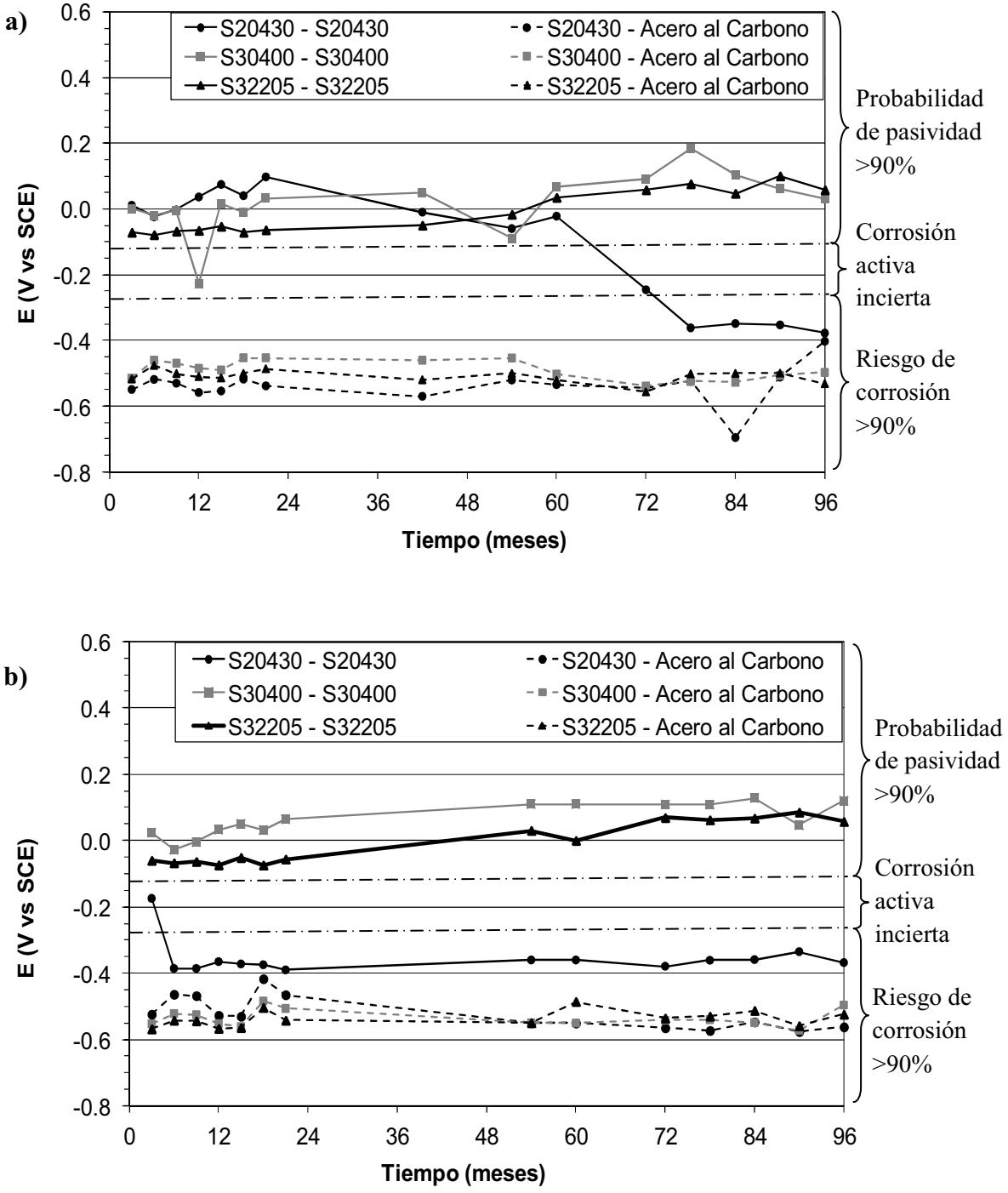

Figura 6.2. Evolución del E_{corr} de los aceros inoxidables corrugados soldados y embebidos en morteros carbonatados. Limpieza de los óxidos de soldadura mediante: a) chorreado con arena y b) decapado químico.

Por otro lado, cuando la soldadura se ha llevado a cabo entre corrugados de acero inoxidable y de acero al carbono, todas los refuerzos evaluados están en la región en la que el riesgo de corrosión es superior al 90% (Figuras 6.1 y 6.2). Este comportamiento puede responder simplemente a la tendencia del acero a carbono a corroerse en estas condiciones y a la polarización que las barras de acero al carbono activas ejercen sobre las de acero inoxidable [3]. Esta polarización tiene lugar aun en condiciones en las que el par galvánico acero inoxidable - acero al carbono tiene una intensidad despreciable en hormigón [4-6]. En conclusión, en este caso las armaduras de acero inoxidable pueden permanecer activas o pasivas, pero la simple medida de E_{corr} no es capaz de ofrecer información sobre el tema.

En la polarización de las probetas tras 8 años de exposición, se observa que los aceros inoxidables embebidos en mortero sin carbonatar la rama anódica tiene la forma típica de un sistema pasivo (Figura 6.3), mientras que los aceros inoxidables soldados frente al acero al carbono muestran claramente una curva activa (Figura 6.3), confirmando la información obtenida de los E_{corr} (Figura 6.1).

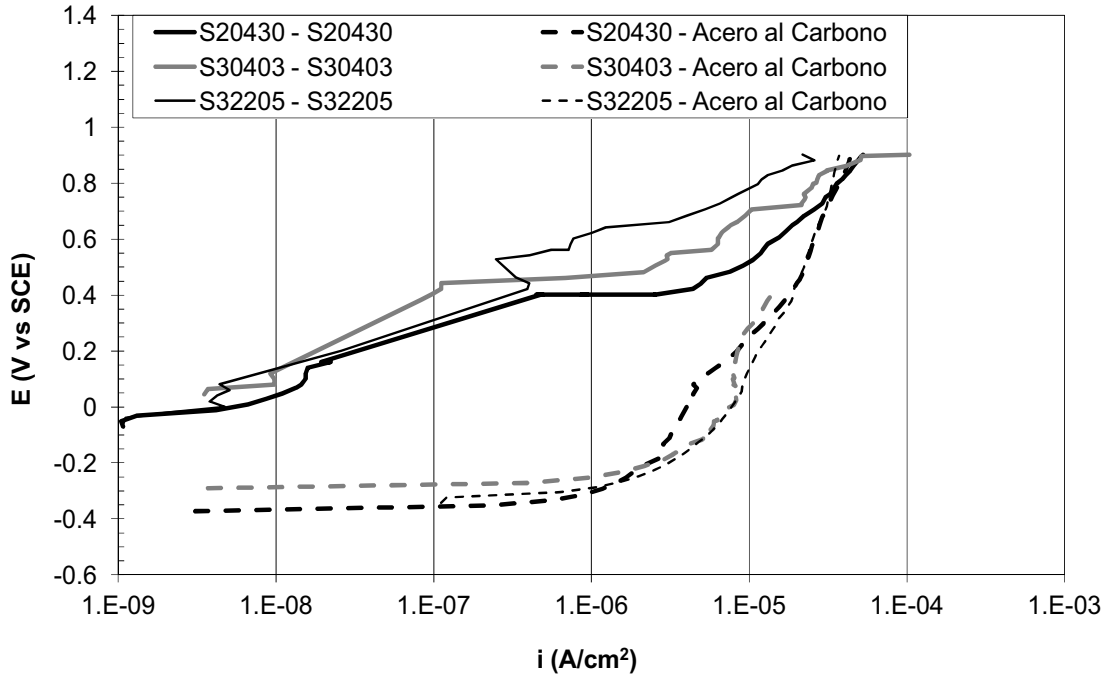

Figura 6.3. Curvas de polarización realizadas después de 8 años de seguimiento en probetas sin carbonatar. Limpieza de los óxidos de soldadura mediante chorreado con arena.

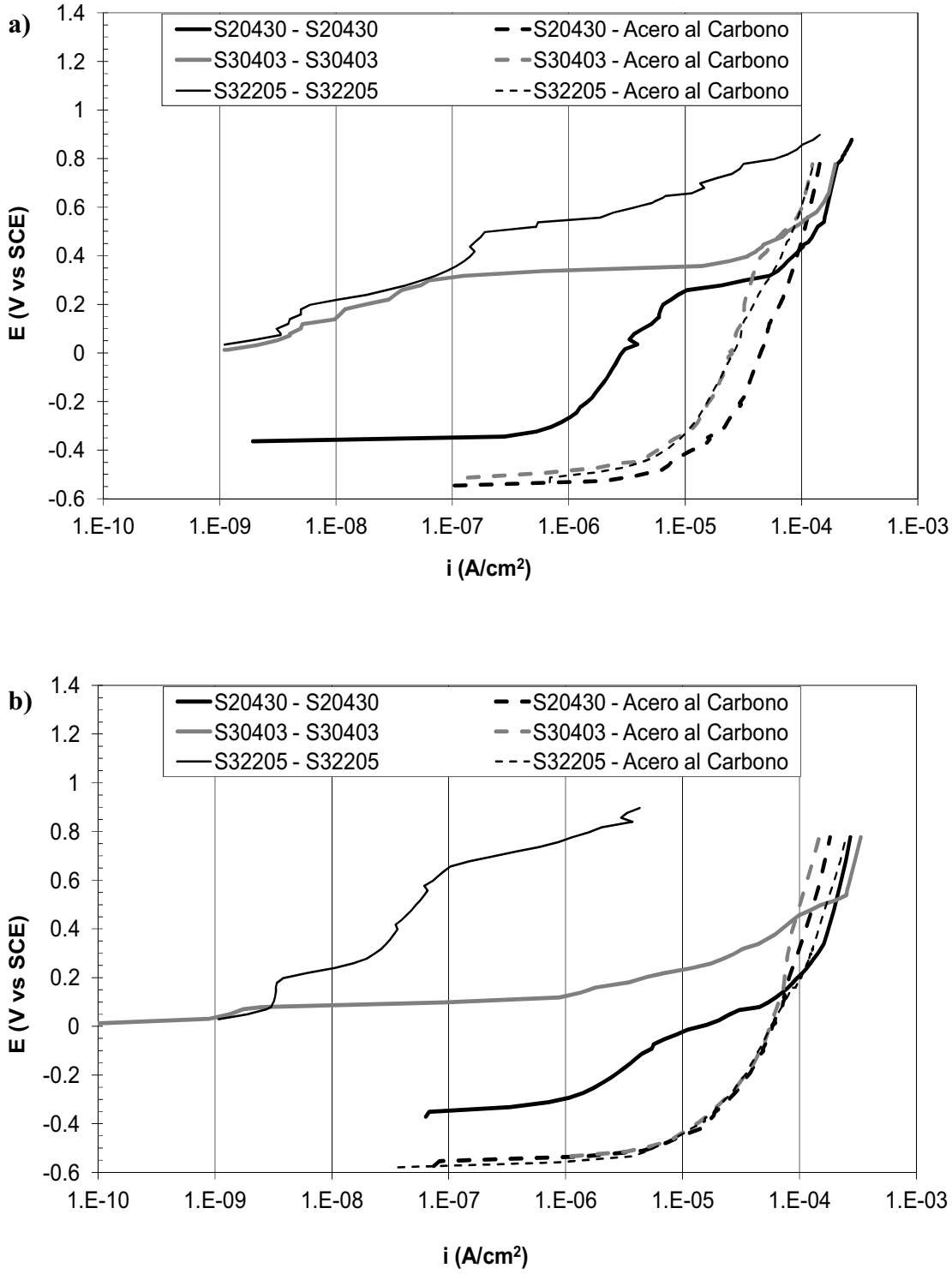

Figura 6.4. Curvas de polarización realizadas después de 8 años de seguimiento en probetas carbonatadas. Limpieza de los óxidos de soldadura mediante:
a) chorreado con arena y b) decapado químico.

En la polarización de los aceros embebidos en morteros carbonatados (Figura 6.4), se muestra el mismo paralelismo entre la forma de la rama anódica y los E_{corr} anteriormente indicado (Figura 6.2). Las diferencias en el comportamiento frente a la polarización de los diferentes grados cuando están soldados frente a sí mismos se hacen más visibles que en morteros sin carbonatar. El grado S20430, en estas condiciones de exposición, ofrece una curva anódica característica de materiales activos, de forma similar a las soldadas con armaduras de acero al carbono, pero con intensidades menores para polarizaciones anódicas moderadas (Figura 6.4). Destaca la forma de la curva del S30403 soldado y decapado químicamente (Figura 6.4b), pues aunque su potencial es típico del estado pasivo y existe zona pasiva, la longitud de esta es de unos pocos mV, es decir, que la pasividad de ese sistema es extremadamente inestable. La zona pasiva del acero S30403 soldado frente a sí mismo y chorreado en arena tiene una zona pasiva algo mayor, aunque no muy grande (Figura 6.4a).

Los incrementos de corriente observados en las Figuras 6.3 y 6.4 se pueden deber a diversos fenómenos. Para identificar el origen del incremento de corriente y lograr una mejor comprensión de lo sucedido durante la polarización anódica de las probetas, estas se dejaron expuestas durante 1 año más en los ambientes agresivos tras el ensayo destructivo. El objetivo era que el ataque eventualmente provocado pudiera progresar y se fácilmente detectable. Tras ese año adicional se rompieron los morteros, se limpiaron las armaduras y se analizó mediante una cuidada inspección visual el estado de las barras.

En las barras soldadas frente a acero al carbono, la corriente anódica se debe siempre, y de forma exclusiva, a la corrosión del acero al carbono. El acero al carbono muestra corrosión generalizada en toda su superficie (Figura 6.5) debido a la agresividad del ensayo. Sin embargo, se observa una diferencia significativa en la morfología del ataque cuando el acero al carbono ha sufrido un chorreado con arena y está embebido en mortero carbonatado (Figura 6.5c) en comparación con las otras condiciones (Figura 6.5a, 6.5b y 6.5d). Cuando el acero al carbono soldado y chorreado está en mortero carbonatado, además de una presencia de óxidos relativamente homogénea en toda su superficie, se observa una importante pérdida de material junto al cordón de soldadura. Este fenómeno es no se ve afectado por la naturaleza química del material de aporte y del inoxidable contra el que está soldado, y se ha observado en todas las barras de acero de carbono ensayadas en esas condiciones, independientemente de su diámetro. La razón de esto puede estar en las tensiones introducidas en el acero al carbono durante el chorreado

en área. Obviamente, el proceso de limpieza de óxidos en más intenso en la zona de la barra corrugada más próxima al material de aporte y esa zona de la barra corrugada debe haber sido expuesta a deformaciones superficiales más severas. En morteros sin carbonatar, el efecto sobre el comportamiento frente a la corrosión del acero al carbono no se ve visiblemente afectado por la deformación, pero este fenómeno podría resultar más relevante en condiciones más agresivas y explicar la diferencia en la morfología del ataque.

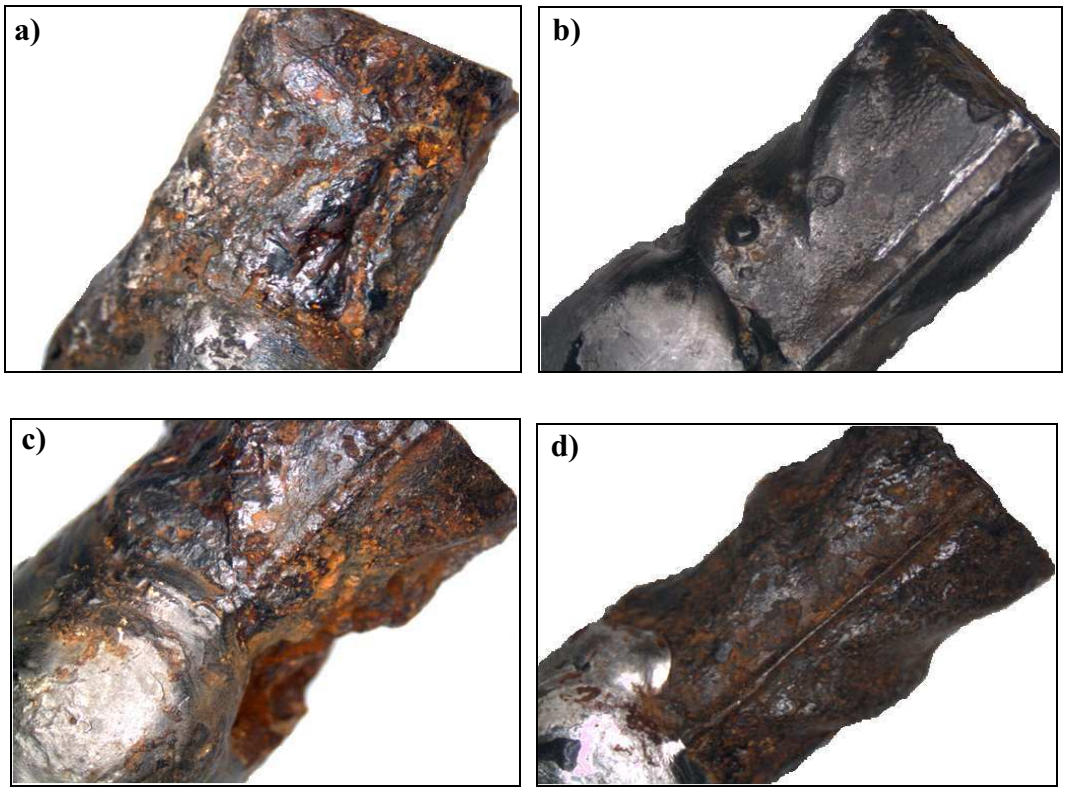

Figura 6.5. Imágenes del estado de las barras de acero al carbono soldadas frente a S30403 tras los ensayos: a) chorreada con arena en mortero sin carbonatar con cloruros; b) decapada en mortero sin carbonatar con cloruros; c) chorreada con arena en mortero carbonatado con cloruros; d) decapada en mortero carbonatado con cloruros.

En las barras inoxidables soldadas frente a sí mismas, el incremento de corriente refleja diferentes fenómenos según la probeta: descomposición del agua a elevadas polarizaciones anódicas, corrosión por picaduras del material de aporte y/o corrosión por picaduras del inoxidable corrugado. En la Tabla 6.1 se resumen las conclusiones obtenidas tras el estudio de las barras tras la polarización anódica. Se puede ver que el

dúplex corrugado S32205 no se corroe ni a altas polarizaciones aunque haya sido soldado. El pequeño incremento de corriente que aparece a altos sobrepotenciales no corresponde tampoco a la evolución de O_2, como ocurría en el mismo material sin soldar, sino a la aparición picaduras en el material de aporte. Estos datos demuestran que aunque el material para el cordón de soldadura se ha seleccionado siguiendo las especificaciones de los fabricantes para un grado S32205, el uso de un inoxidable más aleado como material de aporte podría llegar a ser una opción a considerar para estas aplicaciones.

Tabla 6.1. Fenómenos responsables del incremento de corriente en la polarización anódica de los corrugados inoxidables soldados frente a si mismos. Se han introducido como comparación los resultados de los inoxidables sin soldar en ensayos similares.

Grado soldado frente a sí mismo		**S20430**	**S30403**	**S32205**
Sin carbonatar	**Arena**	Picaduras en barra	Picaduras en el cordón y barra	Picaduras en el cordón
	Sin soldar	Picaduras en barra	Evolución O_2	Evolución O_2
Carbonatado	**Arena**	Picaduras en el cordón y barra	Picaduras en el cordón y barra	Picaduras en el cordón
	Decapada	Picaduras en el cordón y barra	Picaduras en el cordón y barra	Picaduras en el cordón
	Sin soldar	Picaduras en barra	Picaduras en barra	Evolución O_2

En la Tabla 6.1 también se ve que, en el caso de los austeníticos, las picaduras aparecidas durante el ensayo aparecen en la barra corrugada y, a veces, también en el cordón, no siendo el material de aporte en este caso el factor que limita la resistencia a la corrosión.

Para comparar de forma sencilla y cuantitativa los resultados de los ensayos de polarización de los diferentes materiales soldados, se han representado en la Figura 6.6 los potenciales anódicos para los cuales se alcanzan densidades de corriente de 2×10^{-6} A/cm^2. Este criterio es el mismo utilizado en **P7** y **P8** para analizar los resultados de ensayos similares en corrugados inoxidables sin soldar. Esta densidad de corriente seleccionada corresponde a elevadas velocidades de corrosión, similares a las que experimenta el acero al carbono en esas condiciones de exposición, siempre que no se

deban a los casos previamente identificados en la Tabla 6.1 como descomposición del agua. Además, se han incluido en la Figura 6.6, para utilizarlos como referencia, los datos correspondientes a los mismos grados sin soldar y que ya se analizaron con profundidad en **P7** y **P8**.

Dada la ausencia de corrosión en la barra corrugada S32205 en ninguna de las condiciones (Tabla 6.1), si se comparan los potenciales de los austeníticos S20430 y S30403 representados en la Figura 6.6, se puede ver que, en morteros carbonatados, como era de esperar, son necesarias menores polarizaciones para que refuerzos similares alcancen la misma intensidad de corrosión.

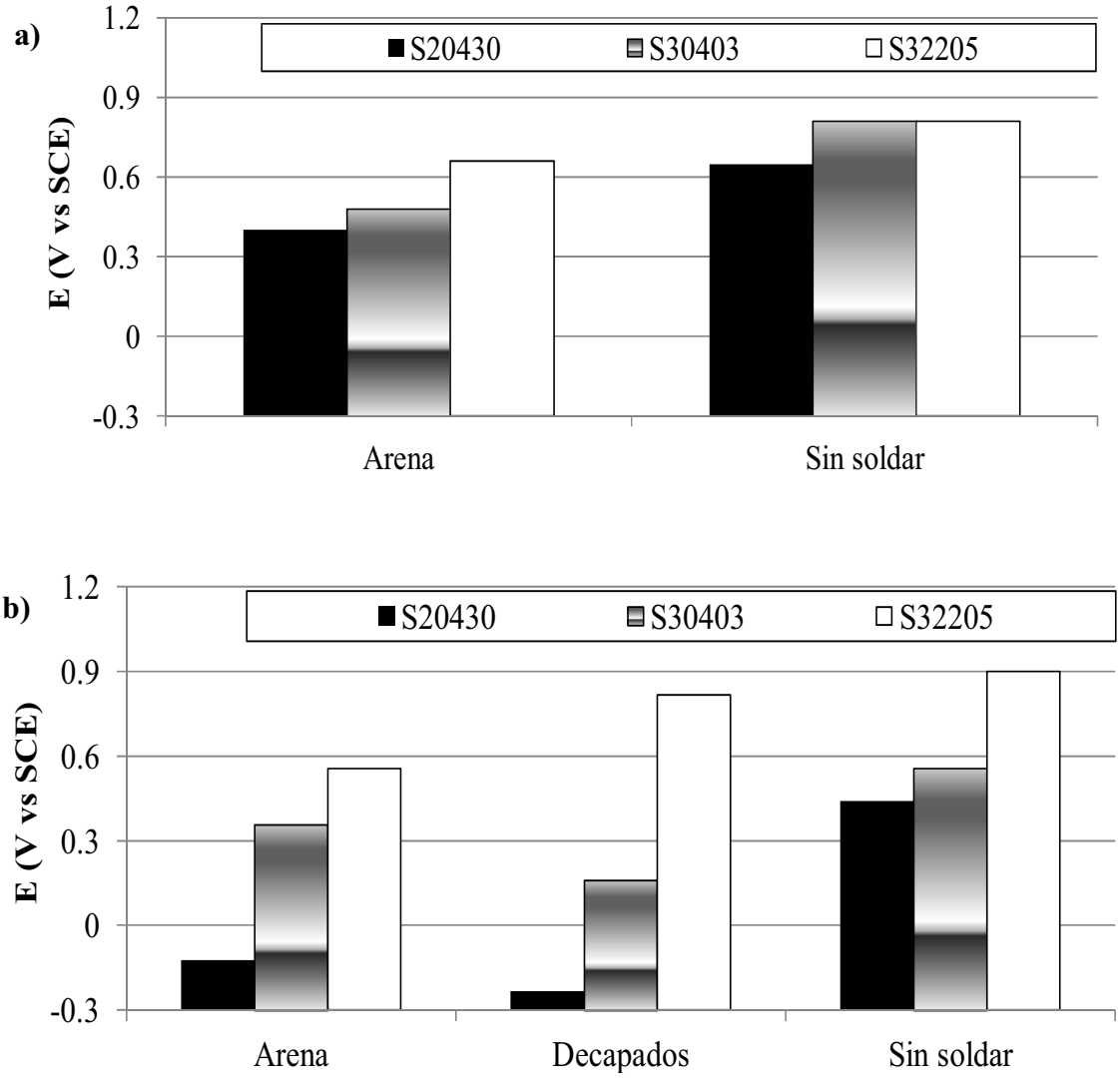

Figura 6.6. Potenciales anódicos a los cuales los corrugados inoxidables soldados frente a si mismos alcanzan densidades de corriente de 2 x 10^{-6} A/cm^2: a) en mortero sin carbonatar con cloruros; b) en mortero sin carbonatado con cloruros.

Para morteros con el mismo nivel de alcalinidad, el efecto perjudicial de la soldadura se confirma de nuevo si se comparan los resultados de las barras sin soldar con las soldadas (Figura 6.6). Los procedimientos de limpieza de óxidos considerados son incapaces de restaurar la resistencia a la corrosión de los inoxidables hasta sus valores originales.

Los datos de la Figura 6.7 confirman que no hay ningún efecto de aceleración de la velocidad de corrosión del acero al carbono debido a la formación de par galvánico con el acero inoxidable. Es más, la durabilidad de probetas soldadas de inoxidable – acero al carbono era mucho mayor que las que contenían sólo armaduras de acero al carbono en ensayos llevados a cabo en las mismas condiciones en nuestro laboratorio.

Este comportamiento puede explicarse teniendo en cuenta no sólo la menor superficie de material activo expuesto al mortero en las probetas soldadas, sino también el efecto positivo que pueden tener sobre la resistencia a la corrosión de las barras de acero al carbono los tratamiento empleados para la limpieza de los óxidos de soldadura. Los corrugados de acero al carbono chorreados con arena han demostrado que requieren de una concentración de cloruros más alta para que iniciar la corrosión que aquellos sin tratar [7,8]. Los procedimientos de eliminación de óxidos de soldadura en el material de aporte también deben contribuir a eliminar los óxidos formados en la atmósfera sobre las barras de acero al carbono. Se ha demostrado que la presencia de estos óxidos perjudica las características protectoras de la capa pasiva del acero en hormigón [9].

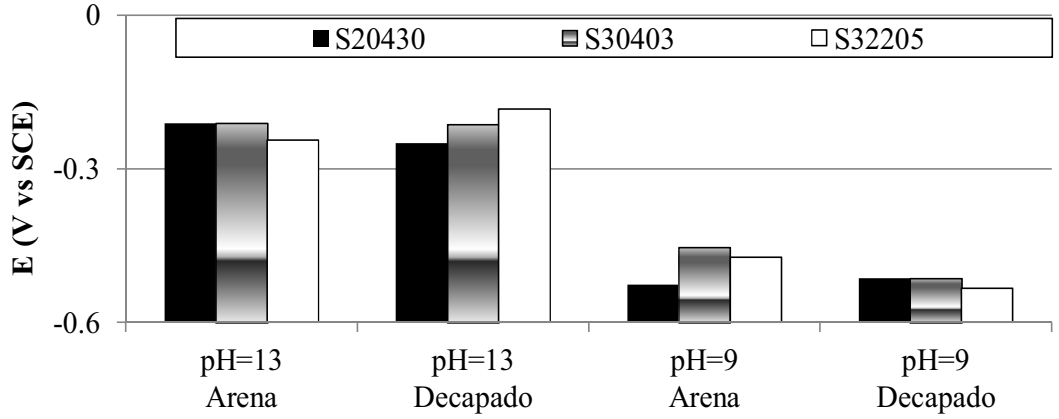

Figura 6.7. Potenciales anódicos a los cuales los corrugados inoxidables soldados frente acero al carbono alcanzan densidades de corriente de 2 x 10^{-6} A/cm^2.

Además, en la Figura 6.7 puede observarse que la polarización necesaria para que el acero al carbono alcance una determinada intensidad de corrosión es independiente del grado de acero inoxidable frente al cual está soldado, y no parece tener tampoco una relación clara con el método de limpieza de los óxidos. Sin embargo, estos valores sí cambian con el pH del medio. En morteros carbonatados, pese a su mayor resistividad, que es un parámetro que frecuentemente controla la velocidad de corrosión, se necesitan menores polarizaciones para alcanzar densidades de corriente anódicas de 2 x 10^{-6} A/cm^2. Las diferencia en la morfología de la corrosión mostradas en la Figura 6.5 no parecen verse reflejadas en este parámetro.

6.2 COMPORTAMIENTO EN MORTERO DE LOS ACEROS DÚPLEX DE BAJA ALEACIÓN

El objetivo de este apartado es conocer el comportamiento frente a la corrosión en mortero de los aceros inoxidables dúplex de baja aleación cuyo comportamiento en disolución se ha investigado en la presente Tesis Doctoral (**P1**). Se han fabricado probetas y se expuesto en 5 condiciones agresivas diferentes: mortero sin carbonatar en inmersión parcial en 3,5% NaCl (PI), mortero carbonatado en inmersión parcial en 3,5%NaCl (PI9), mortero son carbonatar con adición de $CaCl_2$ y expuesto a alta humedad relativa (HRHCl), mortero carbonatado con adición de $CaCl_2$ y expuesto a alta humedad relativa (HRH9Cl); mortero sin carbonatar con adición de $CaCl_2$ y parcialmente sumergido en alta humedad relativa (PICl). Para esta última condición, no incluída en otras investigaciones en mortero (**P7** y **P8**) se armaron también morteros con corrugados inoxidables de diferente composición para poder utilizarlos como referencia.

En esta parte de la investigación se ha realizado hasta el momento un seguimiento periódico del E_{corr} para evaluar la probabilidad de corrosión de los refuerzos siguiendo los criterios utilizados en las **P7** y **P8** (norma ASTM C876 [1]).

Los aceros dúplex de baja aleación embebidos en mortero sin carbonatar tienen E_{corr} por encima de -0,280 mV vs SCE (Figuras 6.8-6.10), por lo que los aceros parecen capaces de mantener el estado pasivo en los 36 meses de ensayo transcurridos hasta el momento. Esta pasividad durante los 3 primeros años de exposición en PI (Figura 6.8) y

HRHCl (Figura 6.9) es un comportamiento simular al mostrado por el dúplex S32205 y los austeníticos ensayados en esas condiciones en P7.

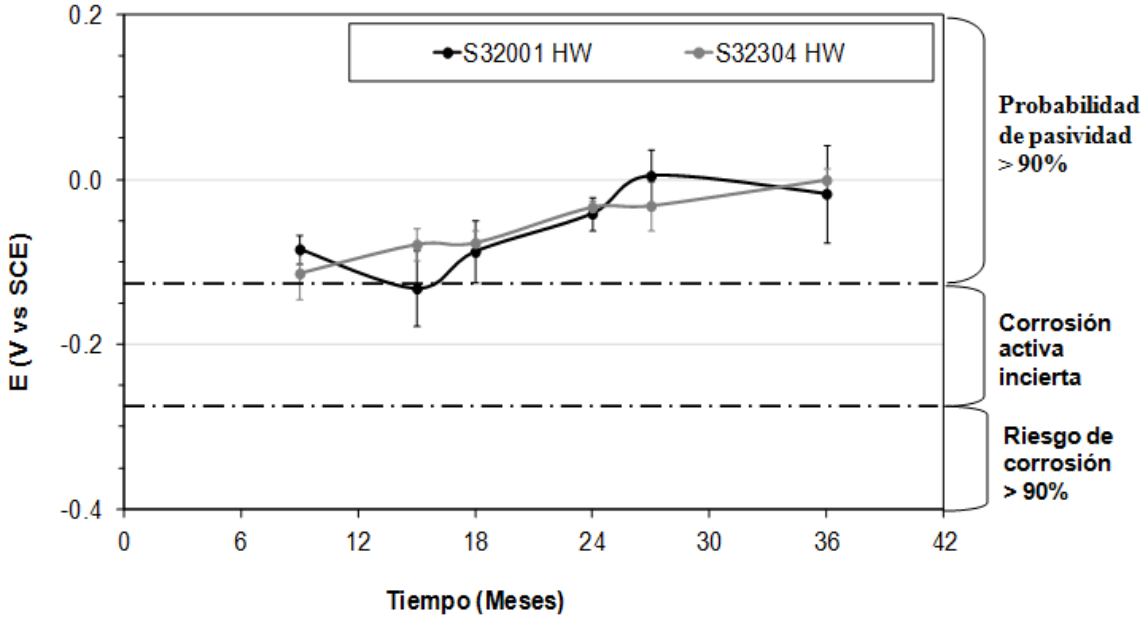

Figura 6.8. Evolución del potencial de corrosión de armaduras expuestas en PI.

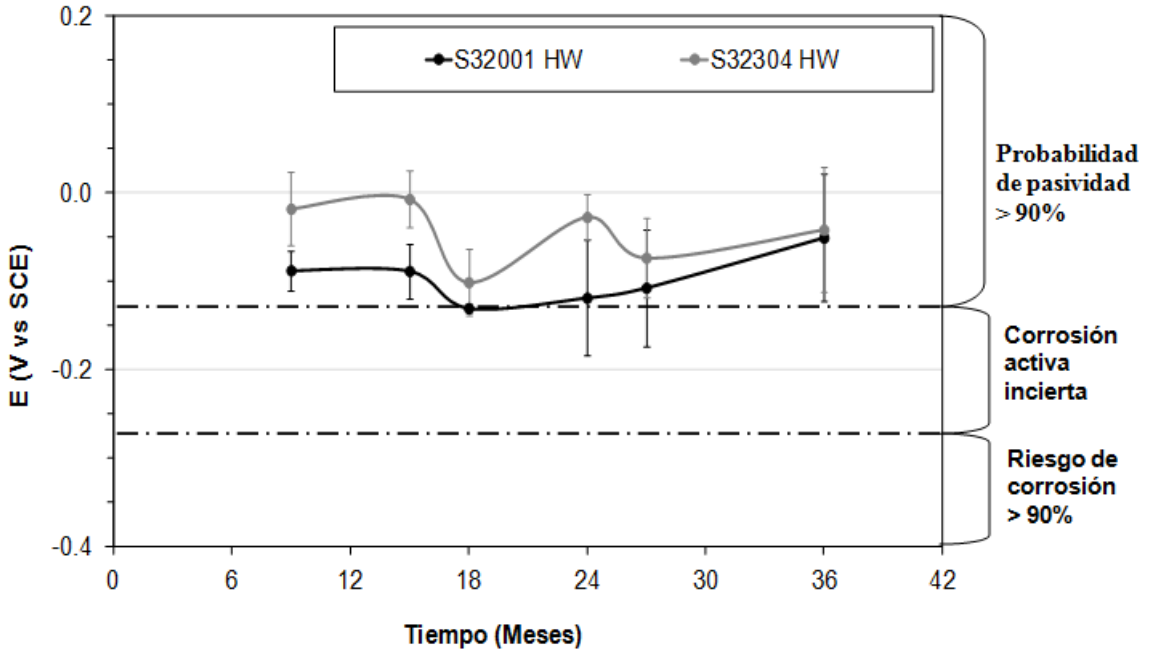

Figura 6.9 Evolución del potencial de corrosión de armaduras embebidas en mortero en HRHCl.

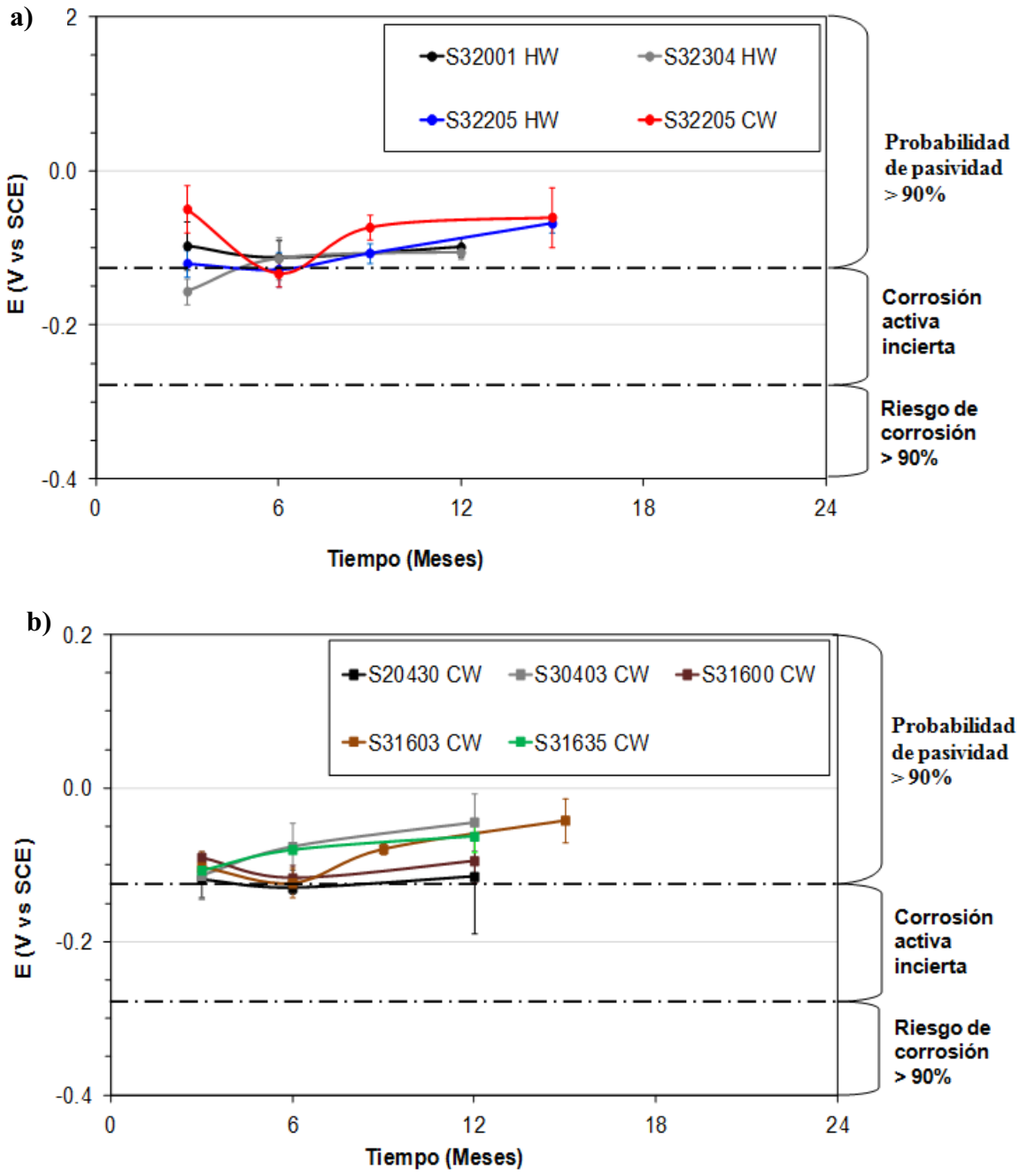

Figura 6.10. Evolución del potencial de corrosión de armaduras embebidas en mortero en PICl: a) corrugados dúplex; b) corrugados austeníticos.

En la condición PICl, potencialmente más agresiva que las anteriores, todos los dúplex ensayados parecen mantener su pasividad (Figura 6.10a), incluyendo los de baja aleación, aunque en este caso el periodo de exposición es todavía reducido. Las medidas de E_{corr} también sugieren un buen comportamiento para los austeníticos en PICl durante el

primer año, incluso para el S20430 (este corrugado había fallado espontáneamente de ha detectado a los 7 años en PI, según se vio en **P7**).

Sin embargo, los resultados de E_{corr} en morteros carbonatados en presencia de cloruros sugieren riesgo de corrosión para el dúplex menos aleado de los ensayados, el S32001 (Figura 6.11). El E_{corr} de este dúplex desciende bruscamente hasta la zona límite entre la probabilidad de corrosión mayor del 90% y la actividad de corrosión incierta a los 3 años en PI9. Este resultado podría reflejar un inicio de corrosión, que en cualquier caso habría que verificar con otros ensayos actualmente en curso o planeados (EIS y observaciones visuales del corrosión). Si el descenso de E_{corr} fuera significativo, el S32001 podría llegar a tener una durabilidad comparable a la del austenítico de baja aleación S20430 en morteros carbonatados, con cloruros y condiciones de inmersión parcial (**P8**). Sin embargo, los ensayos previos en disolución habían sugerido para el S32001 un comportamiento similar al tradicional austenítico S30400 (**P1**). Por otro lado, el austenítico de baja aleación había demostrado una resistencia a la corrosión en disoluciones carbonatadas y con cloruros inferior a la del S30400 [10]. Una hipotética confirmación del fallo en mortero del S32001, pondría de relieve la importancia que pueden tener en el inicio del proceso de corrosión en mortero factores irreproducibles mediante ensayos en disolución (como los citados en **P7**). En cualquier caso, los resultados obtenidos hasta el momento sobre el tema, aunque potencialmente interesantes, no dejan de ser preliminares.

Por otro lado, cuando los morteros se exponen en HRH9 (Figura 6.12), la presencia de carbonatación y cloruros, en ausencia de condiciones de aireación diferencial, no parece capaz de comprometer la pasividad en mortero de ninguno de los dúplex de baja aleación. Estos resultados confirman la información sobre la agresividad relativa de las diferentes condiciones, previamente discutida en **P8**.

Merece la pena resaltar, en cualquier caso, que los resultados correspondientes al S32304 en las 5 condiciones agresivas ensayadas son, sin lugar a dudas, excelentes en los 3 años de ensayo, siendo este material más barato que los austeníticos tradicionales.

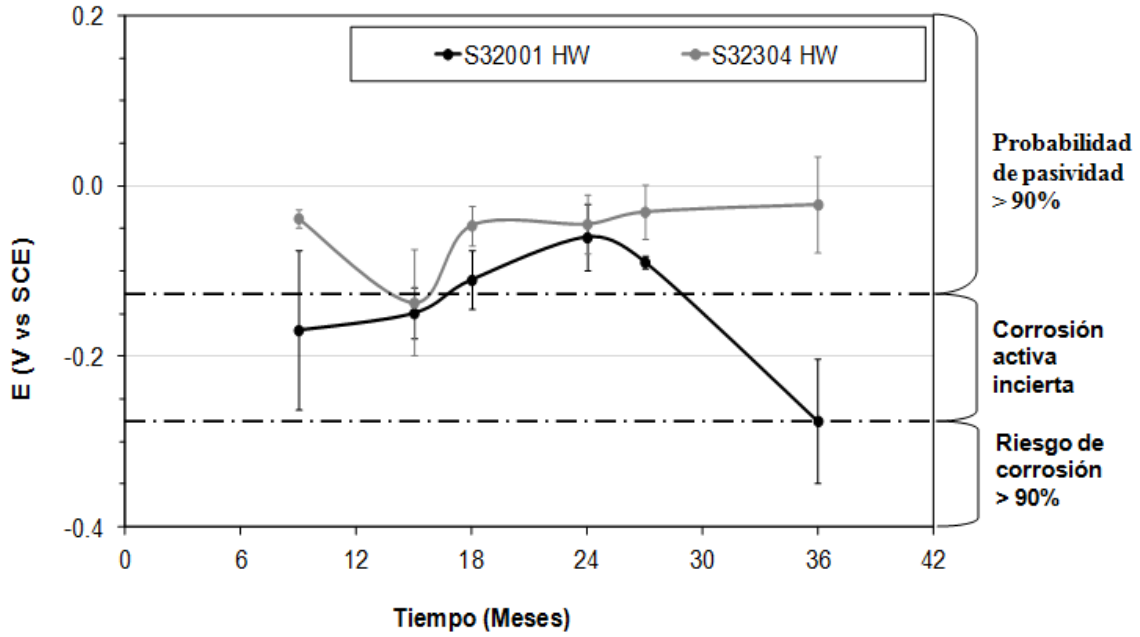

Figura 6.11. Evolución del potencial de corrosión de armaduras embebidas en PI9.

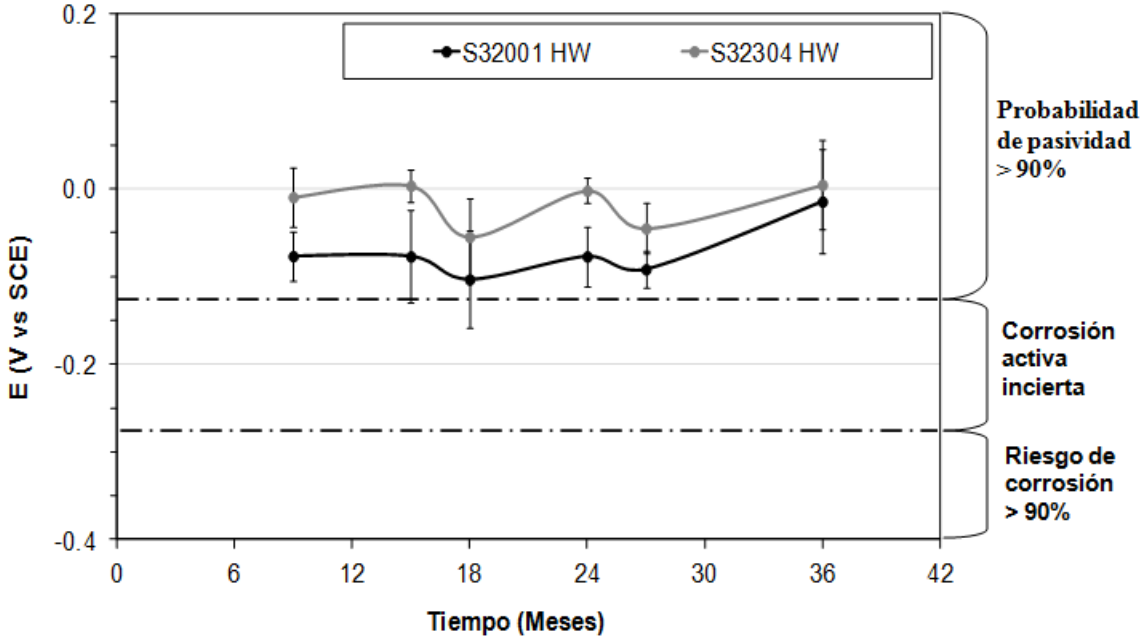

Figura 6.12. Evolución del potencial de corrosión de armaduras embebidas en mortero en HRH9Cl.

6.3 BIBLIOGRAFÍA

[1] ASTM C876-09 Standard. "*Standard Test Method for Corrosion Potentials of Uncoated Reinforcing Steel in Concrete*".

[2] A. Bautista, G. Blanco, F. Velasco, M.A. Martinez, "*Corrosion performance of welded stainless steels reinforcements in simulated pore solutions*", Construction and Building Materials, 21, pp.1267–1276 (2007).

[3] J.A. González, E. Ramírez, A. Bautista, *"Behaviour of steel reinforcement under the effect of strong cathodic or anodic polarizations"*, Magazine of Concrete Research, 50, pp. 201-208 (1998).

[4] M.C. García-Alonso, J.A. González, J. Miranda, M.L. Escudero, M.J. Correia, M. Salta, A. Bennani, "*Corrosion behaviour of innovative stainless steels in mortar"*, Cement and Concrete Research", 37, pp. 1562-1569 (2007).

[5] J.T. Pérez-Quiroz, J. Terán, M.J. Herrera, M. Martínez, J. Genesca, "*Assessment of stainless steel reinforcement for concrete structures rehabilitation*", Journal of Constructional Steel Research, 64, pp. 1317-1324 (2008).

[6] L. Bertolini, P. Pedeferri, "*Laboratory and field experience on the use of stainless steels to improve the durability of reinforced concrete*", Corrosion Reviews, 20, pp. 129-152 (2002).

[7] T.U. Mohammed, H. Hamada, "*Corrosion of steel bars in concrete with various steel surface conditions*", ACI Materials Journal, 103, pp. 233-242 (2006).

[8] M. Manera, O. Vennesland, L. Bertolini, "*Chloride threshold for rebar corrosion in concrete with addition of silica fume*", Corrosion Science, 50, pp. 233-242 (2008).

[9] E. Mahallati, M. Saremi, "*An assessment in the mill scale effects in the electrochemical characteristics of the bars under DC-polarization"*, Cement and Concrete Research, 36, pp. 1324-1329 (2006).

[10] A. Bautista, G. Blanco, F. Velasco, "*Low-Ni Corrosion behaviour of low-nickel austenitic stainless steels reinforcements: A comparative study in simulated pore solutions*", Cement and Concrete Research. 36, pp. 1922-1930 (2006).

Capítulo VII

Conclusiones Generales

Las principales conclusiones de los trabajos ya publicados y de otros resultados obtenidos a lo largo de la investigación desarrollada a lo largo de la presente Tesis Doctoral podrían resumirse de la siguiente forma:

Conclusiones de los ensayos en disoluciones alcalinas

1. El grado dúplex S32304, de bajo contenido en Mo, es claramente más resistente a la corrosión que cualquiera de los grados austeníticos estudiados, estimándose que este material puede costar alrededor de un 9% menos que un grado S30403 tradicional. La resistencia a la corrosión del corrugado S32304 en estos medios es, sin embargo, menor que la del dúplex S32205.

2. La resistencia a inicio de la corrosión del nuevo dúplex S32001 es bastante similar a la del tradicional austenítico S30403, o incluso ligeramente mejor, siendo el S32001 alrededor de un 15% más barato.

3. El dúplex S32205 no se corroe mediante ensayos de polarización en ninguna de las disoluciones ensayadas.

4. La microestructura de los inoxidables dúplex, en comparación con la de los austeníticos, limita el progreso del ataque una vez iniciado.

5. En el dúplex S32304 se corroe preferentemente la ferrita en todas las soluciones alcalinas con cloruros estudiadas. En el dúplex S32001, en las mismas condiciones, se corroe preferentemente la austenita.

6. La superficie corrugada presenta una probabilidad de corrosión mucho mayor que el núcleo de la barra y, cuando el ataque se induce por polarización, es menos localizado en la superficie que en el núcleo. Esto se debe a que el proceso de formación de las corrugas modifica fuertemente la microestructura de los aceros inoxidables.

7. Para una composición de inoxidable dada, la superficie corrugada de barras austeníticas HW comienzan a corroerse a menores sobrepotenciales anódicos que las CW. Sin embargo, el ataque de la superficie en las barras CW tiende a desarrollarse en una forma más rápida y localizada que en los HW.

Conclusiones de los ensayos en disoluciones ácidas

1. Las capas pasivas formadas anódicamente en las corrugas necesitan mayores polarizaciones que las formadas en material del núcleo, y sus características protectoras son más limitadas.

2. Una excepción entre los materiales ensayados son los dúplex S32205, en los que domina en el comportamiento a corrosión el efecto de la beneficioso de la textura sobre otros adversos generados por el proceso de conformado en la superficie.

3. Se ha comprobado la presencia de cantidades variable de martensita inducida por deformación en los aceros inoxidables austeníticos y en la fase austenítica de los dúplex. La cantidad de martensita en la microestructura depende de la composición química y el tipo procesado. Los grados menos aleados tienen mayor tendencia a formar martensita durante el procesado.

4. En el medio ácido ensayado, la martensita de los corrugados austeníticos tiende a corroerse selectivamente frente a la austenita, aunque un incremento de potencial (o una disminución de pH) favorecerían la disolución selectiva de la austenita frente a la de la martensita.

5. En los corrugados dúplex, la ferrita se disuelve selectivamente a E_{corr} o a potenciales ligeramente superiores. En ausencia de polarizaciones, la martensita inducida por deformación en la fase austenita, presenta una resistencia a la corrosión claramente mayor que la de la ferrita.

6. La contribución de las diferentes fases presentes en la microestrutura de los corrugados inoxidables a la región de corrosión activa de las curvas anódicas en medio ácido puede cuantificarse mediante el software diseñado en el grupo de investigación.

7. La ferrita es más sensible que la austenita a la disminución de la resistencia a la corrosión causada por el conformado.

Conclusiones de los ensayos en mortero

1. Los ensayos en mortero expuesto a diferentes condiciones agresivas confirman el excepcional comportamiento frente a la corrosión del grado S32205 sugerido en los ensayos en disolución, no corroyéndose ni en presencia de elevadas polarizaciones anódicas, ni siquiera tras haber sido soldado (aunque en este último caso pueden aparecer picaduras en el material de aporte).

2. Los aceros inoxidables en mortero carbonatado o sin carbonatar, si se corroen, lo hacen por picaduras, que se localizan en las zonas más deformadas de la superficie o se distribuyen por toda ella, dependiendo del grado de deformación plástica previo de la barra.

3. Los grados austeníticos tradicionales sin soldar no se han corroído espontáneamente durante los ensayos de larga duración y, si llegan a desarrollar corrosión en algunos medios especialmente agresivos, lo hacen sólo tras ser sometidos a polarizaciones muy elevadas.

4. El grado S20430 ha revelado ser claramente susceptible a la corrosión en condiciones de inmersión parcial en presencia de cloruros, especialmente si el mortero está carbonatado.

5. El grado S20430 cuando ha sido sometido a un proceso de soldadura y se embebe en mortero carbonatado con cloruros, se corroe fácilmente, aunque se hayan realizado procedimientos de limpieza de óxidos y no esté en condiciones de inmersión parcial.

6. Los resultados provisionales de E_{corr} sugieren que el S32001 podría presentar riesgo de corrosión en presencia de cloruros si el mortero está carbonatado y parcialmente sumergido en NaCl.

Capítulo VIII

Líneas de Trabajo Futuras

La realización de esta Tesis Doctoral ha permitido la obtención de información muy importante sobre el comportamiento frente a la corrosión de armaduras de acero inoxidable austeníticos y dúplex tradicionales embebidas en mortero durante 9 años. Sin embargo, sobre los nuevos aceros inoxidables dúplex de baja aleación (de gran interés tras los datos previos obtenidos en ensayos en disolución), la confirmación necesaria de resultados mediante medidas en mortero se limita a 3 años. Por ello se continuará avanzando en el conocimiento de estos nuevos refuerzos corrugados, trabajando en las siguientes líneas:

1. Continuación con las medidas electroquímicas (E_{corr} y EIS) de las armaduras de aceros inoxidables dúplex de baja aleación embebidas en mortero durante 4-5 años más de tiempo.

2. Realización de ensayos destructivos sobre las probetas de mortero reforzadas con dúplex de baja aleación y expuestas en condiciones agresivas y análisis posterior de la morfología del ataque.

Además, para lograr una mejor comprensión de los datos de comportamiento frente a la corrosión de armaduras inoxidables soldadas en mortero, es necesario que se complete la tarea, actualmente en curso:

3. Análisis de los espectros de EIS obtenidos de las probetas soldadas durante su exposición a lo largo de 8 años en ambientes agresivos.